MECHANISMS OF CHEMICAL AND PHYSICAL TRANSDERMAL PENETRATION ENHANCEMENT

BURRINDER SINGH GREWAL

Doctor of Philosophy

ASTON UNIVERSITY

July 1999

Aston University

MECHANISMS OF CHEMICAL AND PHYSICAL TRANSDERMAL PENETRATION ENHANCEMENT

by
Burrinder Singh Grewal
Submitted for the degree of Doctor of Philosophy, 1999

THESIS SUMMARY

The transdermal route is an alternative route for administering drugs to humans which may circumvent many of the problems associated with the more common oral route. The underlying theme of this thesis is one of exploring the processes involved in the enhancement of percutaneous absorption.

The development of an attenuated total reflectance Fourier-Transform infrared (ATR-FTIR) spectroscopic method to analyse diffusion of suitable topically applied compounds in membranes is described. Diffusion coefficients (D/h^2) and membrane solubility (A_O) for topically applied compounds were determined using a solution to Fick's second law of diffusion. This method was employed to determine the diffusional characteristics of a model permeant, 4-cyanophenol (CP), across silicone membrane as a function of formulation applied and permeant physicochemical properties. The formulations applied were able to either affect CP diffusivity and/or its membrane solubility in the membrane; such parameters partially correlated with permeant physicochemical properties in each formulation.

The interplay during the diffusion process between drug, enhancer and vehicle in stratum corneum (SC) was examined. When enhancers were added to the applied formulations, CP diffusivity and solubility were significantly enhanced when compared to the neat propylene glycol (PG) application. Enhancers did not affect PG diffusivity in SC but enhancers did affect PG solubility in SC. PG diffusion closely resembled that of CP, implying that the respective transport processes were inter-related. Additionally, a synergistic effect, which increases CP diffusivity and membrane solubility in SC, was found to occur between PG and water. Using 12-azidooleic acid (AOA) as an IR active probe for oleic acid, the simultaneous penetration of CP, AOA and PG into human stratum corneum was determined. It was found that the diffusion profiles for all three permeants were similar. This indicated that the diffusion of each species through SC was closely related and most likely occurred *via* the same route or SC microenvironment.

Iontophoresis is a physical means of transdermal penetration enhancement that induces an increased migration of ions or charged molecules through the skin when an electrical potential gradient is applied. This technique was applied in conjunction with chemical enhancement strategies, to assess the combined effect on macromolecular transport across SC. Transdermal enhancers modulated the passive and iontophoretic delivery of a model, anionic macromolecule (Dextran-cascade blue®, (D-CB) M_w=3kDa). While the separate application of enhancers and iontophoresis all improved macromolecular cutaneous delivery, the efficiency of a combined chemical and iontophoretic approach was dependent upon the relative charges of the permeant, enhancer and driving electrode. The greatest flux across SC occurred after pretreatment with a positively charged surfactant (dodecyltrimethylammonium bromide (DTAB)) followed by application of current.

Using two-photon excitation microscopy, real-time analysis provided visual verification of DTAB- and DTAB/iontophoretically-enhanced D-CB transport across human stratum corneum. While passive transport following DTAB pretreatment was characterised by significant intercellular D-CB distribution, the supplementary application of a current also resulted in intracellular uptake. The novel methodology employed offered distinct advantages over other conventional techniques.

Keywords: Attenuated total reflectance Fourier-transform infrared spectroscopy; transdermal penetration enhancement; iontophoresis; two-photon excitation microscopy; macromolecular delivery.

To my family and in loving memory of dad

ACKNOWLEDGEMENTS

I would like to express my appreciation to Professor Bill Irwin for his continual supervision, invaluable advice and encouragement and to Dr Aarti Naik for her guidance and suggestions.

I also extend special and most sincere thanks to Dr Joke Bouwstra from The Department of Pharmaceutical Technology at The Leiden/Amsterdam Centre for Drug Research in The Netherlands, for her vital collaboration, continual support and helpful discussions relating to iontophoresis and visualisation work.

I must also acknowledge the technical help I have received from Chris Bache at Aston and from Gert Gooris, Peter Roemelé (The LACDR) and Kees de Grauw (University of Utrecht). Thanks a lot chaps.

I am grateful to Aston University for the award of a research grant, The James Watt Memorial Foundation for awarding me a Prize Fellowship, The International Pharmacy Federation for the award of a Prize Travel Scholarship, The Nagai Foundation for a CRS Graduate Student award and the Netherlands Foundation for Pharmacological Sciences for a travel award.

I have met many wonderful people during the course of producing this thesis, most of whom, I am very fortunate to call my friends now. They have all added a great deal to my life. There are too many to mention but I would like to acknowledge the help of all my friends for being entertaining, offering companionship, help and advice and *always* being up for it.

Finally, my family have given me a great deal of comfort throughout this project and I would like to thank them for their tremendous support, encouragement and love. Thanks mum.

CONTENTS

LIST OF FIGURES

LIST OF TABLES

ABBREVIATIONS

a	absorptivity
b	path length of sample in cm
c	concentration of sample in g/l
A_{CP}	saturated plateau level for cyanophenol
AOA	12-azidooleic acid
ATR-FTIR	attenuated total reflectance Fourier-Transform infrared
AUFS	absorbance units full scale
C	concentration of permeant in membrane at time t
C_o	concentration of permeant in membrane layer $x = 0$
CB	Cascade blue®
CLSM	confocal laser-scanning microscopy
cm	centimetres
CP	cyanophenol
Da	daltons
d_p	depth of penetration
D-CB	dextran-Cascade blue®
DMSO	dimethyl sulphoxide
DMPS	dimethyl polysiloxane
DTAB	dodecyltrimethylammonium bromide
epi	epidermis
EL	epidermal lipids
EPL	effective pathlength
EtOH	ethanol
F	fluorescence
FL	fluorescein
FITC-PLLs	fluorescently-labelled poly-L-lysines
FM	fluorescence microscopy
FTIR	Fourier-Transform infrared
g	grammes
h	hours/membrane thickness
HPLC	high-performance liquid chromatography
IPM	isopropyl myristate

IR	infrared
IRE	infrared element
IS	internal standard
J_{SS}	steady-state flux
K	partition coefficient
kDa	kilo Daltons
kOhm	kilo Ohm
L	lag-time
logP	log partition coefficient
mg	milligrams
min	minutes
ml	millilitre
mm	millimetres
M_W	molecular weight
n	number of replicate runs
n_1	refractive index of crystal
n_2	refractive index of sample
NMP	N-methyl-2-pyrrolidone
NR	nile red
OA	oleic acid
OTG	n-octyl-β-D-thioglucoside
P	partition coefficient/radiant power transmitted by a sample
P_O	radiant power incident on a sample
PBS	phospate buffered saline
PG	propylene glycol
r	correlation coefficient
RI	refractive index
rpm	revolutions per minute
SC	stratum corneum
SDS	sodium dodecyl sulphate
SEC	size-exclusion chromatography
s.e.m.	standard error of the mean
Si-Me	silicone-methyl
SNA	sodium nonivamide acetate

t	time
T	ratio of radiant power transmitted by the sample to the radiant power incident on the sample
t-test	student's t-test for statistical significance
TDS	thiamine disulphide
TEWL	transepidermal water loss
TPE	Two-photon excitation
TPEM	Two-photon excitation microscopy
UV	ultra-violet
v/v	volume in volume
w/v	weight in volume
ε	molar absorptivity
θ_I	anlgle of radiation striking crystal
θ_c	critical angle
θ_R	angle of refraction
λ	wavelength
μl	microlitres
μm	micrometres
%	percentage
^oC	degrees centigrade
4-CP	4-cyanophenol

CHAPTER ONE

INTRODUCTION

General

There are various routes by which therapeutic entities can enter into the human body to treat illness. The most common is the oral route, but drugs are also administered successfully *via* the buccal and nasal epithelia, intraocularly and intravenously, through the rectum and into the lungs. Drug delivery using the skin as a portal for drug ingress, more precisely referred to as the transdermal route, can also be added to the above list.

Commonly, the success and general acceptance of *alternative* drug delivery systems is judged by comparisons with the oral route. On this basis, being able to administer drugs *via* skin represents a very advantageous strategy. From a pharmacokinetic standpoint, this route avoids first-pass metabolism in the liver or gastrointestinal tract and allows for a constant rate of drug release into the body. This avoids peaks and troughs in drug plasma profiles and thus eliminates the possibility of toxic or subtherapeutic drug plasma concentrations. Inter-patient variance in drug absorption can potentially be avoided since the rate of drug delivery can be inherently system-controlled. Further, treatment can be terminated rapidly by removal of the application. From the viewpoint of the clinician and patient, frequent dosing can be avoided to aid patient compliance.

However, the number of transdermal applications on the market today is still relatively small; at present only seven systemically active transdermally-delivered drugs are marketed in the United States (Guy, 1996). In practice, it is evident that only a small quantity of drug is capable of traversing the skin, inferring that these systems are most applicable for administration of highly potent medicaments. The difficulty in delivery is attributable, not surprisingly, to the nature of skin. This integument, although being a remarkably thin organ, has proved to be an excellent barrier to the ingress of medicaments and further, is prone to exhibit allergic or irritant responses to systems applied. Therefore, research efforts are primarily directed towards reversibly perturbing the excellent barrier properties of skin, which in theory should allow for the enhanced ingress of topically applied entities.

1.1 SKIN: FUNCTION AND STRUCTURE

Skin is one of the most readily accessible and heaviest organs of the human body, comprising one-twelfth of total body mass and receiving about one third of total circulating blood; its unique structure acts as a major interface between the body and its environment. Skin is remarkably tough (but only has a thickness of 1-3 mm (Odland, 1991) and is resistant to many chemical and physical agents, yet is quite viable and permits considerable freedom of movement. Furthermore, skin functions as a thermostat in maintaining body temperature, it plays a role in the regulation of blood pressure and it protects the human body against penetration of harmful ultraviolet rays.

The gross structural features of skin are shown in Figure 1.1. Human skin consists of two major compartments, the relatively thin outer compartment known as the epidermis and the thicker inner compartment known as the dermis. The epidermis and the dermis are separated by a basement membrane which contains genetically defined epidermal ridges and papillae which define a persons fingerprint. A fatty subcutaneous layer or the hypodermis resides beneath the dermis.

Figure 1.1 Gross structural features of human skin (De Bruijn and Den Breejen, 1995)

1.1.1 The dermis

The dermis is approximately 3mm thick which is divided into the subepidermal stratum papillaris (consisting of loose connective tissue, capillaries and sensory nerves) and the deeper, more massive denser stratum reticularis (consisting of bundles of collagenous and elastic fibres). It behaves as a connective tissue layer that supports the overlying epidermis. Its main constituent is the fibrous protein collagen (making up 77% of the fat-free dry weight of skin (Odland, 1991)) which is secreted by dermal fibroblasts. The constituents of the dermis determine its strength and extensibility, which varies with age. Blood vessels present in the dermis serve to remove compounds once absorbed through the epidermal surface thus creating 'sink' conditions. Underlying the dermis there is areolar tissue and varying amounts of fat.

1.1.2 Skin appendages

Various structures exist in the dermis called appendages, such as sensory (somatic) nerve endings, sweat glands and their ducts, hair roots, hair follicles and hairs, sebaceous glands and the arrectores pilorum (involuntary muscles attached to their hair follicles). The skin appendages represent a fractional area for drug absorption of about 0.1%, hence it is generally acknowledged that the passage of drugs *via* these appendages does not contribute significantly to the total drug flux (Grasso, 1971). However, the route may show potential for allowing ions and large polar molecules passage across the stratum corneum (Illel, 1997).

1.1.3 The epidermis

The epidermis (the most superficial layer of skin) is a stratified squamous epithelium which varies in thickness in different parts of the body (usually 75 - 150μm), being thickest on the palms of the hands and soles of feet (0.4 – 0.6mm). There are no blood vessels or nerve endings in the epidermis but its deepest layers are bathed in interstitial fluid, which is drained away as lymph. The epidermal expanse is made up of cells, which are in several stages of differentiation (Figure 1.2). The cells divide and migrate upwards from the basal membrane at the dermal-epidermal junction to the upper part of the skin where they desquamate. This process takes on average 15 to 30 days.

Figure 1.2 Epidermal cell differentiation (Montagna *et al.*, 1992)

Stratum basale or germinativum

This, the inner most layer of the epidermis is made up of proliferative columnar cells responsible for the continuing generation of all epidermal cells. Each cell contains a large nucleus, is approximately 6μm wide and arranged at right angles to the dermo-epidermal junction. Hemidesmosomes attach these cells to the basal membrane whilst desmosomes connect adjacent cells to each other including those making up the stratum spinosum.

Stratum Spinosum

This layer is also known as the Prickle cell layer by virtue of its morphology, characterised by prickles which form during histochemical changes in the basal layer; the result is flattened cells with shrunk nuclei which are interconnected by fine prickles. The prickles enclose an extension of the cytoplasm and adhere to the adjacent cell by intercellular bridges known as desmosomes. The desmosomes serve to maintain the integrity of the epidermis. Transport of nutrients and oxygen to cells is permitted by way of capillary spacings, which are filled with tissue fluid and exist between each desmosome. As cells move upward from this layer they become flattened and loose their cell organelles. This transition is accompanied by the development of membrane-bound granules (often referred to as lamellar bodies) in upper spinosum cells which are involved in the barrier formation at the stratum granulosum-stratum corneum junction.

Stratum Granulosum

This granular layer operates as an important transitional zone between the viable epidermal cells below and dead keratinised cells above. Cells making up this layer manufacture keratohyalin granules, which later develop into keratin.

Stratum Lucidum

Stratum lucidum (not visible in Figure 1.2) is only evident in palmar and plantar epidermis. It is translucent in nature and sits above the granular layer.

Stratum Corneum

The stratum corneum is the thin but compact outermost surface layer of the epidermis protecting against external assault and desiccation. It is made up of terminally differentiated, anucleated flat hexagonal shaped cells devoid of any cell organelles called corneocytes. Each corneocyte forms part of a continuous sheath of keratin-enriched cells embedded in an intercellular matrix enriched with non-polar lipids and organised in lamellar lipid bilayers (Fartasch, 1996). Depending on location, stratum corneum consists of approximately 15-25 cell layers, each cell being 0.5μm thick and 30-40μm wide. The entire layer is 10-20μm thick.

1.2 BARRIER PROPERTIES OF THE STRATUM CORNEUM

Stratum corneum functions as the major barrier to the percutaneous absorption of topically applied drugs and is the major barrier against water-loss from the epidermis (Blank, 1952). Several lines of experimental data support the concept that the stratum corneum is the major epidermal barrier (Scheuplein, 1978a; Spruit and Malten, 1965). Stripping away the stratum corneum by repeated application of cellophane adhesive tape greatly enhances transepidermal water loss (TEWL). Isolated stratum corneum is almost as impermeable as whole skin and dead skin used in *in vitro* experiments has permeability characteristics analogous to those of living skin; all indicate that viable epidermis is not essential to barrier function.

1.2.1 Morphology

Structural features of the stratum corneum important for barrier function include the following:

i) It is a compact layer of greatly compressed corneocytes

ii) Each cell has a thick membrane resistant to dilute acids and bases, to proteases and to many keratolytic agents

iii) Each cell contains a tough alpha-keratin filament representing about one-half of its mass.

1.2.2 Role of lipids

Stratum corneum structure is commonly referred to as being 'brick and mortar'-like in appearance; corneocytes being the bricks embedded in extracellular lipids which constitutes the mortar. These epidermal lipids (EL) are mainly composed of ceramides (50%), cholesterol (25%) free fatty acids (15%), cholesteryl sulphate (5%) and several minor constituents (Wertz and Van den Bergh, 1998). It is worth noting that phospholipids are not present in stratum corneum. The lipids originate from polar lipid precursors (phospholipids and glycosphingolipids) provided by the cells of the stratum granulosum (as mentioned above) *via* the exocytosis of lamellar disks; hydrolytic enzymes are also secreted along with these contents and could affect metabolism of topically applied drugs. After extrusion into the intercellular spaces of the stratum corneum, the disks fuse, and are transformed into broad multilamellar lipid sheets. At the same time, hydroxyceramide molecules covalently bind to corneocytes forming a unique lipid monolayer envelope.

These intracellular lipid bilayer sheets are responsible for the impermeable behaviour of the stratum corneum (Sweeny and Downing, 1970). The precise arrangement of lipids making up these intercellular bilayers is however currently an area of great debate; the presence of multiple intercellular lamellar structures first being determined by freeze-fracture electron microscopy (Breathnach *et al.*, 1973). More recently, the development of superior staining techniques, using ruthenium tetroxide as a post-fixative (Madison *et al.*, 1987) in transmission electron microscopic studies, have also revealed intercellular lamellae in stratum corneum. The lamellae in such studies appear as an electron-lucent pattern consisting of broad-narrow-broad electron-lucent bands. The broad bands on either side of the intercellular space represent the covalently bound lipid whilst the paired bilayers in the centre are thought to be formed by the edge-to-edge fusion of flattened lipid vesicles extruded from the lamellar granules (Landmann, 1986). The number of lipid bilayers within the intercellular spaces varies, but commonly consists of one or more broad-narrow-broad electron lucent band units (Swartzendruber *et al.*, 1995). It is thought that the dimensions of the broad and broad-narrow-broad units are approximately 5 and 13nm respectively (Bouwstra *et al.*, 1992b; Madison *et al.*, 1987).

Assigning specific barrier functionality to individual lipids is difficult but a number of theories have been proposed. The lipid bilayer stability, or more precisely its rigidity is likely to be attributed to a number of factors. It is thought that ceramide 1 acts as a molecular rivet since its alkyl chain is long enough to span a number of bilayers (Wertz and Van den Bergh, 1998). Furthermore, it is also feasible that the presence of other lipids having varying alkyl chain lengths causes interdigitation of lipid bilayers; the occurrence of both these factors serve to create rigid bilayers. Structurally, ceramides contain hydroxyl groups and have no *cis* double bonds in their structures. This means that adjacent lipid molecules are able to hydrogen-bond with each other and ceramides align closely in lipid bilayers, both points infer a close, tight association between adjacent lipids. However, Potts and Francoeur (Potts and Francoeur, 1991) have suggested that it may be more likely that the unique structural organisation of the SC lipids is more influential in barrier function than the chemical structure of the lipids. Further, at body temperature, stratum corneum lipids exist in a rigid gel phase.

1.2.3 Role of corneocytes

The corneocytes in the SC may also have an important part to play in permeant transport across the SC. Boddé and co-workers (Boddé *et al.*, 1989) investigated the diffusion of mercury (Hg) in combination with Azone® (penetration enhancer) in the stratum corneum using staining and transmission electron microscopy (TEM). They found mercury located intercellularly initially and then also incorporated into apical corneocytes. Finally, as time progressed mercury was also taken up by proximal corneocytes with an intercellular distribution in medial regions of the SC. This occurrence most likely highlights a difference in properties of the cells and/or membranes of the SC. Apical and medial corneocytes may take up hydrophilic drugs more readily than proximal cells, either because they provide more free binding sites for mercury (Bodde *et al* suggest sulphydril groups) or the cells are simply more permeable to mercury. However, the authors did not comment on the toxic effects of mercury in skin.

1.3 ROUTES OF PENETRATION

When a drug molecule is applied to the intact skin surface it first comes into contact with sebum, cellular debris, bacteria and other exogenous materials that coat the skin (Barry, 1983a). Assuming that the molecule is chemically unmodified by such substances, the intact molecule can traverse the skin either (i) through the transfollicular route *via* sweat ducts or through hair follicles with their associated sebaceous glands (A, appendageal), (ii) across the continuous stratum corneum (T, transcellular), or (iii) intercellularly (I).

Aston University

Illustration removed for copyright restrictions

Figure 1.3 Possible routes of transdermal penetration (Scheuplein, 1967)

1.3.1 Transappendageal route

Appendages create invaginations of the skin into which drug molecules can enter and bypass diffusion through the stratum corneum. They penetrate deep into the dermis, enabling drug molecules to rapidly diffuse into surrounding blood vessels. This process often referred to as the *shunt route* has the potential of being a faster penetration pathway for drugs when compared to inter- and intracellular routes because molecules encounter fewer membranes to traverse and avoid rigid lipid bilayers.

In practice, however, appendages constitute less than 0.1% of the total skin surface (Bronaugh *et al.*, 1982) and generally do not contribute significantly to gross flux. Appendageal flux is thought to contribute more in early stages of percutaneous absorption than later stages when transepidermal diffusion is most likely to dominate (Barry, 1983a).

It is thought that this route is important for transport of charged compounds especially when electrophoretically driven by an imposed electric field (Scott *et al.*, 1993).

1.3.2 Transcellular route

This route occurs when a permeant is transported across corneocytes and intercellular lipid bilayers making up the bulk stratum corneum. Geometrically, this route is the favoured direction (Scheuplein, 1967) but generally does not occur because from an energy viewpoint, (Praustnitz, 1997) it involves the crossing of approximately 100 intercellular bilayers which renders this pathway to be extremely slow. However, some studies have demonstrated that chemicals may be able to partition into skin corneocytes and penetration enhancers to interact with keratin causing conformational changes (Guy and Hadgraft, 1992).

1.3.3 Intercellular route

The number of bilayer crossings can be reduced if the topically applied permeant follows the more tortuous route exclusively within the intercellular lipids; drugs are transported along multilamellar bilayers rather than crossing them. This pathway is relevant to both lipophilic and hydrophilic permeants and is probably the major route of transport across the stratum corneum. It is thought that polar compounds may be able to progress across skin *via* polar lipid headgroups and water regions (in hydrated stratum corneum) whilst a nonpolar route is provided by the lipid hydrocarbon chains. Visualisation experiments have elegantly demonstrated the presence of penetrants in intercellular regions (Boddé *et al.*, 1989).

1.4 MATHEMATICAL INTERPRETATION OF DIFFUSION

The stratum corneum acts as a passive (but not inert) barrier to diffusion. Fick's diffusion laws can be used to describe passive diffusion across skin (Crank, 1975) and therefore assess its permeability. The classical description of the transport process is represented in Figure 1.4.

The stratum corneum is assumed to be a homogenous membrane (thickness h). D is the diffusion coefficient of the solute through the membrane. The concentration of solute (C) within the outermost layer of the membrane ($x = 0$) depends on the concentration within the vehicle (C_0) and the partition coefficient (K) between the membrane and the vehicle as given by equation 1.1:

$$C = KC_o \tag{1.1}$$

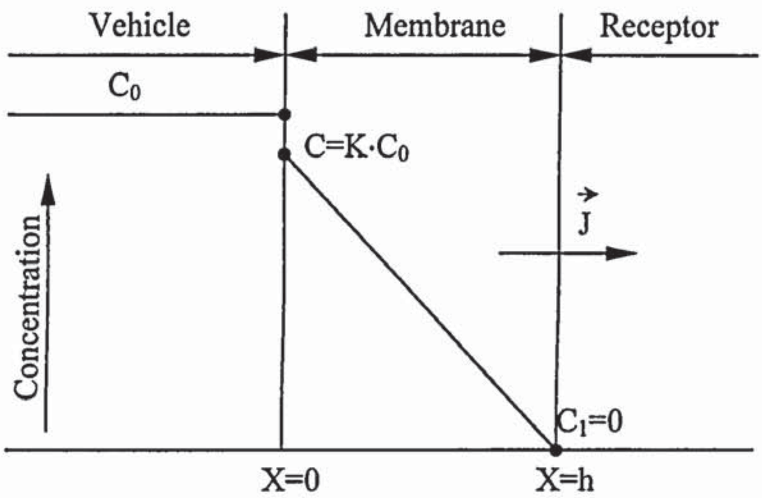

Figure 1.4 Concentration profile across homogenous membrane at steady-state (zero order flux)

Under sink conditions, solute concentration at any time (t), within the innermost membrane layer (x = h), is assumed to be negligible. The change in the cumulative amount of solute (Q) which passes through the membrane per unit area (A) as a function of time is called its flux and is given the following expression:

$$J = \frac{dQ}{Adt} \tag{1.2}$$

which is proportional to the concentration gradient

$$J = -D\frac{dc}{dx} \tag{1.3}$$

where D is the diffusion coefficient or diffusivity (cm^2/sec).

A typical profile of solute flux is illustrated graphically in Figure 1.5. The non-linear portion of the curve corresponds to non steady-state diffusion or the time taken for the amount of solute in the membrane to reach equilibrium. When a steady state is reached, the curve Q(t) is linear reflecting steady-state penetration (net balance in the rate of entry and exit of drug into and out of the membrane) and can be described by the equation below, where J_{ss} corresponds to the steady-state flux (slope of the straight line),

$$J_{ss} = KC_o \frac{D}{h} \tag{1.4}$$

If K, D, and h are combined into a single proportionality constant as below,

$$k_P = \frac{KD}{h} \tag{1.5}$$

where k_P represents the permeability coefficient, substitution into equation 1.4 gives,

$$J_{ss} = k_P C_o \tag{1.6}$$

provided that the donor concentration does not deplete and sink conditions apply throughout the experiment. The lag time (L), the intercept of the straight line on the time axis, is defined by the following equation (1.7) from which the diffusion coefficient can be estimated; in theory steady-state is attained after about 2.7 times the lag time (Barry, 1983a).

$$L = \frac{h^2}{6D} \tag{1.7}$$

The equations listed (1.1 to 1.7) may not always be applicable to Fickian diffusion as other factors can influence diffusion through the skin. For example, significant depletion of the drug in the formulation applied and drug-skin binding will reduce the rate of penetration. If a dilute solution of a solute is used, the vehicle may evaporate leading to an increase in solute concentration and driving force for diffusion as the application time proceeds. Further, certain vehicles such as ethanol and water can also enhance drug delivery.

An equation, shown below, that defines the entire absorption profile rather than the steady-state segment has been given by Scheuplein (Scheuplein, 1978b), provided diffusion is from an infinite dose. The penetration profile shown in Figure 1.5 is therefore more completely described by equation 1.8.

$$M = CK\left\{\frac{Dt}{h} - \frac{h}{6} - \frac{2h}{\pi^2}\sum_{n=1}^{\infty}\frac{(-1)^n}{n^2}\exp\left[\frac{-dn^2\pi^2t}{h^2}\right]\right\} \tag{1.8}$$

where M is the cumulative amount of drug in the receptor solution, C is the drug concentration in the donor cell, D is the diffusion coefficient of the drug through the skin, K is the skin-vehicle partition coefficient, h is the skin thickness and t is the time elapsed.

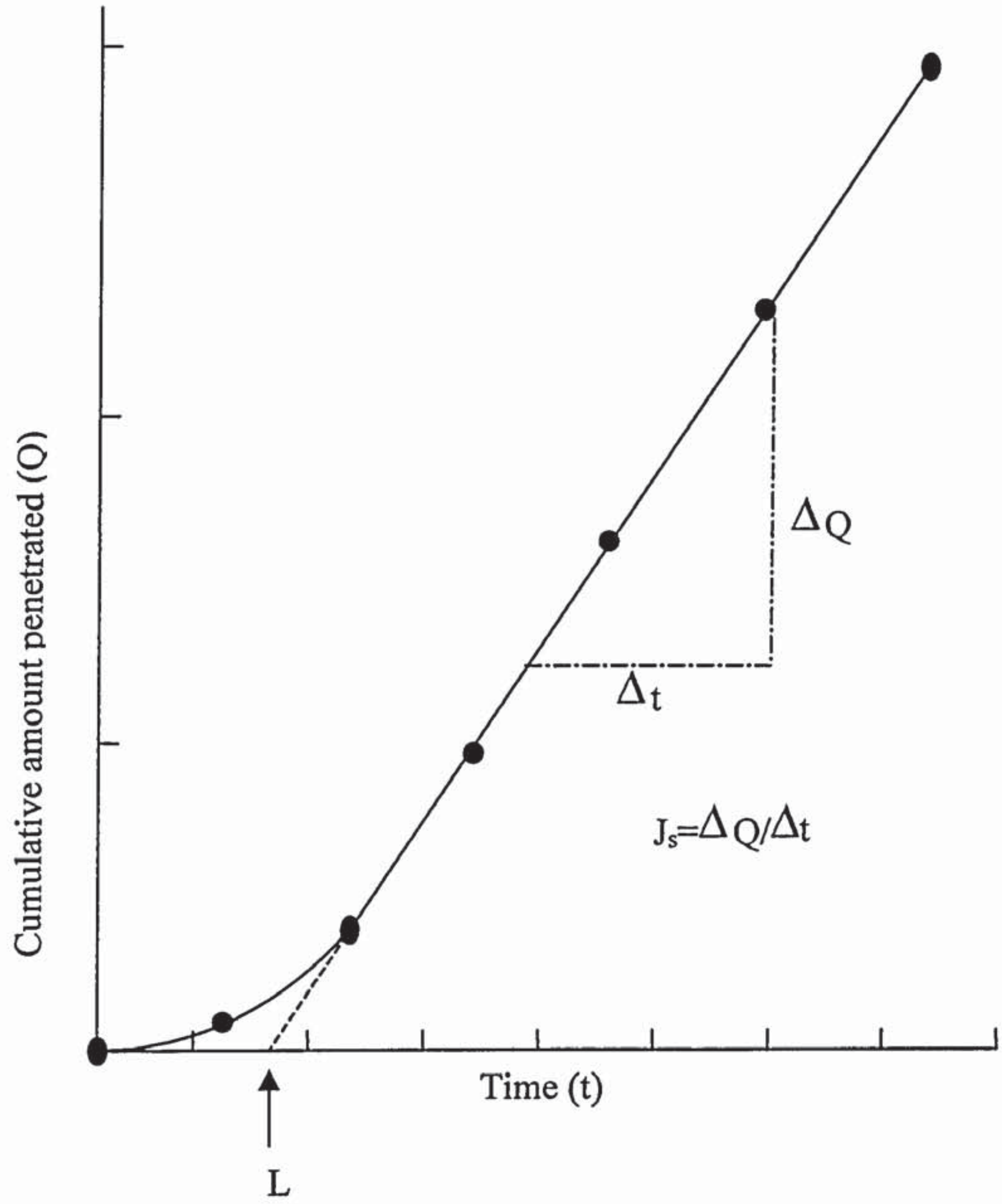

Figure 1.5 Typical profile of concentration versus time for diffusion through the stratum corneum (L = lag time)

1.5 FACTORS AFFECTING PASSIVE DIFFUSION

Passive diffusion of a drug through skin can be affected by the physicochemical properties of the drug, the formulation in which it is applied and the physiological conditions of the skin. During percutaneous absorption, a drug must firstly diffuse out of the formulation, partition into and diffuse across the stratum corneum, pass through the upper part of the papillary dermis and finally be taken up by the systemic circulation (Figure 1.6). Each of these steps can influence the gross amount of drug absorbed.

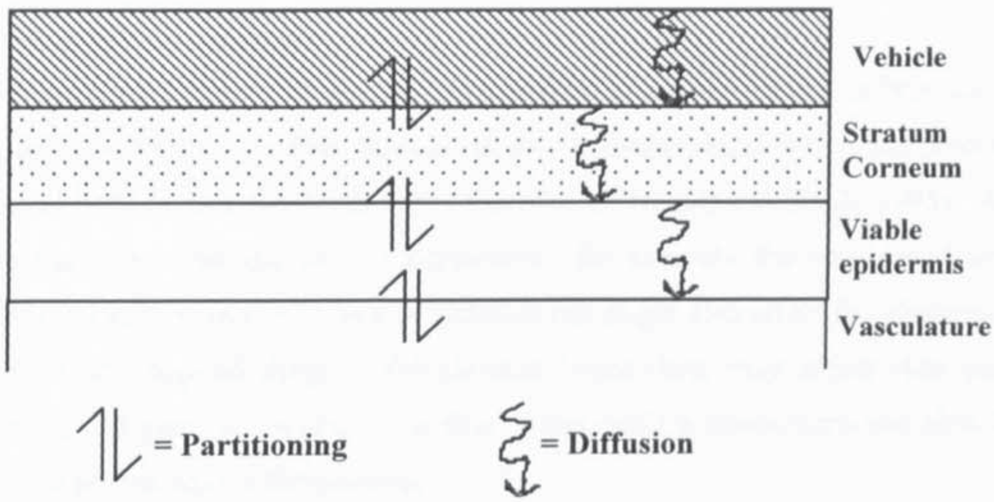

Figure 1.6 The steps involved in the transport of drugs across skin

1.5.1 Physicochemical Factors

Properties of the drug

Generally, an inverse relationship exists between permeant molecular weight and passive percutaneous flux or absorption. A penetrant must be able to partition into both lipid and polar regions of the stratum corneum. Therefore, its partition coefficient (octanol/water) needs to reflect this property; a value approaching 100 (logP = 2) has been correlated with optimal permeability (Hadgraft and Walters, 1995). Likewise a drug needs to dissolve well in stratum corneum lipids and hence those with low melting points make better candidates for transdermal delivery. It follows also that polar or ionised drugs are poor penetrants of the stratum corneum under passive conditions; for drugs containing too many polar substituents, transdermal delivery may not be the best option.

Drug concentration

Increasing the concentration of drug applied increases the escaping tendency of permeant molecules or their thermodynamic activity and enhances percutaneous absorption, with flux becoming optimised from a saturated formulation. Supersaturated solutions may further increase flux but are often less stable (Hadgraft and Walters, 1995).

Skin-drug-vehicle interaction

The interaction between drug-skin, vehicle-skin, and drug-vehicle influences the rate of drug penetration through skin. Substances may interact with skin to either produce a strong chemical bond or van der Waals type of attractions (Singh and Singh, 1993). A drug-skin interaction may alter the rate of penetration, for example the vasoconstrictor effect of steroids not only slows their own penetration but might also affect the absorption of other concomitantly applied drugs. Vehicle-skin interactions may affect skin permeability, hydration and permeant solubility in skin. Drug-vehicle interactions can slow the rate of permeant release from a formulation.

1.5.2 Biological Factors

The age, site, and degree of skin hydration can all affect the extent of percutaneous absorption. Increases in skin water content (Roberts and Walker, 1993) has been shown to increase the diffusion coefficients of a series of phenols. Absorption of topical steroids occurs more readily in children than adults (Singh and Singh, 1993) due to the greater water content of infant skin. Roberts *et al* (Roberts *et al.*, 1982) have shown that skin permeability of methyl salicylates *in vivo* from different sites of the human body was in the rank order: abdomen>forearm>instep>heel>plantar. Further, relative *in vitro* skin permeability rankings have been reported which generally suggest that skins of laboratory animals such as guinea pig, rat and rabbit are more permeable than human skin (Barry, 1983b). Skin from the pig and monkey are the closest models to human skin. Finally, skin may also affect percutaneous absorption by metabolising a drug due to the presence of catabolic enzymes and thus affecting its topical bioavailability. It is known that skin contains proteases such as endopeptidases which are capable of splitting bonds inside peptide chains making up proteins (Steinstrasser and Merkle, 1995). Therefore, it is important to know about any significant enzyme activity causing a loss of drug (e.g protein drug) due to metabolism.

1.6 PERCUTANEOUS ABSORPTION ENHANCEMENT

Since the stratum corneum provides such a great obstacle to the ingress of topically applied molecules, it is often the case that scientists wish to perturb its barrier properties in order to optimise drug delivery. It could be that the drug applied is not very potent and therefore to achieve therapeutic blood levels, a higher amount must diffuse across the stratum corneum and into the dermis or, alternatively, the drug may be very expensive, making it uneconomical for high amounts to be incorporated into a transdermal system.

In order to optimise drug delivery, strategies can be employed to enhance transdermal drug penetration. These are usually grouped as subclasses under the two broad headings of (a) Chemical and (b) Physical enhancement.

1.7 CHEMICAL TRANSDERMAL PENETRATION ENHANCEMENT

Chemical enhancement usually involves the application of exogenous chemicals to skin that perturbs its structure in such a way that results in an increase in drug flux across the membrane. If enhancement is achieved *via* this mechanism, the chemical is referred to as a *transdermal enhancer.* An ideal enhancer should be pharmacologically and chemically inert, have reversible effects on the skin, be compatible with other excipients in a formulation and be non-irritant and cosmetically soluble acceptable. Most often, such enhancers are firstly dissolved in solvents (e.g. propylene glycol) and then applied to skin.

During the last fifty years or so, a number of classes of compounds have been identified (Santus and Baker, 1993) which have been shown to exhibit enhancing activity. Accordingly, in the medical literature available there are a number of reviews and texts which report on such chemicals (Hadgraft and Walters, 1995; Smith and Maibach, 1995; Walters and Hadgraft, 1993). The most commonly investigated enhancers or groups are Azone®, oleic acid, dimethyl sulphoxide, surfactants, terpenes and the simplest of them all water. A more recent innovation is the topical application of epidermal enzymes which behave as penetration enhancers (Patil *et al.*, 1996). Such enzymes are thought to breakdown epidermal phospholipids and thus altering the production of non-polar lipids which contribute to the barrier function of the stratum corneum. Figure 1.7 shows the structures of commonly used enhancers.

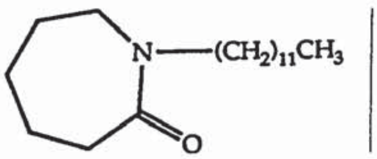

1-Dodecylazacycloheptan-1-one (Azone®)

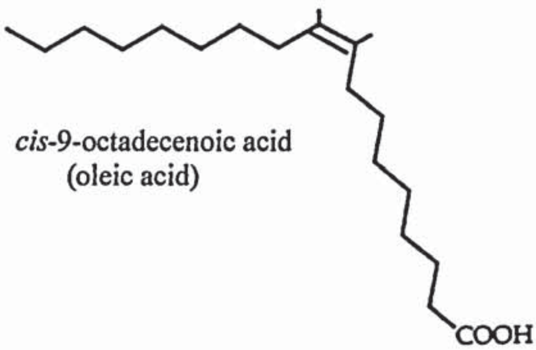

cis-9-octadecenoic acid
(oleic acid)

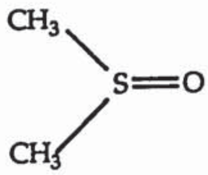

Dimethyl sulphoxide (DMSO)

Figure 1.7 Some common transdermal penetration enhancers

Most of the research concentrates on, after realising enhancer activity, defining the mechanism of action of enhancers. Since enhancer structure is quite diverse amongst the above groups it is unlikely that one single mechanism is responsible for the enhancer activity observed, rather a number of different processes are more likely to be involved. For the purposes of brevity, research relating only to the enhancers that will be used in these studies will be reviewed here.

1.7.1 Azone®

Azone® (1-Dodecylazacycloheptan-1-one) was developed specifically to enhance transport of topically applied compounds. It has been shown to be very effective in increasing absorption of both hydrophilic and hydrophobic drugs (Hadgraft *et al.*, 1993; Wiechers, 1989). It is extremely lipophilic ($\log P_{octanol/water} = 6.0$), is compatible with most solvents and seems to be most effective at low concentrations, usually between 1 and 10% v/v.

Its mode of action is thought primarily to be one of perturbing the structured intercellular lipid bilayers present in stratum corneum resulting in an increase in the fluidity of these hydrophobic regions and thus leading to a decrease in the diffusional resistance of the skin. Hadgraft *et al* (Hadgraft *et al.*, 1993) have shown that the addition of increasing concentrations of Azone® to dipalmitoyl phosphatidylcholine (DPPC) liposomes lowered their phase-transition temperature indicating that Azone® has the capacity to interact with structured lipids. Further work (Hadgraft and Walters, 1995; Michniak *et al.*, 1995) employing Langmuir trough and neutron scattering studies showed Azone® to possess favourable molecular dimensions, enabling it to insert itself into lipid bilayer structures and push apart ceramide head groups. This creates free volume in the alkyl chain region with an associated increase in lipid structural disorder. Some studies have likened the shape of Azone® to a "soup spoon" (Brain and Walters, 1993; Hoogstraate *et al.*, 1991; Lewis and Hadgraft, 1990). Such work suggests that Azone® in the presence of lipid bilayers alters its conformation. It is suggested that the polar carbonyl moiety of the amide present in Azone® distances itself from non-polar lipid alkyl chains; the carbonyl group being the strongest hydrogen bond forming functionality present, enables Azone® to turn and insert into polar regions of membrane lipids. This requires a "twist" in the ring pushing it upwards so as to create a "soup-spoon" conformation.

A number of studies have reported that an alkyl side-chain of at least 12 carbon atoms is a prerequisite for optimal enhancement activity (Hoogstraate *et al.*, 1991; Michniak *et al.*, 1998). It is possible that such a side-chain length is necessary to provide a difference in polarity between the head group in Azone® and its alkyl side-chain to obtain the "soup-spoon" conformation and subsequent lipid perturbation. The C_{12} side-chain of Azone® corresponds to the dimensions of the stratum corneum cholesterol skeleton, leading to the possible disruption of ceramide-cholesterol or cholesterol-cholesterol interactions. Many studies have been performed which have altered the structure of Azone® with an aim to optimise activity. For example, it has been shown that a cyclic structure was not an absolute requirement for enhancer activity (Michniak *et al.*, 1995).

1.7.2 Fatty acids and oleic acid

Fatty acids when applied to skin can enhance solute transport across it, and in some instances, to greater extents when compared to other transdermal enhancers (Aungst *et al.*, 1986; Goodman and Barry, 1989). The degree of enhancement is drug dependent, but fatty acids can promote the diffusion of both lipophilic and hydrophilic compounds across skin. Structurally, fatty acids consist of an aliphatic hydrocarbon chain and a terminal carboxyl group. Structures within in this group differ due to differences in chain length, in the number and the position of double bonds in the molecule and whether the chains are branched and/or contain other substituents. Aungst *et al* (Aungst *et al.*, 1986) have demonstrated how altering fatty acid structure affects the degree of enhancement. Using Naloxone they showed that a parabolic relationship existed between flux and saturated alkyl chain length, with C_{12} being the most effective. They also found that increasing the number of *cis* double bonds in the C_{18} chain resulted in an increasing flux, but this was lower than that seen with the saturated C_{12} chain. It may be, since the C_{12} alkyl-chain length corresponds to the length of the steroid nucleus of cholesterol, that fatty acids are able to disrupt ceramide-cholesterol or cholesterol-cholesterol interactions. Therefore, short-chain fatty acids seem to affect the structure and barrier properties of the skin less than medium-chain fatty acids.

In particular, most research has concentrated on the effects of oleic acid (OA), an eighteen-carbon molecule having a *cis* double bond between carbons 9 and 10. Oleic acid (*cis* –9-octadecenoic acid) has been shown in many studies to be an effective transdermal enhancer, promoting permeation of a variety of drugs such as 5-fluorouracil (Yamane *et al.*, 1995) piroxicam (Francoeur *et al.*, 1990) and propranolol (Ogiso and Shintani, 1990), whereas stearic acid, the corresponding saturated molecule does not have any enhancing activity. Golden *et al* (Golden *et al.*, 1987), using porcine stratum corneum, have further shown that *cis* isomers of oleic acid, where a single double-bond was positioned at C_9 or C_{11} were more effective enhancers than the corresponding *trans* isomers.

The mode of action of oleic acid has been an area of great interest. A number of biophysical techniques have been utilised to determine its possible mechanism of action. To assess whether oleic acid was able to increase disorder of intercellular bilayers, investigators have used differential scanning calorimetry (DSC) (Golden *et al.*, 1987) and infrared analysis (Golden *et al.*, 1986; Knutson *et al.*, 1987) to show that oleic acid-treated skin caused both an increase in fluidity of membrane lipids and alterations in the freedom and motion of the intercellular lipid hydrocarbon chains. These effects were similar in nature to that observed upon heating. Increases in fluidity were then correlated with changes in permeability to salicylic acid. This, therefore, seems to suggest that oleic acid enhances permeant diffusivity by disordering lipid domains.

It is thought that the *cis* double-bond present in oleic acid causes a kink in its structure (Golden *et al.*, 1987). As a result, it has been suggested that this has the effect of disordering tightly packed lipid bilayers and allowing enhancer molecules to position themselves in intercellular regions. This theory is backed up by the fact that the complementary saturated C_{18} stearic acid has a much less effect on flux enhancement.

Reports have also have suggested that oleic acid does not homogenously distribute itself amongst lipids but is present as a separate phase. It is implied that oleic acid exists as pools of fluid within the stratum corneum resulting in areas of enhanced permeant diffusivity (Ongpipattanakul *et al.*, 1991; Walker and Hadgraft, 1991). However, it also is apparent that oleic acid may be able to extract lipids (Takeuchi *et al.*, 1993) following pretreatment of rat skin. The authors of this IR spectroscopic based report claim that this would create a void volume to allow the permeation of solutes or solvents.

1.7.3 Surfactants

Most pharmaceutical formulated products such as cosmetics contain surfactants. Surfactants are characterised by the presence of both polar and non-polar regions in their structures. They are classified according to the charge carried by the hydrophilic region, thus they can be either anionic (e.g. sodium dodecyl sulphate (SDS)), cationic (e.g. dodecyl trimethyl ammonium bromide (DTAB)) or non-ionic (e.g. polyoxyethylene sorbitan monopalmitate). All three classes of surfactant have demonstrated percutaneous enhancement activity (Walters, 1989) to varying degrees. Generally, cationic surfactants are thought to be more irritating than anionic ones, with non-ionic surfactants exhibiting the least irritancy towards the skin. The ability of these surfactants to alter skin permeability generally also follows in a similar manner.

The precise mode of action of these chemicals is still an area of debate. It has been shown that non-ionic surfactants penetrate into skin faster than ionic types because they do not possess a charge, but enhance skin permeability to a lesser degree than charged surfactants (Ashton *et al.*, 1992a). Anionic surfactants have been shown to interact with and bind to epidermal proteins. This has lead to the hypothesis that surfactant alkyl chains interact with the protein substrate leaving the negative end-group exposed and thus creating additional anionic sites in the membrane. This would lead to the development of repulsive forces that separate the protein matrix, uncoiling keratin filaments and exposing more water-binding sites. The end effect would be an increase in hydration and skin permeability. Cationic surfactants have been reported to extract lipids and penetrate into the intercellular lipid matrix of the cornified layer of stratum corneum (Kushla and Zatz, 1991). Both mechanisms would result in the impairment of cutaneous barrier function. Non-ionic surfactants have a limited effect on enhancing skin permeability. A series of polysorbates has been tested by Cappel and Kreuter (Cappel and Kreuter, 1991). Data from this study demonstrated that polysorbates had a limited impact on the transdermal penetration of methanol (maximum flux enhancement being about 2-3 fold). However, the study did show that the more lipophilic polysorbates altered the skin barrier properties to a greater extent than the hydrophilic analogues.

1.7.4 Dimethylsulphoxide (DMSO)

Dimethylsulphoxide was one of the earliest compounds identified to behave as an enhancer of percutaneous absorption. It is thought to increase permeant diffusivity across stratum corneum by either denaturing intercellular proteins, promoting lipid fluidity and/or extracting stratum corneum components (lipids and proteins) (Walker and Smith, 1996). An alternative view is expressed by Barry (Barry, 1991) who postulates that DMSO applied in high concentrations creates solvent-filled spaces with greater solubility for drugs than untreated stratum corneum.

1.7.5 Solvents

Most often, penetration enhancers are dissolved in suitable solvents and then applied to skin. Therefore, the possibility exists that co-administered solvents may have an inhibitory or additive effect on solute permeation. Commonly, the solvents used are either ethanol or propylene glycol (PG). It is thought that these chemicals are able to penetrate into stratum corneum and increase its solubility parameter. Since non-polar enhancers such as Azone® are generally thought to enhance permeant diffusivity by perturbing membrane intercellular bilayers, clearly there is potential for a synergistic or additive effect that may elevate permeant flux when such two component systems are applied to skin. These types of mixtures have worked particularly well for lipophilic permeants such as steroids (Berner and Liu, 1995). A number of studies have reported a synergistic effect on permeant enhancement resulting from the co-application of different enhancers in propylene glycol (Bendas *et al.*, 1995). The precise mechanism of action of PG is still unclear though. It has been suggested that PG is capable of altering both intercellular lipid and corneocyte structures (Barry, 1987; Barry, 1991), enhances permeant membrane solubility (Barry, 1987) and that both constituents (enhancer and solvent) mutually enhance each others penetration across skin (Mollgaard, 1993).

1.8 PHYSICAL - IONTOPHORETIC PENETRATION ENHANCEMENT

A number of technologies have been employed to physically enhance the transdermal penetration of topically applied compounds. Such methods include phonophoresis (Kost, 1998), the application of low or high frequency ultrasound to drive molecules across skin, electroporation (Prausnitz, 1998), the application of transient high-voltage electrical pulses to cause rapid permeabilisation of the stratum corneum and iontophoresis. It is this last mode of delivery that will be investigated in this thesis.

1.8.1 Definition

Iontophoresis is a process that induces an increased migration of ions or charged molecules through the skin when an electrical potential gradient is applied. The idea of applying an electric current to enhance the penetration of a charged compound into a tissue probably was originated by Veratti in 1747 (Riviere and Heit, 1997), with the first documented experiments appearing in the literature at the beginning of the 20th century by LeDuc in which a positively charged ion, strychnine sulphate, caused tetanic convulsions in a rabbit when placed at the positive electrode but had no effect from the negative electrode (LeDuc, 1900).

1.8.2 Theory

In essence, during iontophoresis, charged molecules, dissolved in a suitable electrolyte solution (donor), are brought into contact with a "driver" electrode of similar polarity and skin. The circuit is completed by connecting this electrode to one of opposite charge which is likewise placed in an electrolyte solution also in contact with skin. When an electromotive force is applied, electro-repulsion occurs at the driving electrode surface, serving to propel the drug into the adjacent skin (Figure 1.8). Therefore, positively and negatively charged molecules are delivered from anodal and cathodal chambers respectively.

The flux resulting from iontophoretic delivery is made up of three components as defined by the Nernst-Planck equation (see equation 1.9). Total flux of an ionic solute across a membrane is made up of passive diffusion resulting from the solute concentration gradient, electrically facilitated diffusion due to the presence of a potential difference which serves to drive charged species across the membrane by electrorepulsion and solute transport due to convective flux or electroosmosis. Electroosmosis occurs because skin carries a net negative charge at physiological pH (Riviere and Heit, 1997). This permselective property encourages the net transport of cations or counterions into skin which collide with the surrounding solvent molecules and thus transfer some of their own momentum.

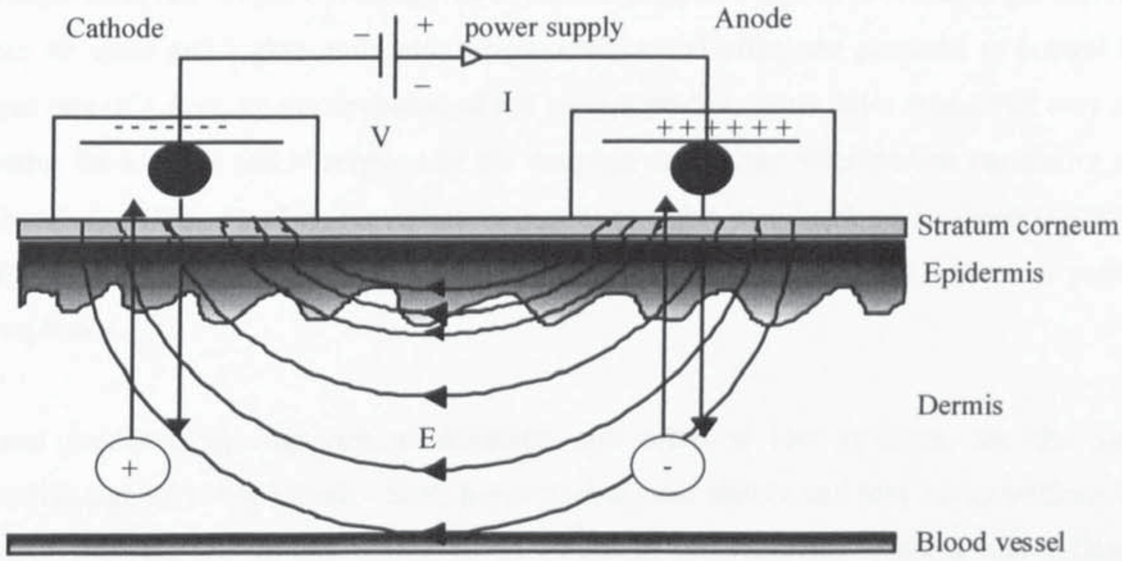

Figure 1.8 Schematic diagram of iontophoretic process

This results in an electro-osmotic flow of water across the skin in the anode-to-cathode direction which is capable of transporting with it uncharged solutes dissolved in the solvent. Hence, electro-osmotic flow allows the delivery of neutral compounds and aids the delivery of cationic solutes.

$$J_i = -D_i \frac{\partial C_i}{\partial x} - D_i \frac{C_i z_i F}{RT} \frac{\partial E}{\partial x} \pm C_i J_v \qquad (1.9)$$

J_i = Flux of ionic solute

$\frac{\partial C_i}{\partial x}$ = solute concentration gradient

$\frac{\partial E}{\partial x}$ = electrical potential difference

D_i = diffusion coefficient of solute

z_i = solute charge

C_i = concentration of solute

J_V = velocity of convective flow

F = Faraday constant

R = Gas constant

T = absolute temperature

1.8.3 Advantages and Limitations

Iontophoresis has several advantages over passive drug delivery. It provides larger delivery rates for ionic and higher-molecular-weight entities and offers the potential to control the input rate of a drug by manipulation of the current profile. This latter aspect not only can control the kinetics and absorption of the drug but can reduce inter-patient variability and side-effects. The use of an iontophoretic patch may also avoid risk of localised infection, inflammation and fibrosis associated with injection and infusion and improves patient compliance.

Burns produced by high-current densities, and often at low voltages, are the main disadvantage of iontophoresis. Such burns tend to heal slowly and may occur without the patient knowing (Singh and Singh, 1993). Further, iontophoresis is not a very efficient method of drug delivery. This is because only a fraction of the total available current is carried by the desirable solute, the bulk of the charge is shared between the more mobile electrolyte ions present in the iontophoretic delivery system. It has been suggested also that iontophoretic delivery of substances such as penicillins, which have a greater risk of causing allergic reaction when applied to the skin, should not be delivered iontophoretically (Theiβ and Lucker, 1991). From a commercial viewpoint, the cost of iontophoretic systems is also a factor in their long-term availability.

1.8.4 Factors affecting Iontophoresis

Physicochemical

Iontophoretic delivery depends on a number of physicochemical variables that both are similar to those encountered during passive delivery across the skin and specific to electrical modes of delivery. The latter factors will be detailed below.

Current Density

The transport number of a given ion, t_i, is defined as the proportion of total current carried by a particular ion, and may be expressed in following manner:

$$t_i = \frac{I_i}{I_T} = \frac{J_i z_i F}{I_T} \tag{1.10}$$

where

I_i = current carried by ion itself

I_T = total current density

J_i = steady - state molar flux of ion

z_i = charge on the ion

F = Faraday constant

During iontophoresis, the current density is the driving force determining the extent of iontophoretic delivery, whereas, during passive diffusion, the driving force is the solute concentration. Therefore, and according to the Nernst-Planck equation, steady-state flux is proportional to current density. A linear relationship has been observed between the flux of a number of compounds such as apomorphine (Van der Geest *et al.*, 1997), azidothymidine (AZT)(Oh *et al.*, 1998) and sodium nonivamide acetate (Fang *et al.*, 1996) and the applied current density. These studies used current densities ranging from 0mA/cm^2 to 1.0mA/cm^2.

To avoid electrically induced skin damage, it is generally thought, the maximum strength of current that can be safely used is $0.5mA/cm^2$.

Vehicle pH and ion competition

The optimum pH for iontophoretic delivery is where the compound exists predominantly in ionised form. This was reported by Siddiqui *et al* (Siddiqui *et al.*, 1985) who showed that iontophoretic transport of lidocaine through human stratum corneum was greatest at the pH where lidocaine exists mainly in the ionised form in an aqueous vehicle. The pH changes are particularly important for protein and peptide drugs, since the pH of the solution affects the charge carried by these molecules according to the Henderson-Hasselbalch equation. One also must bear in mind that hydrogen and hydroxyl ions in the donor solution will compete to carry ionic current thereby reducing flux and therefore it is beneficial to reduce the presence of these and other mobile ions. On the other hand, buffering moieties must be incorporated into formulations to control electrochemically induced pH changes at the electrodes. Increasing donor ionic strength from 0.06 to 0.60M resulted in an approximate eight-fold decrease in the transport of sodium nonivamide acetate (SNA) at pH 4.2 (Fang *et al.*, 1996). This was due to the competition of drug ions and buffers ions for the applied current; most current being carried by buffer ions with higher mobilities and only a small fraction of applied current was carried by SNA ions.

Concentration

Steady-state iontophoretic flux (J_{ss}) has been reported to be proportional to donor concentration for a number of compounds (Behl *et al.*, 1989; Van der Geest *et al.*, 1997). Interestingly, in some studies which delivered positively charged lipophilic peptides, J_{ss} was shown to reach a plateau with increasing donor concentrations (Delgado-Charro and Guy, 1994). This effect was shown to be a result of the higher donor concentrations changing the magnitude of electro-osmotic flow and thus self inhibiting their flux.

Molecular size

Green *et al* (Green *et al.*, 1993) have suggested that since iontophoretic transport follows a porous pathway that enhancement will be size-dependent; as size increases the flux will diminish. This has been shown to be true for a series of positively charged, negatively charged and uncharged solutes (Yoshida and Roberts, 1993).

Convective or electroosmotic transport

Electroosmosis as defined previously, is the bulk fluid flow which occurs when a voltage difference is imposed across a charged membrane. The direction of such a flow is in the same direction as counterions and this may assist or hinder drug transport. At pH 4.0 both human and mouse skins are negatively charged. Therefore, counterion (being positive in this case) and electroosmotic transport is in the anode-to-cathode direction. Thus anodic delivery is assisted by electroosmosis whilst cathodal delivery is retarded. Further, it has been suggested (Pikal, 1992) that electroosmotic flow increases as the size of the drug ion increases.

Continuous *vs* pulsed current

Skin polarisation can be caused by the use of continuous direct current which may result in a reduction of the efficiency of iontophoretic delivery that is proportional to the duration of direct current applied (Singh and Maibach, 1996). This polarisation can be avoided by using a periodically pulsed direct current which allows the skin to depolarise and recover to its near initial pre-current condition. Transdermal iontophoresis of vasopressin in rabbits has been facilitated two-fold using pulse current as compared to simple direct current using the same current density and for the same duration of application (Chien *et al.*, 1990).

1.9 THE AIMS OF THIS THESIS

The underlying theme of this thesis is one of examining the processes and effects involved in the enhancement of percutaneous absorption. Of particular interest was the effect that co-administered constituents, found in topical formulations, had on each others diffusion in membranes. Therefore, a primary aim of this thesis was to develop an analytical technique that could be employed to assess the interplay between co-diffusing permeants, typically drug, enhancer and vehicle. Such a method should ideally allow for the distinct and simultaneous production of permeant diffusion profiles from which relative permeant diffusional parameters may determined.

A further objective of this thesis concerned improving macromolecular delivery across human skin. As outlined in the introduction, iontophoresis is a physical method of enhancing transdermal delivery. Consequently, the aim was to employ an iontophoretic method alone and in conjunction with chemical enhancers to determine the joint effects (if any) on the percutaneous transport of a model charged macromolecule. To shed further light on transport pathways that occurred during penetration enhancement, it was intended that macromolecular transport route(s) in human epidermis during iontophoresis should be visualised following pretreatment with transdermal enhancers.

CHAPTER TWO

SET UP OF ATR-FTIR SPECTROSCOPY METHOD

2.1 INTRODUCTION

This chapter begins by explaining the basis of Fourier-Transform Infrared spectroscopy (FTIR) and the associated modified reflectance technique known as Attenuated Total Reflectance Fourier-Transform Infrared Spectroscopy (ATR-FTIR). It continues by describing the instrumentation used to collect ATR-FTIR spectra and the criteria necessary for its successful employment in the analysis of percutaneous absorption. Possible candidates to act as model permeants to monitor diffusion across stratum corneum are examined. Further, the employment of a synthetic silicone membrane is also validated and diffusion across it analysed and fitted to a diffusion model.

2.2 BASIS OF INFRARED SPECTROSCOPY

All organic substances contain energy (except at absolute zero temperature) causing bonds to stretch and bend and atoms to wag and rock. These vibrations are quantized or discrete and therefore a molecule can only stretch for example at certain frequencies corresponding to certain energy levels.

When mid infrared light having a frequency between 400-4000 cm^{-1} (25-2.5μm) is passed through a sample of an organic compound, some of the frequencies are absorbed, while others are transmitted through the sample without being absorbed. The wavelengths absorbed correspond to those quantized stretching or bending energy levels in the molecule. If one plots absorbance against frequency (or wavelength), the result is an infrared spectrum showing peaks corresponding to absorption bands. Absorption bands correspond to specific molecular motions due to changes in dipole moment between atoms, which are used to interpret the arrangement of atoms or functional groups within a compound. Such information is invaluable in the identification of unknown compounds. Absorption bands of a molecule can also be affected by the environment the molecule finds itself in. Molecular vibrations can differ if the molecule under investigation is in a liquid, if it is adsorbed onto a surface or indeed in the process of diffusing through a membrane such as stratum corneum. Therefore, information relating to the effect a molecule has on its immediate environment and vice versa can also be yielded by this technique.

2.2.1 Molar absorptivity

The absorption bands making up the spectrum of a molecule vary in their intensity. This is dependent on the various bond strengths constituting the molecule. Polar bonds are associated with strong IR absorption while symmetrical bonds may not absorb at all (Sternhell and Kalman, 1986). The bond strength is proportional to the absorbance of that bond at a specific wavelength. Shorter and stronger bonds will have their stretching vibrations at the higher energy end (shorter wavelength) of the IR spectrum than the longer and weaker bonds. Infrared absorptions can be quantified by applying the Beer-Lambert-Bouguer law (commonly abbreviated to Beer's law) (Kendall, 1966). If P_0 represents the radiant power incident on a sample and P the radiant power transmitted by that sample, then

$$P = P_0 10^{-abc} \qquad (2.1)$$

where a = the absorptivity, the inherent sample absorbing power of radiation at a specific frequency, ν

b = the path length of the sample in cm

c = concentration of the sample in g/l

then

$$\frac{P}{P_o} = 10^{-abc} \qquad (2.2)$$

Now $\frac{P}{P_o}$ = the transmittance, T, the ratio of radiant power transmitted by the sample to the radiant power incident on the sample. Equation (2.2) is cumbersome for calculations and can be transformed by taking the logarithm to the base 10 of both sides of the equation. The result is

thus

$$T = 10^{-abc} \qquad (2.3)$$

and

$$\log_{10} T = \log_{10} 10^{-abc} = -abc \qquad (2.4)$$

$$\text{Log}_{10} \frac{1}{T} = abc \qquad (2.5)$$

Now $\log_{10}\frac{1}{T}$ or $-\log T$ is defined as absorbance, A, the $\log_{10}$ of the reciprocal of the transmittance.

Thus

$$\text{Absorbance} = \log_{10} \frac{1}{T} = abc \qquad (2.6)$$

If concentration is expressed in molar concentration and b is in centimeters, the proportionality constant, a, is called the molar absorptivity (having units litre $mole^{-1}$ cm^{-1}) and is designated as ε,

hence $$\varepsilon = \frac{\text{absorbance}}{bc} \qquad (2.7)$$

2.2.2 Instrumentation

There are two basic types of infrared spectrophotometer, characterised by the manner in which the infrared frequencies are handled. The dispersion or grating type have the beam separated into its individual frequencies by dispersion using a rotating grating monochromator (Kemp, 1991). In the second type, known as an interferometric instrument, the infrared frequencies are allowed to interact to produce an interference pattern which is then analysed mathematically, using Fourier-Transforms to determine the individual frequencies and their intensities (Banwell, 1983; Horlick, 1968; Markovich and Pidgeon, 1991). Both types of instrument require in addition, a suitable source of infrared light from which a beam can be directed into the sample and a detector to measure light intensity emerging from the specimen. Dispersive instruments have been widely used during most of this century but modern FTIR instruments have become more commonplace in the last fifteen years. All infrared analyses in this thesis were conducted using a FTIR spectrometer, therefore, the workings and setup of this type of instrument only will be discussed below. A detailed description of the workings of grating instruments is given by Kemp (Kemp, 1991).

2.3 FOURIER-TRANSFORM INFRARED SPECTROSCOPY

FTIR is based on the blending of a Michelson interferometer with a sensitive infrared detector and a digital microcomputer.

2.3.1 The Michelson interferometer

In 1887, a German-born American Physicist, Albert Michelson first perfected this device and used it for several measurements in his study of light. The principle of the Michelson interferometer is illustrated in figure 2.1.

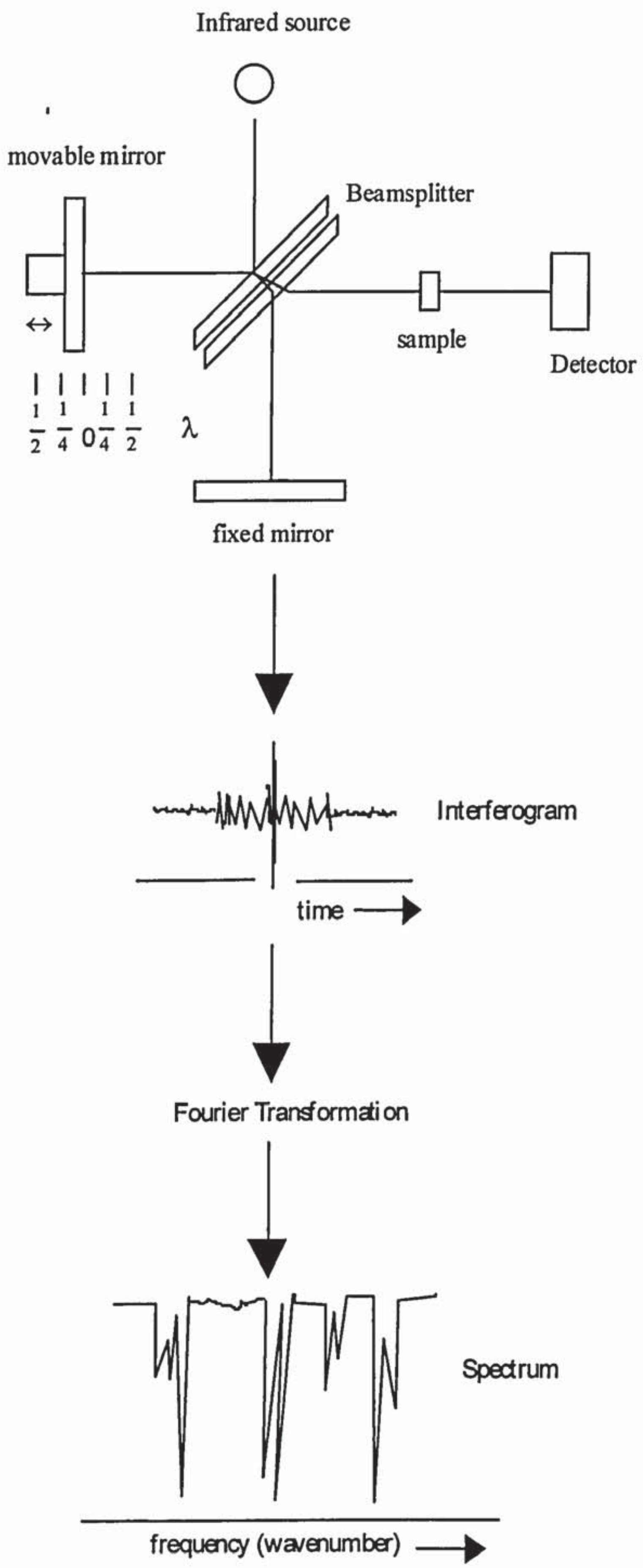

Figure 2.1 Production of a FTIR spectrum

Monochromatic light from an infrared source is passed through a beam splitter consisting of a half silvered mirror which transmits exactly half of the beam to a movable mirror and reflects the other half to a fixed mirror. These two beams are reflected from their respective mirrors and re-combined either constructively or destructively at the beam-splitter depending on the position of the movable mirror. Provided that the pathlengths from the mirrors differ by an integer number of wavelengths (including the situation where the pathlengths are equal), the two emergent beams will recombine with constructive interference, and high-intensity radiation will reach the detector. If the movable mirror moves a distance of $\lambda/4$, the total pathlength differs by exactly $\lambda/2$ and subsequently the two emergent beams are recombined with destructive interference resulting in low-intensity radiation reaching the detector. The moving mirror is the key to the interferometer, because alternate light and dark images will reach the detector if this mirror is slowly moved way from or toward the beamsplitter. The signal from the detector will then be of the form of sine wave. If the source supplies two different frequencies of monochromatic light, the signal from the detector will exhibit a different rhythm or cycle, which will be the result of combining the two separate sine-wave signals for the two different wavelengths. For more complicated polychromatic sources, a complex interferogram arises. The individual frequencies of light which were the origin of this interferogram can be calculated by the use of a Fourier-Transform.

2.3.3 Fourier-Transforms

The complex interference pattern or interferogram produced by the Michelson interferometer appear in the time domain and in this presentation the scientist is unable to extract meaningful information. However, Jean-Baptiste Fourier (1768-1830) was able to define a relationship between the set of sine and cosine frequencies making up an interferogram and the interferogram itself. This resulted in the time domain being converted and presented in the frequency domain. From this presentation, the investigator can more easily comprehend and compare light absorption patterns making up a spectrum.

2.3.4 Advantages of FTIR spectrophotometers

Contemporary FTIR machines have several advantages over the older grating type instruments. In a grating spectrophotometer most of the light from the source does not in fact pass through the sample to the detector, but is lost in the narrowness of the focusing slits, therefore poor sensitivity results. Since the spectrum takes minutes to record in the older instruments this method of identification cannot be applied to fast processes, such as recording the infrared spectra of peaks being eluted from a chromatography column. Grating instruments suffer from wavelength inaccuracies associated with the backlash in the mechanical movements such as in the rotation of mirrors and gratings.

2.4 ATTENUATED TOTAL REFLECTANCE

In 1972, Park and Baddeil (Park and Baddeil, 1972) were the first to use FTIR to study SC. Since then it has been used routinely in studies to detect changes in SC structure under a wide variety of experimental conditions (Edwardson *et al.*, 1991; Edwardson *et al.*, 1993; Lin. and Liang, 1994). An associated technique which allows the detection of diffusing permeants across SC is Attenuated Total Reflectance Fourier-Transform Infrared Spectroscopy (ATR-FTIR). Attenuated Total Reflectance (ATR) was first introduced by Farenfort (Farenfort, 1961) and since has been utilised across many disciplines, being principally employed in the structure determination of plastics, resins and coatings of various kinds (Farinas *et al.*, 1994; Johnson and Mathias, 1994; Margarida *et al.*, 1995; Puttnam *et al.*, 1966; Subramanian, 1995) However, ATR has also become a widely and routinely used technique in the analysis of diffusion across membranes and in particular skin (Harrison *et al.*, 1996b; Watkinson *et al.*, 1995). ATR has also yielded information on skin structure under the influence of topically applied penetration enhancers and drugs (Mak *et al.*, 1990a; Mak *et al.*, 1990b) giving insights into mechanisms of action. This work will be reviewed in detail in chapter 4.

2.4.1 The theory of ATR

ATR is based on the principle of internal reflection and involves the use typically of an instrument whose main component is a trapezoidal shaped crystal positioned in the sampling compartment of a standard FTIR spectrophotometer. A normal infrared beam is directed into this crystal by way of precisely positioned mirrors. The crystal is characterised primarily by a relatively high refractive index when compared to normal synthetic or biological samples. The angle at which the infrared beam enters the crystal *i.e.* the angle of incidence, must be correct for spectra to be produced and is governed by Snell's Law shown below (equation 2.8).

$$n_1 \sin \theta_{I,} = n_2 \sin \theta_R \qquad (2.8)$$

The angle of radiation striking the crystal is θ_I, the angle of refraction is θ_R and the refractive indices of the crystal and sample are represented by n_1 and n_2 respectively.

Three types of reflection arise and can be explained using Snell's Law (Figure 2.2).

I) If $\sin\theta_I < \frac{n_2}{n_1}\sin\theta_R$, some reflection will occur but the larger part of the beam will be refracted since the angle of refraction θ_R is greater than the angle of incident, θ_I .

II) If $\sin\theta_I = \frac{n_2}{n_1}$, then the angle of refraction, θ_R , is 90^o and the radiation will travel along the interface. The sine of the angle of refraction (90^0) becomes 1. In this case θ_I is called the critical angle, θ_c . The critical angle is that angle of incidence that produces an angle of refraction that is equal to 90^0.

III) If $\sin\theta_I > \frac{n_2}{n_1}\sin\theta_R$, then the angle of refraction θ_R becomes imaginary and all the radiation is reflected back into the dense crystal. If the angle of incidence is greater than the critical angle then the angle of incidence becomes larger than the angle of refraction.

This last condition is that of total internal reflection. Fahrenfort and Harrick (Harrick, 1967) have established that, in this case, an evanescent (*i.e.* vanishing) wave having the same frequency as the totally reflected radiation and whose amplitude diminishes logarithmically persists beyond the interface into the rare medium (having a lower refractive index). Both investigators independently recognised that such an evanescent wave was capable of interacting with an absorbing medium just beyond the interface leading to a reduction or "attenuation" of the totally reflected radiation. Thus, if an absorbing substance is placed on the reflecting surface of the prism, the energy that escapes temporarily from the prism is selectively absorbed.

The spectrum of the internally reflected radiation is similar to the transmission infrared absorption spectrum of the substance. The infrared band intensities are the equivalent of a penetration of a few microns depending on the substance and are independent of the

Figure 2.2. The principles of ATR infrared spectroscopy (Colthup *et al*., 1975)

sample thickness (beyond a minimum of 1μm). Hence, sample preparation is simplified for many materials, such as rubbery polymers and stratum corneum.

2.4.2 Factors affecting ATR

The success of ATR spectroscopy depends on a number of factors outlined below.

<u>Depth of penetration</u>

The intensity of absorption bands in ATR spectra depend on the depth of penetration of infrared radiation into the sample. The depth the evanescent wave penetrates the sample, dp, which is defined as the distance from the crystal-sample interface where the intensity of the evanescent wave decays to 1/e (approximately 37%) of its original value, is given by equation 2.9.

$$d_p = \frac{\lambda}{2\pi n_1\left(\sin^2\theta - n_{21}^2\right)^{1/2}} \qquad (2.9)$$

where λ is the wavelength of infrared radiation, n_1 is RI of the crystal, θ is the angle of incidence and n_{21} is that ratio of the refractive indices of the sample and the ATR crystal.

<u>Effective Pathlength (EPL)</u>

The effective pathlength describes the approximate distance infrared radiation travels along within a sample and can be used to compare the expected absorbance intensity of an ATR spectrum with that of a transmission spectrum. The EPL can be calculated from the following relationship

EPL = Penetration depth X Number of reflections (2.10)

Increasing the EPL by increasing the penetration depth or number of reflections will increase absorption band intensities.

<u>Wavelength of infrared radiation</u>

The depth of penetration of infrared radiation into a sample depends on the wavelength of the radiation. The longer the wavelength or smaller the wavenumber of radiation, the greater the depth of penetration. This means that the relative absorption band intensities at high wavenumbers are lower when compared to a transmission spectrum of the same sample. Another difference, rarely observed, is a small shift in the apparent absorption maxima. However, this does not seriously impair the comparison of ATR with transmission spectra (Smith, 1980).

Refractive Index

The relative values of the refractive indices of the crystal and sample can alter the intensity of band absorptions. As the RI of the sample approaches that of the crystal, the ATR spectra become more intense. If the RI of the crystal increases, the depth of penetration decreases. The refractive index also affects the critical angle. The relationship below shows that increasing the refractive index of the crystal decreases the critical angle.

$$\theta_C = \sin^{-1} \frac{n_2}{n_1} \qquad (2.11)$$

Angle of incidence

As explained earlier, in order to obtain an ATR spectrum the angle of incidence must exceed the critical angle. Further, increasing the angle of incidence decreases both the number of reflections and penetration depth of the infrared radiation resulting in a lowering of absorption band intensities.

Efficiency of Sample Contact

It is important that the sample is in close contact with the crystal since the wave of radiation penetrating the sample decays exponentially and rapidly as it protrudes from the crystal surface. The best ATR spectra are therefore those of smooth samples and liquids which wet the crystal surface. Applying pressure onto rough samples can improve absorption bands but care must be taken not to scratch or otherwise damage the crystal.

Area of Sample Contact

The larger the area of sample in contact with the crystal, the greater the number of reflections along the ATR crystal resulting in greater absorption band intensities.

ATR crystal material

In order for internal reflection to be achieved, a crystal having a high RI must be chosen. Generally, crystals possessing a RI greater than 2.2 are used.

Extinction Coefficient of functional group

The extent to which bonds in a chemical are capable of absorbing infrared radiation is dependant on the type and strength of the bond and is also influenced by constituent atoms making up the organic molecule. Therefore, when comparing the relative magnitudes of absorbance exhibited by different chemicals, one must be aware of differences in their extinction coefficients and hence direct comparisons between different permeants are not always possible.

2.5 BASIS OF TRANSDERMAL ATR-FTIR ANALYSIS

Figure 2.3 shows a typical ATR-FTIR spectroscopically determined spectrum of normal human skin *in vitro* (see chapter 4 for method used). The most important and most applicable feature to these investigations is the lack of infrared absorptions between 1700 and 2700cm^{-1} in this spectrum. This infrared transparent `window' can be used to assess the appearance of topically applied substances (by either diffusion/partition/absorbance) in stratum corneum. The essential property such substances need to possess is a distinct inherent functionality that absorbs infrared radiation within the skins infrared transparent region, so as to avoid interference with conflicting infrared absorptions arising from skin components. An analysis of all the peaks constituting the spectrum of stratum corneum is given in chapter 4 (table 4.1).

2.5.1 Determination of suitable labels.

Since the infrared transparent region occurs between 1700 to 2700cm^{-1}, efforts were directed to search for functional groups occurring in organic compounds that absorbed in this region. A search of infrared absorption tables yielded the groups listed in table 2.1 that absorb infrared radiation between the above quoted frequencies. The absorption of the terminal C-H bond found in acetylenes does not appear in the infrared transparent region, but appears at 3296cm^{-1}.

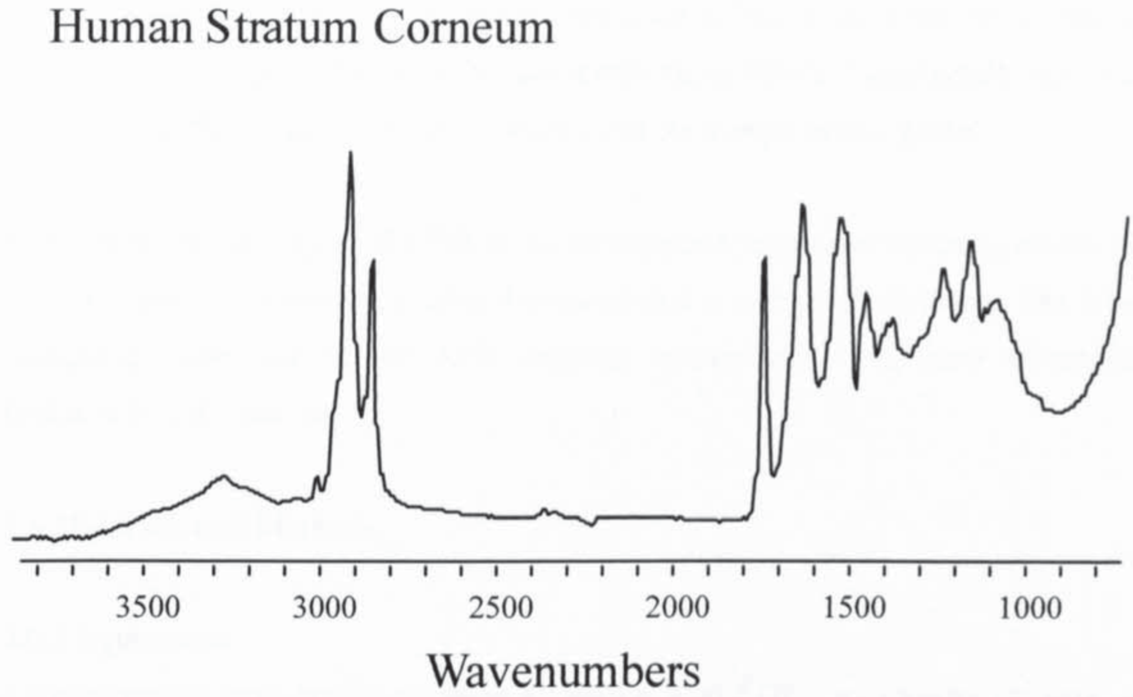

Figure 2.3 ATR-FTIR spectrum of human stratum corneum placed stratum compactum side on crystal (see table 4.1 for assignment of each peak)

Functional group	Frequency of absorption (cm^{-1})	Vibrational motion
$-C{\equiv}N$	2250	stretch
$-C{\equiv}C-$	2116	stretch
$-C{\equiv}C-H$	3296	stretch
$-S-H$	2561	stretch
$-N{=}\overset{+}{N}{=}N^{-}$	2100	stretch

Table 2.1 Infrared absorptions of interest

This strong absorption was also used in experiments as long as there was no interfering O-H stretch in this region. This was the case if anhydrous dimethyl sulphoxide was used as a solvent rather than a hydroxyl-containing solvent such as propylene glycol.

Most studies employing ATR-FTIR in the transdermal analysis of diffusion across stratum corneum have concentrated on using 4-cyanophenol as permeant of choice. The following compounds were chosen for ATR analysis; cyanophenol, 4-hydroxy thiophenol, 1-heptanitrile and 1-octyne.

2.6 Materials and Methods

2.6.1 Equipment

All experiments were carried out using a Mattson 3000 FTIR spectrometer equipped with a deuterated triglycine sulphate (DTGS) detector sensitive to mid infrared radiation produced by a helium-neon laser and a flat-top Advanced ATR accessory® (spectra-Tech). The ATR unit consisted of a teflon box containing a series of precisely positioned mirrors with a rectangular opening at its surface where the internal reflection element (IRE) was placed. The IRE was made of a ZnSe crystal having dimensions of 7.2 x 1.0 x 0.2cm and a refractive index of 2.4. The position of the mirrors dictated that an infrared beam is reflected into the crystal at an angle of 45°C (incident angle) and then reflected internally twelve times. The ATR system is shown in Figure 2.4.

2.6.2 The Trough

In experiments requiring the application of liquids onto membranes placed on the ATR plate, a small Perspex trough was sited onto the membrane and then liquid pippetted into it. This prevented the liquid from spilling over the sides of the membrane and possibly spreading underneath the membrane without first diffusing through it.

2.6.3 Computer software

MacFirst® software run on an Apple Macintosh Quadra 800 computer was used to both operate the spectrometer and analyse the spectra produced.

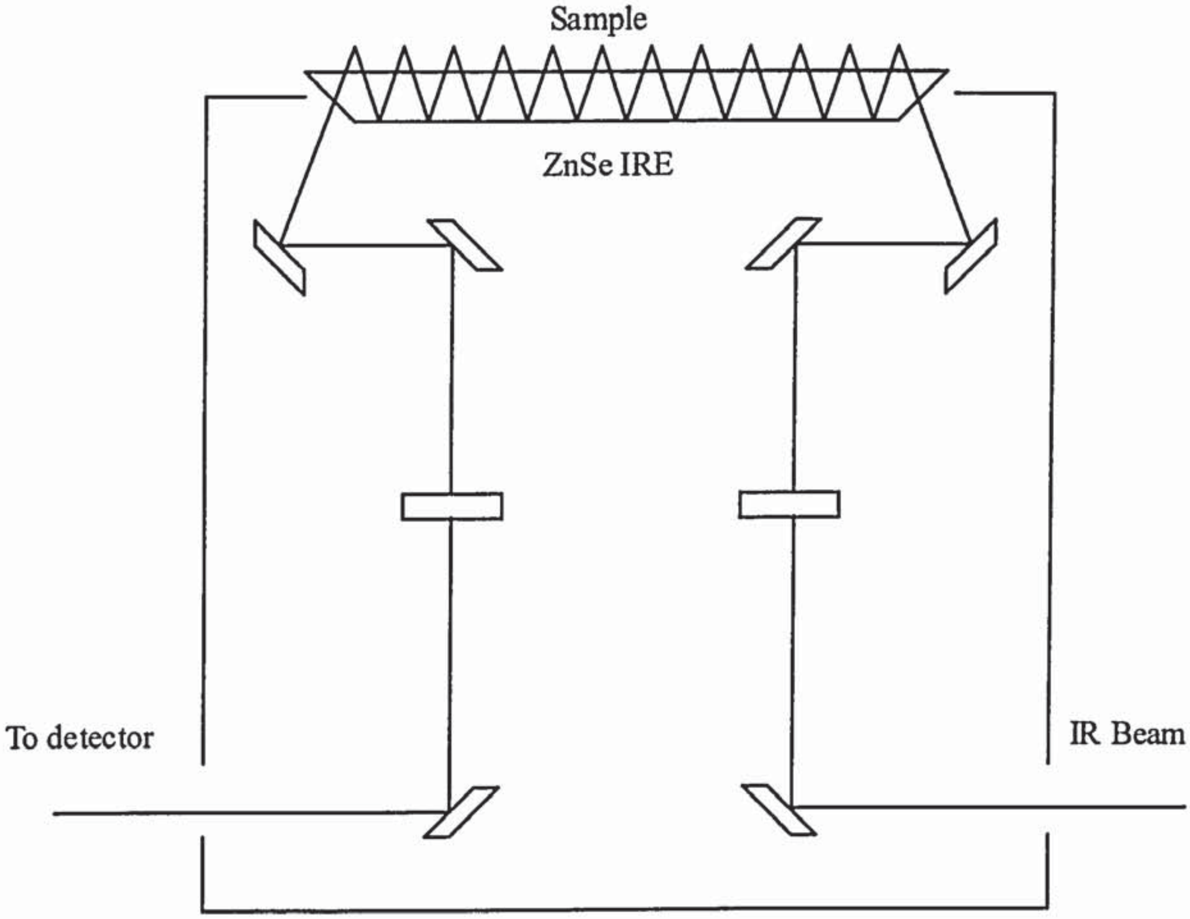

Figure 2.4 The ATR unit used in all experiments

2.6.4 Spectrometer optimization

Resolution and number of scans

The more scans collected and co-added at each time point during an experiment, the greater the signal-to-noise ratio. This is given by the following relationship

signal:noise α $\sqrt{\text{increase in number of scans}}$

It follows therefore that increasing the number of scans by 16 decreases spectral noise by a factor of 4. However, the opposite applies to resolution. Increasing resolution decreases the signal-to-noise ratio. A spectrum having a resolution of $1cm^{-1}$ takes 16 times longer to collect than a $16cm^{-1}$ spectrum and has a signal-to-noise ratio that is four times worse (four times noisier). Therefore, both parameters could not be maximized and a balance had to be achieved. From initial spectra produced and reviewing the published literature, spectra were produced arising from 64 scans and a spectrometer set resolution of $2cm^{-1}$. The time span for each spectral measurement was two minutes and fifty-three seconds.

Gain

Increasing gain settings magnify the whole signal. However, detector noise is also magnified. A gain setting of 20 was employed throughout each experiment.

Kinetics

Rapid automated scanning during experiments was achieved using a kinetics measurement facility within the MacFirst software®.

2.6.5 Molar Absorptivity of IR labels

To assess the relative strengths or weaknesses of chosen IR labels for transdermal analysis, molar absorptivities were determined both in transmission and attenuated total reflectance for each label.

ATR-FTIR determination

Equimolar solutions (5M) 4-cyanophenol, 4-hydroxythiophenol and 1-heptanonitrile were prepared in propylene glycol. A 5M solution of 1-octyne was prepared in dimethylsulphoxide (DMSO). The compounds 1-heptanonitrile and 1-octyne are liquids at room temperature and therefore their densities needed to be determined. This was achieved by weighing 1ml of each liquid at room temperature, determining a weight per ml value and then adding sufficient volume of liquid to solvent to obtain a 5 molar concentration. Infrared spectra of propylene glycol and DMSO were also recorded. Infrared absorptions due to PG and DMSO do not interfere with the absorptions of interest in any of the compounds under investigation.

200μl of each solution was pipetted directly onto the ZnSe crystal and a glass microscope slide positioned directly on top of the sample and a brass weight (25g) placed on top of the slide. An ATR-FTIR spectrum was then recorded and infrared absorbance values for the peaks listed in table 2.1 determined using instrumentation previously described. The above procedure was carried out a total of five times for each sample.

Refractive Index measurements

The refractive index of each 5M solution was determined using an automatic refractometer (GPR U-37, Index instruments, UK) at room temperature. Aliquots (10μl) of solution were pippetted onto a synthetic sapphire receptor plate and refractive index values read of from a digital display.

The molar absorptivity for each compound was then determined by inserting RI values into equation 2.9 to obtain the depth of penetration. This meant that the effective pathlength (EPL) could now be calculated using equation. 2.10. Finally, the molar absorptivity was obtained from equation 2.7. Results are given in table 2.3 (a and b).

Transmission FTIR determination

An infrared 0.1cm pathlength liquid cell (Graseby Specac, UK) consisting of transparent windows with a spacer between them, was used to determine molar absorptivities of the compounds in transmission. Solutions were pipetted into the cell filling the area between the plates and then entrance and exit ports plugged using plastic stoppers. The cell was then inserted into the sampling space of the spectrophotometer. A cell containing solvent only was used as background to eliminate any influence from solvent peaks. Five spectra were then recorded in the normal manner for each sample. Since the pathlength of the cell is known, molar absorptivities were then calculated using equation 2.7 only. Results are given in table 2.2.

2.6.6 ATR experiments using silicone membrane

2.6.6.1 Spectra of silicone membranes in ATR-FTIR analysis

Silicone membrane (Samco Ltd., UK.) having a thickness of 300μm was cut to a size of 2.5 x 9.0cm, gently rinsed in double distilled water and placed directly onto the ZnSe crystal. A glass slide was placed on top of the membrane and a 50g weight positioned on top. An infrared spectrum of the membrane was then recorded.

2.6.6.2 Reproducibility of membrane peaks

Silicone membrane (Samco Ltd., UK.) having a thickness of 300μm was gently rinsed in double distilled water, cut to a size of 2.5 x 9.0cm and placed directly onto the ZnSe crystal. A glass slide was placed on top of the membrane and a 50g-weight positioned on top. An infrared spectrum of the membrane was then recorded. The above procedure was repeated for six different pieces of membrane from the same batch. The area of the Si-Me peak evident within each sample was determined by integration between $1250cm^{-1}$ and $1262cm^{-1}$. The above procedure was repeated again six times within six individual samples of membranes. In this manner, the reproducibility of the Si-Me peak within and between each silicone membrane sample could be assessed.

2.6.7 Assessment of infrared response

To determine the type of relationship between concentration and infrared absorbance during ATR experiments, a series of solutions of different concentrations were prepared. Aliquots of 25μl of each solution and 1μl of dimethylpolysiloxane (Sigma, UK), used as an internal standard, were pippetted directly onto the IRE. A glass slide was placed on top of the liquid, gently pressed into position and a 50g brass weight placed on top. This ensured that liquid was evenly spread along the whole IRE during each experiment. Spectra were then recorded. Relevant peak areas for each different concentration were determined and ratioed to that of the internal standard. Calibration plots were then produced.

2.6.8 Assessment of permeant penetration across silicone membrane

Silicone membrane sheets were positioned onto the ZnSe crystal as described above. A perspex trough was then placed over the membrane (so that its hollow was located precisely over the ZnSe crystal) and sealed in place with white soft paraffin. Solutions of 4-CP, 4-

HTP, 1-heptanitrile and 1-octyne were then pipetted into the trough and the trough sealed with a glass microscope slide and a 50g brass weight. ATR-FTIR spectra were subsequently recorded periodically. The absorbance intensity of the peaks ascertaining to the penetrating molecule and the membrane inherent Si-Me peak were determined and the former normalised by dividing the intensity value with that of the later. This ratio was then plotted as a function of time.

2.6.9 ANALYSIS OF DATA

These series of experiments consider a situation where a membrane is placed on an impermeable material (ZnSe IRE). Diffusion of a permeant in such a situation is therefore bound by two parallel boundaries, an outer boundary which is in contact with the formulation applied and an inner boundary which is in contact with the IRE. These boundaries can then be defined as $x = h$ and $x = 0$ respectively, where h is the pathlength of a permeant. If a permeant-containing formulation of constant concentration, C_0, is applied to the outer surface (x=h) of the membrane, the difference in concentrations between the two surfaces x=h and x=0 will continuously decline as a function of time ($t \geq 0$) until the lower boundary is totally saturated with permeant, exhibiting a permeant concentration in the membrane which may or maynot be equal to C_0, depending on the extent of membrane perturbation by enhancer or solvent in the membrane, solubility of permeant in membrane and the capacity of the membrane to "hold" (possibly by swelling) permeant. Figure 2.5 shows the initial conditions of the experiment. During the experiment, the permeant profile at any point between the boundaries can be given by $C \leq C_0$, $0 < x < h$ and $t \geq 0$.

Using Fick's second law, a diffusion equation that satisfies the above boundary conditions has been derived (Crank, 1975)and is given below:

$$\frac{C}{C_0} = 1 - \frac{4}{\pi}\sum_{n=0}^{\infty}\frac{(-1)^n}{2n+1}\exp\left(\frac{-D(2n+1)^2\pi^2 t}{4h^2}\right)\cos\frac{(2n+1)\pi x}{2h} \qquad (2.12)$$

where C is the concentration of permeant in membrane at time, t, and position,x, in the membrane, and D is the permeant's diffusion coefficient in the membrane. C_0 represents the concentration of permeant in the membrane layer (x = 0) in touch with the impermeable crystal and hence corresponds to the membrane region the ATR-FTIR spectra relate to. Therefore, the cosine function in the above equation becomes 1 and the equation used in our analysis is in the form shown below

$$C = C_0\left[1 - \frac{4}{\pi}\sum_{n=0}^{\infty}\frac{(-1)^n}{2n+1}\exp\left(\frac{-D(2n+1)^2\pi^2 t}{4h^2}\right)\right] \tag{2.13}$$

Finally, the concentration terms can be replaced with ATR-FTIR-determined permeant absorbance values, assuming the Beer-Lambert law applies to obtain the workable equation below

$$A = A_0\left[1 - \frac{4}{\pi}\sum_{n=0}^{\infty}\frac{(-1)^n}{2n+1}\exp\left(\frac{-D(2n+1)^2\pi^2 t}{4h^2}\right)\right] \tag{2.14}$$

where A represents the absorbance of a permeant at time, t , and position, x, in the membrane and A_0 is the absorbance of the permeant, vehicle or enhancer in the saturated plateau region of the membrane, x = 0.

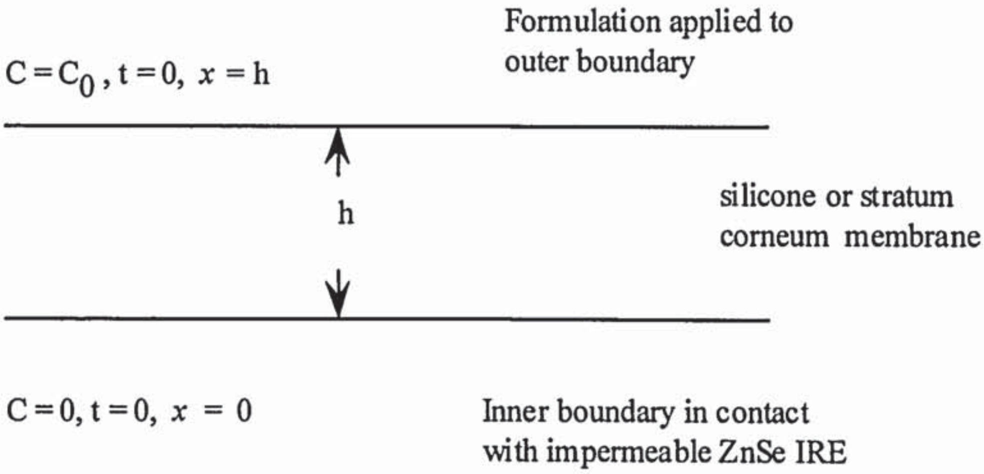

Figure 2.5 Profile of initial membrane conditions for ATR-FTIR experiments

2.7 RESULTS AND DISCUSSION

Figure 2.6 (a-d) shows the ATR-FTIR spectra of the four compounds chosen for diffusional analysis. This choice was dependent on each compound possessing organic functionality that absorbed infrared radiation between the region 1700 to 2700cm^{-1}.

Allied to this criterion, cyanophenol and hydroxythiophenol share a common phenolic structure and a similar molecular weight. The compounds differed due to the substituent found at the carbon-4 position of the benzene ring; cyanophenol having a cyano (-CN) group and hydroxythiophenol possessing a thiol (-S-H) group at this position. These groups were shown to absorb IR strongly at 2230cm^{-1} and 2561cm^{-1} (less strongly) respectively.

Heptanitrile and 1-octyne both shared an aliphatic six-carbon chain with different terminally positioned functional groups, the former having a cyano and the latter an acetylene group attached. It can be seen that the absence of a conjugated benzene ring significantly diminished (when compared to CP) the IR absorption intensity of the -CN bond. The IR absorption spectrum of 1-octyne (Fig 2.6d) shows two absorptions of interest. The weaker absorption at 2116cm^{-1} is due to absorption by the triple carbon to carbon bond. The stronger absorption at 3296cm^{-1} is due to the terminal carbon-hydrogen bond in 1-octyne. This absorption obviously does not appear in the stratum corneum IR transparent region as detailed earlier, but may still be employed to determine diffusion across membranes as long as it does not interfere with any excipient or membrane absorptions. For example, in silicone membrane there is an absence of IR absorptions between 3200-4000cm^{-1}.

Figure 2.7 (a) and (b) shows the ATR-FTIR spectra of the solvents propylene glycol and dimethylsulphoxide. Both solvents have been widely employed in topical formulations and are known to possess penetration enhancement activity (Smith and Maibach, 1995). An important feature apparent in these traces is that they both share an IR transparent region similar to stratum corneum and hence these solvents will not interfere with any solute (*e.g.* cyanophenol absorption at 2230cm^{-1}) which would hinder permeant diffusion analysis. Also, both spectra show strong solvent-related peaks, propylene glycol absorbing at approximately 1020cm^{-1} by virtue of its -C-O- band and DMSO also absorbing at 1020cm^{-1} due it possessing a sulphoxide group. Therefore, one can use these peaks to determine their diffusion characteristics across synthetic (silicone) and stratum corneum membranes.

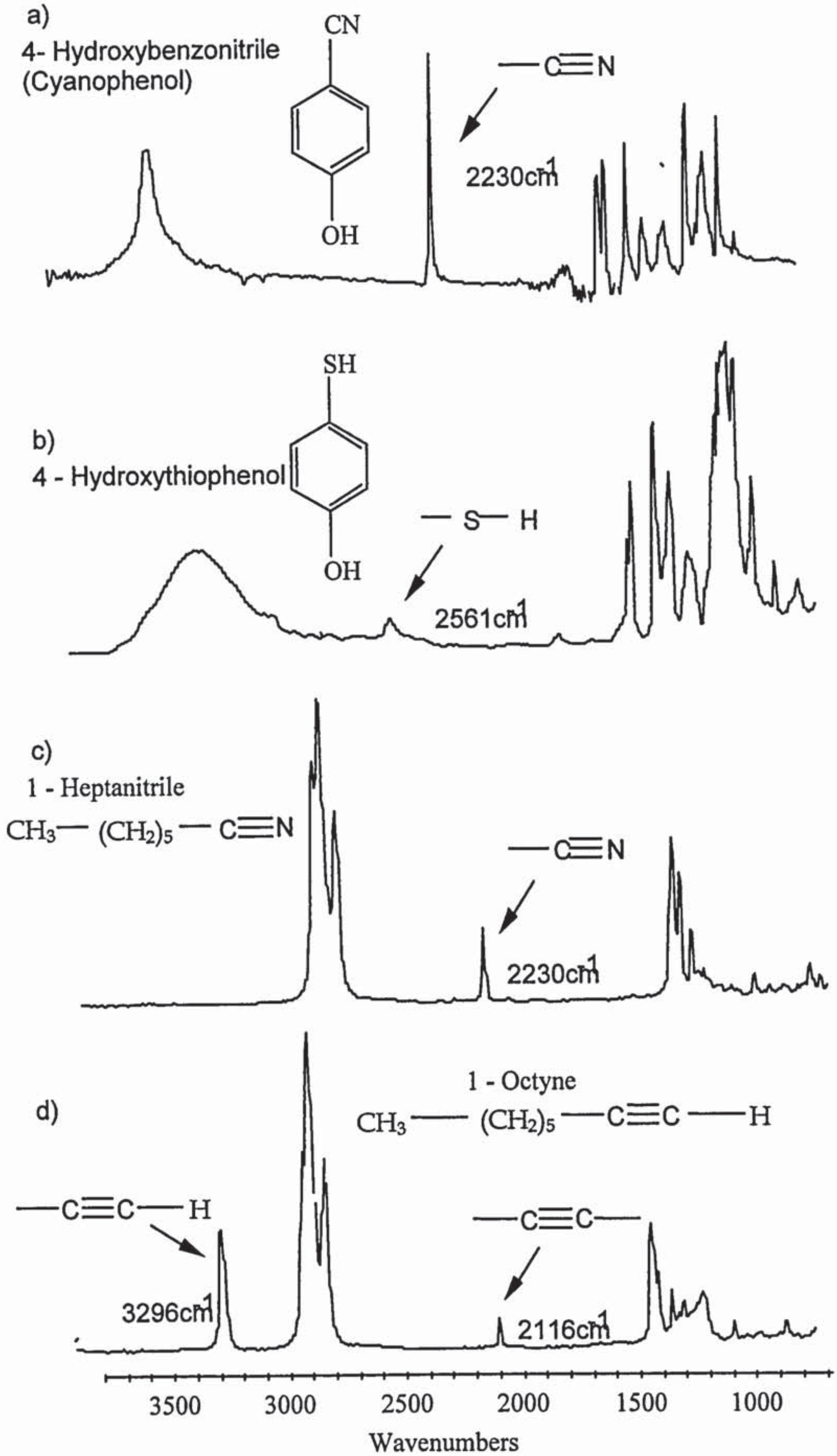

Figure 2.6 (a-d) ATR-FTIR spectra of selected model compounds

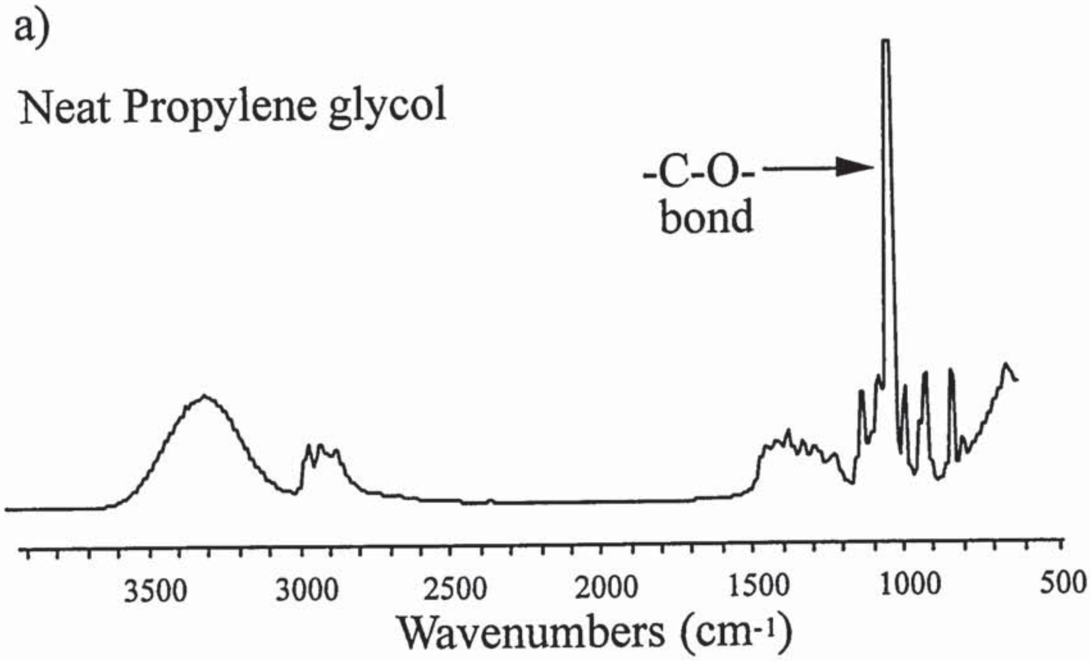

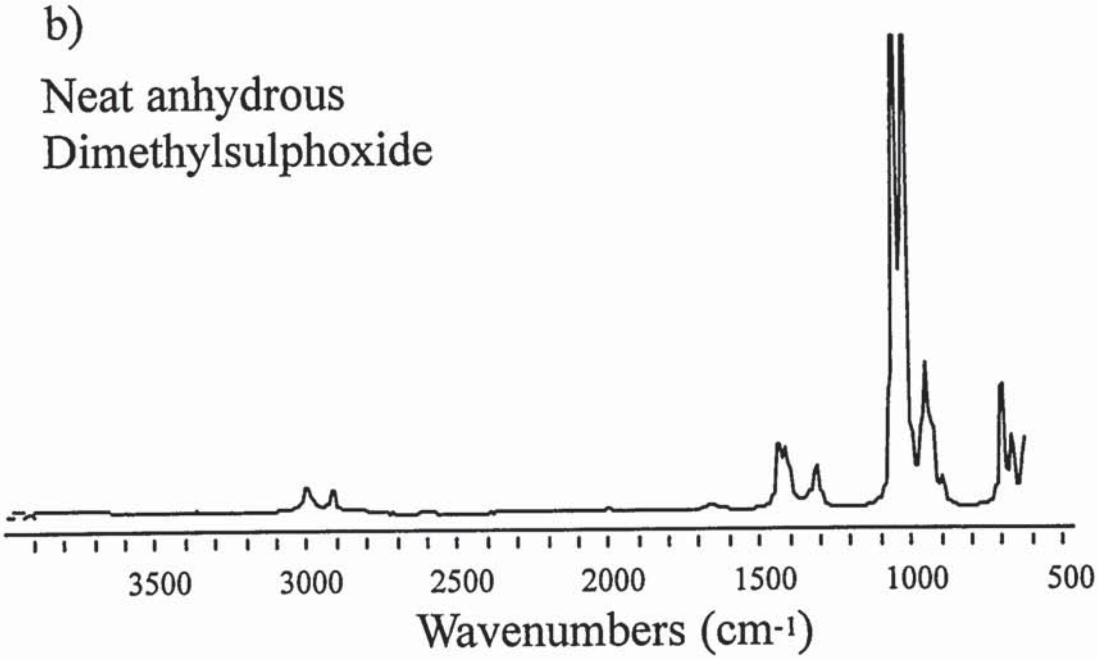

Figure 2.7 ATR-FTIR spectra of solvents used in experiments (a) Neat propylene glycol and (b) dimethyl sulphoxide

In addition to the IR spectra shown in figure 2.6(a-d), efforts were made to clarify relative IR absorption strengths of each of the model compounds. This was done by determining molar absorptivities both in transmission and ATR modes. Table 2.2 shows absorptivities for each compound having identical concentration and cell pathlengths resulting from collection of spectra in transmission. The intensity of IR absorption resulting from the cyano bond in CP was the greatest whilst the absorption attributed to the terminal alkyne bond found in 1-octyne also was strong. Absorptions of interest in the remaining compounds tested ranked in the following order CP>OT (terminal alkyne H bond) >HTP>HeptCN>OT(alkyne bond). A perusal of available literature did not yield quoted absorptivity values, mainly because such values vary depending on the individual instrument used.

Table 2.3(A and B) show the steps involved in obtaining molar absorption values using ATR-FTIR. Equation 2.9 was used to determine depth of penetration of the IR beam into the sample contiguous with the ATR crystal. The value of depth calculated was then used in equation 2.10 to obtain a value for the effective IR beam pathlength along the ATR plate as a function of its and sample refractive index. Final molar absorptivities obtained are listed in table 2.3(B). The intensity of absorptions when compared to those determined during transmission has significantly decreased for all compounds. This is because the pathlength is much smaller when using ATR and the intensity of the IR beam diminishes following each reflection along the crystal and subsequent absorption by the sample. However, molar absorptivities can be ranked in the following order; CP>OT (terminal alkyne H bond)>HeptCN>HTP>OT(alkyne bond). This order is similar to that seen in transmission, the difference being that HeptCN absorbed slightly more than HTP in ATR.

These results give information concerning which of the tested compounds (containing functional groups capable of IR absorption) can be detected using ATR-FTIR to determine their diffusion. However, one must be aware that these determinations were carried out in liquid samples. This means that the calculated absorptivities may be slightly different (due to changes in refractive index) to those of diffusing molecules in a membrane. Nevertheless, the calculations performed give an important indication of relative absorptivities.

From the above classification of model compounds, the next stage was to establish a suitable model membrane that could be employed to monitor permeant diffusion. The fundamental criterion for a suitable membrane (for the purpose of spectroscopic investigations) was that it needed to have an IR spectrum, incorporating an infrared transparent window, similar to that of human stratum corneum (see Figure 2.3).

Table 2.2 Determination of Molar absorptivity in Transmission. Concentrations of all solutions were 5M and pathlength of the IR liquid cell was 0.01cm.

Compound	Bond	IR absorption at (cm^{-1})	Absorbance	Molar Absorptivity (litre mole $^{-1}cm^{-1}$)
4-CP	$—C\equiv N$	2250	4.131	82.62
4-HTP	$—S—H$	2561	0.902	18.04
1-HeptCN	$—C\equiv N$	2250	0.635	12.7
1-Octyne	$—C\equiv \boxed{C—H}$	3296	4.050	81.00
1-Octyne	$—C\equiv C—$	2116	0.404	8.08

Table 2.3(A and B). ATR-FTIR molar absorptivity calculations for IR labels. Concentrations of all solutions was 5M.

Table A

Compound	R.I at 24 ^{0}C	Depth of penetration (μm)	Number of reflections	Effective pathlength (μm)	Effective pathlength (cm x 10^{-3})
4-CP	1.479	1.912	12	22.944	2.2944
4-HTP	1.495	1.982	12	23.784	2.3784
1-HeptCN	1.416	1.701	12	20.0412	2.0412
1-Octyne	1.416	1.701	12	20.412	2.0412

Table B.

Compound	Bond	IR absorption at (cm^{-1})	Absorbance	Pathlength (cm x 10^{-3})	Molar Absorptivity (litre $mole^{-1}cm^{-1}$)
4-CP	$—C\equiv N$	2250	0.592	2.2944	51.60
4-HTP	$—S—H$	2561	0.085	2.3784	7.148
1-HeptCN	$—C\equiv N$	2250	0.072	2.0412	7.153
1-Octyne	$—C\equiv \boxed{C—H}$	3296	0.207	2.0412	20.82
1-Octyne	$—C\equiv C—$	2116	0.048	2.0412	4.703

More specifically, it needed to be IR transparent between the region 1700-2700cm^{-1}. Consequently, a silicone membrane consisting of a dimethylpolysiloxane polymer, available in a thickness of 300μm was used. The IR spectrum of this membrane is shown in Figure 2.8. One can see that a region exists between 1700-2700cm^{-1} where the membrane does not absorb radiation. Hence, bearing in mind the absorption frequencies of the model compounds, membrane components would not interfere with permeant absorptions.

In order to successfully employ this silicone membrane for diffusional analysis, its IR spectra had to be deemed reproducible. This was tested by ensuring that its silicone content, apparent due to the Si-Me bond absorption at 1258cm^{-1}, remained constant when taking spectra of different membrane samples and spectra of different areas within the same sample. Samples from one batch were used in all experiments. Figure 2.9 records the reproducibility of the Si-Me absorption in different regions of six individual membrane samples. No significant difference was observed in silicone content (Tukey B test, $P<0.05$). Figure 2.10 shows the reproducibility between different membrane samples. From the plot, one can also conclude that a significant difference in silicone content did not exist (Tukey B test, $P<0.05$).

To assess correlation between IR absorbance and concentration, different concentrations of CP in PG and PG in water were pipetted onto the ATR crystal. Since the intensity of IR absorption is dependent on the degree of contact between sample and crystal, an aliquot of liquid dimethylpolysiloxane (DMPS) was also pippetted onto the crystal surface. The CP and PG absorptions were then normalised with the Si-Me bond absorption from DMPS, which essentially behaved as an internal standard. Therefore, the ratio of these absorbances gave a value not influenced by contact differences or changes. Figures 2.11 and 2.12 show calibration plots for CP and PG respectively. In both cases a linear correlation existed.
The diffusion of topically applied permeants across silicone membrane was monitored using ATR-FTIR. Figure 2.13 shows the diffusion profile obtained following application over a 12-hour period of a saturated CP solution in PG. CP diffusion has been fitted to Fick's second law (equation 2.14). It is evident that the rate of diffusion across the membrane is greater during the first half of the experiment than the last. As more CP penetrates the membrane, CP concentration in the membrane increases. Eventually, the

membrane should become saturated with the permeant and a plateau obtained. However, even after a 12-hour experimental period a true plateau had not been reached.

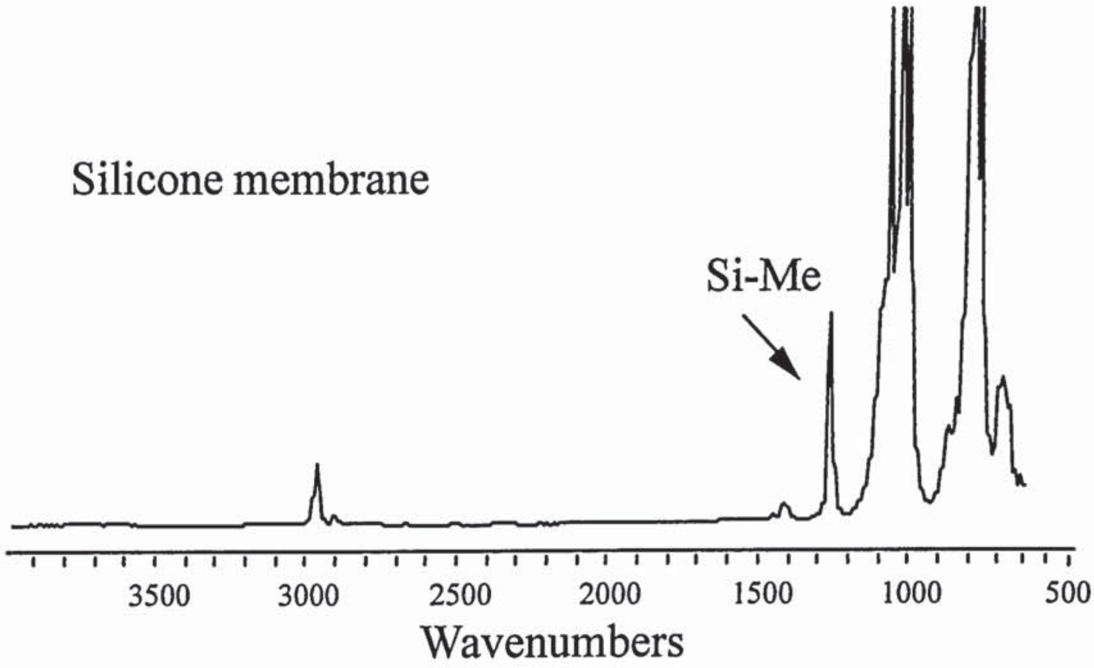

Figure 2.8 ATR-FTIR spectrum of silicone membrane

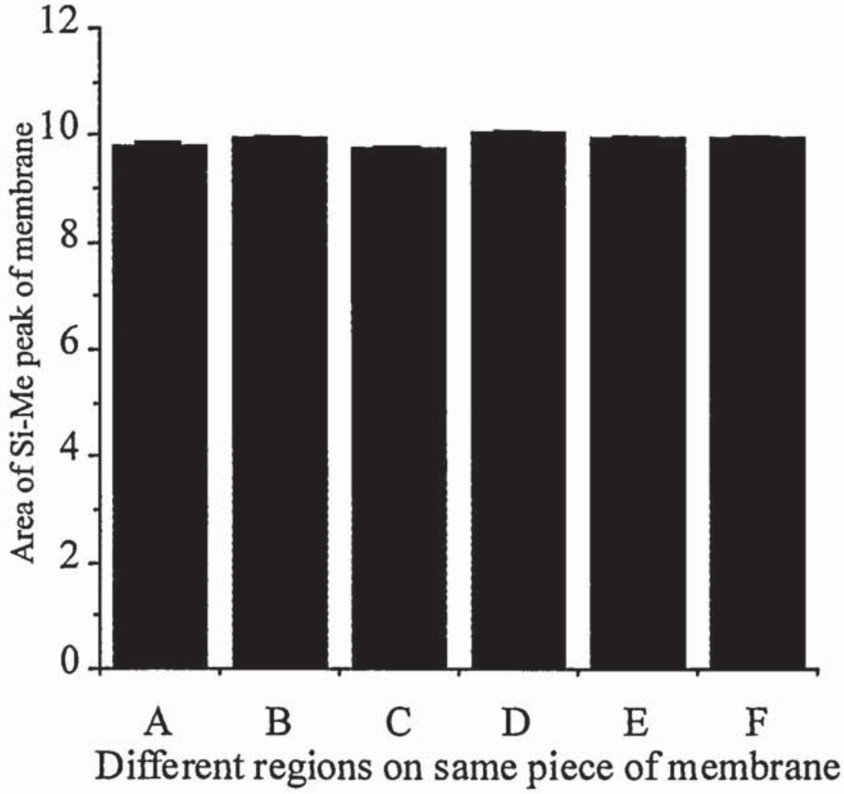

Figure 2.9 Reproducibility of the Si-Me peak area within a sample of silicone membrane

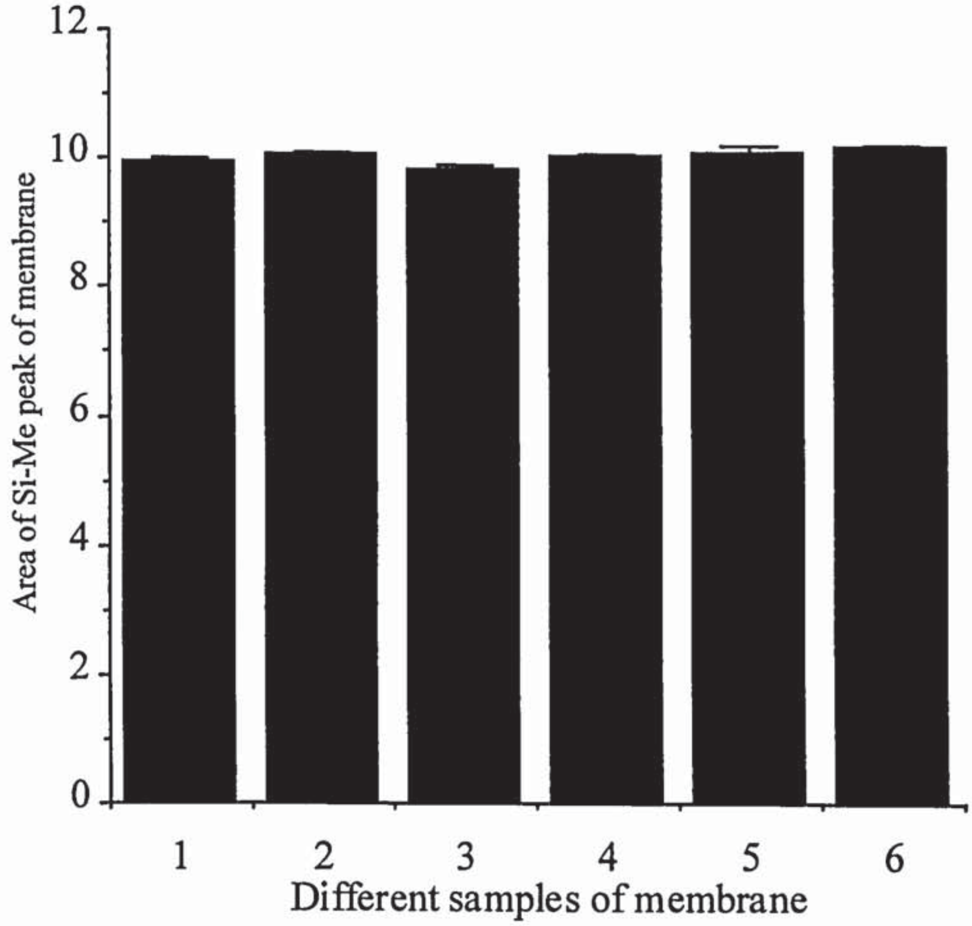

Figure 2.10 Reproducibility of the Si-Me peak area between different samples of silicone membrane

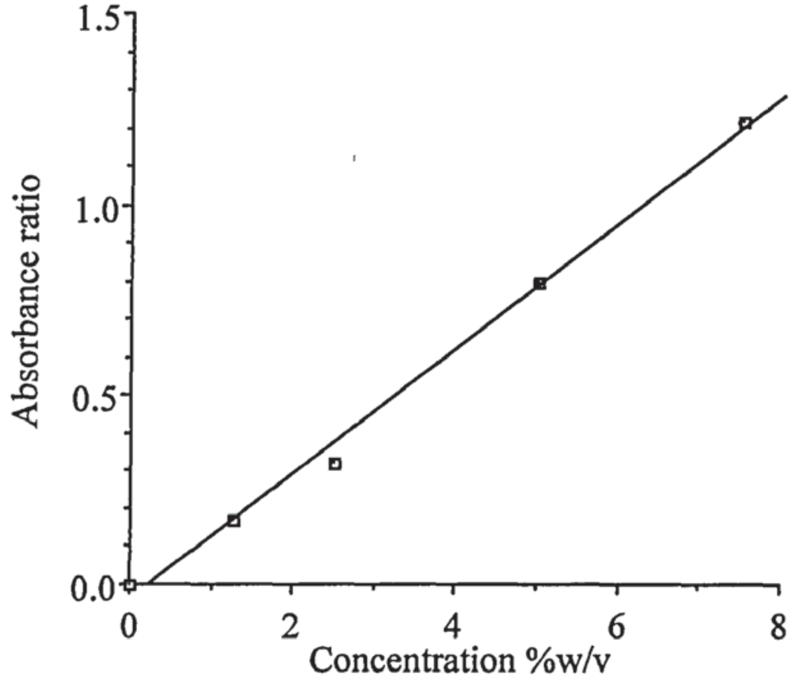

Figure 2.11 Calibration plot for 4-CP in propylene glycol using liquid DMPS as internal standard. The data represents the mean ± sd (n=5).

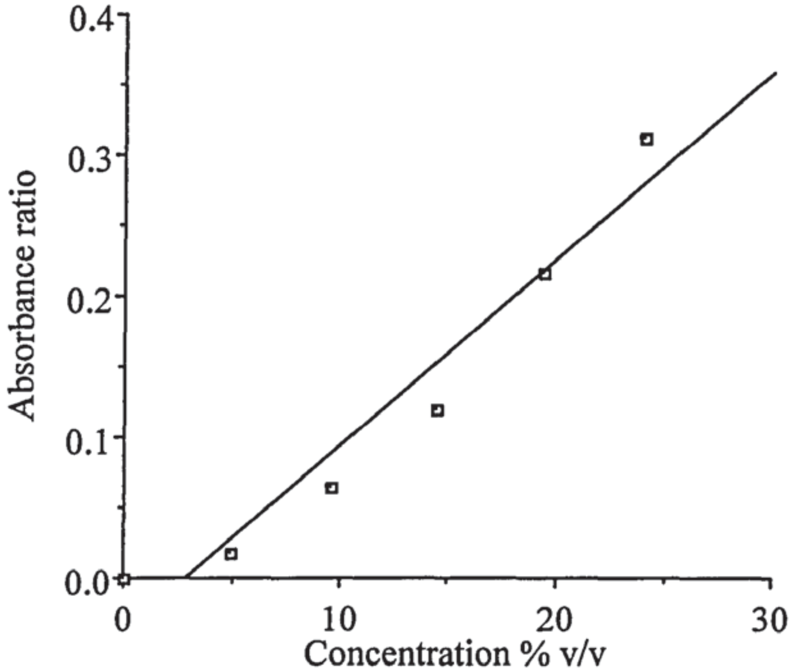

Figure 2.12 Calibration plot for propylene glycol using liquid DMPS as internal standard. The data represents the mean ± sd (n=5).

Figures 2.13 to 2.16 show diffusion profiles across silicone membrane of CP, HTP, OT and HeptCN respectively. The HTP profile is similar to that of CP in the sense that the rate of permeant diffusion is slower in the later part of the experiment. The diffusion of OT and HeptCN did not fit as well to the diffusion model. In both cases, within the first few minutes of application, permeant rapidly diffused across the membrane and then diffusion slowed towards a plateau situation.

Table 2.4 lists parameters determined after performing computer fits for each diffusion profile. Values for D/h^2 and A_O were allowed to vary until the best fit was achieved. The D/h^2 values (pathlength normalised) for each compound were significantly different ($P<0.05$) from each other. Heptanitrile diffused fastest through the silicone membrane followed by 1-octyne, hydroxythiophenol and cyanophenol. Using equation 2.15 and

$$L = \frac{h^2}{6D} \qquad (2.15)$$

knowing the width of silicone membrane used one is able then to calculate the lag times for each permeant, which are listed in table 2.4. It is evident that the greater the rate of diffusion the shorter the lag time. Table 2.4 also shows that the Fickian equation used to model the diffusion of heptanitrile and octyne did not fit to the experimental data as well as that seen for cyanophenol and hydroxythiophenol. Graphically, it was evident that the diffusion of both heptanitrile and octyne was rapid and exhibited a large burst effect. In order to accomadate for this effect, the experimentally determined data was re-fitted to the Fickian diffusion model but differed in that a component that estimates the observed burst effect was incorporated into the fits. The results from these modified fits are listed in table 2.4 and show that the values for D/h^2 are markedly reduced but the revised model still did not fit well to the data. The exact cause of the burst effect seen is not clear although it may be attributed to the compounds reacting with the silicone membrane.

In a series of studies, Pugh and co-workers (Pugh *et al.*, 1996) concluded that the capacity of a permeant to H-bond with membrane components is a major determinant of diffusion and as such is an important predictor of gross permeant diffusion across membranes. Roberts *et al* (Roberts *et al.*, 1996) further showed that the presence of two or more H-bonding groups reduces permeant diffusion coefficients significantly. Therefore, since the value of D/h^2 depends on H-bonding groups present in the permeant, the significantly lower D/h^2 values resulting from the diffusion of the phenols, cyanophenol and hydroxythiophenol, is probably a consequence of their greater ability to H-bond with the silicone membrane when compared to 1-heptanitrile and 1-octyne.

Values for the parameter, A_0, reflect the membrane solubility of each permeant in silicone membrane. However, when comparing A_0 values originating from different permeants, larger values should not be thought to correspond to higher levels of permeant build up. This is because the magnitude of these values is dependent on their IR absorptivity, inferring that high intensity does not always correlate with greater concentrations when comparing values. Further, it is important to keep in mind that the penetration of a permeant into silicone membrane, such as a co-administered solvent, may have an affect on its RI (see equation. 2.9). If this leads to an increase in the depth of penetration of the IR beam into the membrane, then a greater value for A_O would be obtained compared to a system where the membrane RI was unchanged.

The depth of IR beam penetration into silicone membrane would also depend on the wavelength or wavenumber of penetrating radiation. The larger the wavelength, the greater the depth of beam penetration into the membrane and therefore a greater number of diffusing molecules will absorb radiation yielding a larger measured intensity. For example, the cyano group will absorb radiation of wavelength 4.5×10^{-4} which penetrates 50% deeper than radiation of wavelength 3.0×10^{-4} which is absorbed by the terminal C-H bond found in 1-octyne.

However, inspite of the above mentioned limitations to ATR-FTIR analysis one major use of the A_O parameter would be to assess how membrane permeant solubility would be affected by incorporating a given permeant in a variety of topical formulations. This could potentially yield mechanistic information concerning percutaneous transport.

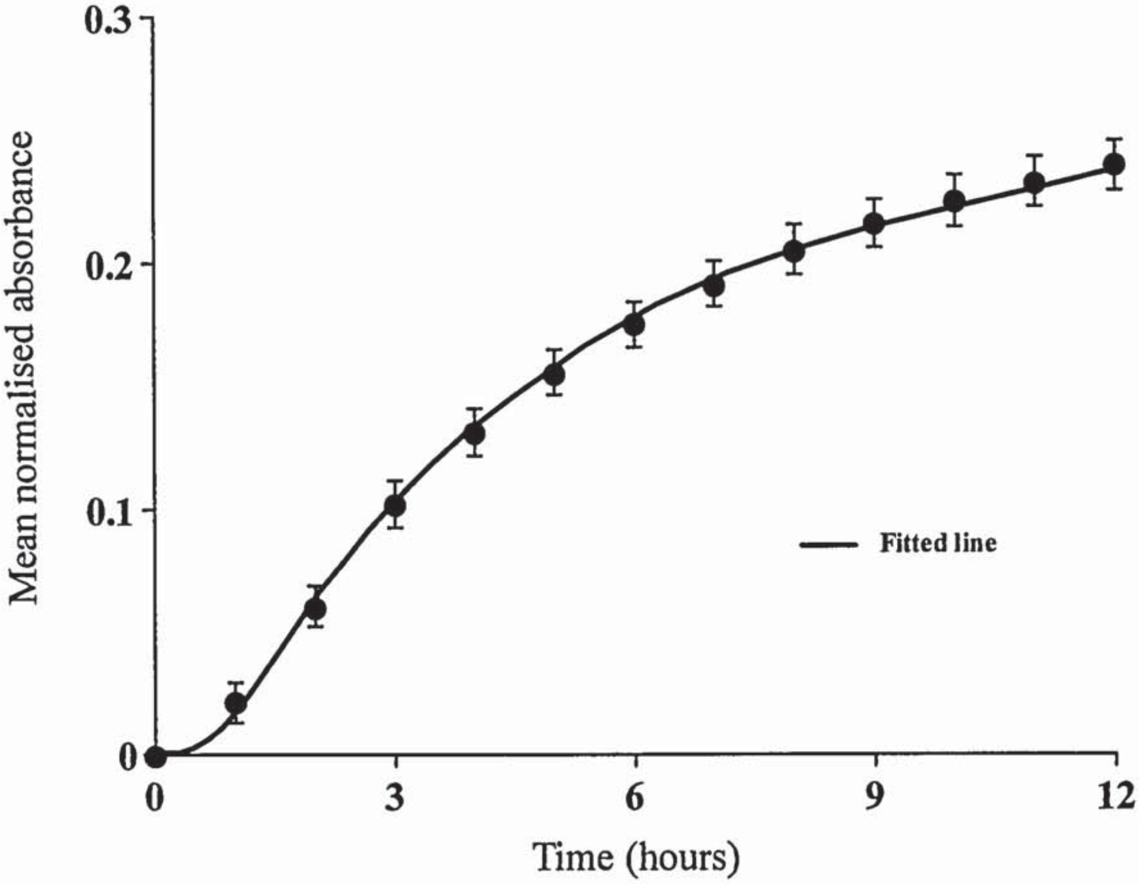

Figure 2.13 Diffusion of 4-cyanophenol across silicone membrane (mean ± sem)

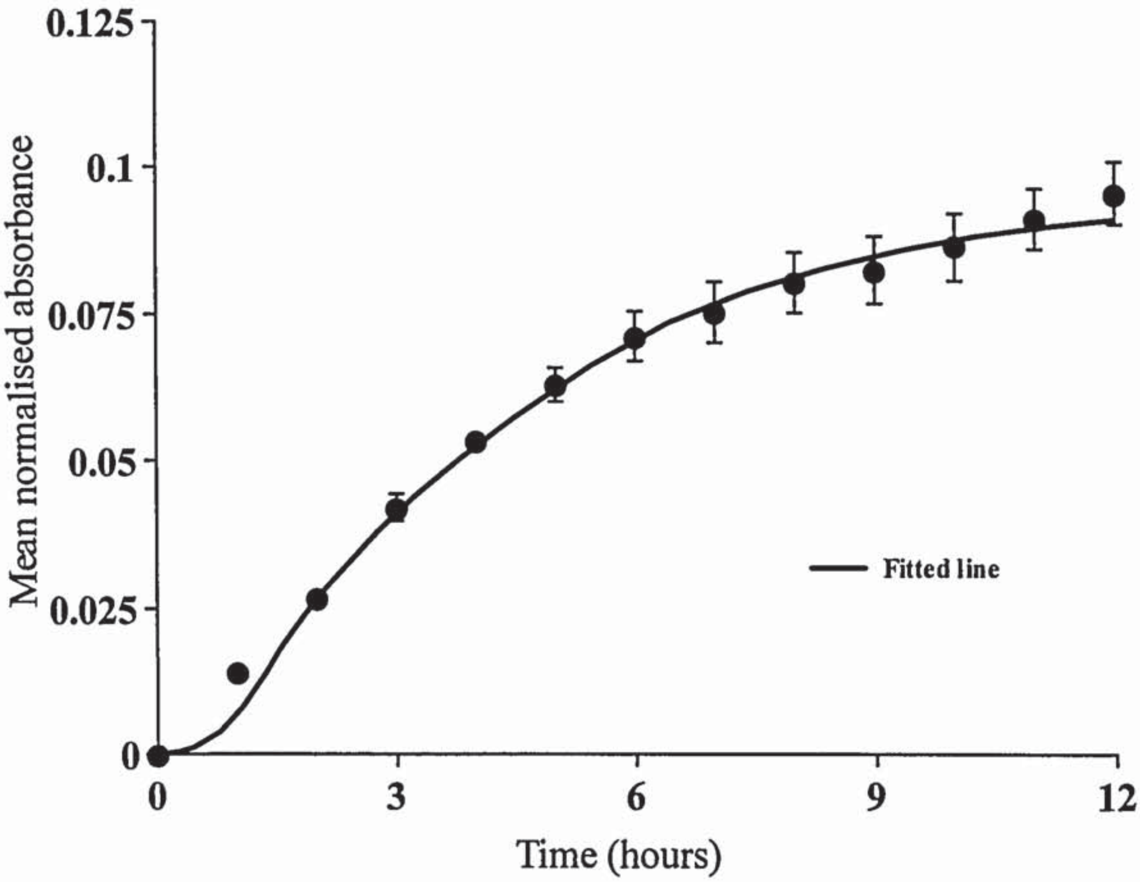

Figure 2.14 Diffusion of Hydroxythiophenol across silicone membrane (mean±sem)

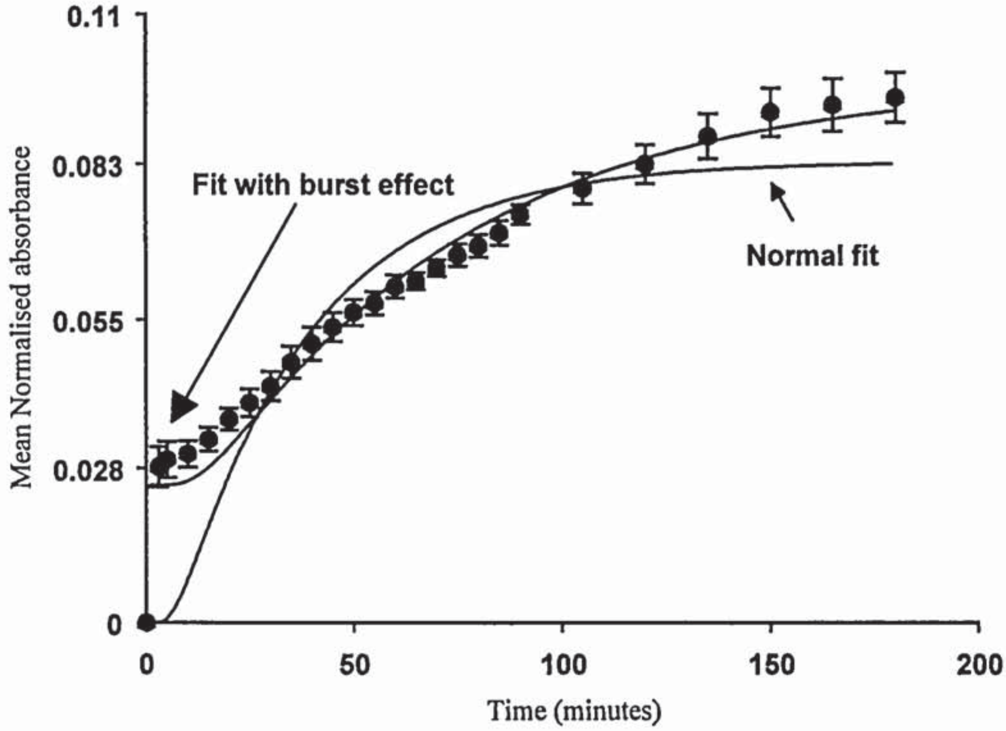

Figure 2.15 Diffusion of 1-octyne across silicone membrane (mean ± sem)

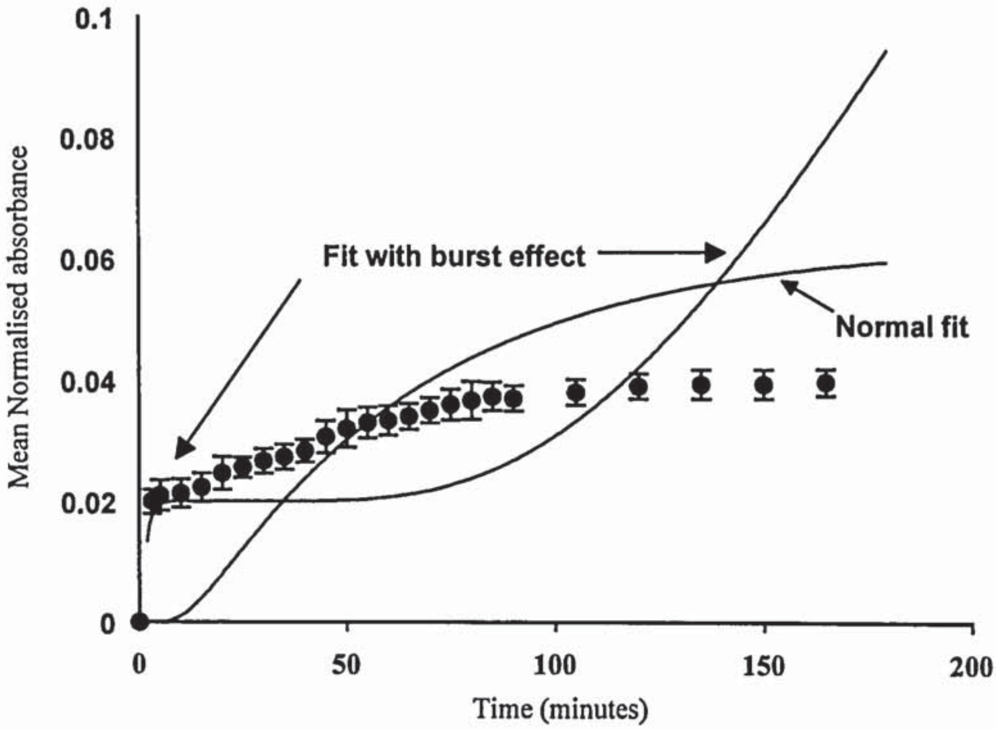

Figure 2.16 Diffusion of heptanitrile across silicone membrane (mean ± sem)

Table 2.4 Diffusion parameters of different IR labeled compounds determined across silicone membrane (300μm thick) using ATR-FTIR.

Compound	$\frac{D}{h^2}$ (h^{-1})	A_0	Lag time (mins)	Correlation coefficient (model v data)
Cyanophenol	0.100 ± 0.006	0.252 ± 0.008	100	0.999
Hydroxy-thiophenol	0.113 ± 0.011	0.095 ± 0.009	88	0.995
Heptanonitrile	1.200 ± 0.358 0.039 ± 0.008*	0.043 ± 0.006 0.944 ± 0.551*	8.3	0.694 0.772*
Octyne	0.783 ± 0.084 0.382 ± 0.034*	0.084 ± 0.004 0.073 ± 0.004*	12.8	0.931 0.973*

* Alternative fit including burst component. Values are the mean ± sem of three determinations.

2.8 SUMMARY

This chapter has developed and optimised a spectroscopic method to analyse the diffusion of topically applied compounds into synthetic membranes and determine diffusion parameters. The technique depends on selecting test permeants which must exhibit infrared absorption bands that do not interfere with inherent membrane IR absorption bands.

Considering the model compounds tested, it was found that relevant bonds in each compound absorbed to varying intensities. Hence, direct comparisons of spectroscopically determined diffusion coefficients for different compounds are not possible. However, the possibility of determining parameters such as diffusion coefficient (D/h^2) and permeant membrane solubility (A_O) for a given topically applied compound from a range of formulations does exist. Comparisons of such data as a function of formulation type, may potentially give insights into the interplay between formulation components during percutaneous diffusion.

The next two chapters will develop this theme and analyse the diffusion of cyanophenol from a range of formulations (consisting of cyanophenol, different transdermal enhancers and vehicles) across silicone membrane and human stratum corneum using ATR-FTIR.

CHAPTER THREE

SOLUTE PENTRATION INTO SILICONE MEMBRANE AS A FUNCTION OF FORMULATION APPLIED

3.1 INTRODUCTION

This chapter uses the method developed in chapter 2 to assess the diffusion of a model molecule (4-cyanophenol) from a series of topical formulations across a synthetic membrane. An artificial model membrane consisting of a dimethylpolysiloxane polymer was chosen. Permeant solubility in each formulation and permeant partitioning from each enhancer/vehicle formulation into silicone membrane was determined to investigate correlations between permeant physicochemical properties and ATR-FTIR determined diffusion parameters.

3.2 USE OF SYNTHETIC MEMBRANES

The use of synthetic membranes in transdermal studies has a number of advantages for example, they provide less time-consuming, less expensive and less morally objectionable alternatives to carrying out experiments on living animals (Houk and Guy, 1988). They can be readily handled allowing rapid determination of drug flux by sandwiching them between simple two compartment Franz type diffusion cells (Walkow and McGinty, 1987a and b). The flux values give an indication of the level and magnitude of drug transported and thus therapeutic bioavailability. Such data can be used to determine, for example, the concentration of donor solutions/suspensions applied to skin tissue, thus optimising experimental parameters and lowering the chance of wasting skin tissue. In essence, results from experiments using such membranes can be used to estimate a molecules potential toxic or therapeutic availability based solely on its physicochemical properties or on its behaviour in the model system (Houk and Guy, 1988).

Further, supplies of such membranes are not limited to the extent that fresh skin tissue is. Often, obtaining a steady supply of fresh skin samples for *in vitro* work is difficult since it generally relies on goodwill on the part of the surgeon and/or hospital. Skin obtained from the surgical removal of breast or abdomen tissue is the most common source for experimental tissue. However, its supply is often not consistent and operations are prone to cancellation, thus often the time spent preparing samples and the related costs are wasted. Further, immediate use or careful storage in a well monitored freezer is essential if not using skin samples immediately (Wester *et al.*, 1998) and then frozen samples needing to be used within three months of freezing.

The development of models is important in comprehending complicated biological processes. Well designed models may allow isolation and examination of individual component processes, for example, simultaneously detecting the diffusion of a series of penetrants across a membrane.

3.2.1 Types of synthetic membranes

Synthetic membranes have been employed to analyse the potential transdermal transport of a wide range of therapeutic entities (Li *et al.*, 1997; Maitani *et al.*, 1995; Walkow and McGinity, 1987b; Yamaguchi, 1997). Such barriers to diffusion have taken the form of egg shells (Walkow and McGinty, 1987a), composite or laminate type sheets (Walkow and McGinty, 1987a; Yamaguchi, 1997; Yuk *et al.*, 1995), zeolites (rigid three dimensional aluminosilicates) which are characterised by having 50% of their volume filled with water (Dyer *et al.*, 1979) and dimethylpolysiloxane or silicone rubber sheets (Garrett and Chemburkar, 1968). The following studies highlight the successful use of silicone membranes during investigations of percutaneous absorptions.

3.2.2 Studies using silicone membranes

Silicone membrane was first used to create a barrier to diffusion of molecules in 1968 (Garrett and Chemburkar, 1968). It was shown to be non-porous and having a higher permeability to neutral rather than ionic species. Following this study, other investigators have utilised its lipophilic nature to assess how molecules of interest may diffuse across lipophilic domains of stratum corneum (Scheuplein and Bronaugh, 1983) in the absence of aqueous regions.

Silicone membranes have served as model membrane in the analysis of *p*-aminobenzoate esters (Flynn and Yalkowsky, 1972; Scheuplein and Bronaugh, 1983), benzocaine (Di Colo *et al.*, 1980) (Botarri *et al.*, 1979) (Botarri *et al.*, 1978; Scheuplein and Bronaugh, 1983)butamben (Juni *et al.*, 1979), chlorpromazine (Bottari *et al.*, 1974), salicylic acid (Bottari *et al.*, 1974; Nakano and Pater, 1970) and steroidal compounds (Friedman *et al.*, 1980; Kincl *et al.*, 1968). Such membranes have been employed, both in Franz-type cells and ATR-FTIR experiments, to shed light on diffusion processes that occur and contribute to drug transport.

3.2.2.1 Diffusion cells

Maitani *et al* (Maitani *et al.*, 1995) have studied the effect ethanol, which is used in topical formulations as both an enhancer and a solvent, has on the true diffusion coefficient of diclofenac (DH) and its sodium salt (DNa) in silicone membrane. Ethanol is reported to influence the transport of several compounds (Knutson *et al.*, 1989; Kurihara *et al.*, 1990) by chemically altering skin structure; its effects are enhanced by increasing its concentration in applied formulations. Maitani *et al* aimed to determine if this phenomenon also occurred in silicone membranes. They were of the opinion that the use of silicone membrane would more easily show ethanol-induced membrane changes when compared to stratum cornuem. They showed that, generally, increasing donor ethanol concentration elevated flux of the hydrophobic DH but had little effect on the hydrophilic DNa.

A study by Lee *et al* (Lee *et al.*, 1987) investigated the permeation of sodium salicylate and sodium warfarin across a dense hydrophobic membrane (composed of a polydimethylsiloxane polymer) from a series of different vehicles with a view to improving the delivery of ionic drugs. Each compound was applied to silicone membranes (sandwiched in diffusion cells) in either an aqueous, ethanol or dioxane/2% DMSO vehicle. Results showed very little flux from the aqueous vehicle but significantly greater flux was achieved from the non-aqueous formulations. The authors state that silicone membrane is predominantly lipophilic in nature. Bearing this in mind, diffusion of the salicylate ion from an aqueous solution is hindered since an aqueous transport pathway is not present. However, the model drugs when applied in a non-aqueous media were able to form ion pairs. Subsequently these neutral species were able to permeate across or partition into the membrane due to their relative greater lipophilicity. Ion pair formation was characterised by NMR. The paper concluded that the delivery of ionic drug salts can be improved by their lipophilisation in non-aqueous formulations.

Megrab *et al* (Megrab *et al.*, 1995a) have also used silicone membrane to predict transdermal drug delivery. One study examined the effect of supersaturation on oestradiol (OE) flux from solutions having different degrees of saturation (Megrab *et al.*, 1995b). The authors chose silicone membrane based on the knowledge that it would be easier to interpret drug permeation characteristics (from often unstable supersaturated solutions) through a simple inert membrane than through a heterogeneous and variable membrane such as skin. The silastic membrane was acknowledged as being lipophilic in nature and this was further enhanced by immersing membranes in isopropyl myristate (IPM) for an hour before performing diffusion cell experiments. Pretreatment with IPM resulted in an 18.5 fold increase of OE flux from a 60% w/w propylene glycol application when compared to untreated silicone membrane. The study goes onto report a positive linear relationship existing between the degree of solution saturation with OE and measured flux. This effect proved (a) silicone membrane to be rate-limiting and (b) was due to increases in permeant thermodynamic activity. Finally the study tested whether the Higuchi assumption (Higuchi, 1960) applied to their formulations of OE in propylene glycol and water. The assumption states that provided OE is incorporated into formulations that are saturated with the drug then flux arising from each preparation should be identical since each formulation has the same thermodynamic activity. The experiment involved the preparation of a series of OE saturated in propylene glycol/water co-solvent systems from which flux across silicone membrane was determined. The results showed flux to increase with increasing PG concentration. Obviously this finding contradicted the Higuchi assumption. The authors attributed this effect to PG being able to penetrate the silicone membrane and thus altering its structure in such a way to enhance flux. Similar solvent effects were noted by Flynn and Smith (Flynn and Smith, 1972).

Another study reported that the application of alcohols to silicone membranes resulted in the formation of simultaneous hydrogen bonds between alcohol molecules and oxygen atoms in the polysiloxane backbone making up the silicone membrane, and perhaps also nonpolar interactions with polymer side-chains (Twist and Zatz, 1988). Therefore, in the oestradiol study mentioned above, the non-ideal behaviour reported, may be a consequence of propylene glycol diffusion into the membrane; PG possibly extracting membrane constituents (such as cross-linking agents) and creating pores. These pores are then filled with the solvent and hence flux is seen to have increased as solvent influx increases membrane permeability of oestradiol.

3.2.2.2 ATR-FTIR

Watkinson *et al* (Watkinson *et al.*, 1994a) have employed ATR-FTIR spectroscopy with a view to assessing the permeability of silicone membrane by applying acetonitrile and a 10%w/v solution (in propylene glycol) of 4-CP to it. Both model compounds possessed a cyano functional group, which allowed analysis of their build up in silicone membrane when placed on an infrared element. The reproducibility of their method was determined by analysing the rapid diffusion of acetonitrile across the membrane and found to be excellent. The experimental data consisting of a time-series of cyano peak area measurements was fitted to their diffusional model, based on a solution to Fick's second law of diffusion, and yielded a good fit.

However, experimental data obtained from the analysis of 4-CP diffusion (in propylene glycol) did not produce a satisfactory plateau (corresponding with membrane saturation by 4-CP) and thus the resulting fit was not so good. This, as the authors suggested, was caused by changes in membrane refractive index bought on by influx of solvent and solute. Any increase in membrane refractive index would result in an increase in the depth of penetration of the IR beam entering the silicone membrane (see equation 2.9 in chapter 2) and thus the depth to which permeants are detected in the membrane would alter during the time course of the experiment. This would explain why there was an absence of a plateau in their graphical analysis. To overcome this effect, the group normalised the permeant cyano signal with an inherent membrane signal attributed to the Si-O peak found in silastic membrane at ~3000cm^{-1}. The experimental data after this procedure yielded a better fit. The study concluded by stating that ATR-FTIR is a useful tool for the detailed investigation of membrane permeation phenomena.

3.2.2.3 Diffusion cells and ATR-FTIR

A number of studies have been published that have examined both permeant diffusion behaviour in membranes and gross flux of permeants by using ATR-FTIR spectroscopic and conventional diffusion cell methodology respectively.

Watkinson *et al* have shown that partition (P) and diffusion (D) coefficients that form part of the permeability coefficient (k_P) expression (see equation 1.5, page 30) can be separately determined (Watkinson *et al.*, 1994b). This is only possible however, in synthetic membranes where the diffusional pathlength or membrane thickness is known.

Firstly, the diffusion coefficient is determined from ATR-FTIR spectroscopic analysis using a solution to Fick's second law of diffusion. This parameter is then inserted into an algebraic expression defining diffusion in a plane sheet (Crank, 1975; Pellet *et al.*, 1997b) which fits a value for the partition coefficient (P) to experimental data derived from diffusion cells. This procedure thus gives a value for the partition coefficient of your test permeant.

In a further study, Pellet *et al* (Pellet *et al.*, 1997a) compared permeability data derived from diffusion cells with that from ATR-FTIR spectroscopic determinations. Pellet found flux and permeability coefficients for CP in a silicone membrane (previously saturated with water), determined by spectroscopic and diffusion cell means, to be in close agreement. However, the permeability parameter differed between the two methods when determined across untreated membranes. This difference was put down to the fact that the only membrane that truly represented an unsaturated membrane was that placed untreated onto the ATR crystal; the untreated membrane in the diffusion cell was thought to have become rapidly hydrated to the same extent as the aqueous pre-saturated membranes. Pellet's overall conclusion, that parameters determined from these two different techniques are in close agreement, seems to hold since the graphs in the paper show that the untreated membrane was only on the crystal for approximately 150 minutes. This is too short a time for complete membrane hydration to have occurred.

3.3 AIMS OF CHAPTER

3.3.1 Physicochemical factors

Studies in this chapter aim to investigate possible correlations between permeant diffusion, for example, values determined for pathlength normalised diffusion coefficient (D/h^2) and membrane solubility (A_{CP}), and physicochemical factors such as the permeant's partition coefficient and solubility in the formulation applied. It has been reported that the relative lipid-water solubility, or apparent partition coefficient, of a drug is an important physical property in determining the rate of penetration through synthetic and biological membrane barriers (Walkow and McGinity, 1987a). The partition coefficient can also provide a measure of a compounds hydrophilic and lipophilic properties and its affinity for the vehicle and the membrane barrier. Several *in vitro* diffusion studies (Bronaugh *et al.*, 1981; Flynn and Yalkowsky, 1972) have investigated the influence of partition coefficient on *in vitro* drug permeability.

3.3.2 Determination of enhancer penetration

This chapter also aims to utilise the ATR-FTIR method described in chapter 2 to determine the diffusional characteristics of concurrently applied topical permeants from multi-constituent formulations in silicone membrane. In particular, it was envisaged that the diffusion or partition of the known transdermal enhancer, oleic acid, could be monitored in silicone membrane by incorporating into the molecule an azido group (Baker *et al.*, 1990) which was capable of absorbing infrared radiation but at the same time did not interfere with infrared peak exhibited by CP. The azido group should absorb at 2100cm^{-1} (Figure 3.1) whilst the cyano group in CP absorbs at 2230cm^{-1}.

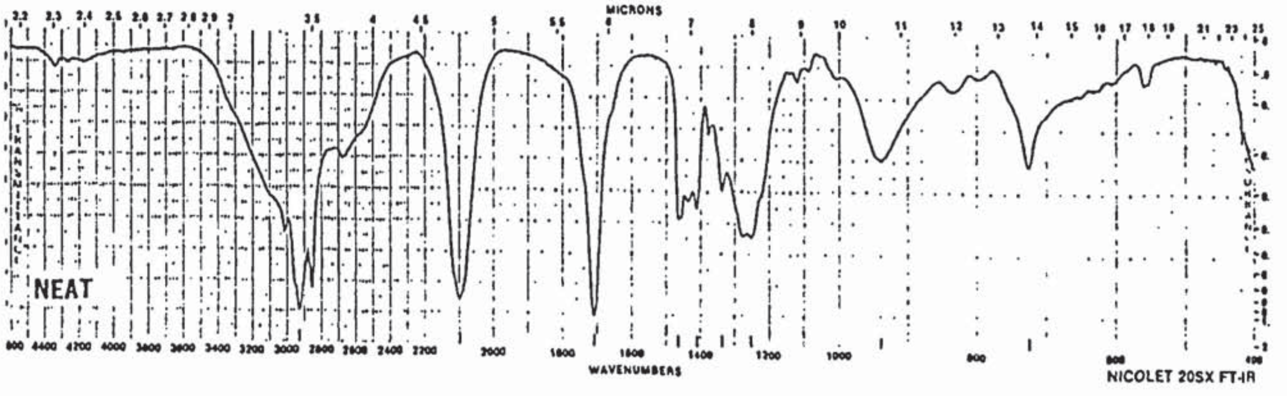

Figure 3.1 FT-IR spectrum of 12-azidooleic acid

3.4 MATERIALS AND METHODS

3.4.1 Materials

The permeant 4-cyanophenol (CP) was purchased from Lancaster Chemicals, UK Test enhancers oleic acid (OA),12-Azidooleic acid (AOA) and the solvent propylene glycol (PG) were obtained from Sigma (Poole, UK). The enhancer Azone® was acquired from Whitby Research (U.S.A).

3.4.2 Preparation of formulations

A series of test formulations (10ml) consisting of 5% v/v enhancer in propylene glycol were prepared. The enhancers were Azone®, oleic acid or 12-azidooleic acid. To each enhancer/vehicle mixture and to 10ml of neat propylene glycol and 10ml of distilled water excess quantities (10g) of CP were added. These mixtures were continuously stirred at room temperature for 48 hours at 400rpm.

3.4.3 Preparation of silicone membranes

Silicone membrane sheets having a thickness of 0.3mm were obtained from Samco (Cambridge, UK). These were used as received, cut to size, rinsed in double distilled water and then blotted dry using lens wipe tissue. The membranes were then mounted onto the IRE.

3.4.4 ATR-FTIR measurements

To produce saturated solutions, aliquots (1ml) of the above CP/enhancer/vehicle mixtures were extracted using a pipette and filtered through 0.2μm Acrodisc® PF syringe filters (Pall Gelman Labs, UK.) before pipetteing directly onto silicone membrane mounted on the ATR-FTIR crystal (see Figure 3.2). A small excess of CP was added to the solution in contact with the membrane to ensure the maintenance of a saturated system. The appearance of CP and 12-AOA (detected by virtue of cyano and azido peaks respectively) at the membrane-crystal interface was then monitored using spectrometer settings as described in section 2.6.4, for a period of twelve hours. Each different formulation was applied to a minimum of three silicone membrane samples. Spectra were evaluated by determining the integrated absorbance of selected peaks. The regions of interest for CP and AOA were between 2200-2250 (cyano peak) and 2150-2030 cm^{-1} (azido peak) respectively; each peak area being normalised to the Si-Me peak found in silicone membrane at 1280 cm^{-1}.

3.4.5 Determination of CP solubility in enhancer/vehicle formulations

The solubility of CP in each formulation was determined in triplicate as follows. Excess quantities (10g) of CP were added to 5% v/v enhancer/propylene glycol formulations (10ml) and continuously stirred for periods of 24 and 48 hours at room temperature (21±1°C). Each mixture was then left to stand for 2 hours and then 1ml aliquots of the supernatant fluid withdrawn and filtered through 0.2μm syringe filters (Acrodisc® PF, UK). Each sample was then diluted appropriately and 200μl mixed with 200μl of 0.5mg/ml propyl parabens (in PG), the latter acting as an HPLC internal standard. CP solubilities were determined by HPLC analysis using a Waters 600E system controller (UK) and a Waters 484 Tuneable absorbance detector set at λ_{MAX} 284nm. The samples were separated on a 10cm reversed phase ODS II column (Jones, UK) using a mobile phase consisting of 35% acetonitrile and 65% water (both HPLC grade, Sigma, Poole, UK) at a flow rate of 1ml/ min. The retention times for CP and internal standard were approximately 4 and 8 minutes respectively.

3.4.6 Determination of membrane partition coefficients

Partition coefficients of CP between enhancer/vehicle formulations and silicone membrane were determined using the method outlined by Leo *et al* (Leo *et al.*, 1971). Silicone membranes having a thickness of 300μm (Samco, UK) were rinsed in distilled water, dried using lens wipe tissue and cut to a size such that each piece weighed approximately 0.5g. One piece of membrane was then inserted into a plastic centrifuge tube (Corning costar, USA) using a pair of forceps and 5g of formulation pipetted into each tube. All formulations consisted of CP (20mg/ml) and 5% v/v enhancer (either Azone®, oleic acid or 12-AOA) in a propylene glycol vehicle. Partitioning of CP from a neat PG vehicle into silicone membrane was also determined. All sample tubes were fitted with screw on tops and mechanically shaken for a period of 12 hours at room temperature. Sample tubes without membranes containing only CP/enhancer/vehicle formulations behaved as controls, to determine if CP was being absorbed by the walls of the plastic centrifuge tubes. After 24 hours, 1ml of the enhancer mixture was removed from the centrifuge tubes using a pipette, and mixed with 1ml of internal standard (0.5mg/ml propyl parabens/PG) and the CP concentration determined by HPLC using the method outlined above. The concentration in the silicone membrane was then obtained by difference. The CP partition coefficient between formulation and membrane was then calculated using the overpage.

$$P = \frac{\text{mass of solute per g of membrane}}{\text{mass of solute per g of formulation}} \qquad (3.1)$$

3.4.7 Statistical analysis

Experimental data relating to CP diffusion across silicone membrane ($n \geq 3$) following the application of different formulations, was fitted to equation 2.14 (see section 2.6.9 in chapter 2) using a non-linear least squares regression program (FigP; Biosoft, UK). Student t-tests were carried out to determine if significant differences existed between fitted D/h^2 and A_o values resulting from the computer fits.

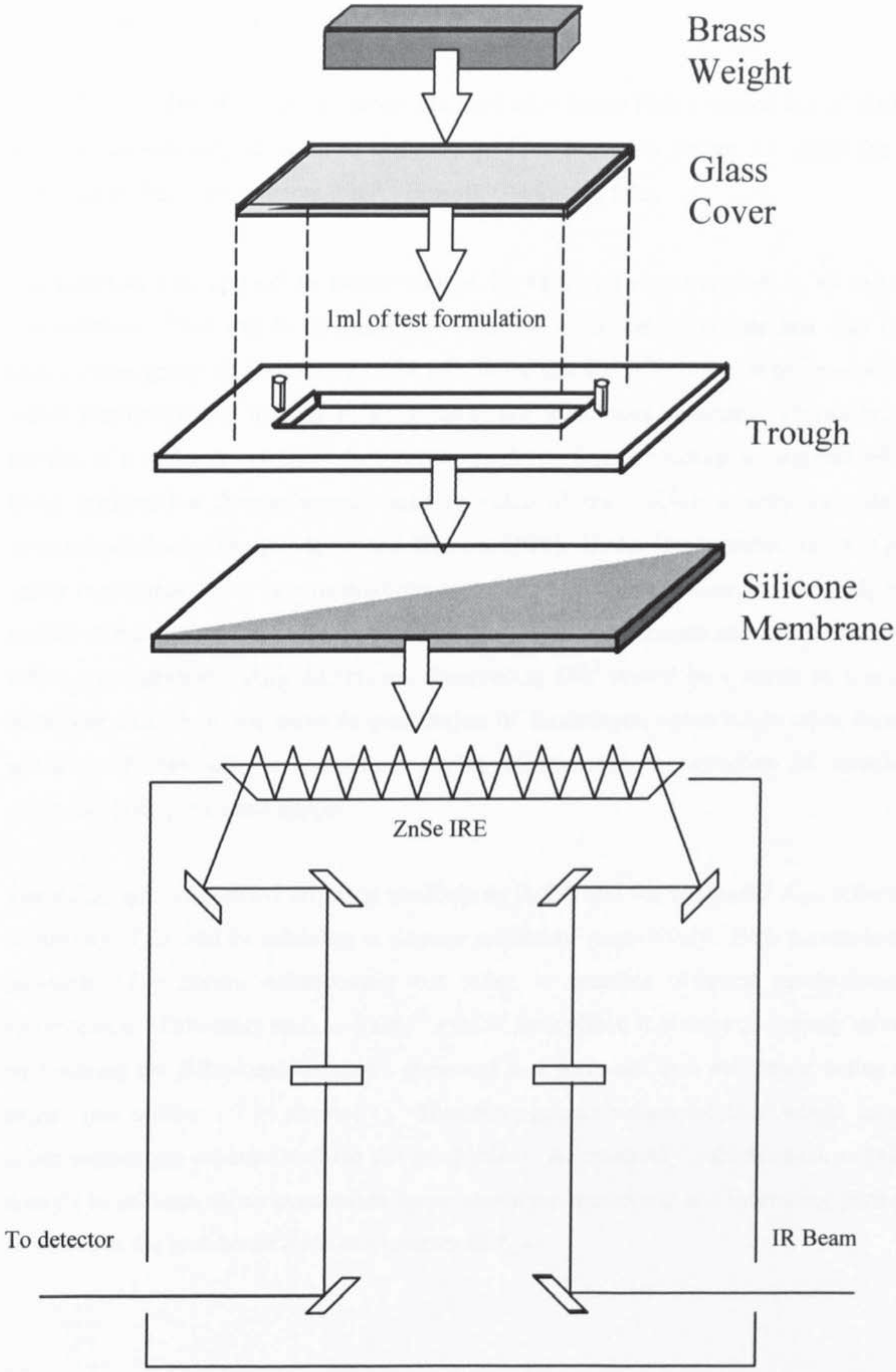

Figure 3.2 Set-up used in ATR-FTIR experiments

3.5 RESULTS AND DISCUSSION

Table 3.1 lists the diffusion parameters obtained after fitting Fick's second law of diffusion to the experimentally determined diffusion profiles shown in Figure 3.3 using the non-linear curve fitting programme, FigP, (Biosoft, Cambridge UK).

Cyanophenol was applied to membranes at its saturated concentration in all enhancer formulations. This was to optimise absorption into silicone membrane and thus obtain strong cyano group IR absorbance in the membrane and secondly it was to try to ensure that solute thermodynamic activity in all formulations tested was constant. Thermodynamic activity of a molecule relates to its escaping tendency from a mixture, a saturated solution being attributed a thermodynamic activity value of one, which is only exceeded by supersaturated solutions (Hadgraft and Walters, 1995). Under ideal conditions, for a given solute incorporated into various mixtures at its saturated concentration, its thermodynamic activity and therefore its rate of penetration (D/h^2) would be constant and independent of its solute concentration. Any differences observed in D/h^2 would be a result of non-ideal behaviour caused by for example penetration of formulation constituents other than the solute itself into silicone membrane during experiments or extraction of membrane components by permeants applied.

The pathlength normalised diffusion coefficients (D/h^2) and the parameter A_{CP}, reflect the diffusivity of CP and its solubility in silicone membrane respectively. Both parameters are measures of permeant enhancement but relate to possible different mechanisms of enhancement. Enhancers such as Azone® exhibit their effect, it is most commonly thought, by lowering the diffusional resistance presented to a permeant by a membrane acting as a barrier (see section 1.7 in chapter 1). Therefore, greater values for D/h^2 would indicate solute permeation enhancement *via* this mechanism. Alternatively, vehicles such as PG are thought to enhance solute penetration by penetrating a membrane and increasing permeant solubility in the membrane (seen as increases in A_{CP}).

Table 3.1 ATR-FTIR-determined diffusion parameters for CP as a function of co-administered enhancer and vehicle.

Enhancer/vehicle formulation	$\frac{D}{h^2}$ (h^{-1})	Lag time (min)	A_{CP}
Azone®/PG	0.110 ± 0.006 (1.25)	91	0.290 ± 0.002 (3.92)
PG only	0.100 ± 0.007 (1.14)	100	0.252 ± 0.008 (3.41)
AOA/PG	0.084 ± 0.006 (0.94)	120	0.259 ± 0.003 (3.5)
Oleic acid/PG	0.073 ± 0.004 (0.83)	137	0.256 ± 0.007 (3.46)
Water only	0.088 ± 0.01	114	0.074 ± 0.003

D/h^2 = pathlength normalised diffusion coefficient

A_{CP} = membrane saturated plateau level

Enhancement ratio (in brackets) = (diffusional parameter from enhancer formulation/diffusional parameter from aqueous formulation)

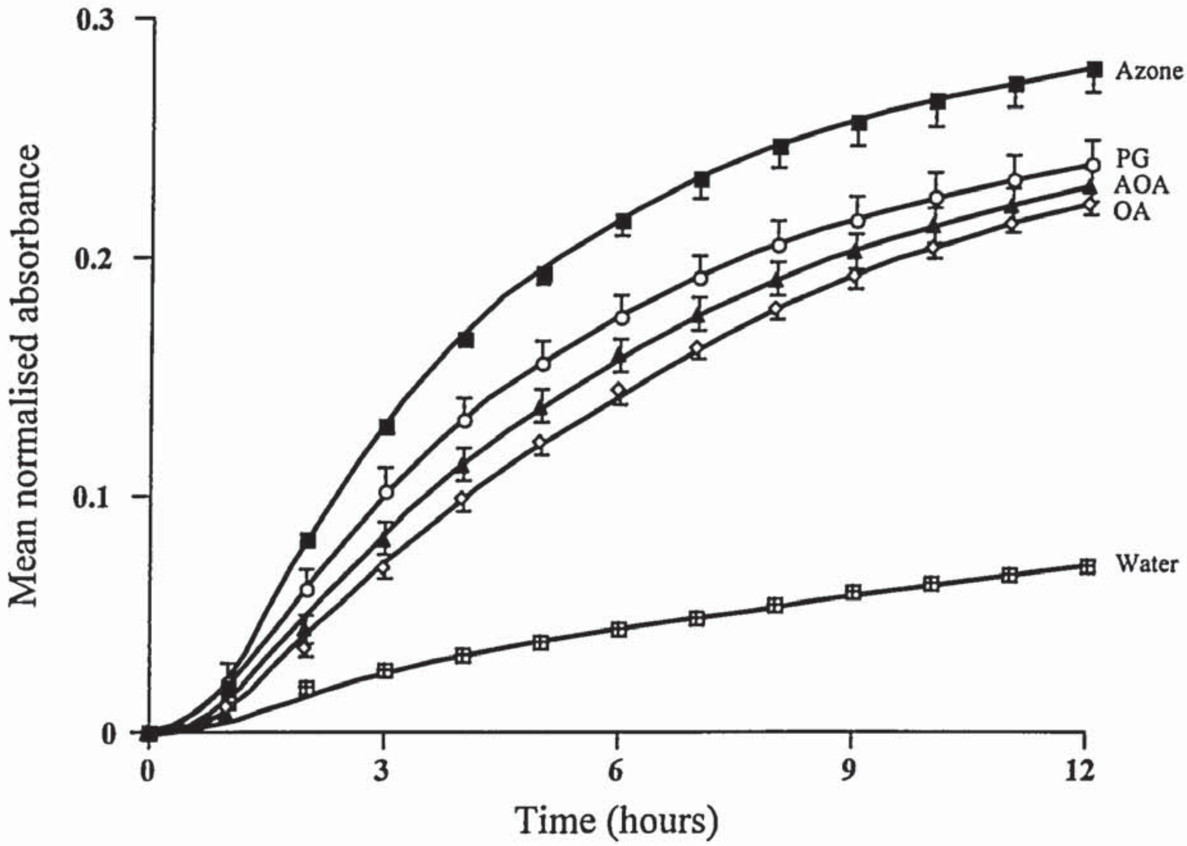

Figure 3.3 ATR-FTIR spectroscopically determined diffusion profiles showing build up of CP at the membrane/crystal interface as a function of topically applied enhancer/vehicle formulations(mean ± sem).

From table 3.1, it is evident that CP diffusivity is dependent on the enhancer formulation applied. There was no significant difference in CP diffusivity (D/h^2) between Azone®/PG and neat PG (t test, $P>0.05$) indicating a lack of synergistic activity between enhancer and vehicle. However, D/h^2 from these formulations was significantly greater when compared to the other enhancer treated membranes. Cyanophenol diffusivity from OA/PG was significantly lower (t test, $P<0.05$) when compared to other tested formulations. Cyanophenol diffusion from a simple aqueous suspension was found to be greater than that from formulations containing OA and AOA. This would suggest that CP might also diffuse across silicone membrane *via* an aqueous diffusional pathway resulting from ingress of water into the membrane. Further, it has been shown previously (Pellet *et al.*, 1995) that water can diffuse and saturate silicone membrane of a similar thickness within three hours of application. The membranes used in these experiments remained in contact with water for 12-hour periods, making it probable that CP diffusion into membranes was facilitated from an aqueous suspension by concurrent membrane hydration.

The other diffusional parameter listed in table 3.1 is A_{CP}, reflecting permeant solubility in silicone membrane. Again, it is evident that this parameter is dependent on the formulation applied.

A_{CP} from neat PG was greater (0.252 ± 0.008) than that determined from the aqueous CP formulation (0.074 ± 0.003). Of more interest would be the affect the co-administered enhancers have on A_{CP}. Plateau (A_{CP}) values obtained from all formulations tested were significantly greater than that observed from the aqueous control (t test, $P<0.05$). A_{CP} values determined from Azone®/PG was found to be significantly greater than from other enhancer/PG formulations. There was no difference in A_{CP} from OA/PG, neat PG and AOA/PG formulations indicating that these enhancers did not contribute to the magnitude of A_{CP}.

The partitioning of CP from test enhancer formulations into silicone membrane was determined (logP) as well as CP solubility in each formulation in an attempt to determine if any relationship existed between these physicochemical properties and CP diffusional parameters determined from ATR-FTIR experiments. Cyanophenol concentrations were determined by HPLC. Figure 3.4 shows a typical HPLC trace obtained under the HPLC parameters listed (Kirkland, 1971).

Since A_{CP} is related to the extent of CP partitioning into membranes from formulations applied, its partition coefficient (logP) between treatments applied and the membrane was determined separately experimentally. Table 3.2 shows the results obtained along with log octanol/water partition coefficients for enhancers present in each formulation.

The log of the partition coefficient, logP, is a constant and refers to a single molecular species partitioning between two phases; in this case the two phases are the formulation applied containing cyanophenol and the silicone membrane. The table shows that LogP values for cyanophenol determined from each formulation were significantly different ($P<0.05$). Plastic centrifuge tubes used during logP determinations were found to absorb a small quantity of cyanophenol and therefore, all values were corrected for this. CP partitioning into silicone membrane was greatest from the Azone®/PG formulation, followed by AOA/PG, OA/PG, Neat PG and aqueous applications. The data in the table suggest that enhancer present in the formulation applied is penetrating the lipophilic silicone membrane and enhancing CP partitioning into it when compared to the neat PG control in the order Azone®>AOA>OA>PG. Relative enhancer penetration into lipophilic domains can also be determined by assessing their $\log_{(\text{octanol:water})}$ partition coefficients. Table 3.2 also lists these values for each enhancer.

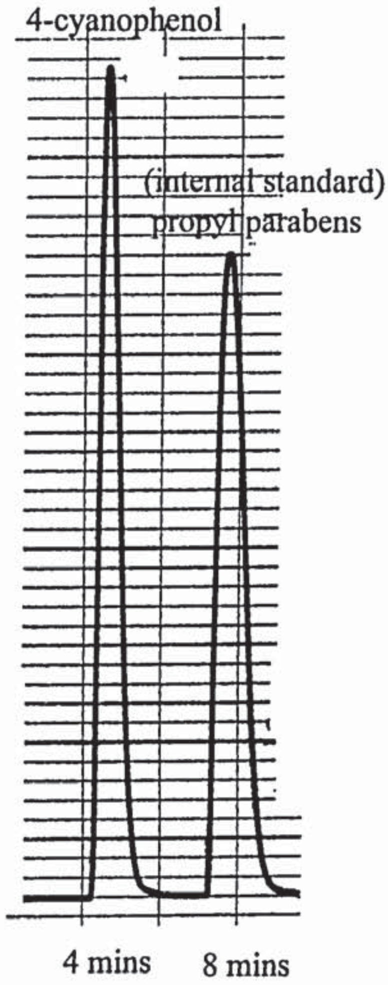

Efficiency and charactersistics of HPLC method.

Parameter	Description	Calculated value	Acceptable range
K'	Capacity factor (Retention factor)	3	1 - 10
N	Column efficiency	4000	2500 - 10000
R_S	Peak resolution	5	>1
H	Column efficency	25μm	25 - 100μm

Figure 3.4 Example HPLC chromatogram of CP and propyl parabens (internal standard). Loop size: 20μl; sensitivity: 0.500AUFS; flow rate: 1ml/min; chart speed: 0.25cm/min.

Table 3.2 LogP values for cyanophenol between 5% enhancer/PG vehicles and silicone membrane at room temperature

Enhancer formulation	A_{CP}	Log P (± sem)	Enhancer log $_{oct/water}$ partition coefficient
Water only	0.074 ± 0.003	-0.90± 0.06	N/A
Neat PG	0.252 ± 0.008	0.59 ± 0.06	-1.34 ± 0.21[a]
OA/PG	0.256 ± 0.007	1.04 ± 0.05	4.5[b]
AOA/PG	0.259 ± 0.003	1.21 ± 0.04	5.46 ± 0.26[a]
Azone®/PG	0.290 ± 0.002	1.35 ± 0.06	6.0[b]

[a]calculated value using ACD/logP version 1.0 software (ACD labs, Toronto, Canada)

[b]from (Kalia and Guy, 1997)

It is possible that enhancers are partitioning into octanol in the order Azone>AOA>OA>PG which is an identical trend to that mentioned above for CP partitioning from enhancer formulations, suggesting further that the enhancers present in the formulation are penetrating silicone membrane to varying extents and affecting CP partitioning. It is clear that the greater the enhancer log $_{(octanol:water)}$ partition coefficient, the greater the partitioning of CP into silicone membrane.

There is partial correlation between the experimentally determined cyanophenol logP values and A_{CP}. The highest plateau value (from Azone®/PG) and the lowest (from the aqueous formulation) correlates with the highest logP value experimentally determined (1.35) and the lowest value (-0.90±0.04) respectively. Cyanophenol partitioning from OA/PG into silicone membrane was lower than that observed from Azone®/PG:silicone membrane which correlated with a lower A_{CP}. However, A_{CP} values from OA/PG, neat PG and AOA/PG were not significantly different (P>0.05) whilst corresponding logP values were.

The differences between A_{CP} and membrane partition coefficients listed above may also be explained due to differences in experimental conditions. During logP determinations the formulations and membrane were constantly shaken for 12 hours whilst during the ATR experiments the donor phases were not mechanically agitated. This may have resulted in enhancers partitioning more effectively during logP determinations. Secondly, the A_{CP} value is affected by changes in membrane refractive index (RI) which may be increased or decreased during the course of an experiment due to permeant membrane penetration. Since Figure 3.3 shows that a "perfect" plateau had not been reached after 12 hours, it is likely that the membrane RI was increased; such an affect as dictated by equation 2.9 (section 2.4.2 in chapter 2) would increase the depth of the IR beam into silicone membrane, bringing a greater number of penetrating molecules into contact with it (leading to a greater beam attenuation and stronger absorption) and therefore delaying or preventing the establishment of a plateau. This phenomenon would also then affect comparisons between A_{CP} and logP.

Cyanophenol concentration in the formulations applied may have affected the diffusional parameters obtained. Table 3.3 lists cyanophenol concentration in each enhancer/vehicle formulation. Cyanophenol solubility in each formulation was determined in triplicate separately after 24 and 48-hour periods. This was to ensure that the viscous formulations had been stirred adequately to produce truly saturated solutions. The formulation solubilities for CP in Table 3.3 show that for each type of application, saturation had been achieved after 24 hours; saturated solubilities determined after 48 hours were not significantly different (P>0.05) when compared to solubilities determined after 24 hours for each formulation type.

Table 3.3 Cyanophenol solubility (mg/ml) in test 5% enhancer/PG vehicles determined after 24 and 48 hours

Enhancer Formulation	24 hours	48 hours
Water only	15.06 ± 0.12	15.10 ± 0.12
Oleic acid/ PG	787.33 ± 14.81	806.67 ± 13.54
12-AOA/PG	915. 67 ± 8.55	920.20 ± 2.90
Azone®/PG	968.33 ± 3.67	982.67 ± 6.06
Neat PG	969.00 ± 7.23	975.67 ± 8.33

Comparing diffusion parameters between Azone® and neat PG treated samples, one notes that CP diffusivity (D/h^2) was not significantly different but membrane solubility (A_{CP}) was. Since CP concentration in these formulations was similar but logP values were significantly different, the correlation suggests that, under these experimental conditions, diffusivity (D/h^2) is related to permeant concentration in donor whilst CP membrane solubility (A_{CP}) was related to its formulation/membrane partitioning. Therefore, Azone at the concentration applied, was having little effect (compared to the neat PG control) on the rate of CP diffusion but was enhancing its partition into the membrane. This may suggest therefore, that CP transport across silicone membrane from an Azone®/PG formulation was a two-step process; an initial Azone®-mediated partition into the membrane followed by diffusion along a more aqueous propylene glycol mediated path or route.

The above relationship also holds when comparing OA/PG with AOA/PG formulations, CP solubility in each formulation was markedly different as was D/h^2; CP being ~12% less soluble in OA/PG resulting in significantly lower diffusivity. LogP values however, were of the same order corresponding to similar CP membrane solubility.

However, only partial correlation exists between CP physicochemical properties and fitted diffusion parameters. This is because CP diffusivity from the aqueous formulation is of the same order as that from OA/PG and AOA/PG but CP donor concentration is substantially lower (~15mg/ml). Also CP partitioning from neat PG into silicone membrane is significantly lower than that from OA/PG and AOA/PG treated membranes but membrane solubility (A_{CP}) is very similar. These results could be explained by the fact that during logP experimental determinations, the formulations applied to silicone membrane samples were continuously shaken for a 12-hour period allowing the enhancers to partition into the membrane more effectively than during the ATR-FTIR experiments.

3.5.1 Simultaneous detection of enhancer and solute penetration

The diffusion of CP reported above may have been related to the concurrent diffusion of vehicle and/or enhancer. Initially an attempt was made to assess the appearance of the solvent PG in silicone membrane. It was envisaged that absorptions relating to the -C-O- stretch present in the IR spectrum of PG which absorbs at ~1035cm^{-1} could be visualised in collected ATR-FTIR spectra. Unfortunately, silicone membrane IR absorptions in this region were too strong and masked any absorption originating from PG. Further, it was not possible to identify PG diffusion by monitoring its -O-H absorptions at ~3300cm^{-1} because cyanophenol also possess a hydroxyl moiety which absorbs at this wavelength. Other investigators (Watkinson *et al.*, 1995) have reported the membrane penetration and diffusion coefficients of vehicles such as ethanol and PEG 400 possessing hydroxyl groups by monitoring the hydroxyl stretch at ~ 3300cm^{-1}. However, the authors did not recount how they eliminated solute hydroxyl group contributions from the total absorbancies at 3300cm^{-1}.

A simple experiment to determine PG diffusion into silicone membrane was performed. Neat PG (1ml), was pippetted directly onto silicone membrane placed on an ATR-FTIR crystal; its appearance in the membrane being monitored by the emergence of hydroxyl group absorbencies (~3300cm^{-1}) at the membrane:crystal interface. Since no solute was present and silicone membrane did not absorb at this wavelength then the penetration of vehicle could be assessed, all be it independently. Over a normal 12-hour experimental period, absorbencies due to the hydroxyl groups found in PG increased as a function of time indicating vehicle penetration into the membrane.

The penetration of enhancer into silicone membrane was detected. Azidooleic acid was used as a probe to simulate the diffusion of oleic acid. This was possible due to its azido group absorbing at ~2150cm^{-1}; this absorption did not interfere with any absorptions arising from membrane or other formulation constituents. Figure 3.5 shows the simultaneous detection and appearance of CP and enhancer (AOA) at the membrane/crystal interface and Table 3.4 lists the fitted diffusion parameters determined.

The table shows that CP and AOA diffusion in silicone membrane are closely related and of the same order. Figure 3.6 serves to show the closely related concurrently determined diffusion profiles for CP and AOA in silicone membrane.

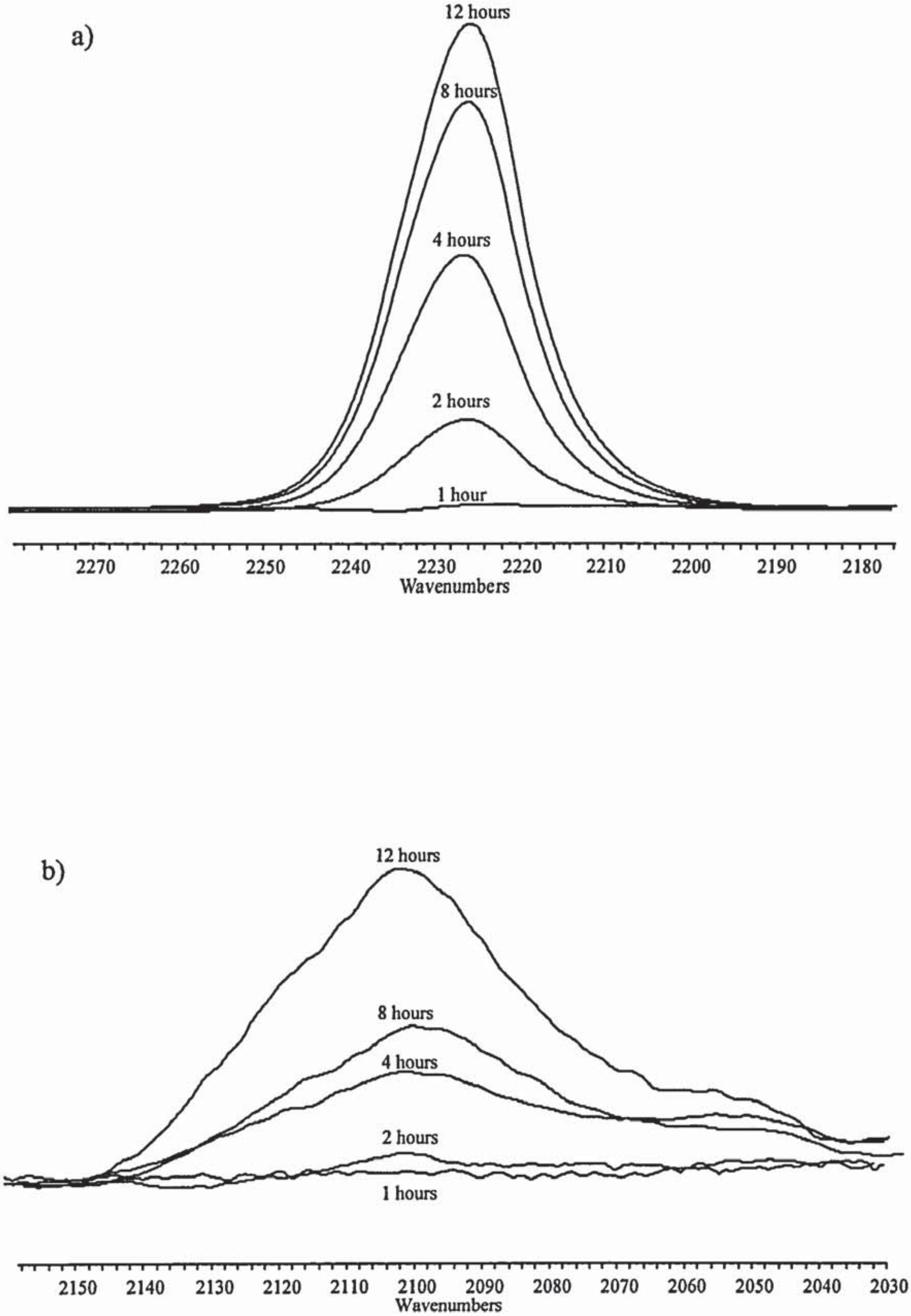

Figure 3.5 Simultaneous detection of (a) solute (CP) and (b) enhancer (AOA) in silicone membrane

Table 3.4 Concurrent determination of diffusional parameters for cyanophenol and azidooleic acid in silicone membrane

Membrane penetrants	$\frac{D}{h^2}(h^{-1})$	A_o
Cyanophenol (solute)	0.084 ± 0.006	0.256 ± 0.007
Azidooleic acid (enhancer)	0.079 ± 0.006	0.080 ± 0.002

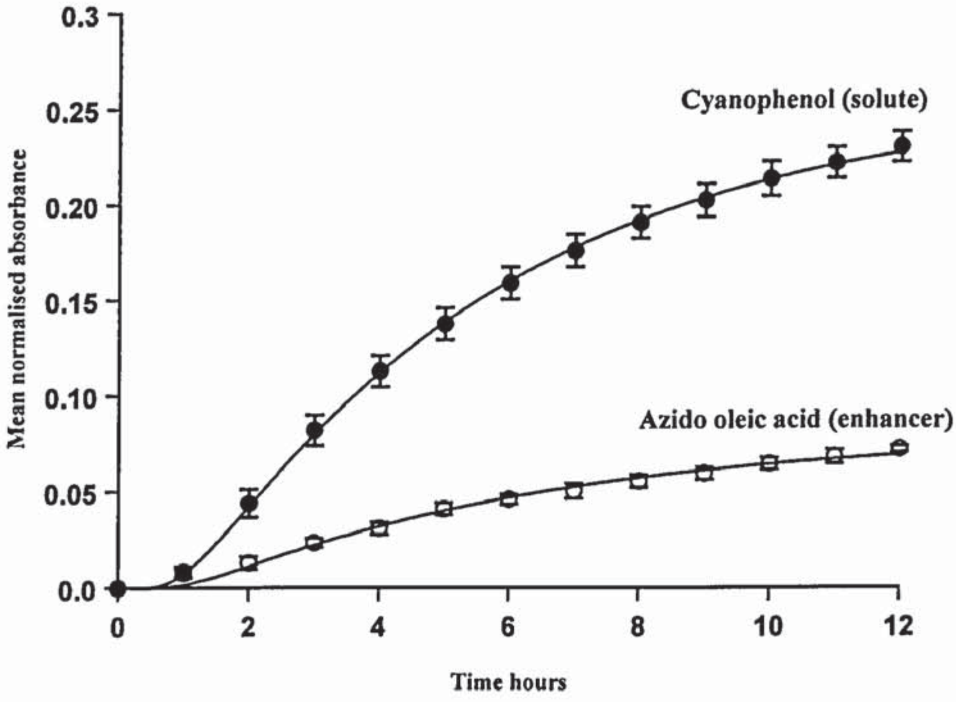

Figure 3.6 Concurrent cyanophenol and azidooleic acid diffusion profiles in silicone membrane.

3.6 SUMMARY

The diffusion of cyanophenol (CP) across silicone membrane from a variety of enhancer/vehicle formulations (saturated with CP) was spectroscopically analysed by virtue of fitting experimentally determined diffusion profiles to a solution of Fick's second law yielding parameters that reflected CP diffusivity (D/h^2) and solubility in the membrane (A_{CP}). The formulations applied were able to either affect CP diffusivity and/or its membrane solubility in the membrane. Cyanophenol diffusion was dependent on the enhancer formulation applied. The greatest diffusivity was observed from the Azone®/PG and neat PG formulations whilst diffusion from OA/PG and AOA/PG and aqueous formulations was not different. Cyanophenol membrane solubility was greatest when CP was applied in the Azone®/PG formulation; the A_{CP} value being 11% greater than the value determined after CP in neat PG was applied. It is likely therefore that Azone® was enhancing the partition of CP into the membrane and thus contributing to the magnitude of the A_{CP} parameter, although spectroscopically it was not possible to identify distinct IR absorptions originating from Azone® molecules. CP membrane solubility (as determined by comparisons of spectroscopically determined A_{CP} values) from OA/PG, neat PG and AOA/PG formulations was indifferent.

Although many studies have employed an ATR-FTIR method to obtain information relating to the diffusion of chemicals across membranes or other barriers such as semisolid ointments (Wurster *et al.*, 1993) this study aimed to correlate these diffusional parameters with experimentally determined formulation:membrane partition coefficients and permeant solubility in the formulations applied. In either case a partial relationship between these physicochemical properties and values for CP diffusivity and membrane solubility was established.

CHAPTER FOUR

PENETRATION OF SOLUTE, ENHANCER AND VEHICLE IN HUMAN STRATUM CORNEUM

4.1 INTRODUCTION

Following on from the previous chapter, the aim here is to trace simultaneously, co-administered and topically applied permeants in human stratum corneum. Formulations consisting of putative enhancer, model drug and vehicle were applied to human stratum corneum sheets *in vitro*. Diffusional profiles and characteristics for each permeant in the stratum corneum have been determined by spectroscopic analysis. The interplay between the diffusion of each permeant was assessed. Further, the influence of stratum corneum hydration on the diffusion of putative enhancer, model drug and vehicle was also examined. The chapter begins with a summary of some studies reporting the interplay between drug, enhancer, and vehicle in topically applied formulations in human skin.

4.2 PERMEANT PENETRATION IN HUMAN SKIN

Transdermal and topical formulations that are applied to the skin do not simply contain the active drug. Commonly, such applications consist of the drug, a vehicle or solvent and a transdermal penetration enhancer. Each component of the formulation therefore has the potential to diffuse or partition into the stratum corneum and exert an effect on transdermal penetration. For example, the composition of the vehicle may affect the barrier function and thereby influence the diffusion pattern. This was shown for the antipsoriatic agent dithranol which shows good penetration into the skin from a petrolatum base, whereas from polyethylene glycol it penetrates to a far lesser degree (Idson, 1983). Understanding the role of each excipient and the interplay that exists between excipients in the process of diffusion through skin is therefore important when designing transdermal delivery systems.

4.2.1 Information from diffusion cells

Wotton *et al* (Wotton *et al.*, 1985) have examined the concurrent diffusion of propylene glycol and metronidazole from a formulation containing varying amounts of Azone®. Using open glass diffusion cells, they applied various formulations to human skin. Each application consisted of a constant concentration of metronidazole but differing concentrations of Azone® in an ethanolic propylene glycol (PG) vehicle. They showed that the incorporation of Azone at a concentration of 1%v/v into the vehicle considerably enhanced the permeation of metronidazole (by a factor of 25) with a concurrent reduction in lag time. Perhaps more interesting though, was the effect Azone® had on the diffusion of

PG through skin. When comparing PG diffusion across the skin from a formulation containing 1% Azone® with that lacking Azone®, it also became evident that Azone® was enhancing the diffusion of the vehicle. Moreover, the metronidazole and PG permeation profiles showed a similar time-course. This was explained by the authors who suggested that the observed correlation between metronidazole and PG permeation was due to metronidazole becoming dissolved in PG whilst it permeated the skin barrier. It was also implied that the transport of metronidazole and PG was through the same microenvironment (where Azone® is effective) of skin, based on the similar permeation-time profiles.

This study also investigated the effect of changing the vehicle on drug diffusion. Omission of PG from the formulation reduced the permeation of metronidazole. Replacement with a different vehicle, PEG 400, produced extremely slow drug permeation. This latter effect was thought to be due to the drug not being released from the PEG 400 vehicle. This vehicle had previously been shown not to penetrate the skin itself (Mollgaard and Hoelgaard, 1983). Overall, the study shows that choice of vehicle is an important factor and that an enhancer can only behave as such if the drug is made available by the vehicle itself.

Some investigators have tried to improve the transdermal penetration of nitroglycerin by varying the concentration range of aqueous ethanol in their delivery system (Berner *et al.*, 1989). They reported the skin permeation of both the drug and the vehicle, ethanol. It was found that nitroglycerin and ethanol flux increased concurrently in a linear fashion, when the drug was incorporated into an aqueous based system having an ethanol volume fraction range between 0.1 to 0.5. Above this range, flux was independent of ethanol volume fraction with a plateau being obtained. This effect may be due to increasing concentrations of ethanol dehydrating the stratum corneum. Further, it was observed that ethanol flux across human skin from pure ethanol was considerably less than from 50% aqueous ethanol and even less than from ethanol solutions with nitroglycerin. The paper continues by stating that the above mentioned linearity implies that nitroglycerin transdermal delivery systems can be designed, where the rate of delivery of nitroglycerin across skin can be controlled by the delivery rate of ethanol. For example, to obtain a nitroglycerin flux of $50\mu g/cm^2/h$, an ethanol flux of $1mg/cm^2/h$ is necessary. Therefore, it was suggested that a reservoir formulation containing approximately an ethanol volume fraction of 0.7 should be used for optimum and therapeutic delivery of nitroglycerin. In conclusion, this study highlighted the complex interdependence of the penetration of ethanol, water and nitroglycerin. It was seen that ethanol not only increased nitroglycerin flux, but also that water increases ethanol transdermal flux; between ethanol volume fractions of 0.7 and 1.0, the flux of ethanol was halved due to dehydration. Perhaps more suprisingly, nitroglycerin also enhanced ethanol transport. In the presence of the drug, ethanol penetration into the skin increased by a factor of three. Mechanistically, the linear relationship between nitroglycerin and ethanol flux was suggested to be a consequence of ethanol affecting the local stratum corneum permeability for the drug and itself in the same manner; in the simplest terms the two permeants follow each other through the stratum corneum.

The relationship between the cotransport of permeant and solvent has also been probed by investigating ethanol-enhanced estradiol skin transport (Liu *et al.*, 1991). Estradiol in aqueous ethanol solutions was applied to human skin sandwiched in Franz diffusion cells; the receptor solution consisting of only water. Again, as in the case for nitroglycerin and ethanol, the flux of estradiol across human cadaver epidermis was linearly correlated with ethanol flux.

The *invitro* percutaneous transport of thiamine disulphide (TDS, indicated for the prophylaxis and treatment of thiamine deficiency), from a series of propylene glycol and saturated fatty acids vehicles has been studied (Komata *et al.*, 1992). A synergistic effect on permeation was observed when TDS was applied in a vehicle consisting of a C_{12} (the greatest enhancement) and a C_{14} fatty acid but the addition of the C_{18} fatty acid to PG resulted in a 80% reduction in TDS flux. Therefore, increasing the carbon side-chain length caused a reduction in flux. The authors postulated that the C_{12} fatty acid is able to disrupt the SC lipid structure to a greater extent than C_{14} and C_{18}, quoting the work of Aungst *et al* (Aungst *et al.*, 1986), whilst PG may be able to enhance the solubility of TDS in SC, resulting in a greater TDS flux. This later study states that the C_{18} fatty acid chain is similar in length and conformation to the carbon chains found in normal SC lipids and is thus able to align with these without disrupting their rigid structure.

4.2.2 Information from spectroscopic studies

The appearance in skin of topically applied substances can be determined by ATR-FTIR spectroscopy if the penetrating chemicals possess functional groups that absorb infra-red radiation distinctly from membrane-inherent groups. If this criterion is satisfied, valuable information regarding the simultaneous evaluation of the transport of topically applied chemicals can be obtained. Such data, would aid in the optimisation of transdermal drug delivery.

The percutaneous penetration enhancement of cyanophenol (CP) from various formulations was assessed by ATR-FTIR spectroscopy (Mak *et al.*, 1990b). The model drug, CP, was incorporated into formulations having a CP concentration of 10% w/v in either propylene glycol (PG) or in a PG solution containing oleic acid (OA) present at a concentration of 5% v/v. The formulations were applied to the forearms of volunteers using a gauze pad, for periods of 1, 2 or 3 hours. After the treatment times, the formulations were removed, the skin surface wiped clean and ATR-FTIR spectra recorded of each individuals skin for a period of nine hours. Absorbances at 2230 and 1040 cm^{-1} were used to determine the relative amounts of CP and PG respectively in the stratum corneum after removal of the delivery system. These absorbances were normalised with respect to the SC absorbance at 1741 cm^{-1}, which originated from the C=O stretching vibration of endogenous SC lipids, thus eliminating inter-measurement differences due to variable degrees of skin contact with the IRE. Results produced were in the form of CP absorbance ratio plots as a function of time, following removal of the formulations after 1, 2 and 3 hours and showed the effect of OA in the vehicle. Oleic acid was shown to have two effects. Firstly, as treatment time increased (from 1 to 3 hours) OA progressively increased the disappearance of CP from the SC and secondly, immediately after the removal of the delivery system OA reduced the relative amount of CP observed spectroscopically in SC when compared to the PG only vehicle. The effect of OA on the clearance of PG in SC was also reported. The results showed that OA hastened the transport of PG across the SC. The authors conclude by stating that CP was delivered into the SC at comparable rates from the formulations with and without OA and that the presence of the enhancer promoted the "throughput" of the penetrant.

The *in vitro* percutaneous enhancing mechanism of the known enhancers Azone® and Transcutol® (monoethyl ether of diethylene glycol) in human SC has also been explored using ATR-FTIR spectroscopy (Harrison *et al.*, 1996b). Human SC sheets were placed on a ATR-FTIR crystal (IRE) and pretreated with either ethanol (control) or a 0.05M ethanolic solution of Azone®. After one hour, a saturated aqueous suspension of the model permeant

CP was applied to the SC sheets. Experiments to assess the effects of Transcutol on SC permeability were done so by the application of CP (saturated) in a 1:1 mixture of Transcutol and water. Infrared spectra were then collected every 5 minutes and the areas associated with the CN stretch at 2230cm^{-1} were calculated to give measurements of CP permeation. Parameters relating to permeant diffusivity and membrane solubility were then determined using Fickian analysis of the ATR-FTIR absorbance profiles. Diffusion coefficients for CP were also determined from traditional Franz cells, following pretreatment with enhancers that allowed for comparisons between the two methods. It was shown by both methods that pretreatment with the above mentioned enhancers increased flux of CP by a factor of approximately two. However, only the ATR-FTIR method was able to differentiate between the enhancing mechanisms for Azone® and Transcutol. ATR-FTIR analysis showed that CP diffusivity in SC following pretreatment with pure ethanol and an ethanolic solution of Azone® was significantly different but CP membrane solubility was not. On the other hand, CP diffusivity from the Transcutol:water mixture did not differ whilst CP membrane solubility did (compared to control), suggesting that Transcutol enhanced CP penetration into SC by increasing its solubility in the membrane. This study thus showed that the ATR–FTIR technique could be employed to offer mechanistic information into percutaneous enhancer effects.

In a further study, Mak *et al* (Mak *et al.*, 1990a) examined SC uptake of OA using ATR-FTIR. Even though the SC lipids also contain a small percentage of OA, it was thought that this was very small compared to the exogeneously introduced OA . Therefore, OA was traced in SC by virtue of it possessing a C=O group which absorbed IR at 1710 cm^{-1}. Samples of solutions having varying concentrations of OA in ethanol (in the range 0.5 to 10 % v/v) were applied to human SC and ATR-FTIR spectra recorded. The OA peak at 1710 cm^{-1} was normalised with a SC inherent peak found at 1741 cm^{-1} to normalise results for variation in the degree of contact between subjects arms and the IRE. This membrane absorbance is characteristic of esterified SC lipids and is unaffected by fatty acid treatment. Mean normalised ratios were then plotted against OA treatment concentration and it was shown that OA uptake was proportional to the enhancer treatment concentration.

To probe the mechanism of action of OA in SC further, Naik *et al,* (Naik *et al.*, 1993) have used perdeuterated oleic acid (pD-OA). In their experiments, they applied a 5%(v/v) solution of pD-OA in ethanol to the mid-ventral forearms of healthy human volunteers for a period of 16 hours. At the end of the application period, IR spectra were recorded, each followed by sequential tape-stripping of the skin until 20 spectra were obtained. Each tape-strip was weighed before and after the stripping procedure to determine the mass of SC removed; increases in mass of SC being correlated with increase depth into the membrane. The presence of the putative enhancer, pD-OA, in SC was determined by virtue of a chemical substitution of deuterium for hydrogen. This results in $-CD_2$ symmetric and asymmetric stretching absorbances near 2095 and 2190 cm^{-1} respectively which do not interfere with any inherent IR absorbances of the SC. The appearance of pD-OA in SC was determined from the area under the $-CD_2$ stretching absorbance. The resulting enhancer penetration profile showed that the amount of enhancer present in SC decreased with increasing mass of SC removed or depth into the membrane. This finding was consistent with the existence of sink conditions near the base of the SC. The study continued by probing the effect of pD-OA on the conformational character of the SC lipids by evaluating shifts in their $-CH_2$ stretching vibrations, these being indicators of their alkyl chain order. It was found that pD-OA treatment had no effect on SC lipid alkyl chain conformation, $-CH_2$ absorbances appearing near 2848.5 cm^{-1} for control and treated sites. This inferred that SC lipids in the skin remained predominately in the solid state. In conjunction with this finding, the study also reported that frequencies of $-CD_2$ absorbances at all depths in SC also remained unchanged. Thus, the above two findings implied that the enhancer was present in SC in a semi-solid phase whilst endogenous SC lipids were predominately in the unperturbed solid state. This finding does not agree with postulated mechanisms of OA action that suggest OA is able to fluidise SC lipids leading to an enhancement of skin permeability (Golden *et al.*, 1987) but suggests that the enhancer exists in a separate "semi-solid" phase which is distinct from ordered SC lipids. Therefore the report infers that, and in light of published *in vitro* data (Ongpipattanakul *et al.*, 1991), OA induced permeation enhancement occurs *via* permeable interfacial defects resulting from phase separation in SC lipids. The study further concluded by stating that ATR-FTIR spectroscopy is a sensitive method to distinguish differences in the behaviour of SC lipids and exogenously applied enhancer.

ATR-FTIR spectroscopy has also been elegantly employed to determine the magnitude of permeant diffusion coefficient as a function of stratum corneum morphology (Pellet *et al.*, 1997a). In this study, fully hydrated SC was positioned onto an ATR crystal with either the outer (superficial layer) or inner surface (stratum compactum) in contact with the IRE. Once in place, an aqueous solution saturated with CP was applied to the SC and spectra recorded showing the accumulation of CP in the membrane. The area under the cyano peak occurring at approximately 2230 cm^{-1} was determined, plotted as a function of time and these data fitted to a solution of Fick's second law of diffusion. This yielded relative values for pathlength normalised diffusion coefficients and permeant build up in the SC. In theory, the diffusion coefficient for CP when the inner SC layer was in contact with the ATR should be greater than when the superficial layer was contiguous with the IRE; this being because the permeant is more easily able to diffuse through the less cohesive layers of the upper parts of the SC before reaching the more compact inner mantle. As expected, a greater value (~ 2.4 fold) for the CP diffusion coefficient when the inner side of the SC was on the ATR crystal was obtained together with a lower CP build up (due to this layer consisting of more cohesive cells (Bowser and White, 1985)). As the diffusional pathlength is likely to be similar, irrespective of which side is placed on the ATR crystal, this study confirmed that SC is not a homogenous membrane (the tissue does not consist of a uniform distribution of corneocytes in a matrix of lipids) and that diffusional resistance is greater in the inner layers than the outer layers.

These studies have highlighted the complex interplay that exists between topically applied excipients and that such phenomena have the potential to enhance or limit the transdermal delivery of drugs. The following experiments, outlined in the next part of this chapter, aim to investigate further such interactions in human stratum corneum.

4.3 MATERIALS AND METHODS

4.3.1 Materials

The permeant 4-cyanophenol (CP) was purchased from Lancaster Chemicals, (UK). Test enhancers oleic acid (OA), 12-Azidooleic acid (AOA) and the solvent propylene glycol (PG) were obtained from Sigma (Poole, U.K). The enhancer Azone® was acquired from Whitby Research (U.S.A). Whole skin was obtained from Selly Oak Hospital (Birmingham, UK).

4.3.2 Preparation of formulations

Excess amounts of CP (>10g) were added to a series of propylene glycol/enhancer mixtures to produce 10ml quantities of the following enhancer/propylene glycol formulations: 5% Azone®/PG, 5% OA/PG, 5% AOA/PG and neat PG. CP was also added to 10ml of water only to produce a saturated aqueous solution. The solutions were left to stir continuously for 48 hours at 400rpm.

Excess amounts of CP (>10g) were also added to a series of propylene glycol and water solutions (100%, 70%, 50%, 30% and 10%) to produce 10ml of saturated solution in each case, and left to stir for 48 hours at 400rpm.

4.3.3 HPLC analysis

The solubility of CP in each PG/water formulation was also determined in triplicate as follows. Excess quantities (10g) of CP were added to each propylene glycol/water formulation and continuously stirred for a periods of 48 hours at room temperature (21±1°C). Each mixture was then left to stand for 2 hours and then 1ml aliquots of the supernatant fluid withdrawn and filtered through 0.2μm syringe filters (Acrodisc® PF, UK). Each sample was then diluted appropriately and 200μl mixed with 200μl of 0.5mg/ml propyl parabens (in PG), the later acting as an HPLC internal standard. CP solubility's were determined by HPLC analysis using a Waters 600E system controller (UK) and a Waters 484 Tuneable absorbance detector set at λ_{MAX} 284nm. The samples were separated on a 10cm reversed-phase ODS II column (Jones, UK) using a mobile phase consisting of 35% acetonitrile and 65% water (both HPLC grade, Aldrich) at a flow-rate of 1ml/ min. The retention times for CP and internal standard were approximately 4 and 8 minutes respectively.

4.3.4 Preparation of stratum corneum sheets

Whole female human breast skin was obtained after having been removed during reduction surgery (Burns/Plastic Surgery Department, Birmingham University Hospital, Selly Oak, Birmingham, UK) and stored as received in a refrigerator at -20°C until required. When required, the skin was taken out of the refrigerator and allowed to defrost naturally. When fully thawed, the tissue was smoothed out epidermal side down on a corkboard. Depending on the amount of adhering subcutaneous fat and other debris, such tissue was removed using either a blunt pair of forceps or initially removed using a large pair of tissue cutting scissors. Once the dermis was visible, the tissue was cut to approximately $3cm^2$ dimensions. Each square was then immersed in water heated to 60°C for 60 seconds. On removal from the water, the epidermis was teased away from the dermis using a pair of forceps. Each square of epidermis was then placed in a 0.001% solution of Trypsin (Type II Soya, Sigma, UK) in phosphate-buffered saline at 37°C for 12 hours. The stratum corneum was then gently teased away from the viable epidermal layers. Each piece of stratum corneum was then immersed in distilled water for about 2 hours to wash away any remaining trypsin. Stratum corneum sheets were then, using a pair of blunt forceps, placed on to plastic sheeting (Salton, UK), which had been cut to size, and smoothed out flat; care being taken to avoid creasing the tissue and its turning back on itself. The sheets were then left to dry over silica gel in a sealed desiccator until needed. Stratum corneum required for experiments was then removed from the dessicator and subjected to laboratory relative humidity (~ 28 - 30% at all times, measured using a hygrometer) for 48 hours, after which the tissue was ready for experiments. All experiments were performed on breast tissue obtained from six donors.

4.3.5 ATR-FTIR analysis

ATR-FTIR spectroscopy was performed using a Mattson 3000 FTIR spectrometer equipped with a flat top accessory and mounting stand (consisting of a series of obliquely mounted mirrors), together forming the advanced ATR system® (Spectra-Tech, Cambridge, UK). The spectrometer was further linked to a deuterated triglycine sulphate detector. The flat-top accessory incorporated the ZnSe internal reflection element having dimensions 7.2cm x 1.0cm x 0.2cm and a refractive index of 2.4 at $1000cm^{-1}$ at room temperature. An infrared beam from the spectrometer was reflected into the IRE at an angle of 45^0 (incident angle) which was reflected internally along the ZnSe crystal twelve times. Stratum corneum was cut to size so as to overlap the junction on both sides of the crystal and surrounding plate and smoothed gently out over the crystal. A plastic trough was positioned and sealed with a small amount of white soft paraffin (Sigma, UK) on to the membrane but not obstructing the IRE. An aliquot of formulation (200µl) was pipetted into the trough and a small excess of CP added. The contents of the trough were protected from the laboratory environment by placing a glass microscope slide on top of the trough, which was held, in place by a 50g brass weight. Spectra were taken automatically every 5 minutes until plateau conditions had been reached *via* an Apple Macintosh 800 Quadra computer employing MacFirst® software. A total of 64 scans, using a gain setting of 20, were taken at each time point, requiring 2 minutes and 53 seconds. Spectra produced had a resolution of $2cm^{-1}$.

Absorbances relating to CN, N_3 and CO bond stretches were determined at approximately 2230, 2100 and $1035cm^{-1}$ respectively. All absorbances relating to excipients were normalised to the Amide II absorbance present in human stratum corneum at $1550cm^{-1}$, in order to compensate for changes in contact between the SC and IRE during the experiment. Observed absorbances as a function of time were plotted, and these were fitted to equation 2.14 (see chapter 2) using a non-linear least-squares regression program (FigP; Biosoft, UK) to yield best fit values for D/h^2 and A_o.

4.3.6 Statistical analysis

Student t-tests were carried out to determine if significant differences existed between fitted D/h^2 and A_o values obtained from different formulations applied to stratum corneum. A minimum of three replicates were used for each formulation tested.

4.4 RESULTS AND DISCUSSION

Figure 4.1 shows a representative ATR-FTIR spectroscopic spectrum of human stratum corneum, obtained by positioning (dermal side in contact with crystal) and pressing gently an isolated sheet of SC onto the ZnSe IRE and running a spectrum using the software and parameters described in the method. The peaks making up the spectrum are assigned functionality in table 4.1.

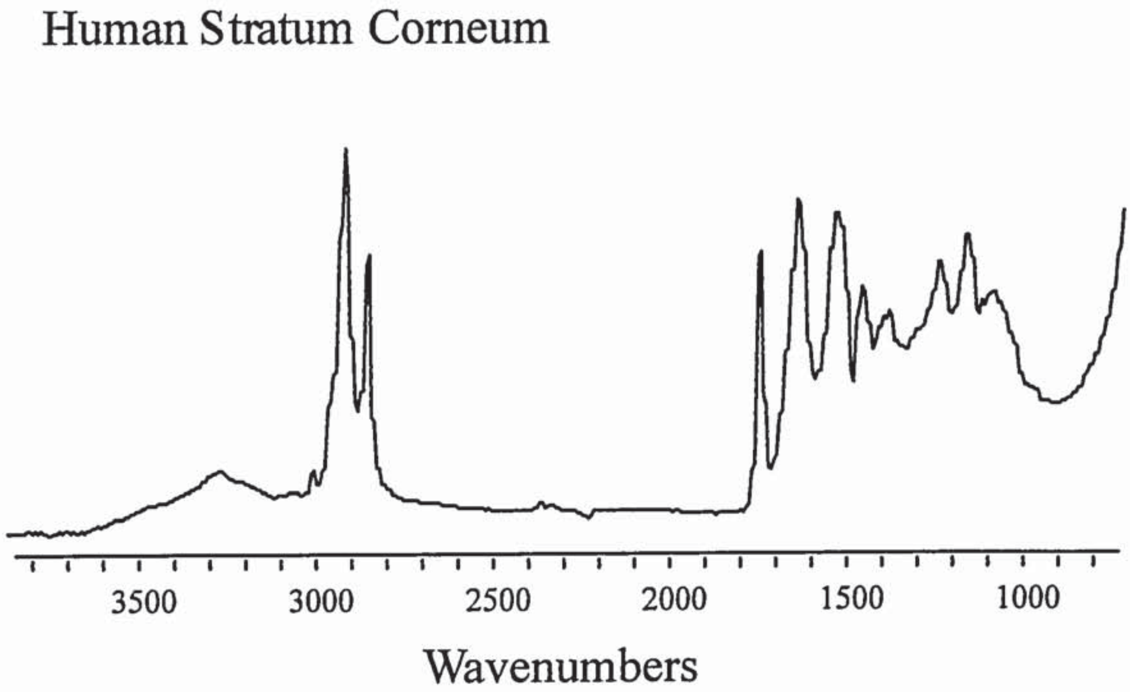

Figure 4.1. ATR-FTIR spectrum of human stratum corneum placed stratum compactum side on crystal

The spectrum shows a region between 1700 to 2700cm^{-1} where the SC does not absorb infrared radiation. This infrared transparent region is of interest as it allows the detection of compounds having functional groups that absorb in this region as they are diffusing or are transported across the SC. The spectrum also clearly shows the IR absorptions that occur at 1565 cm^{-1} which are due primarily to the C-N stretching and N-H bending vibrations of protein amide groups (making up SC corneocytes) although sphingolipids may also contribute due to the presence of amide groups within polar head groups. The IR intensities in SC of all diffusing species from topically applied formulations were normalised to the

Table 4.1 Infrared absorptions of human stratum corneum

Wavenumber (cm^{-1})	Origin	Vibrational Mode
3500-3400	Water	O-H stretch
3400-3300	Protein,Lipid	N-H stretch
2920	Lipid	C-H asym stretch
2850	Lipid	C-H sym stretch
1740	Lipid	C=O
1640	Protein	C=O stretch (amide I)
1565	Protein	N-H bending (amide II)
1565	Protein	C-N stretch (amide II)
1470-1400	Lipid, Protein	C-H bending and twisting

intensity of this amide II peak of SC to correct for changes in contact (between SC and the ATR crystal) and pressure dependent changes in absorbance during each experiment.

4.4.1 Penetration of cyanophenol (drug)

A series of experiments were conducted to assess the penetration of cyanophenol across human SC from a variety of topically applied formulations using the ATR-FTIR method previously described. The area under the –CN peak was taken to be directly proportional to the concentration of CP at the SC crystal interface. Figure 4.2 shows the diffusion profiles of CP as a function of formulation applied and time. The diffusion profiles show that for each CP diffusion profile, the spread of data is relatively small, highlighting the excellent reproducibility of the method. Further, CP is shown to rapidly diffuse across the SC and that a CP plateau level was achieved in all cases. Values for CP pathlength normalised diffusion coefficients (D/h^2) and plateau levels (A_o) were obtained after fitting the

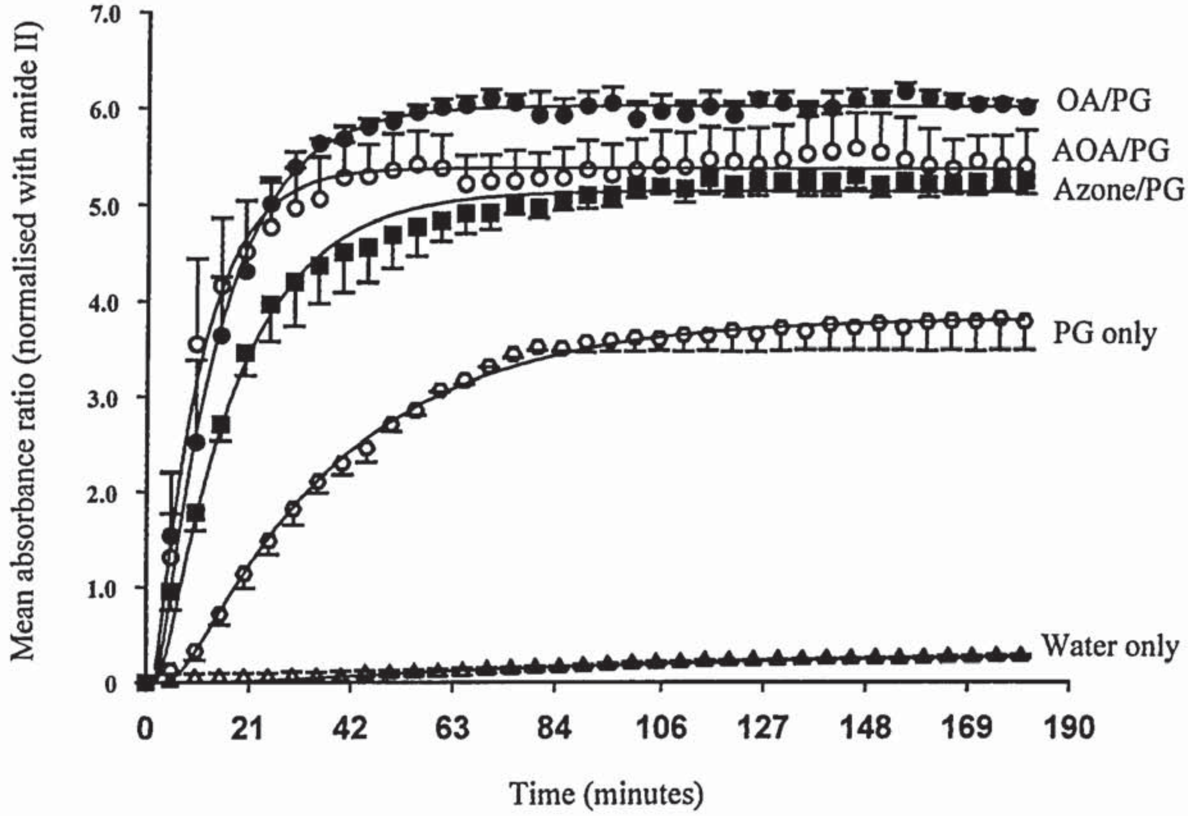

Figure 4.2 Diffusion profiles for cyanophenol across human stratum corneum from various enhancer/propylene glycol (vehicle) formulations (mean ± sem)

Formulation	$\frac{D}{h^2}(h^{-1})$	A_o
AOA/PG	2.88 ± 0.72	5.41 ± 0.33
OA/PG	2.28 ± 0.54	6.04 ± 0.14
Azone®/PG	1.56 ± 0.18	5.17 ± 0.11
Neat PG	0.75 ± 0.06	3.84 ± 0.21
Water only	0.36 ± 0.18	0.37 ± 0.12

Table 4.2 Values for cyanophenol diffusivity and solubility in human stratum corneum as a function of formulation applied

experimental data to Fick's second law of diffusion (see equation 2.14 in chapter two) and are summarised in Table 4.2. These data show (assuming *h* is invariant) an increase in CP diffusivity, as the enhancer/vehicle combination is modified, in the order AOA>OA>Azone®>PG>water. CP diffusivity from the AOA, OA and Azone® applications was not significantly different from either of these formulations but all were significantly greater than the diffusivity seen from neat PG ($P<0.05$). Harrison *et al* (Harrison *et al.*, 1996b) have also determined the value for D/h^2 for CP following pretreatment with an ethanolic solution of Azone®. In their experiments, SC was pretreated with Azone® for one hour before an aqueous solution of CP was applied. The authors report a D/h^2 of 1.33 ± 0.15 hr^{-1} that compares favourably with the value determined in this study of 1.56 ± 0.18 hr^{-1} and indicates that the method of enhancer pretreatment does not affect the value of D/h^2. CP diffusivity from both the OA and AOA formulation was ~4 times greater than from the neat PG formulation.

CP diffusion across SC from neat PG was not significantly greater ($P>0.05$) than that from a simple aqueous solution suggesting that PG and water are equally effective as vehicles for CP. The D/h^2 value determined here for CP from an aqueous solution (0.36 h^{-1}) is consistent with a value of 0.30 h^{-1} derived *in vivo* (Pirot, 1996). However, an *in vitro* value for D/h^2 of 1.660 h^{-1} has also been reported in the literature for CP (Pellet *et al.*, 1997a), which is between four to five times greater than the value obtained in this study. One reason for this difference maybe that Pellet *et al* used fully hydrated SC in their experiments whereas the SC employed in this study had a much lower water content. It has been shown previously in many studies that the level of SC hydration can affect the permeation and diffusivity of topically applied permeants (Barry, 1983b; Roberts and Walker, 1993).

These results indicate that the enhancers are having an effect on the diffusion of CP across SC, by lowering SC diffusional resistance, and are equally effective at doing so. The microenvironment the enhancers are acting on in the SC to lower diffusional resistance is not clear from these experiments; enhancers can either perturb SC lipid bilayers or perhaps affect the structure of SC corneocytes (Barry, 1991).

The effect of enhancers on human SC lipid fluidity has been studied using FT-IR spectroscopy and a perdeuterated analogue of Azone® (Harrison *et al.*, 1996a). The effect

Azone® had on SC lipids was determined by assessing the organisation of the lipid acyl chains (reflected by changes in the frequency of the C-H_2 symmetric stretching frequency, see table 4.1) and the rate of motion of the lipid chains within the rigid intercellular environment of the SC (reflected in changes in the bandwidth of the C-H_2 symmetric stretching frequency at half maximum height). The perdeuterated Azone® analogue (D-Azone®) was used in order to discriminate between signals due to the acyl chains of the SC lipids and the enhancer and applied to SC at two different concentrations (5mg/cm^2 or 15mg/cm^2) following which IR spectra were recorded for each piece of SC. The authors reported that application of D-Azone® at the lower and higher concentration, resulted in conformational changes of SC lipids in the form of an increase in the number of gauche conformers (indicative of melting of lipid acyl chains) along lipid hydrocarbon chains, corresponding with frequency shifts to higher values which is associated with an increase in SC lipid fluidity. This action could suggest how the penetration of molecules, such as CP, is enhanced through the skin by Azone®.

Extrapolation of the plateau level to the y-axis (see Figure 4.2) furnished the value of A_0 for CP as a function of formulation applied to SC, which is a measure of the solubility of the permeant in SC. These values are also significantly elevated with respect to the aqueous formulation. The presence of the enhancers in the formulations also increased CP membrane solubility in the order OA>AOA>Azone®>PG>water. This order compares well to the order the enhancers affect CP diffusivity in SC indicating that higher CP diffusivity correlates with higher membrane CP solubility or vice versa.

However, this is not strictly true when comparing the CP diffusional parameters obtained from neat PG and aqueous formulations. Here the CP diffusivity is indifferent but CP membrane solubility is much higher after the neat PG application. Therefore, it is evident that PG has a greater capacity to increase the solubility of CP in SC, which is logical since CP solubility in PG is greater than in water. These findings seem to agree with other reports that comment on the mode of action of PG and other vehicles in transdermal drug delivery, such work suggesting also that PG is able to enhance delivery across the SC by increasing drug solubility in the skin (Barry, 1991; Mollgaard, 1993).

It is also evident from the results that the presence of enhancers is increasing CP membrane solubility. Enhancers are generally thought to penetrate into SC lipid domains and lower the resistance of these rigid regions and hence increase drug permeability and the accumulation of CP in SC. Therefore, increases seen in A_0 may suggest that this is what is occurring.

Alternatively, the value of A_o at saturation can be taken as being proportional to CP partitioning into SC. The addition of enhancers to PG increases the lipophilicity of the formulations. This in theory, should lower the partitioning of CP between the formulation and the lipophilic domains in SC resulting in a lowering of A_o. However, A_o increases when formulation lipophilicity increased upon the addition of enhancers compared to neat PG. Therefore, it is possible, since CP has both lipophilic and hydrophilic domains ($\log P_{oct/water} = 1.56$) (Barry, 1991), that more partitions into hydrophilic areas of the SC when enhancers are present in the formulation, resulting in the increase in A_o compared to neat PG. Furthermore, Pellet *et al* (Pellet *et al.*, 1997a) have previously suggested that CP has an affinity for SC corneocytes since it most likely traverses SC *via* this route.

4.4.2 Penetration of propylene glycol (vehicle)

The penetration of the vehicle into SC during each experiment was traced by monitoring the C-O infrared vibration at 1035 cm^{-1} as a function of time and formulation applied. Figure 4.3 shows the PG diffusion profiles obtained during the concurrent penetration of PG and CP into SC (shown in Figure 4.2) and Table 4.3 summarises D/h^2 and A_o parameters for PG as derived from four different formulations.

Again, the diffusion of propylene glycol in SC fitted well to Fick's second law of diffusion with the data spread being small. In each case, the vehicle diffused rapidly into the SC and a plateau achieved (when the SC was totally saturated with PG) around 63 minutes. The values for diffusivity across SC for PG and CP (see Table 4.2) were very similar from each different enhancer formulation applied; indicating that both vehicle and drug most likely penetrated SC *via* the same route.

The D/h^2 value for PG from the neat PG application (control) was not significantly different to D/h^2 values determined from enhancer/PG formulations indicating that the enhancers applied

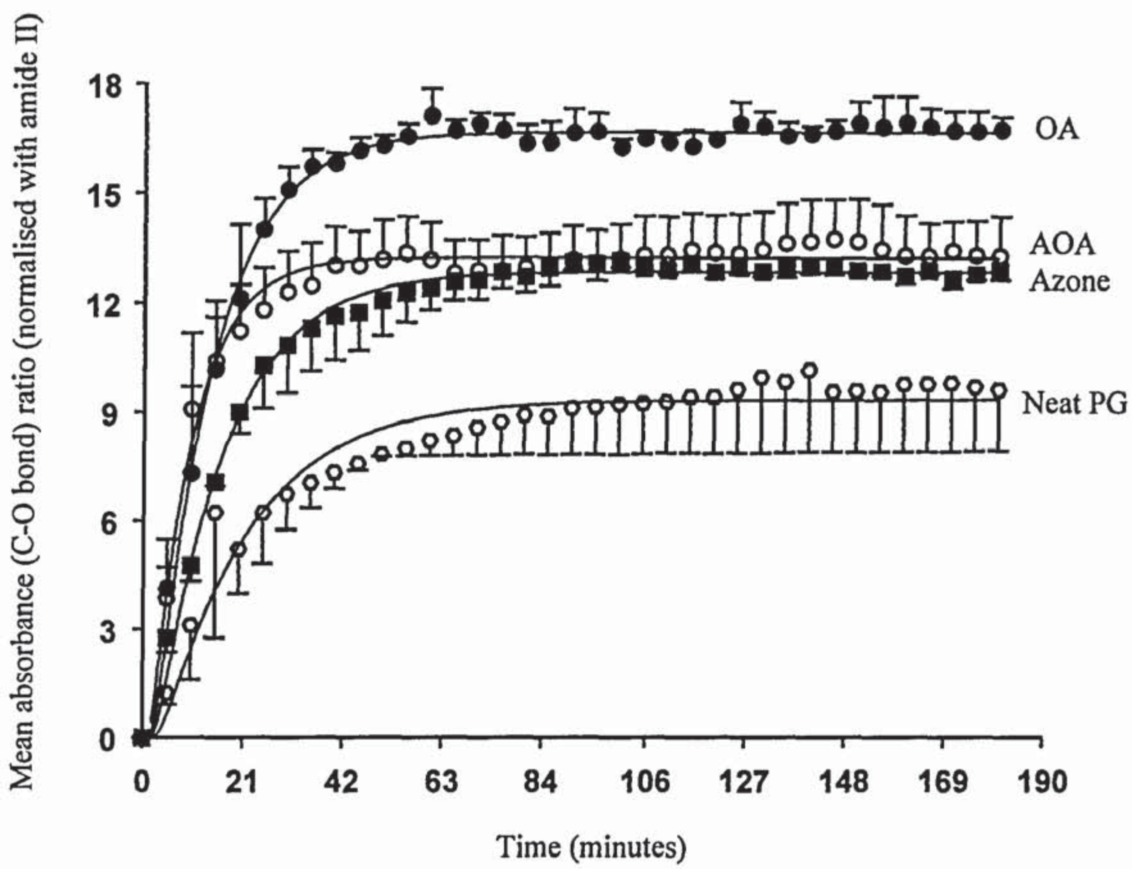

Figure 4.3 Diffusion profiles for propylene glycol (vehicle) across human stratum corneum from various cyanophenol saturated enhancer/propylene glycol formulations (mean ± sem)

Formulation	$\frac{D}{h^2}(h^{-1})$	A_o
OA/PG	2.22 ± 0.42	16.7 ± 0.40
AOA/PG	3.00 ± 0.66	13.3 ± 0.99
Azone®/PG	1.68 ± 0.18	12.9 ± 0.23
Neat PG	1.58 ± 0.52	9.74 ± 1.83
Water only	--------------	-------------

Table 4.3 Values for propylene glycol (solvent) diffusivity and solubility in human stratum corneum as a function of formulation applied

had little effect on PG diffusivity in SC ($P>0.05$). This may be because enhancers generally tend to increase permeant diffusivity by perturbing the rigid lipid structure of the SC whilst PG may not traverse the SC through lipid domains but perhaps has an affinity for SC corneocytes instead. However, the enhancers did affect the amount of PG accumulating in SC when compared to the neat PG application, which is shown by the different values for A_o listed in table 4.3, suggesting possibly enhancer-corneocyte interactions (Barry, 1991). These data show an increase in PG membrane content as the enhancer/vehicle combination is modified, in the order OA>AOA>Azone®>PG; the plateau level from the OA/PG formulation being ~2-fold greater when compared to that from neat PG. Hence, if PG is penetrating through corneocytes then the enhancers also may be able to alter corneocytic affinity for PG. This rank order is identical to that observed for CP penetration into SC as a function of enhancer/PG formulations (see table 4.2) applied. This suggests that the diffusion of drug and vehicle is equally affected by the enhancers applied and that the respective transport processes are not independent, but inter-related.

The appearance of PG in the dermis of rat skins from formulations having different OA acid concentrations has been previously reported (Takeuchi *et al.*, 1995). It was shown that PG did not penetrate skin (not detectable in the dermis using ATR-FTIR spectroscopy) from OA/PG applications having an OA concentration of 0.01 or 0.05M but did appear in the dermis from 0.15M OA/PG. This is the same concentration of OA used in this study. The PG diffusion *vs.* time profiles were similar to the ones shown in Figure 4.3, with a PG plateau being established after about 60 minutes. Interestingly, and in contrast to the results reported here, the results from the above study by Takeuchi *et al* showed that PG did not penetrate skin from a neat PG application, the authors thus implying that OA facilitated vehicle penetration into skin. They proposed that OA was able to extract SC intercellular lipids, which aided the passage of PG molecules into the SC (Takeuchi *et al.*, 1993).

4.4.3 Penetration of enhancer

The chemical, 12-azidooleic acid (AOA), was employed in these studies to behave as an IR active marker for the putative transdermal enhancer oleic acid. The similarity of CP diffusional parameters obtained from OA and AOA containing formulations (see Table 4.2) indicated that AOA is a suitable IR-active marker for OA. The appearance of AOA in SC was traced by virtue of it possessing an azido group (N_3) that absorbed IR radiation at

~2150 cm^{-1}. Penetration of CP (solute) and PG (vehicle) were monitored by changes in their IR absorptions at 2230 and 1040 cm^{-1}. Figure 4.4 shows the time-dependent, and simultaneously monitored, appearance of AOA, CP and PG (from a saturated solution of CP in 5% AOA/PG) at the SC-crystal interface. It shows that all three species were able to concurrently penetrate into SC, and saturate the deepest layers; penetration of all three permeants following a similar time course.

The diffusion of solute or drug (CP), vehicle and enhancer all fitted well to Fick's second law of diffusion; the plateau for solute and vehicle being reached at approximately the same time highlighting the inter dependence of the diffusing species. Figure 4.5 shows the spectral traces representing the solute (CP), the enhancer (AOA) and solvent (PG) when SC had become saturated with each permeant i.e., once a plateau level had been reached. In all experiments, this was from approximately 63 minutes onwards.

The data in table 4.4 shows that the pathlength normalised diffusion coefficient (D/h^2) for each species is of a similar magnitude. The absolute values of A_0 for each permeant could not be compared since their molar absorptivities varied but AOA has previously been shown to increase the membrane solubility of CP (Figure 4.2) and PG (Figure 4.3) above that of control (neat PG). These findings are similar to other published results (Wotton *et al.*, 1985). Azone® has been shown to enhance the diffusion of metronidazole and vehicle (PG), where both drug and vehicle penetration exhibited similar diffusion *vs.* time profiles. This correspondence in diffusion time course for drug and vehicle evident in this study may be due to the drug (CP) becoming dissolved in PG whilst PG penetrates the skin barrier. Further, such similarities suggest that the transport of CP and PG is through the same microenvironment (where 12-AOA is most effective) in SC.

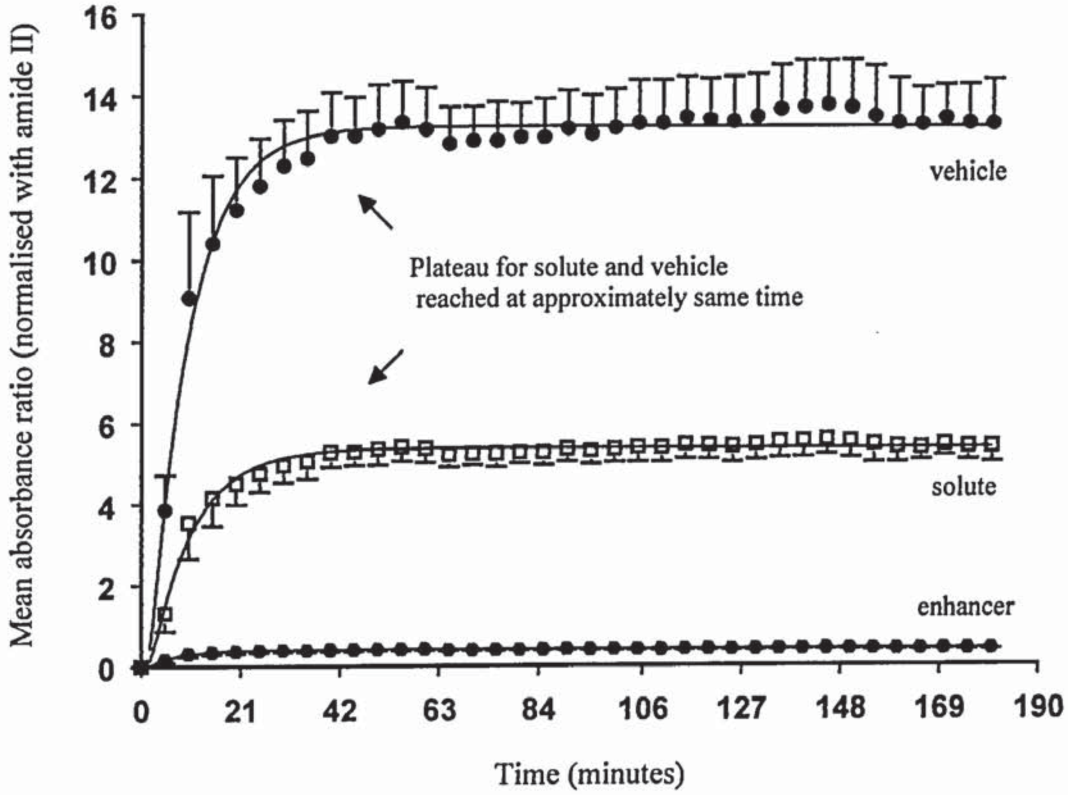

Figure 4.4 Simultaneous detection of cyanophenol, azidooleic acid and propylene glycol in human stratum corneum (mean ± sem)

Substance	$\frac{D}{h^2}$	A_o
Cyanophenol	2.88 ± 0.72	5.41 ± 0.33
Propylene glycol	3.00 ± 0.66	13.3 ± 0.99
12-azidooleic acid	3.90 ± 1.32	0.41 ± 0.02

Table 4.4 D/h^2 values for CP, PG and AOA following application of a saturated CP solution in 5% AOA/PG.

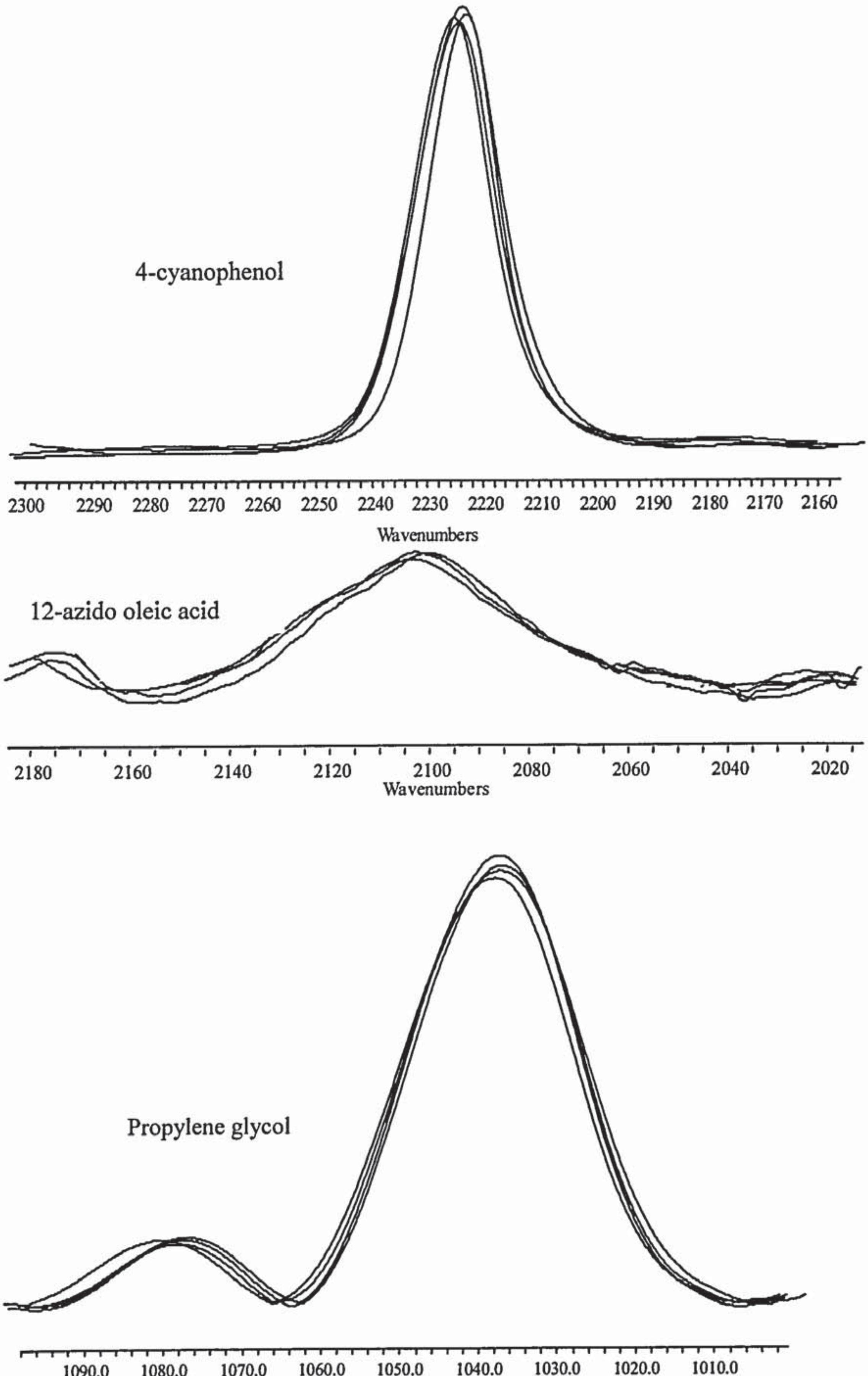

Figure 4.5 Simultaneous detection of solute, enhancer and solvent in human SC: typical peaks between 1 and 3 hours of each experiment (plateau region)

4.4.4 Cyanophenol and propylene glycol penetration from PG/water formulations

To probe the interplay between CP and PG penetration into SC further, the penetration of both species from a series of PG/water co-solvent systems was also assessed. No enhancers were present in the formulations applied to SC. Saturated solubilities of CP in different PG/water co-solvent systems were determined and are shown graphically in Figure 4.6.

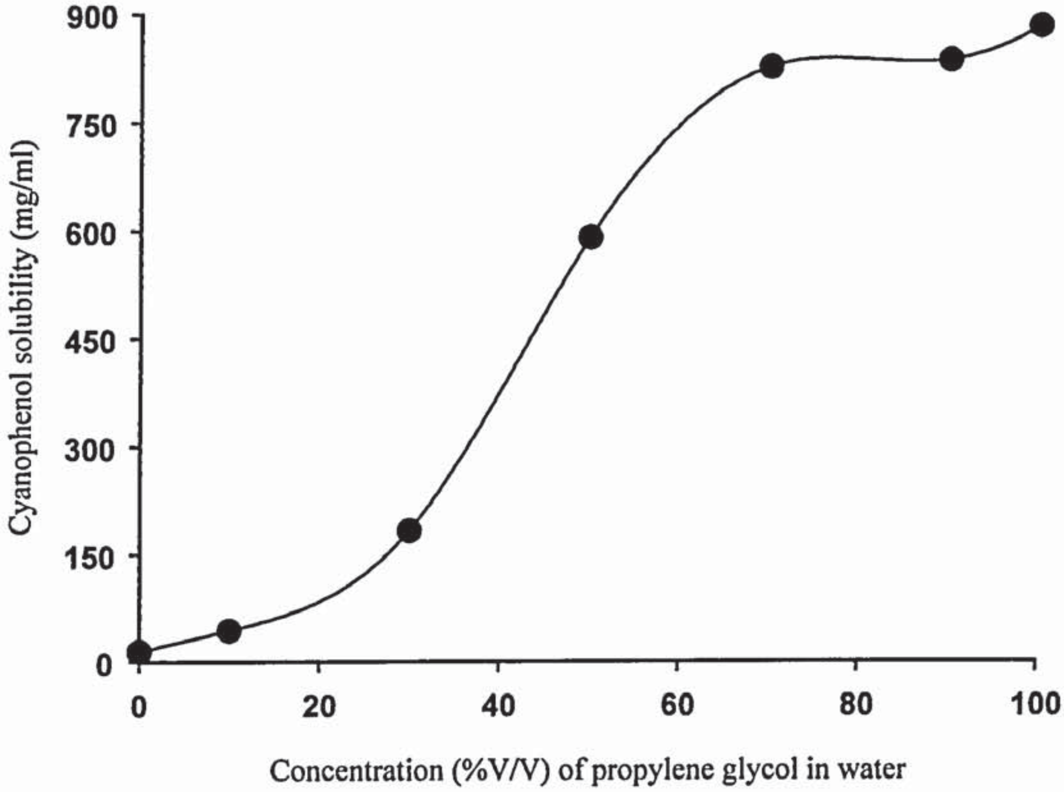

Figure 4.6 Solubility of cyanophenol in PG/water vehicles (mean ± sem)

The above data show that, as the percentage of PG increases, the saturated solubility of CP increases in an exponential manner with a plateau being reached at higher levels of PG concentration. This phenomenon has also been observed in other studies (Megrab *et al.*, 1995b)and it has been shown that the effect depends upon the polarity of the drug with respect to the solvent or co-solvent.

Figure 4.7 profiles CP penetration in SC as a function of co-solvent system with the respective diffusional parameters being listed in table 4.5. The table shows that CP diffusivity (D/h^2) from the neat PG and aqueous formulations was not statistically different ($P>0.05$), indicating that PG and water are possibly facilitating the diffusion of CP *via* the same pathways in SC. The solubility of CP in SC (A_o) is markedly different from these formulations. This is probably due the greater solubility of CP in PG in the SC, compared to water (PG has been shown to penetrate SC previously see Figure 4.3). These results are similar to those reported by Watkinson *et al* (Watkinson *et al.*, 1995) who found that permeant diffusion coefficients from water or ethanol vehicles were indifferent but corresponding permeant plateau levels varied significantly.

When water is added to the PG formulations, CP diffusivity increases as shown in Table 4.5. Diffusivity of CP increases from 0.75 ± 0.06 (CP in neat PG) to 1.08 ± 0.09 and 1.68 ± 0.06 for the 30%PG/70%water and 50%PG/50%water formulations respectively. These results infer the occurrence of a synergistic effect between PG and water which serves to promote CP diffusivity (since the additive effect of PG and water on CP diffusivity is greater than the sum of their individual effects).

Further as the concentration of PG increased from 30 to 50 to 100% so did the solubility of CP in SC (exhibited by increasing A_0 values, see table 4.5). This increase in CP membrane solubility can be correlated to the amount of PG penetrating SC from different PG/water vehicles. Figure 4.8 and table 4.6 show that as the formulation PG concentration increased, so did its accumulation in SC (increasing values of A_0). Therefore, this would provide an environment where PG is able to enhance solute (CP) solubility in SC.

Overall, these studies show that the diffusivity of CP from neat PG and water is indifferent, that when water is added to the formulation CP diffusivity increases and that CP membrane solubility increases as the penetration of PG increases into SC.

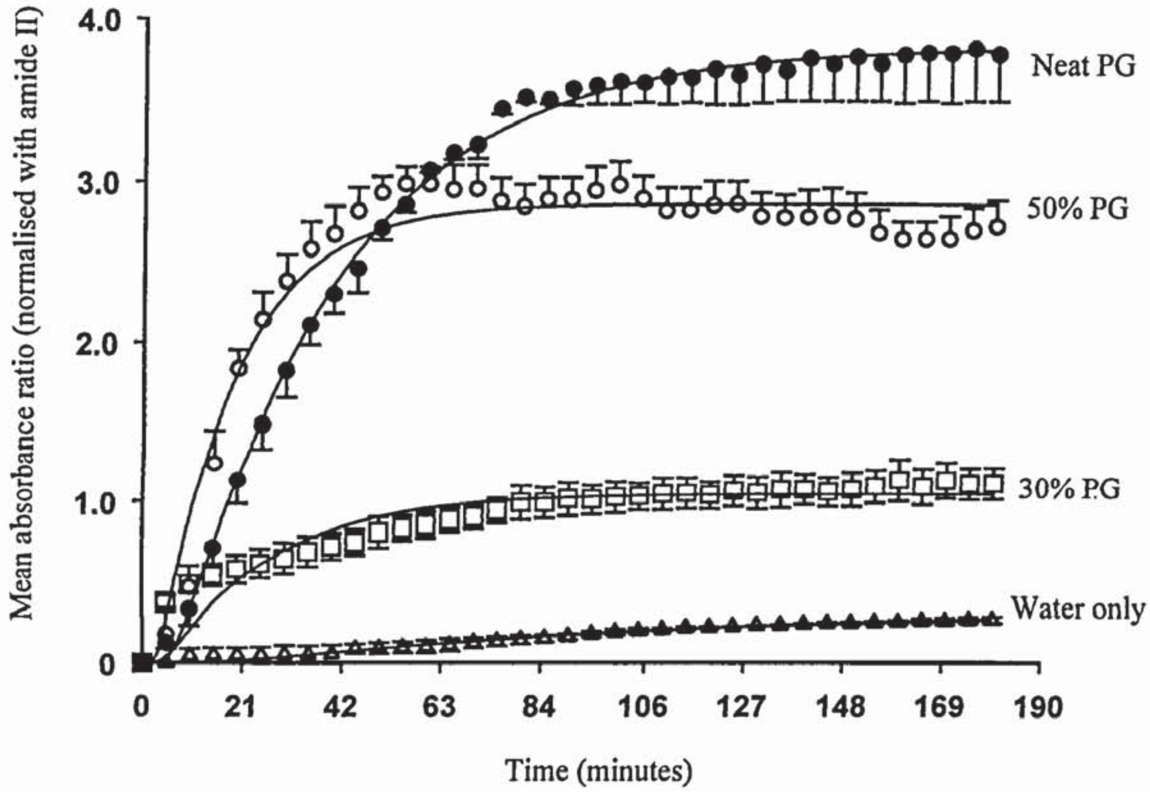

Figure 4.7 Diffusion profiles for cyanophenol across human stratum corneum from various propylene glycol:water vehicles (mean ± sem)

Formulation	$\frac{D}{h^2}(h^{-1})$	A_o
Neat PG	0.75 ± 0.06	3.84 ± 0.21
50% PG/ 50% water	1.52 ± 0.06	2.86 ± 0.18
30% PG/ 70% water	1.08 ± 0.09	1.05 ± 0.10
Water only	0.36 ± 0.18	0.37 ± 0.12

Table 4.5 Values for cyanophenol diffusivity and solubility in human stratum corneum as a function of PG/Water formulation applied

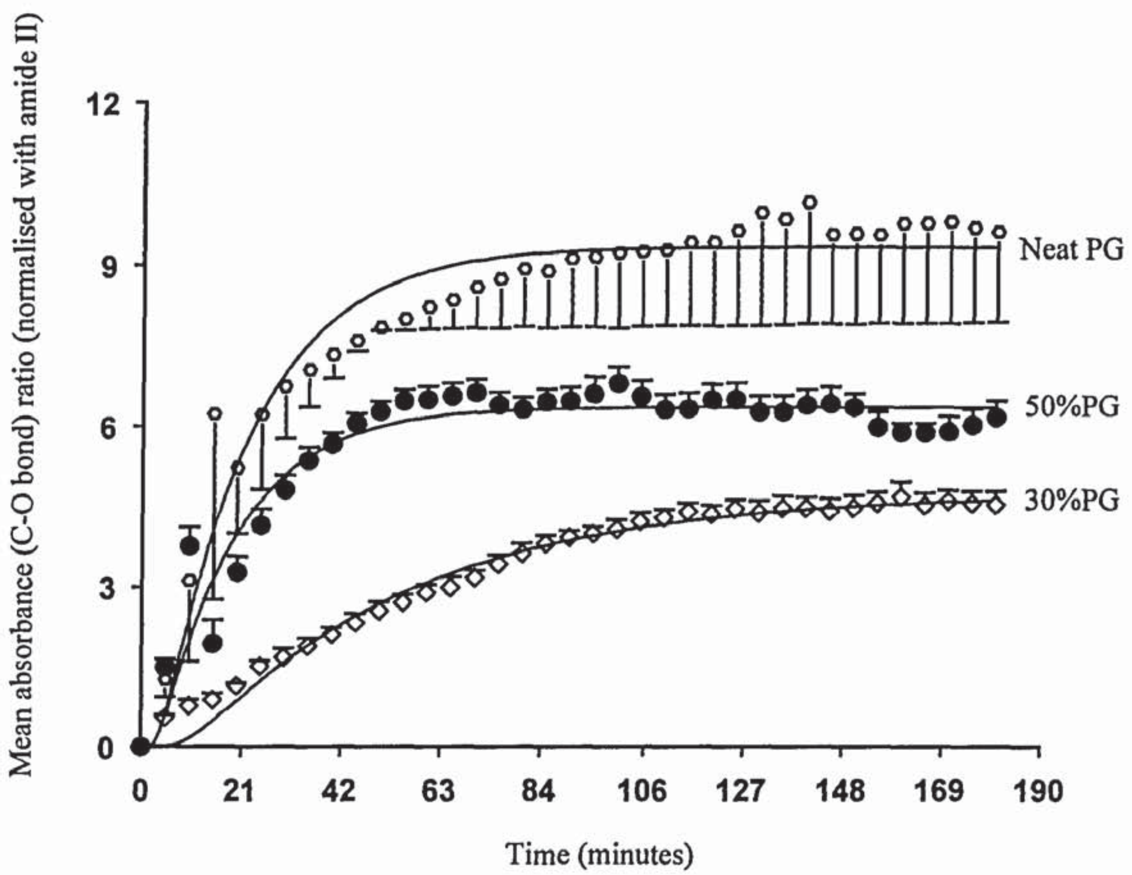

Figure 4.8 Diffusion profiles for propylene glycol across human stratum corneum from various propylene glycol:water vehicles (mean ± sem)

Formulation	$\frac{D}{h^2}(h^{-1})$	A_o
Neat PG	1.58 ± 0.52	9.74 ± 1.83
50% PG/ 50% water	1.49 ± 0.11	6.38 ± 0.14
30% PG/ 70% water	0.52 ± 0.2	4.75 ± 0.10
Water only	------------------------	------------------------

Table 4.6 Values for propylene glycol diffusivity and solubility in human stratum corneum as a function of PG/Water formulation applied

4.5 SUMMARY

The diffusion of CP into SC from a series of enhancer/PG vehicles was determined by ATR-FTIR spectroscopic analysis. When enhancers were added to the applied formulations, CP diffusivity was significantly enhanced when compared to the neat PG application. Cyanophenol solubility in SC was also enhanced by the presence of enhancers. Enhancers may have penetrated SC and perturbed SC lipid domains to promote CP diffusion across SC, although CP also shows an affinity for SC corneocytes.

Diffusional profiles and characteristics for the vehicle propylene glycol were also determined as a function of enhancer formulation. It was found that the enhancers did not affect PG diffusivity in SC (probably because PG penetrates SC *via* a corneocytic route rather than *via* a lipid pathway) but enhancers did affect PG solubility in SC suggesting enhancer-corneocyte interactions. Propylene glycol diffusion closely resembled that of CP, implying that the respective transport processes were inter-related. Additionally, a synergistic effect, which increases CP diffusivity and membrane solubility in SC, was found to occur between PG and water.

Using 12-azidooleic acid as an IR active probe for oleic acid, the simultaneous penetration of drug, enhancer and vehicle into human stratum corneum was determined using a spectroscopic method. It was found that the diffusion profiles and hence diffusivity for all three permeants were similar. This indicated that the diffusion of each species through SC was closely related and most likely occurred *via* the same route or SC microenvironment.

CHAPTER FIVE

TRANSDERMAL MACROMOLECULAR DELIVERY: EFFECT OF ENHANCERS AND ELECTRICAL CURRENT

5.1 INTRODUCTION

The objective of this chapter is to investigate the *in vitro* transdermal delivery of a model macromolecule by passive and iontophoretic means following pretreatment with a series of C_{12} penetration enhancers and to investigate prevalent mechanisms of action. The chapter begins by mentioning the importance of delivering macromolecules through the skin followed by a discussion of relevant studies employing both a chemical and physical approach to improve transdermal delivery of molecules. Subsequently, the method section details the experimental techniques involved in this study succeeded by a discussion of macromolecular diffusion profiles determined. The overall findings are then summarised.

5.2 TRANSDERMAL MACROMOLECULAR DELIVERY

Recent advances in the biotechnological sciences, for example in the area of genetic engineering, have led to the large-scale production of a series of hydrophilic macromolecules such as proteins, peptides and oligonucleotides. These entities cover a multitude of therapeutic areas and potentially have the capacity to treat a number of disease states (Maher, 1996). However, being able to realise the promise of such molecules is complicated because their delivery into humans is made difficult for a number of reasons; generally biologically active macromolecules have low oral bioavailability and short biological half-lives, making oral delivery impractical. Therefore, being able to deliver these chemicals across skin is one method of circumventing these problems. Principally, transdermal delivery would avoid drug degradation in the stomach, intestine or first-pass metabolism in the liver and has the potential for steady or time-varying controlled delivery.

However, the skin represents a formidable barrier to diffusion of applied drugs (see chapter 1) and efforts so far have generally concentrated towards delivering solutes having molecular weights of less than 1000Da (Yoshida and Roberts, 1993), whilst the new generation of chemicals have much larger masses. Clearly, therefore, in order to successfully deliver macromolecules transdermally into humans, robust delivery strategies need to be employed that are not only able to (i) reversibly perturb the skins barrier function but also (ii) allow the penetration of large molecular weight entities. With this goal in mind, experiments in this chapter combined both chemical (use of transdermal penetration enhancers) and physical (iontophoretic) modes of percutaneous enhancement in an attempt to deliver a model macromolecule. The following sections discuss some relevant reports concerning this bimodal delivery strategy.

5.2.1 Iontophoretic enhancement

Iontophoresis is an alternative method for promoting the flux of charged molecules across skin. It normally refers to the transfer of ionic solutes through biological membranes under the influence of an electric field. In essence, charged molecules, dissolved in a suitable electrolyte solution (donor), are brought into contact with a "driver" electrode of similar polarity and skin. The circuit is completed by connecting this electrode to one of opposite charge, which is likewise placed in an electrolyte solution also in contact with skin. When an electromotive force is applied, electro-repulsion occurs at the driving electrode surface, serving to propel the drug into the adjacent skin.

Iontophoresis can be applied to transdermal macromolecular delivery on the basis that many polypeptides exist as ions at physiological pH. As discussed in chapter one, the extent of delivery is determined by (i) magnitude of the electric field applied across skin, (ii) extent of membrane alteration caused by the applied field and (iii) extent of water transport induced by the electric field (electroosmotic flow). Table 5.1 summarises a number of studies that have employed iontophoresis to deliver macromolecules transdermally. In one study, Green *et al*, (Green *et al.*, 1992) investigated the delivery of a positively charged tripeptide (Threonine-Lysine-Proline) across nude rat skin. *In vitro* studies showed that iontophoresis significantly enhanced peptide delivery compared to passive transport, and that delivery was directly proportional to the amount of current applied (over the range 0.18-0.36mA/cm^2). Further, current was found not to degrade the peptide in any compartment of the transport cell used or cause any gross morphological changes in skin. However, the authors also point out the inefficiency of iontophoresis since, at a current of 0.36mA/cm^2, only 0.07% of the total applied dose was delivered after three hours. This is because most of the applied current was carried by the smaller and more mobile ions such as Na^+ and Cl^- that are present in skin and the formulation applied.

A number of studies have focused on delivering insulin *via* the skin as this would alleviate the discomfort and inconvenience experienced by diabetics due to repeated subcutaneous

Table 5.1 Reports of iontophoretic delivery of macromolecules

Macromolecular drug	Molecular weight (kDa)	Reference:
Angiotensin 2	1.0	(Clemessy *et al.*, 1995)
Octreotide	1.0	(Lau *et al.*, 1994)
Arginine-Vasopressin	1.1	(Lelawongs *et al.*, 1989)
Desmospressin	1.1	(Martin *et al.*, 1991)
Luteinizing hormone releasing hormone	1.2	(Miller *et al.*, 1989)
Nafrelin	1.3	(Delgado-Charro and Guy, 1995)
Calcitonin	3.5	(Thysman *et al.*, 1994)
Growth hormone releasing factor	3.9, 5.0	(Kumar *et al.*, 1992)
Carboxy- Insulin	5.2	(Pikal and Shah, 1989)
Insulin	~6.0	(Banga and Chien, 1993)

insulin injections (Banga and Chien, 1993; Langkjaer *et al.*, 1998); in particular, iontophoresis has the potential to control insulin input (either pulsatile or continuous) (Langkjaer *et al.*, 1998). These studies have shown that insulin in sufficient quantities can be transported across animal skin by electrical means to treat small diabetic animals. However, scaling up to humans would involve the use of too large a patch or device rendering its use impractical. Nevertheless, monomeric insulin (exhibiting greater charge and faster absorption than the parent insulin) after being delivered iontophoretically has been reported to achieve therapeutic insulin plasma levels for an adult diabetic (Langkjaer *et al.*, 1998).

Overall, the iontophoresis literature shows that despite success with animal skin, clinically relevant iontophoretic protocols have been capable of transporting macromolecules across human skin in just a few cases, generally limited to compounds of approximately 1 kDa in size (Praustnitz, 1997).

5.2.2 Chemical enhancement

The use of chemical enhancers to ease the diffusion or partition of drugs into stratum corneum has been well documented, many different groups of percutaneous enhancers having now been identified (Smith and Maibach, 1995). Generally, it is accepted that a saturated side-chain of 10-14 carbons is a pre-requisite to ensure significant enhancement activity (Aungst *et al.*, 1986; Bouwstra *et al.*, 1992a; French *et al.*, 1993; Kushla and Zatz, 1991; Ogiso and Shintani, 1990; Scheuplein and Dugard, 1973). However, the capability of enhancers to promote the transport of macromolecules across skin has not been well demonstrated (Praustnitz, 1997) and the few reports available show low enhancement factors. One study (Hoogstraate *et al.*, 1991) has reported on peptide transdermal flux following skin pretreatment with N-alkylazacycloheptanones of varying hydrocarbon chain length. The flux of desglycinamide arginine vasopressin (DGAVP) across human stratum corneum following PG or hexyl- or octyl-Azone® did not vary significantly from control skin (untreated). However, permeability did increase (although only moderately) following pretreatment with decyl-Azone® (1.9 fold), dodecyl-Azone® (3.5 fold) and tetradecyl-Azone® (2.5 fold).

Generally, it is thought that although chemical transdermal enhancers have been shown to be successful in promoting the flux of low molecular weight drugs, their affect on enhancing flux of macromolecules is limited (Praustnitz, 1997).

5.2.3 Electrical and chemical (bimodal) enhancement

Transdermal iontophoresis and the use of percutaneous penetration enhancers are electrical (physical) and chemical means to improve the delivery of topically applied drugs into and through skin. If employed together, it would be under the premise that a synergy between the different methods would result in greater flux at lower applied voltages and/or concentration of enhancer. Inevitably, this would lead to a reduction in the chances of inflammatory response during system application. Both methods ultimately aim to reversibly perturb the excellent naturally occurring barrier function of the stratum corneum. Separately, the mechanisms (chapter one) of action of both modes of delivery have been well documented (Walters and Hadgraft, 1993). What is less clear, however, is the mechanism of chemical enhancer action in conjunction with iontophoresis; early reports suggest that the charge which an enhancer carries is important (Fang *et al.*, 1997; Hirvonen *et al.*, 1993; Van der Geest, 1998) while some studies have reported no significant additive affect (Gay *et al.*, 1992, Wearley and Chien, 1990). Table 5.2 lists most of the studies that have reported on chemical and physical transdermal enhancement.

Table 5.2 Reports combining chemical and iontophoretic means of transdermal delivery

Drug	Molecular weight	Charge	Chemical enhancer	Current applied (mA/cm^2)	Synergy reported	Reference:
Leuo-prolide	1209	+ ve	Ethanol	Not given	Yes	(Srinivasasn *et al.*, 1990)
LHRH[a]	1200	+ ve	SFA[b]	0.2	Yes	(Bhatia and Singh, 1998)
			UFA[b]		Yes	
CCK-8[d]	1150	- ve	Oleic acid	0.2	Yes	(Bhatia *et al.*, 1997)
CCK-8[d]	1150	-ve	Ethanol	Not given	Yes	(Srinivasasn *et al.*, 1990)
Metoprolol	685	+ ve	Azone®	0.53	Yes	(Ganga *et al.*, 1996)
Cromolyn sodium	512	- ve	Ethanol	0.1	Yes	(Gupta *et al.*, 1994)
			SLS[e]	0.1	No	
			SDS[f]	0.1	No	
Piroxicam	315	- ve	Oleic acid[g]	0.07	No	(Gay *et al.*, 1992)
				0.36	No	
				0.5	Yes	
			Oleic acid[h]	0.36	Yes	
Apo-morphine	312	+ ve	DTAB[i]	0.5	No	(Van der Geest, 1998)
			LA[j]	0.5	No	
			$C_{12}EO_3$[k]	0.5	Yes	
Sotalol	272	+ ve	NNDA[l]	Not given	No	(Hirvonen *et al.*, 1993)
			Azone®	Not given	No	
AZT[m]	252	Neutral	Oleic acid	0.5	Yes	(Oh *et al.*, 1998)
AZT[m]	252	Neutral	$C_{10}MSO$[n]	0.157	No	(Wearley and Chien, 1990)

[a]leutinising hormone releasing hormone, [b]SFA/[c]UFA=saturated fatty acid/unsaturated fatty acid, study showed that UFA with iontophoresis resulted in greater enhancement than SFA with iontophoresis; additional double bonds did not affect the degree of enhancement, [d]cholecystokinin (peptide), [e]sodium lauryl sulphate, [f]sodium dodecyl sulphonate, [g]oleic acid present in gel applied, [h]skin pretreated with oleic acid and then gel applied, [i]dodecyl trimethyl ammonium bromide, [j]lauric acid, [k]trioxyethylenedodecyl ether, [l]N,N-dimethylamino acetate [m]azdiothymidine, [n]N-decylmethylsulfoxide

5.3 AIMS OF CHAPTER

It is well accepted that for iontophoretic and chemical modes of enhancement, an inverse relationship exists between drug flux and permeant molecular weight (Brand *et al.*, 1998; Pikal and Shah, 1989). However, the challenge to deliver effectively into the body the new generation of biotechnologically produced drugs (Berner and Dinh, 1998) is (amongst other factors) intrinsically linked to their comparative large molecular weights (Brand *et al.*, 1998; Green *et al.*, 1992; Green *et al.*, 1993). The objectives of this study were to combine iontophoresis and the use of enhancers in an attempt to assess transdermal flux of the model macromolecular compound, Dextran (M_w=3kDa) (Figure 5.1) and to investigate the prevalent mechanisms of enhancement. Electrically assisted and passive diffusional profiles together with steady state-flux values have been determined and contrasted.

Dextran is a hydrophilic bacterial *exo*-polysaccharide. It is biologically inert due to its uncommon of α-1,6-linked D-glucopyranose residues, making it resistant to cleavage by most endogenous cellular glycosidases. Dextrans also have a low percentage of α-1,2, α-1,3 and α-1,4-linked side-chains (Van Dijk-Wolthuis, 1997). Dextrans with defined molecular weights are obtained by partial depolymerization and subsequent fractionation of the high molecular weight native compound (about 10^3 kDa) (Van Dijk-Wolthuis, 1997).

Dextran (D) used in the experiments described here carried three negative charges by virtue of coupling to the fluorescent probe, Cascade Blue® (CB), thus ensuring its capacity to be delivered by iontophoresis (Figure 5.2). CB is water-soluble (~8% for the lithium salt), has high absorptivity (absorbs fluorescence at 400 and emits at 420 nm), is highly fluorescent and unlike most dyes resists quenching upon conjugation (Haugland, 1996). CB is coupled to dextran and yields a strong amide linkage (degree of substitution in all experiments was 0.7).

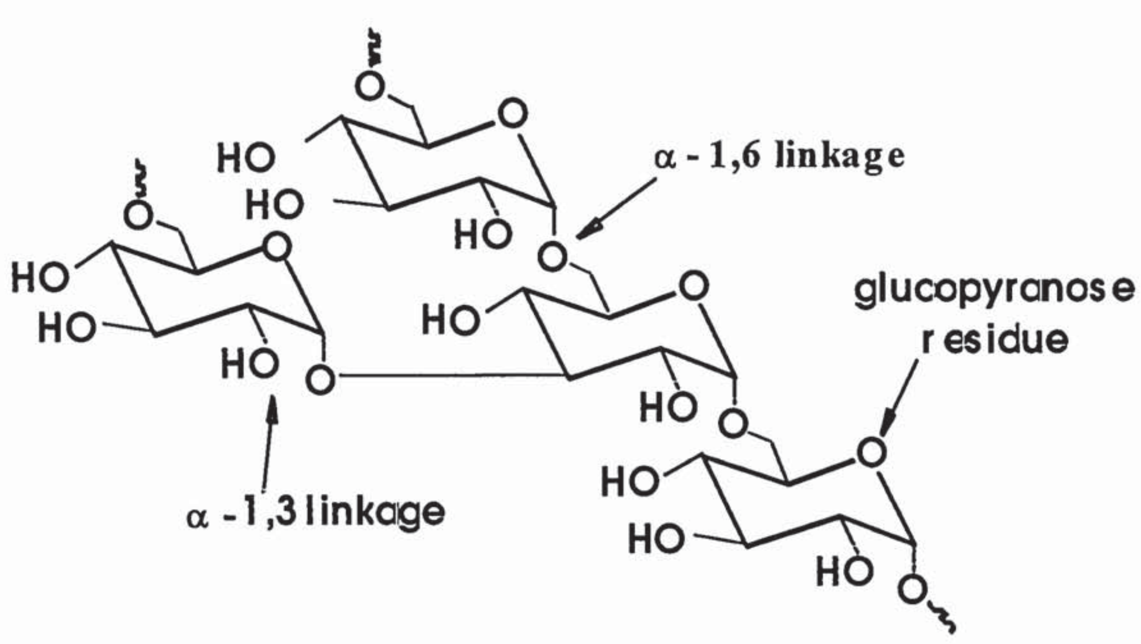

Figure 5.1 Structural features of dextran used in experiments

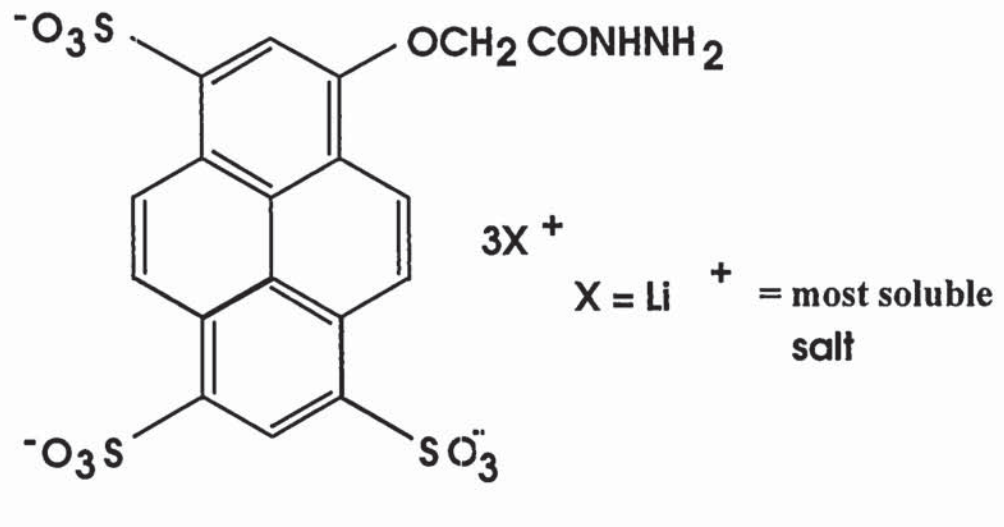

Figure 5.2 Structure of the fluorescent label, Cascade Blue®

5.4 MATERIALS AND METHODS

5.4.1 Materials

Dextran labelled with cascade blue® (D-CB) of molecular weight 3kDa and free label cascade blue® were purchased from Molecular Probes (Leiden, Holland). All enhancers, dodecyltrimethylammonium bromide (DTAB) and sodium dodecyl sulphate (SDS) (apart from Azone®) and propylene glycol were obtained from Sigma Chemicals (St. Louis, USA). Azone® was a gift from Whitby Research Ltd. The buffer used was phosphate-buffered saline (PBS) pH 7.4 (8mM Na_2HPO_4, 1.5mM KH_2PO_4, 139mM NaCl, 2.5mM KCl in Millipore water). Solutions of D-CB were prepared in PBS.

5.4.2 Preparation of electrodes

AgCl electrodes (cathode) were produced as follows. Silver wire was cut to a length of 5 cm. At one end, the wire was then bent back onto itself to form a small loop. The wire loop was then dipped into molten AgCl powder until a regular shaped bulb was formed at the tip. The wire was then left to cool for three hours after which the cathodes were ready for experimental use.

After each experiment, Ag was removed from cathodes by placing them in regeneration solution (having the following composition; KCl =16g and concentrated HCl = 25ml in one litre of Millipore water) and a current being applied for approximately three hours.

Ag foil or plate having dimensions 5cm x 0.4 cm x 0.2 cm was used as the anode. Anodes were regenerated by gently rubbing off AgCl (deposited on them during experiments) with sand paper. All Ag products were purchased from Aldrich (Holland).

5.4.3 Epidermis and Stratum Corneum preparation

Whole thickness abdominal skin was obtained from local hospitals following cosmetic surgery; the underlying subcutaneous fat together with other adhering debris was removed using a surgical scalpel and the skin was then dermatomed to a thickness of 200μm (Padgett Electro Dermatome Model B, Kansas City, USA). The epidermal sheet was spread flat on filter paper soaked in 0.1% trypsin solution (type III from bovine pancreas, Sigma Chemicals, St. Louis, USA) and stored in a refrigerator at 4°C overnight. The following day, the skin was removed and placed in a oven at 37°C for one hour after which the SC was carefully teased away from the remaining underlying epidermis. Each SC sheet was then washed in an aqueous 0.1% trypsin inhibitor solution (type II from soybean, Sigma Chemicals, St. Louis, USA) by gentle shaking for 30 seconds. Sheets of SC were subsequently rinsed twice in Millipore water, transferred to wire gauze, left to dry at room temperature and finally stored over silica gel in a nitrogen-rich and airtight atmosphere until needed for experiments.

5.4.4 Iontophoresis Experiments

(i) Pretreatment with enhancers

SC sheets were floated on Millipore water (dermal side being in contact with water) and left to hydrate for two hours. Dialysis tubing membrane (DM) having a molecular weight cut off of 50,000Da (Hicol bv, Holland) was immersed in a beaker of water containing 1%w/v $NaHCO_3$ (Sigma, UK), boiled for 30 minutes, allowed to cool and washed in water. Using a steel punch and dye, circular discs (having a diameter of 13mm) were cut out from SC and DM, and each piece of SC was carefully positioned on a DM disc to provide support for the tissue. Two pieces of SC were then sandwiched in each of the three compartmental iontophoretic cells as shown in Figure 5.3. PBS was pippetted into cell acceptor compartments to prevent dehydration of the SC and 120μl of enhancer solution (0.16M in PG) pippetted into the cathodal (donor) chamber ensuring that the entire SC surface was covered. The cells were left positioned vertically for 18 hours after which the SC was washed three times with PBS to remove any traces of enhancer.

(ii) Transport studies

Transport experiments to determine steady-state flux as a function of donor concentration and enhancer pretreatment were performed. PBS and D-CB solutions (2ml) were pippetted into the receptor and donor compartments and Ag (anode) and AgCl (cathode) electrodes were inserted into these chambers respectively. Silver measuring electrodes were also placed in both chambers to record the electrical resistance of SC during each experiment. The electrodes were connected to a 6-channel computer-controlled current source powered by a +/- 40-volt supply (Electronic Department, Leiden University).

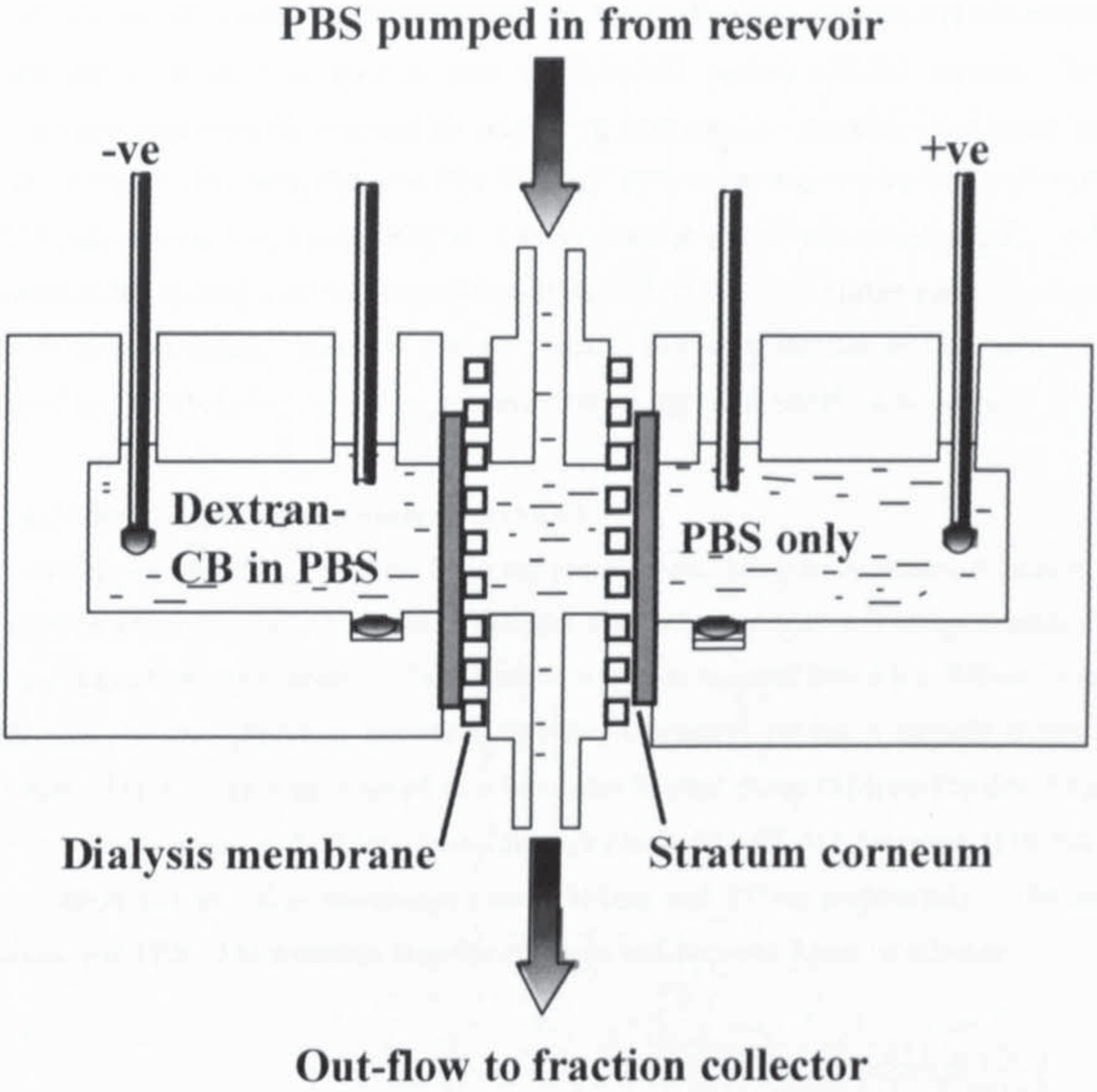

Figure 5.3 Cross section diagram of three-compartment horizontal diffusion cell used in experiments.

Anodal and cathodal chambers were continuously stirred at 375rpm. PBS was continuously pumped at a rate of 7ml/hour, through the central acceptor compartment (volume 0.5ml) from a reservoir to a Retriever IV fraction collector (Isco, Holland) using a peristaltic pump (Ismatec SA, Switzerland). Fractions were collected hourly in test tubes and then assayed for dextran content. Each experiment started with a six-hour passive period (no current) and was followed by nine hours of current application (500µamps/cm^2) and finally a six-hour passive post iontophoretic period without current. Dextran concentrations were determined by measuring fluorescence intensity on a Jasco 821-FP (H.I.Ambacht, Holland) detector (Ex 401, Em 431) connected to an autosampler (Gilson 234 autoinjector, UK.) using PBS as mobile phase at a flow rate of 0.5ml/min. A linear relationship existed over the range 7.5ng-100ng/ml ($r^2 = 0.99$). Fluxes versus time profiles were then produced. Relevant transport studies involving the use of free label Cascade blue® in PBS (0.1mM) were also performed following an identical methodology.

5.4.5 Size-exclusion chromatography (SEC)

To determine the integrity of D-CB in the presence and absence of electrical current, SEC analysis was performed. Samples of solution were taken from all cell compartments during all stages of transport studies. Each sample was then injected into a 8 x 300mm Suprema 30 SEC column (Polymer Standards Service, Germany) having a particle diameter of 10µm. The column was attached to a Isochrom solvent pump (Spectra-Physics, England, flow rate: 1ml/min) and a fluorescence detector (Jasco 821-FP, H.I.Ambacht, Holland). The excitation and emission wavelengths were 401nm and 431nm respectively. The mobile phase was PBS. The retention time for all peaks was between 7 and 10 minutes.

5.4.6 Statistical analysis

All transport cell results are represented as the means of 4 to 11 experiments ± standard errors. Statistical difference was tested for by using an unpaired Student's t-test, statistical significance being defined as $p<0.05$.

5.5 RESULTS AND DISCUSSION

5.5.1 Untreated Stratum Corneum

The dependence of dextran transport on donor concentration is illustrated by Figure 5.4, which summarises steady state flux (J_{SS}) values for Cascade blue®-labelled dextran (D-CB), as a function of donor concentration and treatment regimen (stage 1:- 6 hours of passive transport; stage 2:- 9 hours of iontophoresis, and stage 3:- 6 hours of passive delivery).

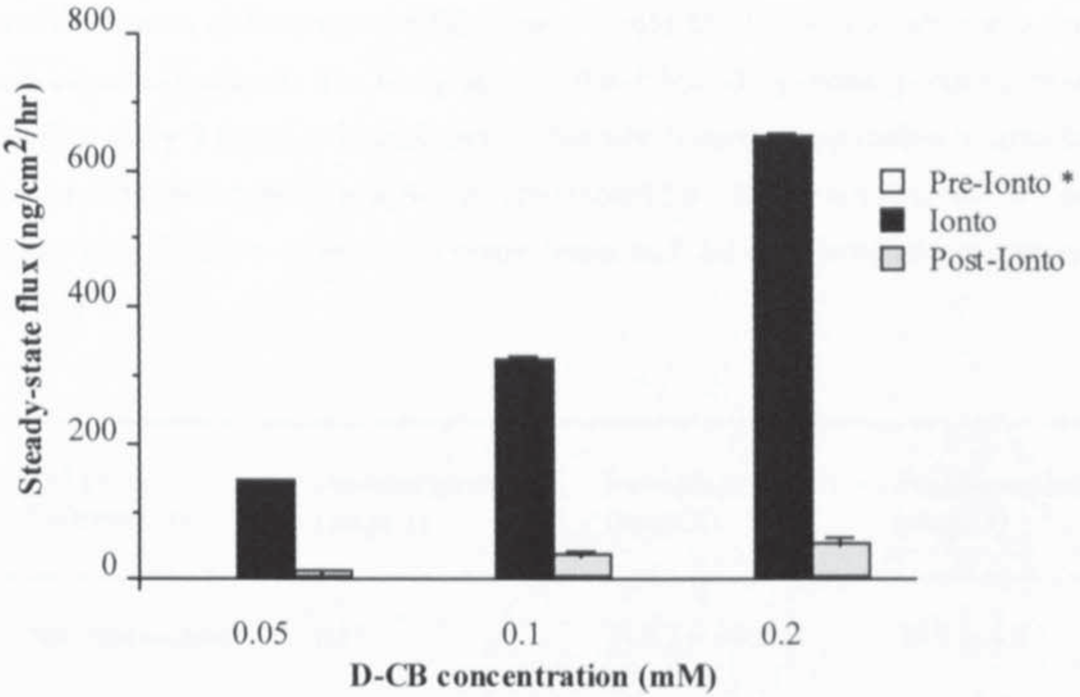

Figure 5.4 Effect of D-CB donor concentration on permeant steady-state flux across untreated human SC. *Note: pre-iontophoretic (passive) D-CB transport was below the limit of detection

The corresponding permeation profile for an applied D-CB concentration of 0.1mM is shown in Figure 5.5. Dextran transport across untreated SC was not detected during stage 1 (indicating the need for facilitated means) but was significantly enhanced during, and subsequent to, the application of an electrical potential (stages 2 and 3, respectively). On application of current (500μamps/cm^2), an immediate increase in D-CB flux was observed, with iontophoretic fluxes reaching steady state within 5 hours and being linearly proportional to the applied drug concentration ($r^2 = 0.99$). Typically (Volpato *et al.*, 1995), J_{SS} six-hours post iontophoresis did not return to passive pre-iontophoretic levels, but ranged between 8-10% of that during iontophoresis, indicating possible current or water induced perturbation of SC permeability, (see also table 5.3).

5.5.2 Pre-iontophoresis

To increase dextran transport, SC was pretreated with either a cationic (DTAB), anionic (SDS) or uncharged (Azone®) transdermal penetration enhancer (0.16M) in PG. Figure 5.5 profiles dextran diffusion across SC from a 0.1mM D-CB donor solution as a function of pretreatment employed. The first phase (t = 0 to 6 hours) represents passive diffusion; this is followed by 9 hours of iontophoresis, after which current application is terminated, and (post-iontophoretic) passive diffusion is monitored for a further 6 hours. D-CB steady-state values as a function of enhancer pretreatment and delivery protocol are summarised in Table 5.3.

Enhancer Pretreatment	Pre-iontophoresis (stage 1)	Iontophoresis (stage 2)	Post-iontophoresis (stage 3)
No Pretreatment	nd*	313.7 ± 10.9	26.5 ± 4.9
DTAB	47.5 ± 7.2	477.2 ± 29.3	52.2 ± 3.1
PG only	11.8 ± 2.6	272.7 ± 17.0	28.8 ± 2.1
Azone®	22.7 ± 3.1	210.3 ± 9.6	33.6 ± 2.2
SDS	11.5 ± 1.7	172.7 ± 7.0	17.2 ± 1.5

Table 5.3 Steady-state flux ($ng/cm^2/hr$) for D-CB transport as a function of chemical pretreatment during passive and/or iontophoretic modes of delivery, *not detectable

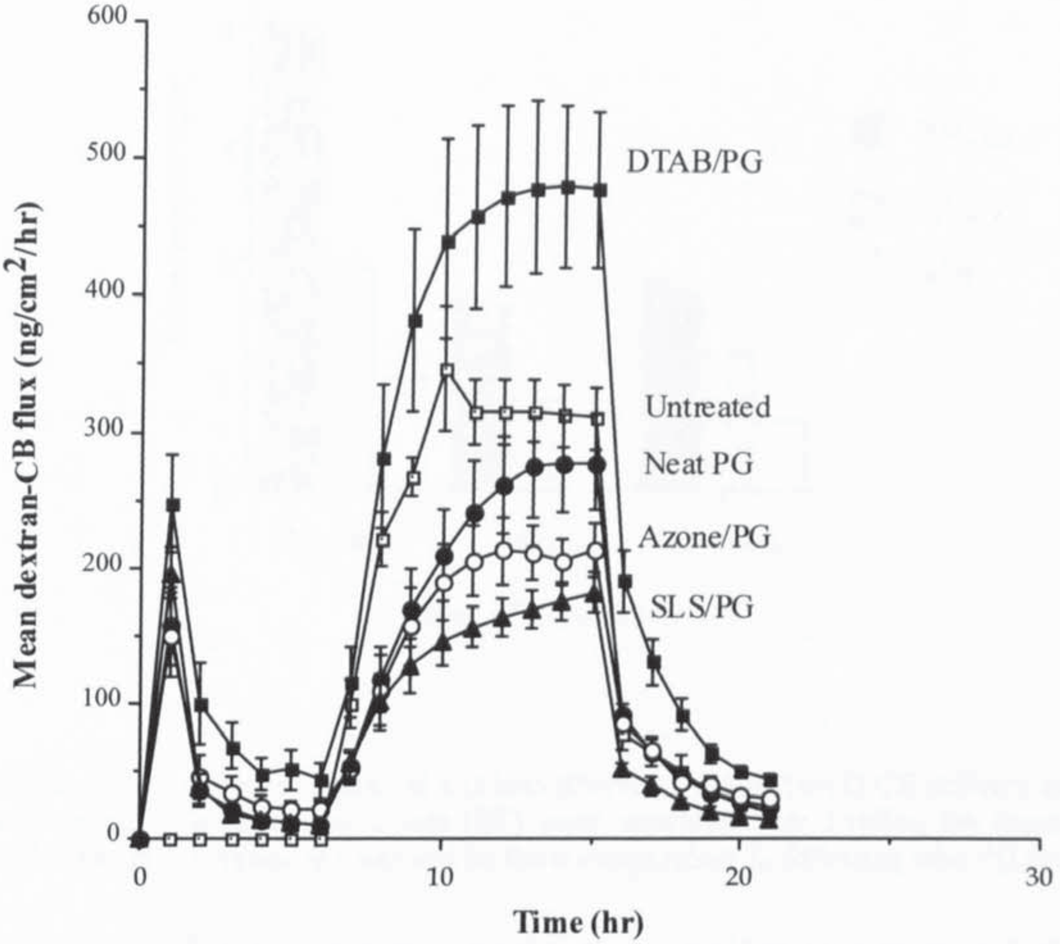

Figure 5.5 Passive and iontophoretic permeation profiles of D-CB across untreated human stratum corneum (—□—) and following pretreatment with 0.16M DTAB/PG (—■—), neat propylene glycol (—●—), 0.16M Azone®/PG (—○—) and 0.16M SDS/PG (—▲—).

During stage 1, all systems (including PG) significantly elevated passive D-CB flux relative to that of untreated SC. When compared to the PG-treated control (to differentiate between vehicle and enhancer effect), the greatest degree of "passive enhancement" was achieved by DTAB (x 4-fold), followed by Azone® (x 2-fold), while the activity of SDS was equivalent to that of the solvent, PG (see Figure 5.6).

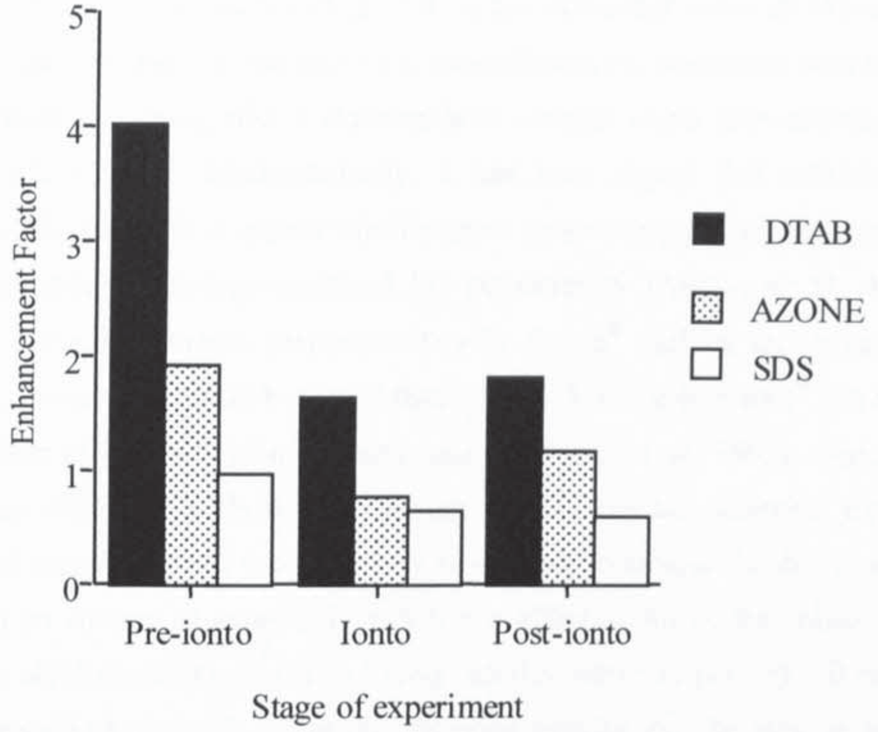

Figure 5.6 Effect of chemical and iontophoretic treatment on D-CB delivery across human SC. Enhancement factors (EF) were determined by dividing the appropriate J_{ss} following given enhancer treatment by the corresponding J_{ss} following neat PG treatment.

Interestingly, flux measurements recorded during the first hour of stage 1 showed an unexpected spike for each enhancer-mediated profile (Fig.5.5). One possible explanation for this decline in flux after t=1hr was considered to be enhancer washout from SC during the first hour of permeation. This could potentially have abated enhancer effects and thus invalidated any comparison of enhancer performance (derived from D-CB steady state-flux determinations) during iontophoresis. In order to resolve this issue, experiments which excluded stage 1 (thereby ruling out any possibility of passive enhancer washout from the SC) but comprising stages 2 and 3 (following DTAB pretreatment) were conducted. The steady-state flux produced under these conditions was not significantly different ($P>0.05$) from that obtained earlier (Table 5.3 under stage 2). Consequently, it was concluded that the spike was not caused by enhancer washout during stage 1 and that its occurrence did not affect chemically enhanced iontophoretic steady-state flux. Although the exact cause of this spike remains unknown, the observation that this peak is absent in untreated skin but present in all PG-treated samples (including PG alone) suggests it is solvent-mediated.

Returning to the diffusion studies (Figure 5.5), the difference between DTAB and SDS mediated J_{ss} was ~4 fold. On the face of it, this difference is consistent with the literature reporting greater enhancing effects attributable to cationic rather than anionic surfactants (Ashton *et al.*, 1992a). Mechanistically, it has been shown that cationic surfactant treatment of SC results in a greater birefringence measurement when compared to their anionic counterparts, inferring enhanced SC permeability (Ashton *et al.*, 1992b). In comparison, stratum corneum pretreatment with Azone® yielded questionable results; exhibiting J_{ss} above that of SDS but lower than DTAB. Previously Azone® has been shown to enhance flux of a variety of macromolecules (Hadgraft *et al.*, 1993). Since evidently enhancers are affecting D-CB flux to varying extents, but all enhancers are known to penetrate and perturb the SC, it was thought reasonable to look at the differences in their structures in an attempt to explain their differing effects. All of the enhancers share a common C_{12} alkyl chain but possess a headgroup that varies in polarity. Bearing this in mind, one possible hypothesis is that this differing polarity may be altering the negative charge the skin carries (Burnette and Ongpipattanakul, 1987) and modulating the flux of anionic D-CB. For example, cationic DTAB may lower SC negativity, *reducing* electrostatic repulsions between similarly charged SC and D-CB thus yielding a greater flux. Alternatively, SDS could add to the skin's negative charge, leading to *enhanced* repulsion between membrane and permeant and thus hindering flux. This relationship is summarised in Table 5.4. Although this theory is mainly conjecture without the inclusion of further permeants of varying charge and negative controls (neutral similarly sized permeants) it does raise applicable points and forms a basis for further investigations.

5.5.3 Iontophoresis

The effect of iontophoresis, alone and in combination with chemical enhancers, on the transdermal delivery of D-CB was investigated in the subsequent series of experiments. While the impact of chemical pretreatment upon D-CB permeation across the SC was notable, but not substantial, the effects of electrically-enhanced D-CB delivery were more intriguing (Figures 5.5 /5.6 and Table 5.3). The iontophoretic steady-state flux of D-CB (in the absence of chemical pretreatment) reached a value of 313.7 (±10.9) $ng.cm^2.hr^{-1}$ after ~6 hours of current application, compared to a passive D-CB flux which was 'undetectable'.

Table 5.4 Summary of charge relationships between skin, drug and enhancer during passive delivery.

Net skin charge	Charge of drug	Charge of enhancer	Comparative* effect on J_{SS}
negative	negative	positive	increase
negative	negative	negative	decrease
negative	negative	neutral	decrease

*Compared to control dextran J_{SS} flux following pretreatment with neat PG (solvent)

When an iontophoretic current was applied in combination with enhancers (that is, following chemical pretreatment of SC), to drive D-CB across the membrane, the resulting D-CB fluxes revealed interesting phenomena. For instance, the data indicate that iontophoresis increased values of J_{ss} by a factor of at least 10, relative to the corresponding passive fluxes and that DTAB pretreatment coupled with iontophoresis achieved the highest absolute D-CB flux (477 ± 29.3 ng.cm^2.hr^{-1}) of all the treatment protocols described (Table 5.3).

While these data suggest a co-operative effect between iontophoresis and chemical enhancers, comparison of the *'iontophoresis + chemical pretreatment'* fluxes relative to the '*iontophoresis + PG pretreatment*' fluxes (note that all the chemical enhancement regimes comprised PG as the solvent), further probes the influence of the enhancer *itself* on the iontophoretic effect (Figure 5.6). Hence, this type of analysis reveals that DTAB has the greatest impact (albeit an approximately 2-fold enhancement; $p<0.05$), while Azone® and SDS markedly *attenuate* the iontophoretic driving force ($p<0.05$). In other words, the impact of iontophoresis on the transport of D-CB appears to be subdued by the co-administration of certain enhancers, rather than be 'synergistically' augmented, as one might expect. Furthermore, PG pretreatment prior to iontophoresis offers no additional benefit (compared to the iontophoresis *alone* protocol).

5.5.3.1 Stratum corneum resistance

During all iontophoresis facilitated transport studies, measuring electrodes were used to determine changes in the resistance of stratum corneum. The resistance of skin is a function of its permeability to mobile ions (Cranne-van Hinsberg *et al.*, 1994). Resistance values can therefore potentially indicate the integrity of the skin barrier to ionic transport. Figure 5.7 profiles skin resistance as a function of both time and pretreatment regimen. Table 5.5 summarises the initial skin resistance and gives a value for steady state resistance of stratum corneum depending on enhancer pretreatment. All profiles were similar and showed a marked and immediate decrease in SC resistance on the application of current. After one hour, SC resistance is virtually identical for all pretreatments. Table 5.6 shows that the initial resistance of untreated SC was significantly ($P<0.05$) higher than that for pretreated SC samples. This finding is consistent with other reports quoting similar measurements (Cranne-van Hinsberg *et al.*, 1994). In theory, this decrease in SC resistance (following pretreatment) should show an overall increase of the conductance of the pathways for small ions due to pretreatment with penetration enhancers. Further, the initial SC resistance values following enhancer pretreatment were indifferent from each other ($P>0.05$).

The steady-state resistance of SC during nine hours of current application is also recorded in Table 5.5. The lowest value for resistance was for DTAB pretreated SC, whilst the highest was for SDS treated SC. This equates well with D-CB flux findings (Table 5.3) since one would expect SC resistance after DTAB pretreatment to be lower than SDS pretreated SC because flux was greater following DTAB treatment. However, closer inspection of Table 5.6 reveals that there was no significant difference in SC resistance between untreated and DTAB treated SC, whilst D-CB flux was significantly elevated following enhancer application. In addition, all enhancer mediated D-CB fluxes were different during iontophoresis but this was not the case for corresponding SC resistance values. Therefore, clearly SC resistance only partially correlates with the trend for D-CB flux observed during these experiments. Previously, it has also been reported elsewhere that SC resistance cannot be taken as an accurate marker for levels of drug flux (Van der Geest, 1998).

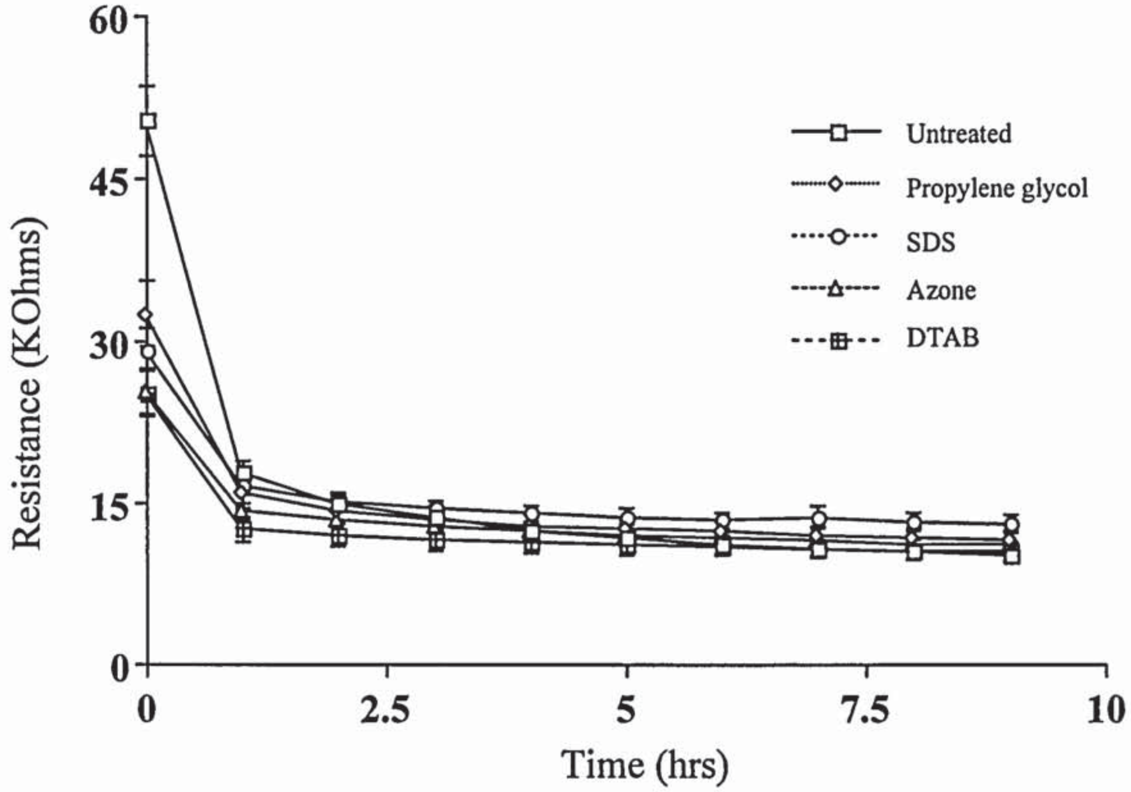

Figure 5.7 Stratum corneum resistance during iontophoresis as a function of pretreatment

Enhancer	Initial point	Steady-state resistance (kOhm)
No pretreatment	50.216±3.161	11.111±0.348
DTAB	29.091±1.959	10.876±0.127
PG only	32.428±3.030	12.224±0.192
Azone®	25.350±2.147	11.698±0.210
SDS	25.673±2.051	13.467±0.150

Table.5.5 Initial and steady state resistance values (kOhms) for human stratum corneum during iontophoresis of 0.1mM dextran-cascade blue following pretreatment with transdermal penetration enhancers.

Although skin resistance to ionic current is localised in the SC, actual values vary between donors, within the same donor and between different body sites (Yamamoto and Yamamoto, 1976). The reason why skin resistance drops so markedly on the application of current is still an area of debate. Reports have suggested an irreversible electrical or thermal breakdown of lipid bilayers, mechanical rupture due to solvent flow, accumulation of ions within the skin, loss of structural components or electroporation of the multilamellar bilayer membranes of the SC (Chizmadzhev *et al.*, 1998; Cranne-van Hinsberg *et al.*, 1994).

5.5.3.2 Effect of molecular weight

In addition, the dependence of the degree of enhancement on permeant molecular weight was assessed for the enhancer, Azone®. The influence of Azone®/PG on the transport of the anionic label cascade blue® (CB; 548 Da) was investigated. The resulting permeation profiles, and steady-state fluxes are shown in Figure 5.8 and Table 5.6, respectively. As with D-CB, passive transport of CB across untreated skin is below the analytical limit of detection, but is greatly enhanced by all treatment regimens. Additionally, the data show that the passive (following PG pretreatment) and iontophoretic transport of this smaller M_w anion is significantly ($P<0.05$) elevated relative to the delivery of D-CB, under identical experimental conditions. This is clearly consistent with the physicochemical laws governing transport across a resistant membrane. In contrast, the passive transport of CB following Azone® pretreatment, is not significantly ($P>0.05$) different to that of the larger anion, D-CB, despite a 6-fold difference in M_w. Moreover, as for D-CB transport, the combined application of Azone®/PG and iontophoresis significantly *decreases* the delivery of CB relative to the corresponding regimen without Azone®.

The combined results in this chapter, demonstrate that (a) of the chemical enhancers tested, pretreatment with cationic DTAB produces the greatest enhancement of passive D-CB transport; (b) DTAB pretreatment coupled with iontophoresis achieves the highest absolute D-CB flux of *all* the treatment protocols described; (c) the enhancing ability of iontophoresis + chemical pretreatment is not greater than the sum of the effects of iontophoresis or chemical pretreatment employed individually, (there is no evidence of synergism between the two enhancement regimens) (d) in fact, the dual application of chemical pretreatment (Azone® or SDS) and iontophoresis can *attenuate* the iontophoretic

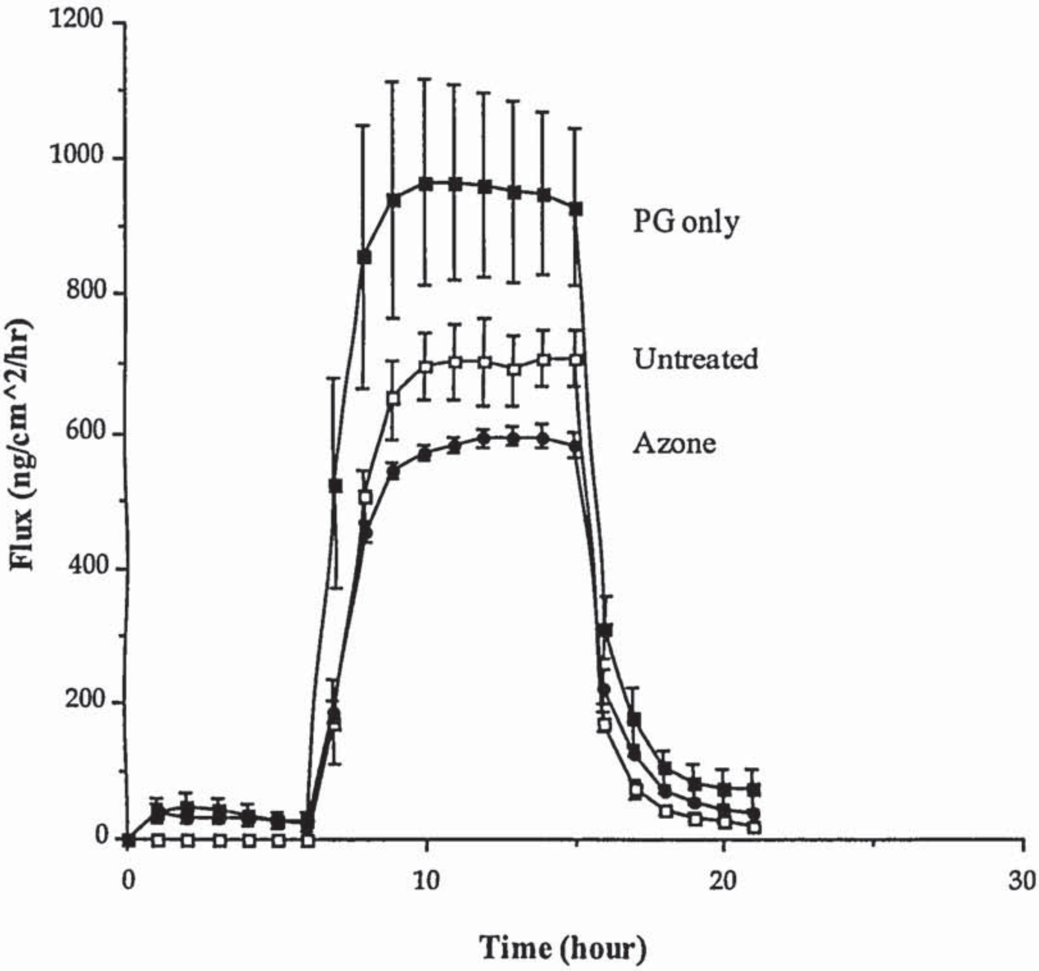

Figure 5.8 Passive and iontophoretic permeation profiles of free Cascade blue® (0.1mM) across untreated human stratum corneum (—□—)and following pretreatment with 0.16M Azone®/PG (—●—) and neat propylene glycol (—■—).

Enhancer Pretreatment	Pre-iontophoresis (stage 1)	Iontophoresis (stage 2)	Post-iontophoresis (stage 3)
No pretreatment	nd*	703.6 ± 21.3	27.3 ± 3.0
Azone®	27.7 ± 1.3	589.8 ± 6.7	47.1 ± 1.7
PG only	30.9 ± 7.7	950.9 ± 54.2	79.1 ± 14.7

Table 5.6 Steady state flux values for free Cascade blue® ($ng/cm^2/hr$) transport as a function of chemical pretreatment during passive and/or iontophoretic modes of delivery, *not detectable.

driving force for D-CB transport; and (e) this latter phenomenon is also observed for the iontophoretic delivery of the smaller anion, CB, following Azone® pretreatment.

The observation that DTAB enhances the percutaneous iontophoretic transport of D-CB, while Azone® and SDS retard the electrically-mediated delivery of this anionic macromolecule warrants further discussion. The application of an iontophoretic driving force (at constant current) would be expected to non-selectively enhance the delivery of all similarly charged and sized donor solution constituents. While enhancer pretreatment, and consequent barrier disruption, of the membrane might be expected to further elevate this transport, the observed selectivity of the enhancers tested is puzzling. One possible interpretation of this behaviour is based on the relative charges of the membrane, permeant, enhancer and driving electrode. The permselective nature of the skin, conferred by its net negative charge at physiological pH (Burnette and Ongpipattanakul, 1987; Chizmadzhev *et al.*, 1998), favours the transport of neutral and positively charged permeants in the anodal to cathodal direction (Chizmadzhev *et al.*, 1998; Kim *et al.*, 1993). Consequently, the cathodal delivery of anionic permeants is regarded to be considerably less efficient compared to the anodal transport of similarly sized cations of equal valence. In other words, the cathodal transport of D-CB is already at a relative 'disadvantage'. Furthermore, it is also reasonable to surmise that pretreatment with chemical enhancers offers a means to modify this membrane permselectivity. Indeed, the modulation of skin permselectivity has recently been the subject of considerable investigation (Fang *et al.*, 1997; Hirvonen *et al.*, 1993; Van der Geest, 1998; Wearley and Chien, 1990). Although the experimental design of the studies presented here (enhancer pretreatment of skin adjacent to the cathodal surface only) does not permit elaboration concerning the electroosmotic and electrorepulsive contributions to net D-CB iontophoretic flux, it is not unreasonable to expect the charge of the enhancer to influence these parameters. For example, it is conceivable that application of the positively-charged enhancer, DTAB, can aid the 'neutralisation' of the skin's negative charges, thereby facilitating cathodal delivery of the negatively-charged D-CB across a membrane which no longer 'discriminates' against anions. Similarly, it is reasonable to expect the negatively-charged SDS to 'augment' the skin's negativity, and hence, retard the cathodal transport of D-CB. However, the attenuating effect of the uncharged enhancer, Azone®, remains unexplained by these scenarios. One could also argue that the negatively-charged SDS is likely to be repelled at the cathode, driving it from the SC and therefore, attenuating its enhancing effect. Similarly, DTAB would be expected to be retained at the cathodal surface, prolonging its effect. Clearly, there are a number of possible mechanisms responsible for the observations presented here, which can only be discerned by further prudent and discriminating experiments.

5.5.4 Post-iontophoresis

Subsequent to the termination of current, D-CB flux values declined rapidly and reached steady state approximately 3 hours after current cessation. With the exception of the DTAB treatment set, these passive J_{SS} values (Table 5.3) remained significantly greater than those measured passively prior to current application ($P<0.05$). Indeed, the data suggest that DTAB treatment perturbs the SC barrier to a greater extent (at least, for a longer duration) than does current application.

5.5.5 Size-exclusion chromatography

The donor D-CB solution consisting of dextran (M_W= 3kDa) was poly disperse in nature. Therefore, the possibility existed that SC could behave permselectively, favouring the diffusion of slightly smaller dextran fragments and hence affect true flux. To determine the characteristics of dextran transported across stratum corneum, SEC was performed. The size-exclusion chromatograms of solutions in different cell compartments during transport studies are shown in Figure 5.9(a-d). Figures 5.9(a) and (b) represent the size-exclusion chromatograms for the 3kDa D-CB (used as the donor solution) and neat cascade blue®, respectively. The free label (cascade blue®) is retained on the SEC column longer than D-CB by virtue of its smaller molecular weight (548 Da); the data indicate negligible levels of free label in the applied donor solutions.

Figures 5.9(c) and (d) show the molecular weight distribution of dextran in receptor compartments (after dextran has been transported through the SC) during the passive and iontophoretic experimental stages respectively. In both cases, the chromatograms were essentially identical to that of the donor, confirming that the SC was not behaving permselectively and that dextrans were not being degraded in the SC or indeed by the application of current. Further, Figures 5.9 (e) and (f) show chromatograms of the molecular weight distribution of D-CB in donor compartments of cells following passive (e) and iontophoretic (f) modes of delivery. It is evident that the two chromatograms are identical to each other and to 5.9(a), indicating that dextran structural integrity was

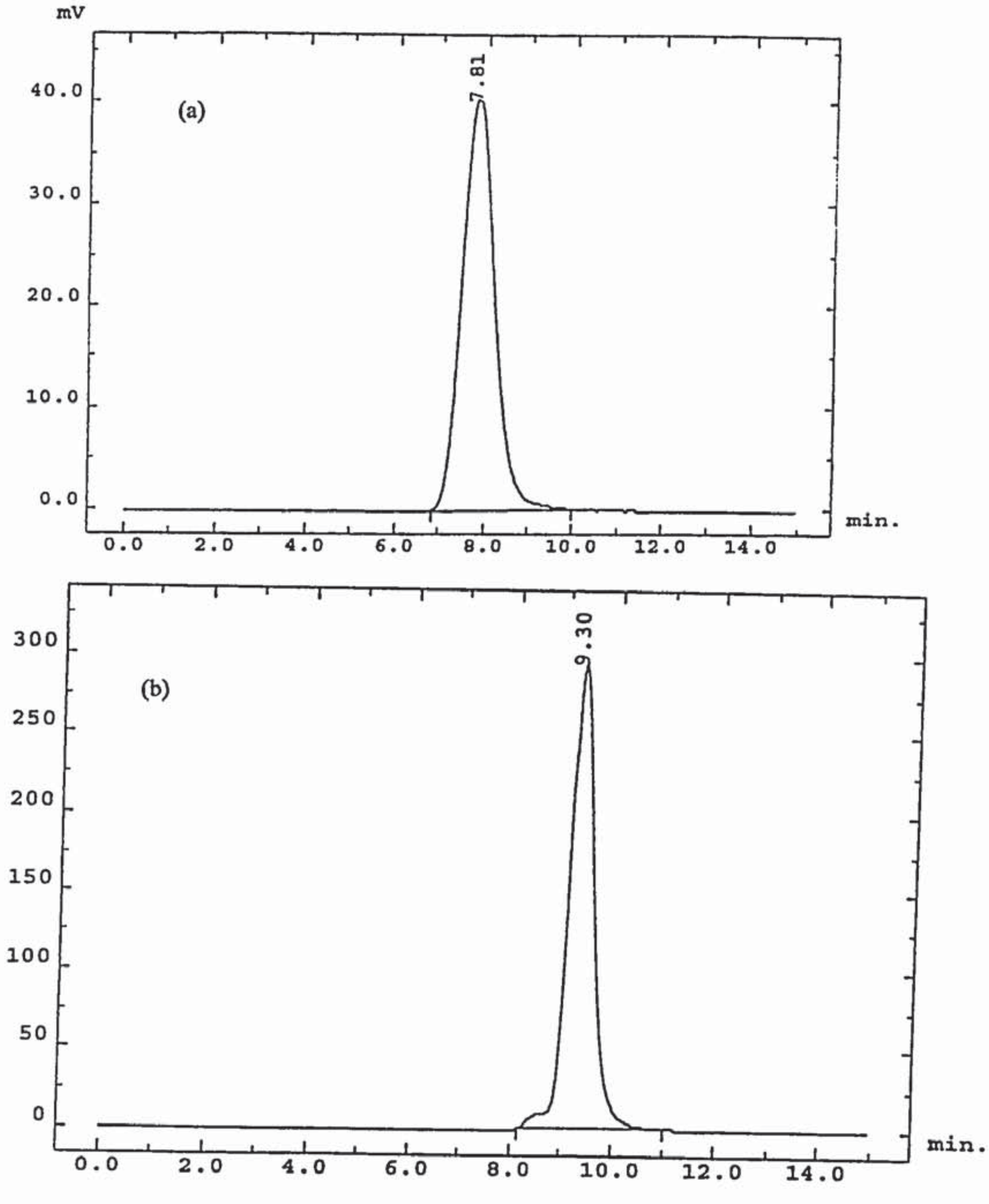

Figure 5.9 (a-b) Size-exclusion chromatograms of (a) Dextran-Cascade blue® used in donor chambers of transport cells and (b) Free label Cascade blue®. Digits in traces represent the retention times of each species on the column.

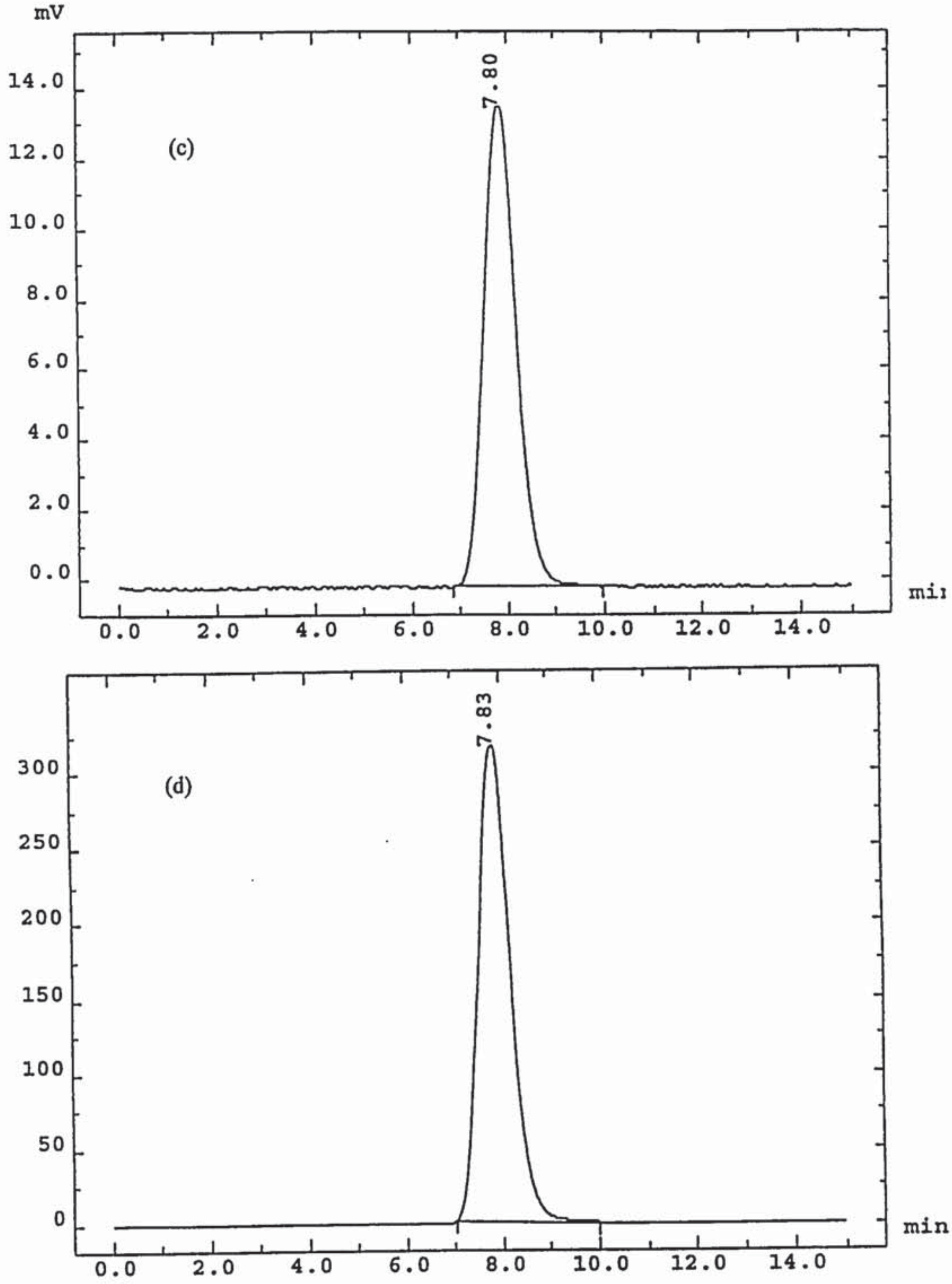

Figure 5.9 (c-d) Size exclusion chromatograms of (c) Dextran-Cascade blue ® present in acceptor chambers after passive diffusion and (d) Dextran-Cascade blue® present in acceptor chambers following iontophoresis. Digits in traces represent the retention times of each species on the column.

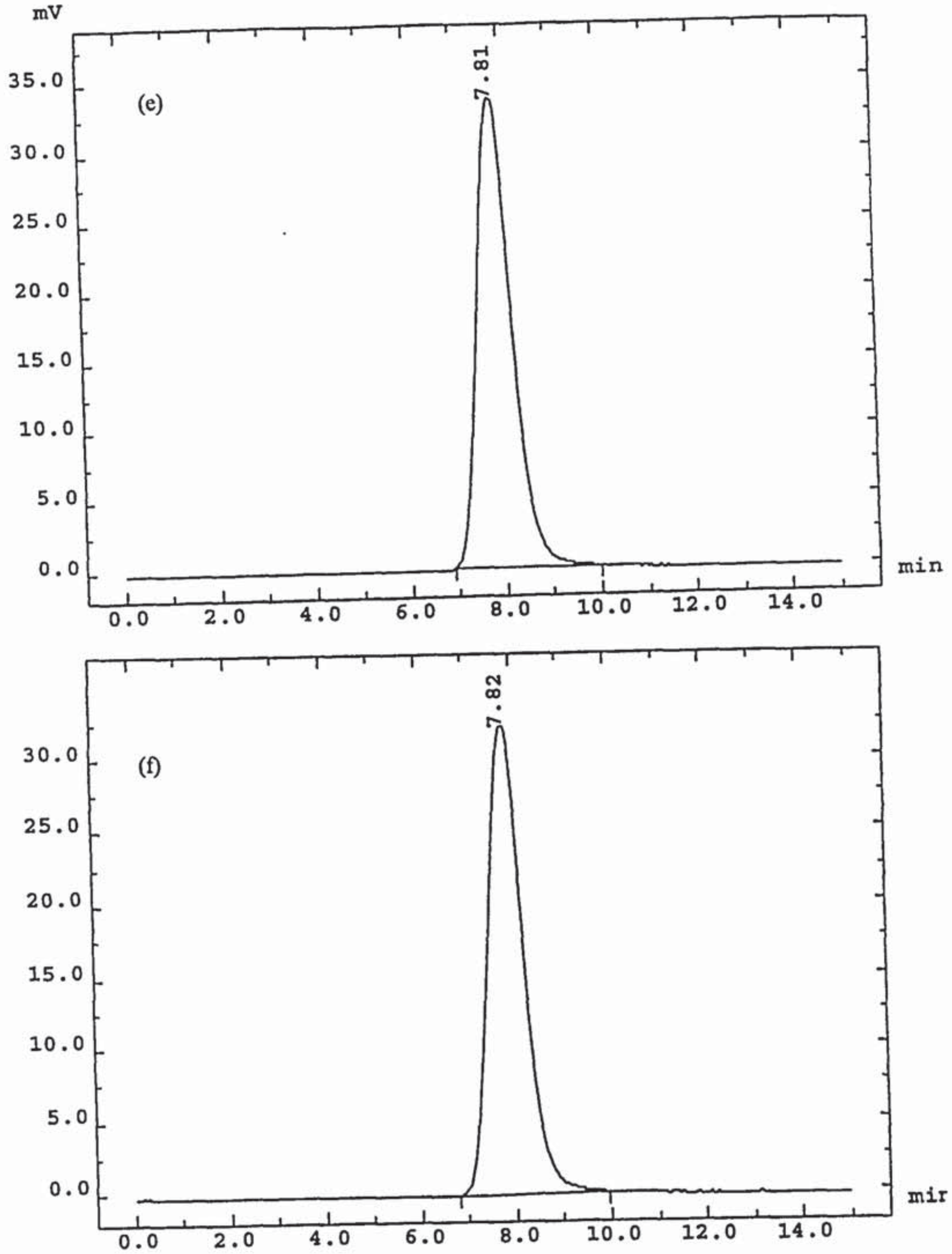

Figure 5.9 (e-f). Size-exclusion chromatograms of Dextran-Cascade blue® used in donor chambers of transport cells, (e) after passive and (f) after iontophoretic modes of delivery. Digits in traces represent the retention times of each species on the column.

maintained throughout experimental lifetime. Finally, these chromatograms also show that the D-CB content of donor and receptor compartments was not bound to membrane and/or formulation constituents, nor existed as ion-pairs (with for example, DTAB).

5.6 SUMMARY

The results presented demonstrate the ability of transdermal enhancers to modulate the passive and iontophoretic delivery of a model, anionic macromolecule (M_w=3kDa). While the separate application of DTAB, SDS, Azone® and iontophoresis all improved the cutaneous delivery of D-CB, the efficiency of a combined chemical and iontophoretic approach appeared to be dependent upon the relative charges of the permeant, enhancer and driving electrode. Clearly though, further studies incorporating a comprehensive range of permeants and enhancers of varying polarities and charges are necessary to fully understand the mechanism(s) influencing chemically- and electrically-mediated modes of percutaneous enhancement.

CHAPTER SIX

TRANSDERMAL MACROMOLECULAR DELIVERY: REAL TIME VISUALISATION OF CHEMICAL AND PHYSICAL PENETRATION PATHWAYS IN HUMAN EPIDERMIS

6.1 INTRODUCTION

Gross macromolecular flux across human stratum corneum, as a function of enhancer and/or electrical treatment, was determined in the previous chapter. This chapter aims to elucidate and visualise the penetration pathways macromolecules take as they traverse human epidermis using microscopic means. The following sections describe what is currently known about the route penetrants take across skin followed by a discussion of microscopic techniques used to obtain such information. The procedure employed in this particular study to visualise penetration pathways is described in Materials and Methods. Finally, digital images of macromolecular transport in epidermis are exhibited in the results and discussion section. Subsequently, all findings are summarised.

6.2 PENETRATION PATHWAYS THROUGH SKIN

As described in chapter one, topically applied drugs can penetrate through epidermis *via* either an intercellular, intracellular or shunt route (*via* skin appendages, see Figure 1.3). The actual pathway(s) that prevail(s), can be affected by the formulation applied, physiochemical properties of the permeant and is a function of the penetration enhancing system employed, be it chemical or physical in nature (Illel *et al.*, 1993). This chapter is concerned with the visualisation of epidermal penetration pathways and therefore this introduction will discuss studies that have employed visualisation techniques only as a means of determining permeant transport.

6.2.1 Small molecules

Small molecules that are delivered passively through the skin are generally classified according to their hydrophilic or lipophilic properties. The path they take to traverse the stratum corneum or epidermis is then commonly correlated to these properties. For example, a hydrophilic compound is usually thought to penetrate stratum corneum through a polar or aqueous route that usually traverses skin corneocytes. Alternatively, a lipophilic molecule is frequently thought to mainly cross the stratum corneum *via* its intercellular region, which is made up of rigid lipid bilayers. This is a rather simplistic approach that often is seen not to be true. For instance, for a drug to pass through the stratum corneum it really needs to possess a balance between the above mentioned properties which would therefore indicate a dual transport pathway in skin. Evidence for the presence of penetration routes will now be discussed.

6.2.1.1 Passive

A number of studies have investigated possible routes that species having a molecular weight below 1000Da utilise to pass across SC. Turner and Guy (Turner and Guy, 1997) have used laser scanning confocal microscopy (LSCM) to determine epidermal penetration pathways (in mouse skin) for hydrophilic (calcein, $M_w = 623$) and lipophilic (nile red (NR) $M_w = 318$) probes. The study showed elegantly different transport pathways as a function of permeant lipophilicity. NR was seen to be transported across SC intercellularly although some intracellular distribution was also noted; there was minimal localisation in viable epidermal cells. In contrast, calcein being charged and hydrophilic did not penetrate SC passively.

Other topically applied permeants (applied passively) have also been visualised in stratum corneum and localised in SC intercellular regions. Using transmission electron microscopy (TEM), Nemanic and Elias (Nemanic and Elias, 1980) showed that *n*-butanol traversed both human and mouse SC *via* intercellular domains; *n*-butanol distribution was extensive but irregular in these regions and was three times more than that found in skin corneocytes.

The time-dependent transport of mercury in SC has also been determined using electron microscopy (Boddé *et al.*, 1991). Following the application of a solution of mercuric chloride (5% w/v in water) to human skin *in vitro*, mercury was seen to accumulate intercellularly initially (within 15 minutes). After one hour, surface (apical) corneocytes had taken up mercury whilst in the lower SC mercury remained distributed intercellularly only. After ten hours, mercury had accumulated uniformly in all apical corneocytes and was present in some of the medial cells but was present only intercellularly in deeper SC layers. The difference in this localisation of mercury was suggested to be due to apical corneocytes possessing a greater number of binding sites for the diffusing species or that they are simply more permeable; access into corneocytes may have been through degrading desmosomes. This study highlighted that hydrophilic entities may traverse the SC *via* the intercellular lipids. The authors postulated that this is possible since permeants may be able to diffuse through the intercellular spaces of the SC by surface diffusion along the polar head groups of the lipids.

6.2.1.2 Chemically enhanced

Visualisation of transport pathways in skin following pretreatment with enhancers has been achieved using electron microscopy (Turner and Nonato, 1997). In one study, mouse SC was pretreated with DMSO to determine chemically enhanced transport of Hg^{2+} and Ni^{2+} (Sharata and Burnette, 1988). Both Hg^{2+} and Ni^{2+} were located within swollen basal SC cells, intercellularly and associated with cell envelopes. The ions were not detected beyond the SC. The paper concluded that DMSO enhanced transport by enlarging the size of basal SC cells, which resulted in an increased free volume for permeant diffusion.

Another study has reported on the effect that skin pretreatment with different azones have on the transport route of mercury across SC (Boddé *et al.*, 1989). Following hexadecyl azone pretreatment (10% v/v in PG), there was no difference in mercury distribution when compared to untreated skin. However, hexyl azone applied at the same concentration enhanced the accumulation of mercury within apical and medial corneocytes and intercellularly within the deeper layers of the SC when compared to the untreated control. The effect of dodecyl-azone was also of interest since it only enhanced intercellular and intracellular distribution of mercury.

LSCM has been used to visualise transport of nile red (NR) through human skin from different vehicles (Simonetti *et al.*, 1995), these were PEG 400, PG and DMSO. The results of the experiments showed that penetration of NR into SC varied depending on the vehicle employed. NR from the DMSO vehicle was located mainly in the intercellular spaces of the viable epidermis. However, NR penetration from PEG 400 or PG was not observed.

In summary, the above mentioned studies serve to highlight that chemically induced enhancement can be visualised using microscopic techniques.

6.2.1.3 Current enhanced

Transport of charged species across skin, following the application of an electrical potential has been determined and visualised to reveal current induced penetration pathways. The major route of iontophoretic transport is believed to be *via* appendageal pores such as sweat ducts and hair follicles, although drugs have been visualised in intercellular domains in SC

also (Singh and Maibach, 1994); the predominant pathway being the one that exhibits the lowest electrical resistance.
A study employing light microscopy has visualised the iontophoretic transport of fluorescein (FL) across human skin (Burnette and Ongipipattanakul, 1988). An optical microscope was positioned on the receptor side of skin mounted in a diffusion cell and then FL delivered iontophoretically. Discrete sites of FL transport were visualised. Microelectrodes were then used to determine the corresponding voltage gradient associated with these transport regions; the maximum potential difference detected was directly over the visualised pathways suggesting that transport did correspond to sites of high current flow. These regions were most likely low resistance shunt routes such as hair follicles or sweat ducts.

Turner and Guy (Turner and Guy, 1997) have visualised current facilitated flux as a function of permeant physicochemical properties. CLSM was used to visualise the transport of nile red (lipophilic) and calcein (hydrophilic) in hairless mouse skin following current application. Calcein was shown to be distributed deep into the epidermis (>20μm) and was predominately found in the pilary canals of hair follicles, although slight intercellular penetration was observed in superficial skin layers. However, fluorescence due to NR was observed primarily on the intercellular domains of the SC and viable epidermis with extensive partitioning also in the intercellular compartment of viable epidermal cells. Further, NR exhibited a high affinity for the hair shafts themselves but was not present in the pilary canal as was the case for calcein. The paper showed elegantly, the different transport routes occurring following current application and the affinity a permeant has for different environments within SC that can be correlated to its hydrophilic/lipophilic nature.

In an earlier study, Cullander and Guy (Cullander and Guy, 1991) also investigated the transport of fluorescent probes having varying lipophilic nature. Their study employed calcein, NBD-diethanolamine (an uncharged and polar molecule) and NR (an uncharged and lipophilic molecule) which were delivered across hairless mouse skin using a current of 0.4mA/cm^2; current was applied for twenty minutes. Confocal images showed calcein and NBD-diethanolamine penetrated into SC intercellular and follicular pathways similarly; in the viable epidermis, the probes were found mainly in the hair follicles. The lipophilic fluorophore, NR, however was localised mostly in the intercellular lipids of the SC and in both inter and intracellular regions of the viable epidermis.

6.2.2 Large molecules

Although an inverse relationship generally exists between permeant flux and molecular weight a number of studies have reported on transdermal macromolecular flux (Green *et al.*, 1993). Therefore, it is of great interest to determine the pathways these molecules take to traverse the SC and epidermis and to assess if they are similar or distinct to those observed for smaller molecules. For example, if the major route of penetration is through a porous pathway (*via* skin appendages and pores), then one may expect that transport along this route would depend on the size of the molecule; as the size of the molecule increases the flux will diminish.

6.2.2.1 Passive

The passive delivery of macromolecules across untreated skin has not been reported as having been visualised in the literature (Turner *et al.*, 1997). However, transport of such large molecules across skin is evident when enhancement is achieved by either chemical or physical means.

6.2.2.2 Chemically enhanced

Ogiso *et al* (Ogiso *et al.*, 1995) have reported on the mechanism involved in the enhancement effect of enhancers on the intercellular penetration of large polar molecules across rat skin. The study determined the flux of different molecular weight fluorescently labelled dextrans (M_w= 4400, 9400 and 69000Da) following skin pretreatment with either water soluble (DMSO, and N-methyl-2-pyrrolidone (NMP)) or water immiscible (n-octanol, laurocapram, isopropylmyristate (IPM), oleic acid, and cineol) enhancers. It was found that pretreatment with water immiscible enhancers significantly increased dextran flux whilst water-soluble enhancers did not enhance flux compared to the control; overall penetration of dextrans was size dependent. The authors suggest that water immiscible enhancers removed intercellular lipids causing dilatations between adjacent cornified cells and thus enhanced dextran penetration through intercellular pathways. However, the authors also compared dextran flux across Wistar rat skin and hairless rat skin (both pretreated with water immiscible enhancers) and found that steady-state flux was higher by a factor of 1.2 to 4.9 across Wistar rat skin. This would seem to indicate that the transfollicular route also plays apart in chemically enhanced transdermal macromolecular transport.

The same authors have also pretreated rat skin with an enhancer that is known to enhance macromolecular transdermal transport to determine the effect molecular weight of water soluble permeants has on measured flux (Ogiso *et al.*, 1994b). Rat skin was pretreated with n-octyl-β-D-thioglucoside (OTG) (Ogiso *et al.*, 1994a) and then different molecular weight fluorescently labelled dextrans (M_w = 4400, 9600 and 69000Da) applied using a typical diffusion cell set-up. Dextran permeability across skin was size-dependent but dextrans penetrated more easily in the presence of OTG (1.5%), with high fluxes being equivalent to those through stripped skin. This result indicated the enhancement effect of OTG on the penetration of macromolecules through SC to be extensive, OTG nearly eliminating the barrier function of the SC. Scanning electron microscopic observations showed that OTG treatment caused exfoliation of cell membranes and dissociation of adherent cornified cells that suggested a significant disturbance of the cohesive laminae and barrier functions.

6.2.2.3 Current enhanced

The penetration pathways of a series of macromolecules (fluorescently-labelled poly-L-lysines, (FITC-PLLs)) across hairless mouse skin following the application of constant current (0.5mA/cm^2) for periods of 4, 8 and 16 hours have been visualised using CLSM (Turner *et al.*, 1997). The FITC-PLLs had molecular weights of either 4, 7 or 26kDa. Confocal images revealed that current induced transport was molecular weight dependent, with penetration of the 4 kDa analogue being greatly enhanced, delivery of the 7 kDa FITC-PLL being slightly elevated whilst iontophoresis had no effect on the transport of the larger 26 kDa FITC-PLL. On closer inspection of the confocal digital images showing macromolecular transport pathways, it was found that iontophoresis of the 4 kDa FITC-PLL localised fluorescence primarily in the hair follicles, especially at the deeper levels of the skin (20 – 40 μm below the surface). However, there was also considerable penetration in non-follicular regions at ~10-15 μm below the surface which decreased with increasing depth. There was negligible SC penetration for the larger 7kDa FITC-PLL following iontophoresis for 4 and 8 hours but it was slightly enhanced after 16 hours of current application; fluorescence once again being localised mainly along the hair follicles. Penetration of the 26 kDa FITC-PLL did not occur even after 16 hours of current application. In summary, this study clearly showed by using visualisation means, that iontophoretic transport was molecular weight dependent and transport pathways in skin were dependent on depth within it.

6.3 VISUALISATION USING FLORESCENCE MICROSCOPY

Florescence microscopy (FM) is a means to visualise drug transport in skin. Fluorescence is the property of some atoms and molecules to absorb light of a particular wavelength and after a brief interval, termed the fluorescence lifetime, to re-emit light at longer wavelengths. Fluorescence requires an outside light source of energy, is the result of the absorption of light, and involves the emission of electromagnetic radiation (light).

FM as a means of detection of drugs through a microscope offers many advantages. For instance, specificity and sensitivity are very high. This is because fluorescence excitation and emission spectra are usually characteristic of a molecules structure and composition. Therefore, different molecules display distinct excitation and emission spectra allowing selective analysis of complex mixtures. Furthermore, fluorescence from a few molecules can be detected ensuring a high degree of sensitivity. FM also allows for quantitative measurements since emitted fluorescence is directly proportional to the fluorescence quantum yield of the fluorophore. Fluorescence is also extremely sensitive to its immediate environment; fluorophores have been designed for assessing changes in pH or viscosity or the concentration of Ca^{2+} (Herman, 1998b).

Of particular relevance to this study, fluorescence detection can be used to view very fast chemical and molecular changes in specimens inferring a high temporal resolution. Further, enhanced spatial resolution is possible as fluorescence can be measured from a single molecule.

6.3.1 Confocal laser-scanning microscopy (CLSM)

Most studies discussed in the introduction to this chapter have employed CLSM to visualise penetration pathways in skin. The technique typically involves mounting skin following some kind of procedure (for example, pretreatment with an enhancer followed by application of a fluorophore) on to the microscope stage. Subsequently, a laser beam is directed onto the sample, the light is absorbed by the fluorescent marker in the tissue and then the emitted fluorescence is detected. Images of optical sections, which are proportional to the numerical aperture of the objective, are then digitally recorded by a computer (that is interfaced to the microscope) at different depths and planes (either xy or xz). These digital images usually display a pattern of fluorescence distribution that can correspond to transport pathways in skin. The main advantages of CLSM are (i) that specimens do not need to be fixed (avoiding artefacts that may be introduced during tissue preparation), (ii) living tissue can be used, (iii) specimens can be prepared and examined rapidly and (iv) permeation pathways can be observed at multiple time-points without difficulty (Cullander, 1996).

6.3.2 Two-photon excitation microscopy (TPEM)

A number of disadvantages are however associated with CLSM. Firstly, the images are not in real time, typically one to four seconds are needed to aquire a full-frame image. Secondly, the laser employed can cause photodamage and photobleaching; photobleaching being a consequence of a high intensity laser continually exciting a fluorophore (without it emitting fluorescence) until it is completely bleached or destroyed. Recently, however, technological advances in the field of lasers have led to the use of different fluorescent microscopes based on the principle of two-photon excitation; as a result, both tissue damage and photobleaching are markedly reduced.

The defining practical difference between a confocal and a TPE system is the specification of the laser light source. Whereas a confocal microscope uses a light source emitting a continuous intensity laser of a few milliwatts, a two-photon system uses a laser emitting ultrashort pulses of light with peak intensities per pulse of tens of megawatts. It is this combination of very high power over a short period of time that allows the "two-photon" mode of fluorescence excitation to occur. This is explained in detail below.

In normal confocal microscopy, fluorescence is the result of the absorption of a single photon of energy (from a continuous short wavelength laser) by a fluorophore and the subsequent emission of that absorbed energy as light (Figure 6.1a). Two-photon absorption is the simultaneous absorption of two photons (from a pulsed laser of long wavelength) in a single quantized event that combines their excitation energies to produce an excitation that is conventionally caused by a single photon of a shorter wavelength (Figure 6.1b). For TPE to occur, the two photons must arrive with in 10^{-18} seconds, which results in an immediate virtual state lifetime of 10^{-17} seconds (Herman, 1998a).

The absorption of two photons infers a number of advantages over conventional confocal microscopy.

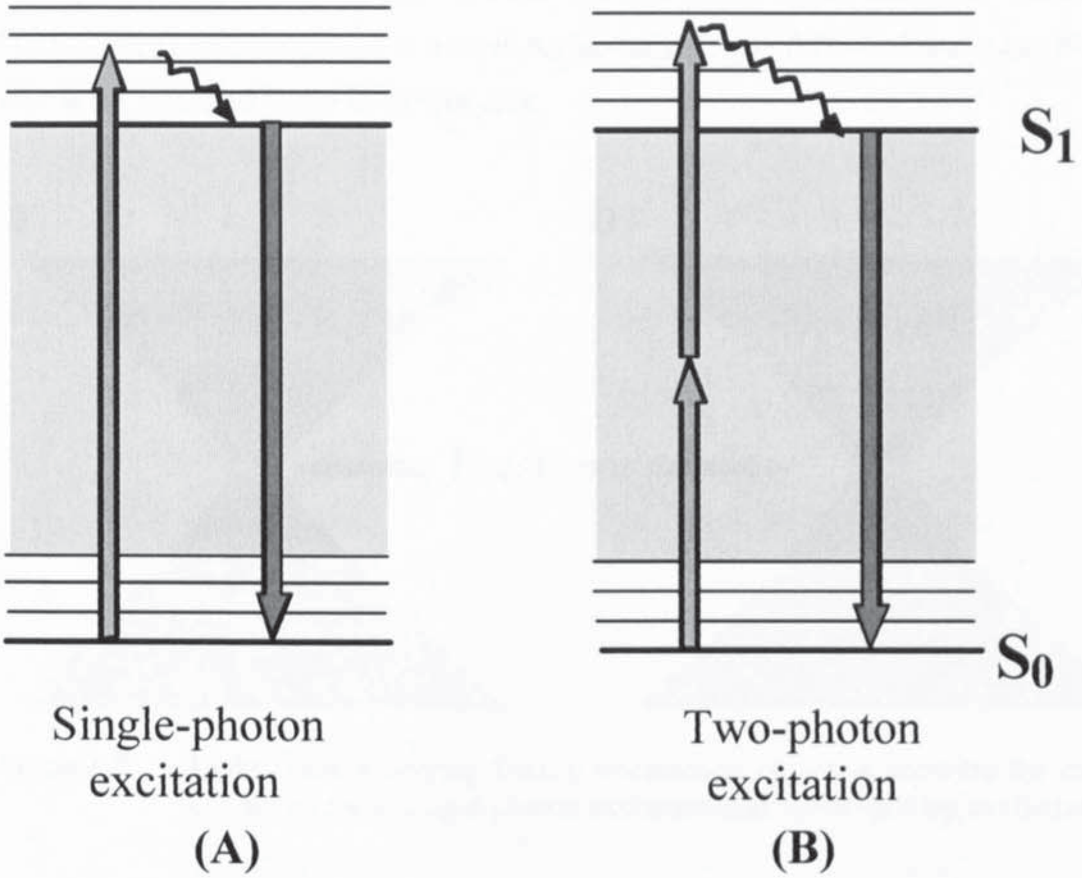

Figure 6.1 Explanation of single and two-photon excitation using energy diagrams

Deeper imaging

TPEM employs a laser having a longer wavelength than that used in CLSM. Light from this laser is scattered much less, which allows deeper penetration of light into a tissue sample. Therefore, the appearance of fluorescent markers can be detected and assessed at much greater depths in a tissue.

Improved cell viability

Light emerging from a confocal microscope objective (single photon) illuminates the whole sample in the field of view even though only one focal section is being observed (Figure 6.2a). Therefore, there is a high possibility of the production of cytotoxic compounds in the cell being imaged. In contrast, in TPEM, fluorescence is only generated at the focus point (Figure 6.2b).

Reduced photobleaching

TPEM employs a very intense pulsed laser, rather than a continuous laser. As a result, fluorophores are not continually excited but allowed to relax and emit fluorescence. Further, excitation is localised to a small region only (Figure 6.2b) and hence any bleaching effects are restricted to the focal spot only.

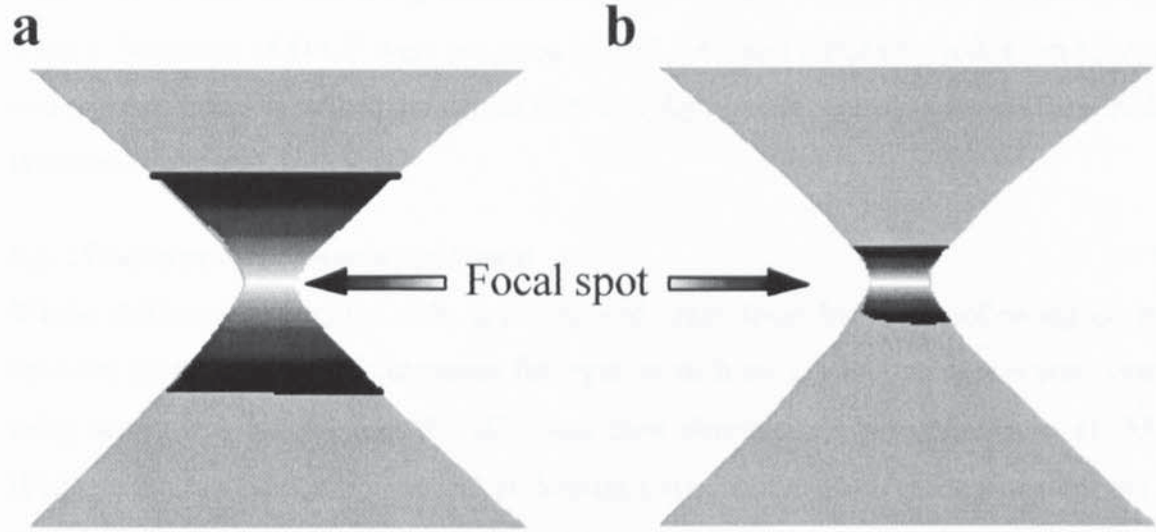

Figure 6.2 Light cones emerging from a microscope objective showing the extent of excitation for a) single-photon excitation and b) two-photon excitation

6.4 AIMS OF CHAPTER

Following on from work in the previous chapter that determined flux of D-CB as a function of chemical and/or physical enhancement, this chapter aims to employ two-photon excitation microscopy to visualise the penetration pathway(s) of D-CB across human epidermis by recording real-time digital images of transport. Images of skin pretreated with enhancer (DTAB) will be compared to untreated skin before and during current application.

6.5 MATERIALS AND METHODS

6.5.1 Materials

Dextran labelled with cascade blue® (D-CB) of molecular weight 3kDa was purchased from Molecular Probes (Leiden, Holland). DTAB and propylene glycol were obtained from Sigma Chemicals (St. Louis, USA). The buffer used was phosphate-buffered saline (PBS) pH 7.4 (8mM Na_2HPO_4, 1.5mM KH_2PO_4, 139mM NaCl, 2.5mM KCl in Millipore water). Solutions of D-CB were prepared in PBS. Ag and AgCl electrodes were prepared and regenerated as described in chapter five. All Ag products were purchased from Aldrich (Barnem, Belgium).

6.5.2 Preparation of human epidermis

Whole thickness abdominal skin was obtained from local hospitals following cosmetic surgery; the underlying subcutaneous fat together with other adhering debris was removed using a surgical scalpel and the skin was then dermatomed to a thickness of 200μm (Padgett Electro Dermatome Model B, Kansas City, USA). Each piece of epidermis was then laid flat inside a plastic Petri dish (dermis side in contact with dish). Using a steel punch and dye, circular discs having a diameter of 13mm were then cut out.

6.5.3 Transport experiments across epidermis

Circular discs (diameter 18 mm) from wire gauze were produced in the same manner as epidermis discs described above. A piece of epidermis was then positioned onto the wire gauze discs to provide support for the tissue. Two pieces of epidermis were then sandwiched in each of the three compartmental iontophoretic cells as previously described in chapter five (Figure 5.3). PBS was pippetted into cell acceptor compartments to prevent dehydration of the epidermis and where epidermis was to be pretreated with DTAB, 120μl of enhancer solution (0.16M in PG) pippetted into the cathodal (donor) chamber ensuring that the entire epidermis surface was covered. The cells were left positioned vertically for 18 hours after which the epidermis was washed three times with PBS to remove any traces of enhancer. Following pretreatment, PBS and D-CB solutions (2ml) were pippetted into the receptor and donor compartments and Ag (anode) and AgCl (cathode) electrodes were inserted into these chambers respectively. Silver measuring electrodes were also placed in both chambers to record the electrical resistance of SC during each experiment. The electrodes were connected to a 6-channel computer-controlled current source powered by a

+/- 40-volt supply (Electronic Department, Leiden University). Anodal and cathodal chambers were continuously stirred at 375rpm. PBS was continuously pumped at a rate of 7ml/hour, through the central acceptor compartment (volume 0.5ml) from a reservoir to a Retriever IV fraction collector (Isco, Holland) using a peristaltic pump (Ismatec SA, Switzerland). Fractions were collected hourly in test tubes and then assayed for dextran content. Each experiment started with a six-hour passive period (no current) and was followed by nine hours of current application (500μamps/cm^2) and finally a six-hour passive post iontophoretic period without current. Dextran concentrations were determined by measuring fluorescence intensity on a Jasco 821-FP (H.I.Ambacht, Holland) detector (Ex 401, Em 431) connected to an autosampler (Gilson 234 autoinjector, UK.) using PBS as mobile phase at a flow rate of 0.5ml/min. Transport experiments on untreated and propylene glycol and DTAB pretreated epidermis were conducted.

6.5.4 Two-photon excitation microscopic visualisation of transport.

A two-photon excitation microscope employing a mode-locked Titanium:Sapphire laser as the light source (Tsunami, Spectra Physics) was used to image transport. The microscope is described fully elsewhere (Vroom, 1998). Whole epidermis, having a thickness of, 200μm, was prepared and pretreated in transport cells as described in section 6.5.3. Following the pretreatment procedure, epidermis was removed from these transport cells and positioned into a different cell that allowed the visualisation of drug penetration into epidermis. A diagram of this cell is shown in Figure 6.3, which also shows the positioning of the skin sample during these experiments. This cell brought the skin surface into contact with a 0.1mM D-CB solution and allowed both the application of current (500μamps/cm^2) across electrodes and penetration of the laser (excitation wavelength 800 nm, average laser power 3mW) into the skin. Electrodes were prepared as described in chapter five. XY images having dimensions of 95x95μm (256x256 pixels) were collected at regular time intervals at 10, 15 and 20 microns deep into the SC during passive and electrically enhanced (500mamps/cm^2) periods of delivery. XZ images were compiled also. The minimal time resolution was approximately 4 minutes using a 60x NAI.2 objective which resulted in an imaging resolution of 0.3μm and 0.7μm in XY and XZ planes respectively.

6.5.5 Statistical analysis

A minimum of three experiments was carried out for each different visualisation procedure. All transport cell results are represented as the means of 4-6 experiments ± standard errors. Statistical difference was tested for by using an unpaired Student's t-test, statistical significance being defined as $p<0.05$.

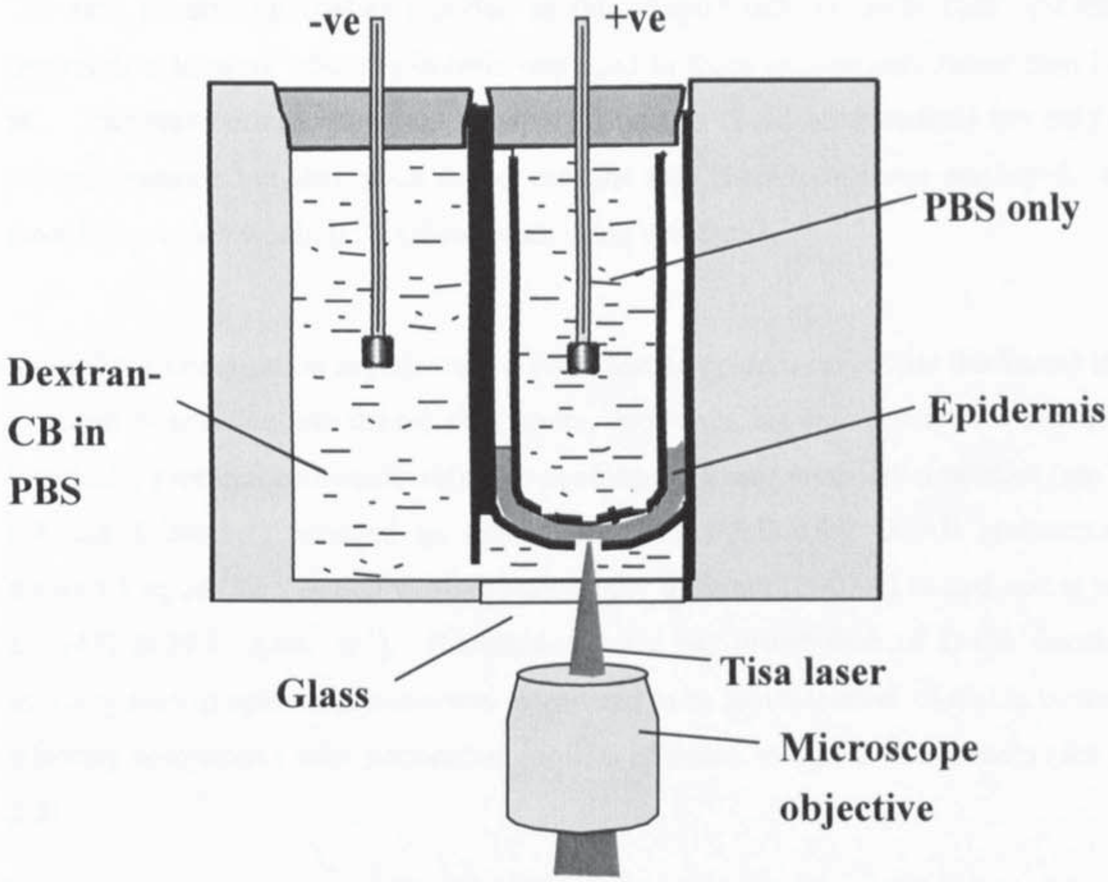

Figure 6.3 Cross-section diagram of transport cell used to visualise macromolecular penetration pathways in epidermis.

6.6 RESULTS AND DISCUSSION

Whole epidermis that had previously been pretreated with 0.16M DTAB (in PG) or left untreated was mounted into the diffusion cell shown in Figure 6.4. A 0.1mM donor solution of the model fluorescent macromolecule, D-CB, was placed into the donor compartment of the cell and PBS in the anodal compartment. Optical digital images were then taken at various depths into the epidermis at different time points, during a period of one hour of passive diffusion and then a two-hour period when current was applied across the epidermis.

The skin penetration studies reported in this chapter differed from those presented in chapter five because whole epidermis was used in these experiments rather than isolated SC. This was because permeant transport pathways could be visualised not only in the stratum corneum but also much deeper into the skin if epidermis was employed. Hence, more information would be obtained when using epidermis.

Since these visualisation experiments utilised human epidermis (200μm thickness) in order to assess penetration into deeper skin layers, corresponding skin permeation studies using identically prepared epidermis were also conducted. These permeation profiles (see Figure 6.4 and Table 6.1) revealed an iontophoretic flux, following DTAB pretreatment, of 496±14.4 $ng.cm^2.hr^{-1}$, which was not statistically different ($P>0.05$) to that across isolated SC (477.2±29.3 $ng.cm^2.hr^{-1}$). Consequently, the SC distribution of D-CB fluorescence intensity seen in epidermal tissue was considered to be representative of that in isolated SC, allowing comparison with permeation profiles obtained using SC membranes (see Figure 5.5).

Passive transport was visualised using TPEM. Figure 6.5a shows xy images, taken by the TPE microscope, of human SC at a depth of 10 microns (before the onset of current) following 18 hours pretreatment with 0.16 DTAB (in PG) during 60 minutes of passive D-CB diffusion from a 0.1mM donor solution. The images clearly show a time dependent build up of fluorescence in SC due to the penetration of D-CB. Skin corneocytes and intercellular domains are clearly highlighted by the distribution of D-CB, whilst some intracellular accumulation is also evident in the treated sample.

Figure 6.4 Dextran-Cascade blue® flux from a 0.1mM donor solution across isolated stratum corneum and whole skin after pretreatment with 0.16M DTAB/PG

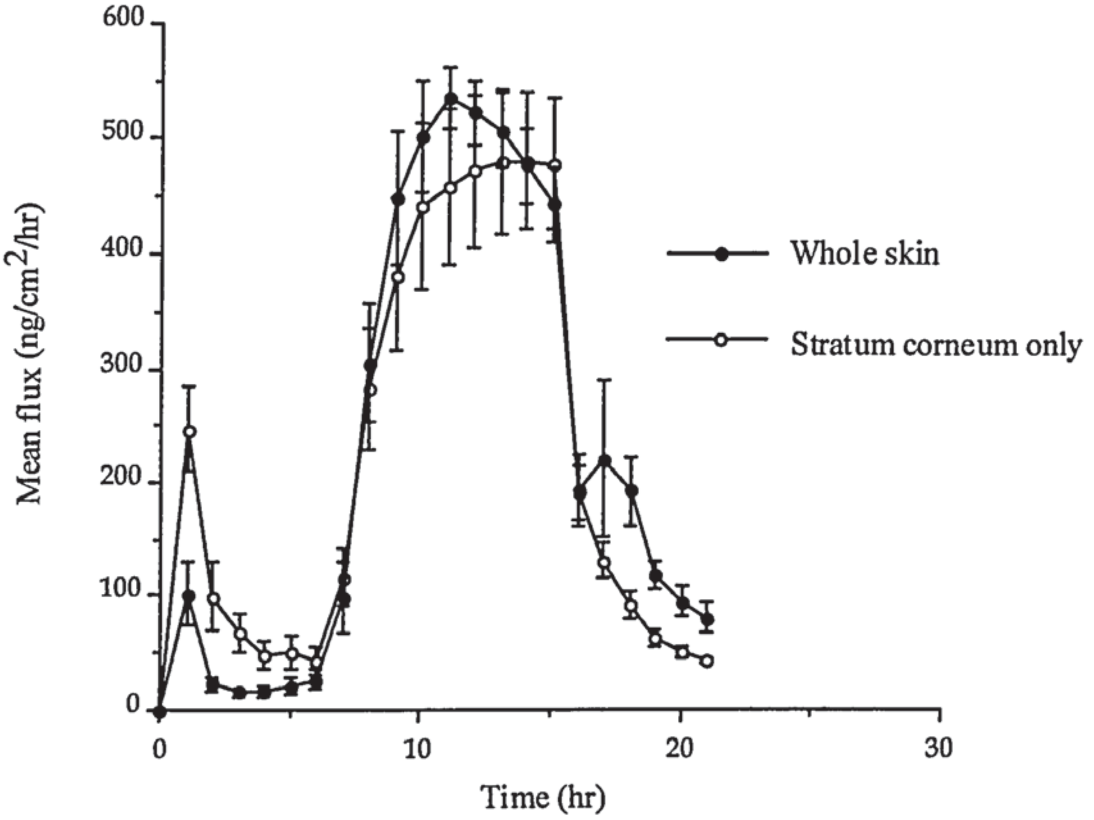

Table 6.1 Steady-state flux values (ng/cm^2/hr) for D-CB transport after DTAB pretreatment of whole skin or stratum corneum only.

Membrane tissue	Pre-iontophoresis (stage 1)	Iontophoresis (stage 2)	Post-iontophoresis (stage 3)
Whole skin	22.28 ± 3.94	496.35 ± 14.35	97.63 ± 8.22
Stratum corneum	47.48 ± 7.16	477.22 ± 29.26	52.18 ± 3.14

However, there is no apparent transport or absorption of D-CB occurring in the untreated sample, as is evident from the images shown in Figure 6.5b.

These findings are similar to those previously reported for calcein at a depth of 10μm in mouse SC (Turner and Guy, 1997) and also parallel the findings of diffusion studies from which one concluded an absence of passive transport in untreated skin (chapter five, Figure 5.5).

Figures 6.6a and 6.6b show a typical series of TPE images (in the xy plane) taken at depths of 10, 15 and 20 microns into SC at varying time points during the iontophoretic delivery of D-CB after pretreatment with DTAB/PG. Control experiments revealed negligible autofluorescence arising from skin tissue. In all series, average fluorescence intensity decreased with increasing depth. The images show that fluorescence intensity and therefore D-CB penetration into SC increased over the hour of passive diffusion. The set of images obtained (at 10μm), initially show a predominant intercellular distribution of D-CB, with corneocyte cell contours being clearly defined. As iontophoresis proceeds, the label intensity increased strongly in certain regions. Images after 60 and 120 minutes of iontophoresis clearly show that these regions of increased intensity correspond with the shape of cells, indicating a significant amount of D-CB uptake into corneocytes. This may be a consequence of surfactant-induced swelling (Rhein *et al.*, 1986) due to DTAB partitioning into SC corneocytes, resulting in increased corneocyte membrane permeability. Alternatively, this partitioning could serve to lower corneocytic negativity ensuing in a greater affinity for D-CB. Deeper into the membrane, D-CB also shows a propensity towards both an inter- and intra-cellular distribution. Control images of untreated skin after equivalent scaling (see Figure 6.6c) exhibited visible label intensity only at a depth of 10μm in SC and was at least an order of magnitude less in intensity than the images shown in figure 6.6a. At depths of 15 and 20μm, iontophoresed samples without DTAB pretreatment exhibited negligible D-CB distribution. Comparison of Figures 6.5a (passive diffusion across DTAB treated SC) and 6.6c (iontophoretic transport across untreated SC) at a depth of 10μm show a greater fluorescent intensity in the former images, in contrast to a higher measured flux during the iontophoretic protocol. These data are consistent with a significant appendageal contribution to iontophoretic transport as reported in the literature

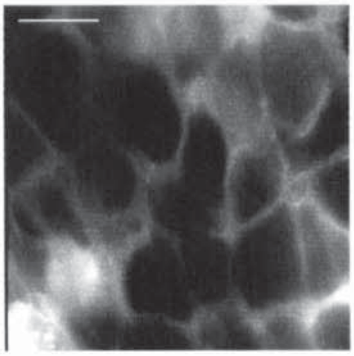

9 minutes passive

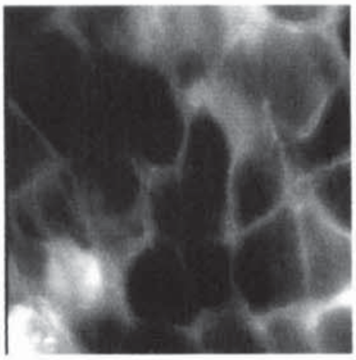

16 minutes passive

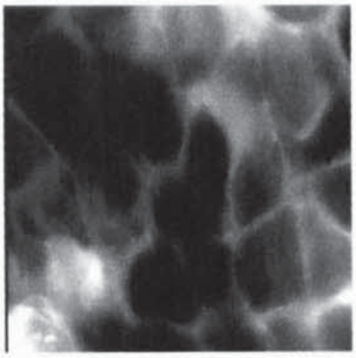

23 minutes passive

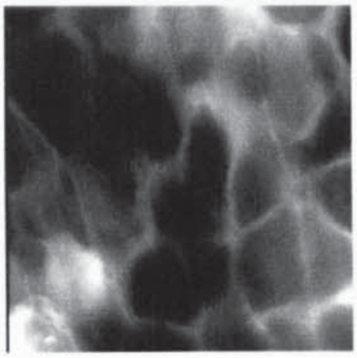

30 minutes passive

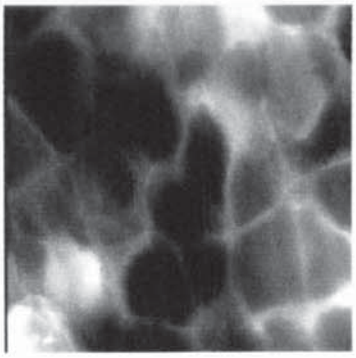

35 minutes passive

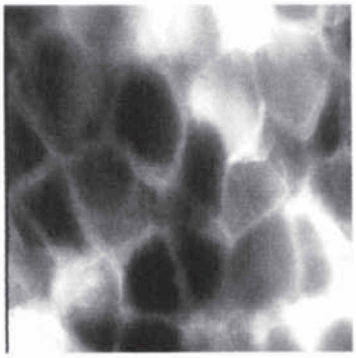

44 minutes passive

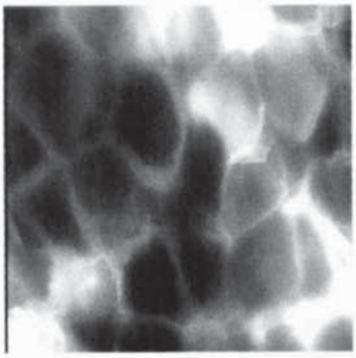

50 minutes passive

Figure 6.5a TPEM xy images (95 x 95μm^2) showing passive D-CB transport across human stratum corneum at a depth of 10μm during 60 minutes of drug application following pretreatment with 0.16M DTAB. Scale bar represents 20μm.

8 minutes passive

39 minutes passive

14 minutes passive

48 minutes passive

25 minutes passive

60 minutes passive

Figure 6.5b TPEM xy images (95 x 95μm^2) showing passive D-CB transport across untreated human stratum corneum at a depth of 10μm during 60 minutes of drug application. Scale bar represents 20μm.

(Green *et al.*, 1993). Other studies have reported the follicular distribution of positively charged fluorescently labelled macromolecules of similar molecular weight to D-CB following cutaneous iontophoresis (Turner *et al.*, 1997). This appendageal distribution was more noticeable at depths ranging from 20-40μm into skin while at more superficial depths significant non-follicular distribution was evident as described for D-CB. However, due to the high magnifications used in the present study, it was not possible to simultaneously visualise possible transport in skin appendages. Whether this transport route is also of importance for anionic macromolecules warrants further TPEM investigations at lower magnifications.

Figure 6.7 is a series of images obtained in the xz plane (perpendicular to the skin surface) of a sample showing dextran transport into DTAB/PG pretreated skin. The white band at the base of each image represents the fluorescent-labelled dextran solution applied to the skin. The SC is expressed by a visible cellular layer (10-20μm) above and adjacent to this band. Following the application of current, the SC becomes less well defined, as D-CB is transported across it and deeper into the epidermis. TPEM imaging is clearly able to show dextran transport upto 80μm deep in the epidermis. From the skin samples examined, substantial enhanced iontophoretic macromolecular transport was visualised. However, the pattern of distribution visualised by xz imaging was variable, when comparing different samples, reflecting the heterogeneity of the tissue; transport most likely taking the route of least resistance in each sample.

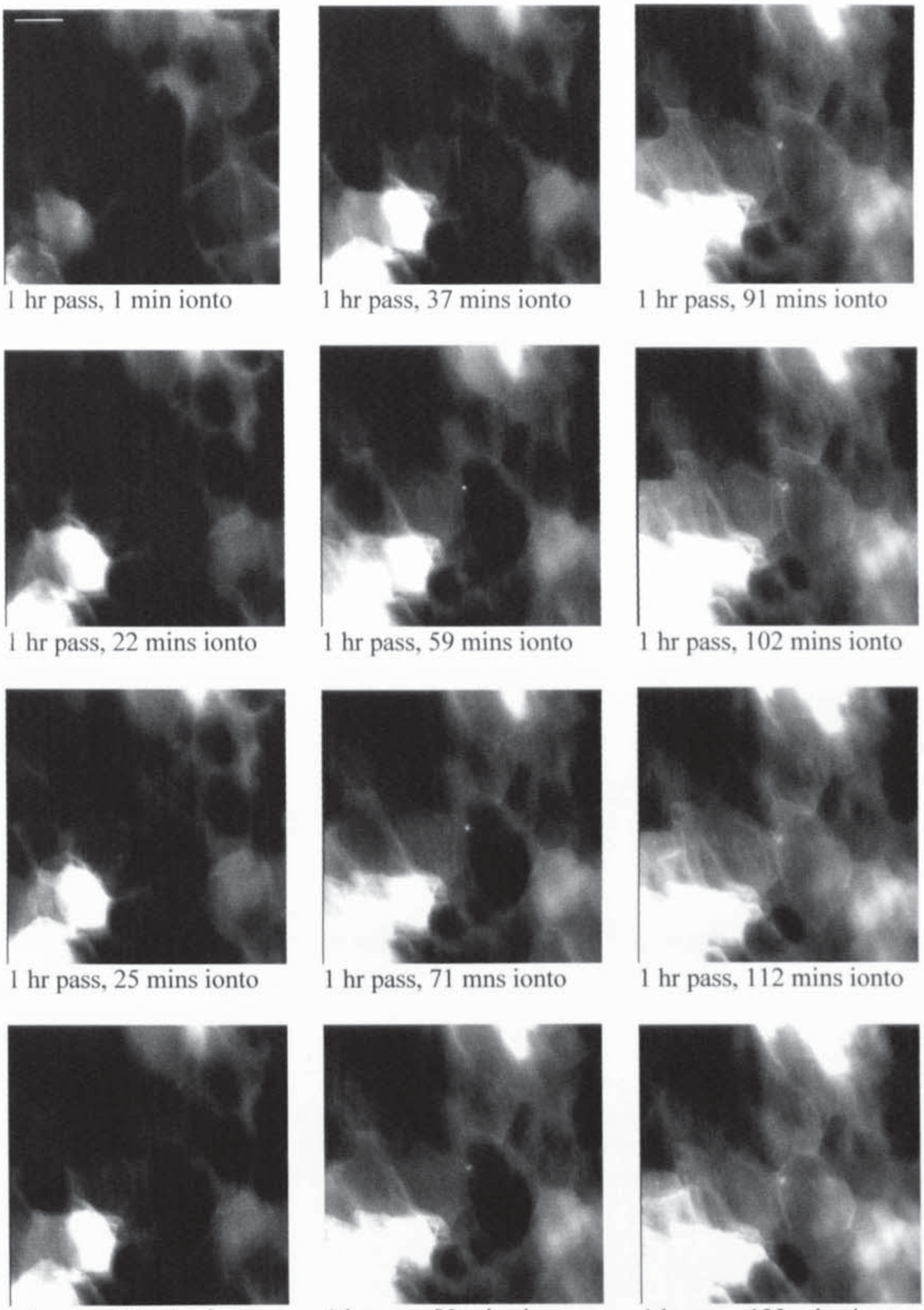

Figure 6.6a TPEM xy images ($95 \times 95\mu m^2$) showing D-CB transport as a function of time at a depth of10microns in SC, during iontophoresis across DTAB/PG pretreated stratum corneum; all images were scaled to the same intensity. Scale bar represents 20μm.

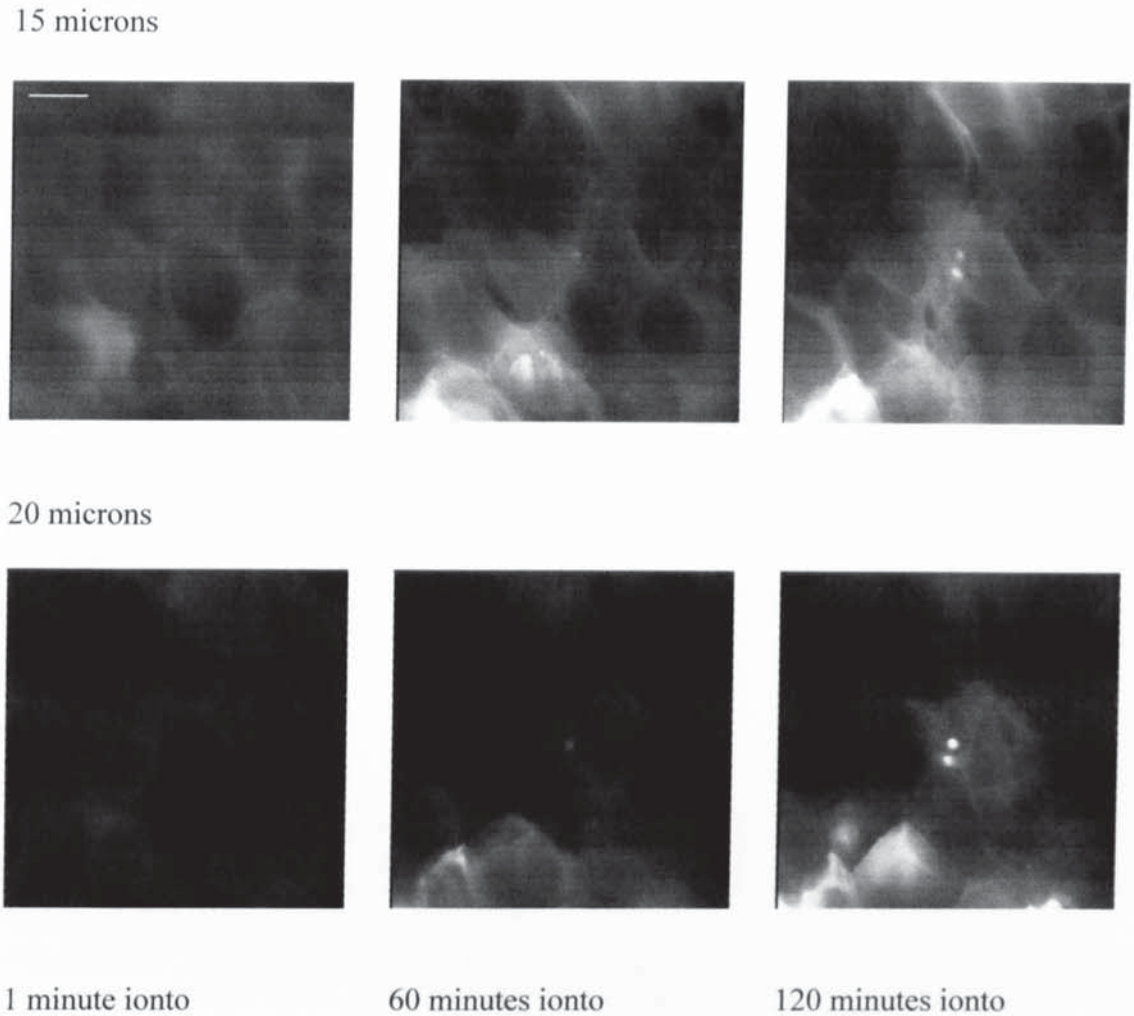

Figure 6.6b TPEM xy images (95 x 95μm^2) showing D-CB transport as a function of time and depth, during iontophoresis across DTAB/PG pretreated stratum corneum; all images were scaled to the same intensity. Scale bar represents 20μm

10 microns

1 minute	60 minutes	120 minutes

Figure 6.6c TPEM xy images (95 x 95μm^2) showing D-CB transport as a function of time and depth during iontophoresis across untreated human stratum corneum; all images were scaled to the same intensity. Scale bar represents 20μm.

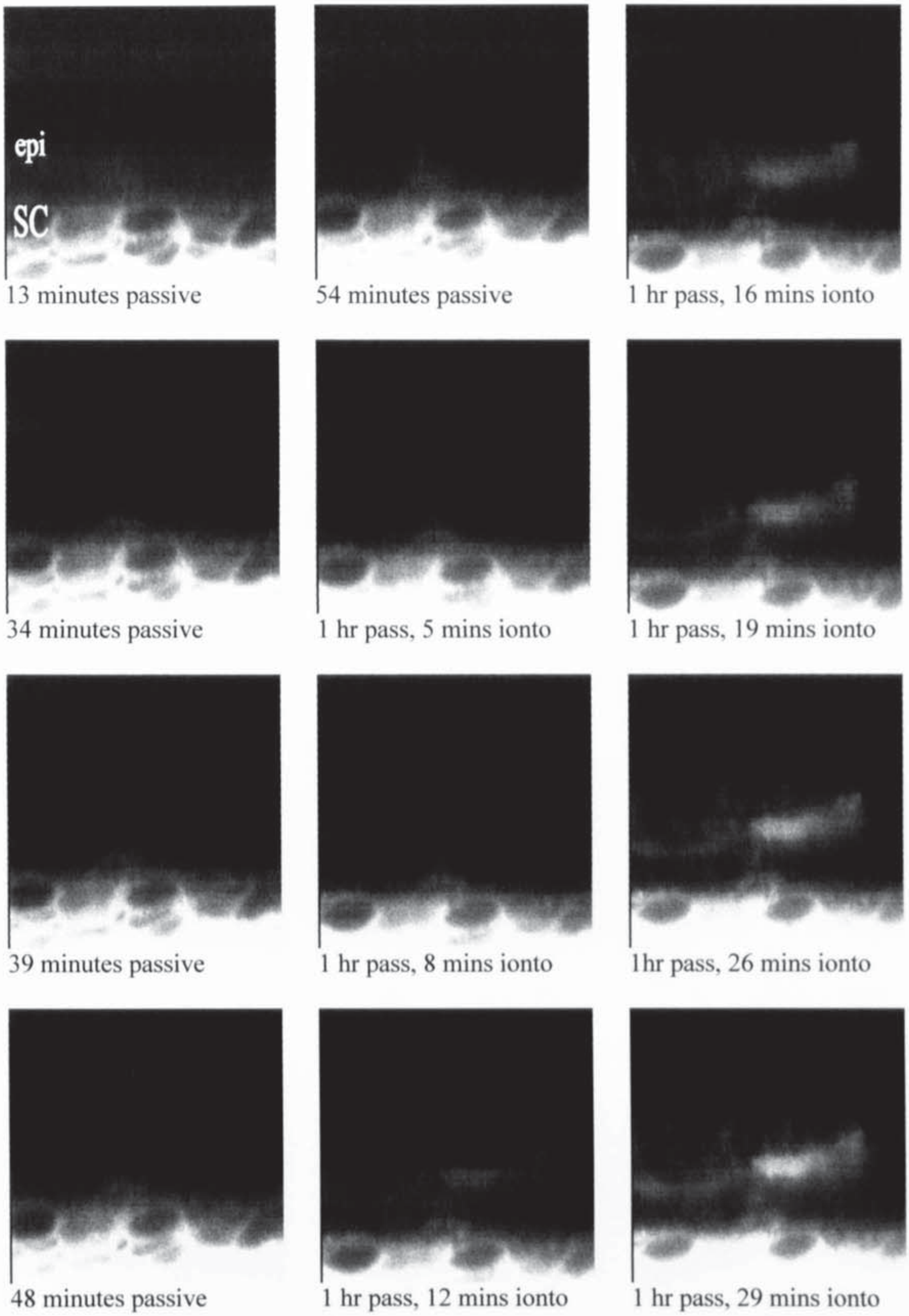

Figure 6.7 TPEM xz images (95 x 95μm^2) showing D-CB transport through DTAB/PG pretreated human epidermis during passive and iontophoretic delivery at various time points. SC = stratum corneum, epi = epidermis. Scale bar represents 20μm.

Figure 6.7 continued

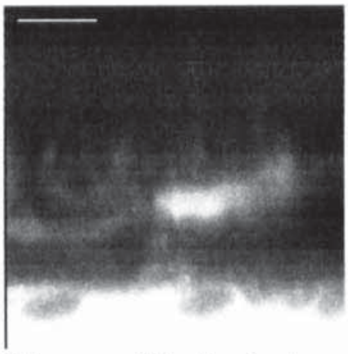

1 hr pass, 35 mins ionto

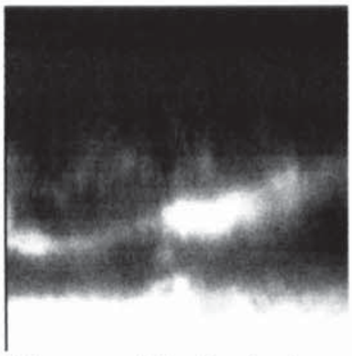

1 hr pass, 60 mins ionto

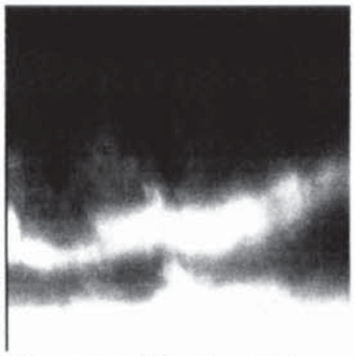

1 hr pass, 95 mins ionto

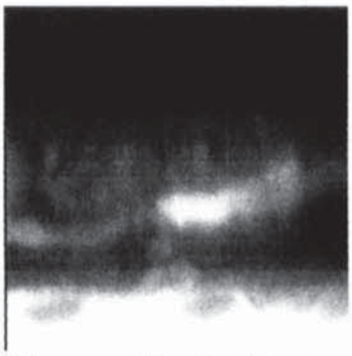

1 hr pass, 41 mins ionto

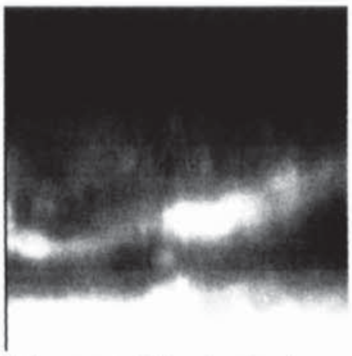

1 hr pass, 63 mins ionto

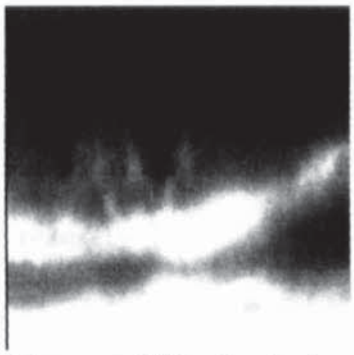

1 hr pass, 106 mins ionto

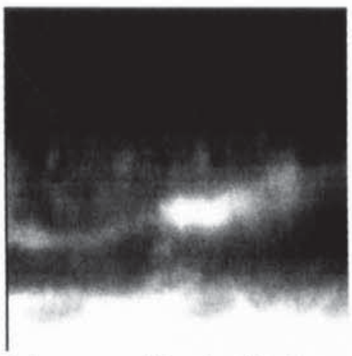

1 hr pass, 46 mins ionto

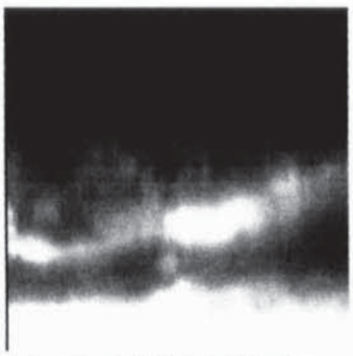

1 hr pass, 75 mins ionto

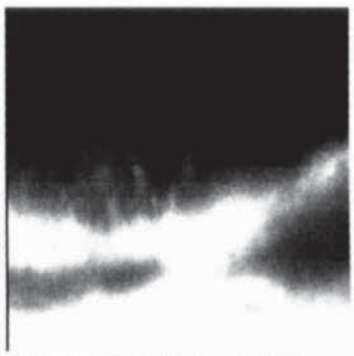

1 hr pass, 116mins ionto

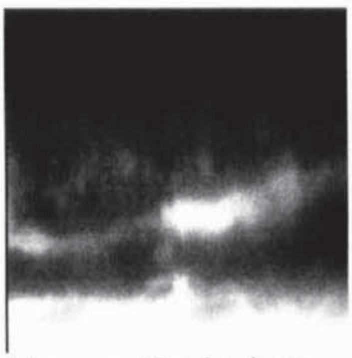

1 hr pass, 53 mins ionto

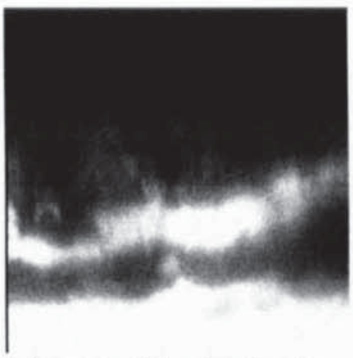

1 hr pass, 84 mins ionto

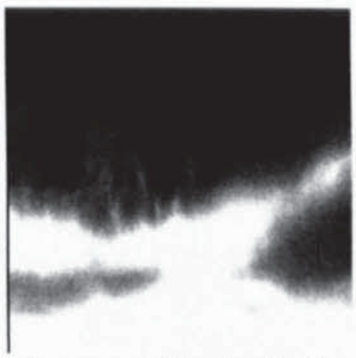

1 hr pass, 127 mins ionto

6.7 SUMMARY

The reported 'real-time' analysis provided visual verification of DTAB- and DTAB/iontophoretically-enhanced D-CB transport across human SC. While passive transport following DTAB pretreatment was characterised by significant intercellular D-CB distribution, the supplementary application of a current also resulted in intracellular uptake. To the best of our knowledge, this is the first study to report the 'on-line' visualisation, using TPEM, of iontophoretic transport across human skin. This methodology offers distinct advantages over conventional techniques, enabling the dynamic visualisation of transport, and consequently, rapid differentiation between 'transport pathways' and static regions of penetrant accumulation, in areas simply having a high affinity for the permeant (exaggerated by virtue of the time-lag between sample preparation and visualisation).

CHAPTER SEVEN

GENERAL SUMMARY

GENERAL SUMMARY

The transdermal route is seen by the pharmaceutical scientist, as a seductive means of administering drugs to humans since many of the problems associated with the more common oral route are circumvented by this approach (chapter one). Transdermal systems over the last two decades have been employed in therapeutic areas such as smoking cessation (nicotine patches), hormone replacement therapy (oestradiol) and pain control (fentanyl). However, not all drugs can be delivered through the skin since potency, molecular weight, lipophilicity and polarity are important determinants for transdermal delivery. One way of expanding the range of drugs that are capable of traversing skin is by developing enhancement strategies that can reversibly alter the skin's impermeable nature, thus allowing the ingress of topically applied permeants. Percutaneous penetration enhancement has been and still is today therefore, an area of great scientific interest.

It is important to initially understand how drugs diffuse into skin in order to develop enhancement strategies and, therefore, analytical techniques are required that can answer this question. An ATR-FTIR spectroscopic method was developed in chapter two to enable the detection of topically applied permeants in membranes. The method was used successfully to determine diffusional characteristics of permeants that penetrated the membrane of interest. A drawback of this method is that it can not be used to assess diffusion of any drug since the IR single from a diffusing species needs to be distinct from any absorption arising from the test membrane. Therefore, this needs to be kept in mind before choosing this analytical tool. Most membranes have an infrared transparent region between 1700-2700 cm^{-1} and therefore the diffusion of compounds possessing either cyano, acetylene, thiol or azido functionality (since they all absorb IR within these limits) are good candidates for diffusional assessment using ATR-FTIR spectroscopy. Direct assessment of diffusion between such drugs is difficult because each functional group has a different molar absorptivity. However, the possibility of determining parameters such as diffusion coefficient and permeant solubility in a membrane for a given topically applied compound as a function of formulation type does exist. Data from such analyses may potentially give insights into the interplay between formulation components during percutaneous diffusion.

The diffusion of cyanophenol (CP) into silicone membrane determined in chapter two gave the strongest IR single and fitted best to the Fickian diffusion model (when compared to the other test permeants) and therefore it was used as the permeant of choice in subsequent experiments. Chapter three assessed and compared the effect of incorporating CP into different formulations had on its penetration into silicone membrane. It was seen that the formulation type, which consisted of a transdermal enhancer in propylene glycol, did indeed affect the diffusion of CP in silicone membrane. Greatest CP diffusivity was observed from the Azone®/PG and neat PG formulations whilst its diffusion from OA/PG and AOA/PG and aqueous formulations was not different. CP membrane solubility was greatest also when CP was applied in the Azone®/PG formulation. This result suggests that Azone® is penetrating into the silicone membrane and enhancing CP partitioning into it. Unfortunately, it was not feasible to directly determine the penetration of Azone® into the membrane, since it was not possible to detect any distinct IR absorptions arising from it during the infrared based diffusional analysis. One way of perhaps clarifying this point would be to use a perdeuterated analogue of Azone®. The C-D symmetric and antisymmetric stretching motions from the analogue would absorb at 2100 cm^{-1} and 2200 cm^{-1} respectively, which are not only distinct from SC $C\text{-}H_2$ symmetric stretching bands that transpire at 2850 cm^{-1} but they also occur in the infrared transparent window of the test membrane.

The possible penetration of oleic acid into silicone membrane was modelled successfully using an analogue incorporating an azido functional group (12-azido oleic acid, (AOA)) that allowed its detection and therefore diffusional analysis. Its diffusivity through silicone membrane was similar to that of CP. However, future work should address the validation of using this AOA as a probe for oleic acid (OA). Experiments determining and comparing OA and AOA physico-chemical properties and their respective effects on gross transport of selected model permeants should be conducted.

The interplay during the diffusion process between drug, enhancer and vehicle in stratum corneum (SC) was examined in chapter four. When enhancers were added to the applied formulations, CP diffusivity and solubility were significantly enhanced when compared to the neat propylene glycol (PG) application. Enhancers did not affect PG diffusivity in SC but enhancers did affect PG solubility in SC. PG diffusion closely resembled that of CP, implying that the respective transport processes were inter-related. Additionally, a synergistic effect, which increases CP diffusivity and membrane solubility in SC, was found to occur between PG and water. Using 12-azido oleic acid as an IR-active probe for oleic acid, the simultaneous penetration of CP, AOA and PG into human stratum corneum was determined. It was found that the diffusion profiles for all three permeants were similar. This indicated that the diffusion of each species through SC was closely related and most likely occurred *via* the same route or SC microenvironment.

Powerful and extensive techniques exist now in molecular biology that have led to the production of therapeutic agents such as peptides, oligonucleotides and cytokines that are capable of potentially treating a whole plethora of diverse ailments in humans. The challenge facing the pharmaceutical scientist is to design systems that can deliver these entities into humans so that they can reach their site of action to elicit a therapeutic action. The traditional oral route in this case is not always the best choice (chapter five) since these biotechnologically produced drugs are susceptible to biological deactivation, before they reach the systemic circulation, and therefore alternative delivery routes are being actively sought.

Iontophoresis is a physical means of transdermal penetration enhancement that induces an increased migration of ions or charged molecules through the skin when an electrical potential gradient is applied. It was applied in chapter five in conjunction with chemical enhancement strategies to assess diffusion of a negatively charged macromolecule across SC. Transdermal enhancers modulated the passive and iontophoretic delivery of the model, anionic macromolecule (Dextran-cascade blue®, (D-CB) M_w=3kDa). While the separate application of enhancers and iontophoresis all improved macromolecular cutaneous delivery, the efficiency of a combined chemical and iontophoretic approach was dependent upon the relative charges of the permeant, enhancer and driving electrode. The greatest flux across SC occurred after pretreatment with a positively charged surfactant (dodecyltrimethylammonium bromide (DTAB)) followed by application of current. Clearly though, further studies incorporating a comprehensive range of permeants and enhancers of varying polarities and charges are necessary to fully understand the mechanism(s) influencing chemically- and electrically-mediated modes of percutaneous enhancement. Further, now that a system that is capable of delivering a macromolecule across SC in detectable amounts has been achieved, it would be interesting to attempt to deliver a drug of similar molecular weight and having a known therapeutic action, to determine if therapeutic fluxes could be achieved.

It was important to realise and visualise the transport pathways that were responsible for macromolecular migration across SC both in the presence and absence of chemical and physical enhancement. Using Two-photon excitation microscopy (chapter six), 'real time' analysis provided visual verification of DTAB- and DTAB/iontophoretically-enhanced D-CB transport across human stratum corneum. While passive transport following DTAB pretreatment was characterised by significant intercellular D-CB distribution, the supplementary application of a current also resulted in intracellular uptake. The novel method employed offered distinct advantages over other conventional techniques such as confocal laser scanning microscopy. This allowed the dynamic visualisation of transport, and consequently, rapid differentiation between 'transport pathways' and static regions of permeant accumulation, in areas simply having a high affinity for the permeant (exaggerated by virtue of the time-lag between sample preparation and visualisation). Further visualisation studies should attempt to compare and contrast macromolecular transport pathways following SC pretreatment with sodium dodecyl sulphate (SDS) and Azone® with those occurring following DTAB pretreatment, since the former two enhancers attenuated D-CB flux during combined chemical and physical enhancement. Also, TPEM should be employed at lower magnifications so as to visualise hair follicles, this would then give information as to the role of appendages in anionic macromolecular transport.

References

Ashton, P., Walters, K.A., Brain, K.R. and Hadgraft, J. Surfactant effects in percutaneous absorption I. Effects on the transdermal flux of methyl nicotinate. *Int. J. Pharm.* **87**:261-264, (1992a).

Ashton, P., Walters, K.A., Brain, K.R. and Hadgraft, J. Surfactant effects in percutaneous absorption II. Effects on protein and lipid structure of the stratum corneum. *Int. J. Pharm.* **87**:265-269, (1992b).

Aungst, B.J., Rogers, N.J. and Sheffer, E. Enhancement of Naloxone penetration through human skin *in vitro* using fatty acids, fatty alcohols, surfactants, sulfoxides and amides. *Int. J. Pharm.* **33**:225-234, (1986).

Baker, N.D., Griffen, R.J. and Irwin, W.J. The percutaneous absorption of m-azidopyrimethamine: A soft antifolate for topical use. *Int. J. Pharm.* **65**:115-125, (1990).

Banga, A.K. and Chien, Y.-W. Hydrogel-based iontotherapeutic delivery devices for transdermal delivery of peptide/protein drugs. *Pharm. Res.* **10**:697-702(1993).

Banwell, C.N. Fourier Transform Spectroscopy. In: *Fundamentals of Molecular Spectroscopy*, edited by Banwell, C.N. Maidenhead: McGraw-Hill, 1983, p. 26-34.

Barry, B.W. Skin Transport. In: *Dermatological Formulations: Percutaneous Absorption*, edited by Barry, B.W. New York: Marcel Dekker, 1983a, p. 95-126.

Barry, B.W. Properties that influence percutaneous absorption. In: *Dermatological Formulations:Percutaneous Absorption*, edited by Barry, B.W. 1983b, p. 127-233.

Barry, B.W. Mode of action of penetration enhancers in human skin. *J. Control. Rel.* **6**:85(1987).

Barry, B.W. Lipid-Protein-Partitioning theory of skin penetration enhancement. *J. Control. Rel.* **15**:237-248, (1991).

Behl, C.R., Kumar, S., Malick, A.W., Del Terzo, S., Higuichi, W.I. and Nash, R.A. Iontophoretic drug delivery: Effects of physicochemical factors on the skin uptake of nonpeptide drugs. *J. Pharm. Sci.* **78**:355-360, (1989).

Bendas, B., Neubert, R. and Wohlrab, W. Propylene Glycol. In: *Percutaneous Penetration Enhancers*, edited by Smith, E.W. and Maibach, H. New York: CRC Press, 1995, p. 61-77.

Berner, B., Mazzenga, G.C., Otte, J.H., Steffens, R.J., Rong-Hwei, J. and Ebert, C.D. Ethanol: Water mutually enhanced transdermal therapeutic system II: Skin permeation of ethanol and nitroglycerin. *J. Pharm. Sci.* **78**:402-407, (1989).

Berner, B. and Liu, P. Alcohols. In: *Percutaneous Penetration Enhancers*, edited by Smith, E.W. and Maibach, H. New York: CRC Press, 1995, p. 45-60.

Berner, B. and Dinh, S.M. Electronically assisted drug delivery: An overview. In: *Electronically Controlled Drug Delivery*, edited by Berner, B. and Dinh, S.M. New York: CRC Press, 1998, p. 3-7.

Bhatia, K.S., Gao, S. and Singh, J. Effect of penetration enhancers and iontophoresis on the FT-IR spectroscopy and LHRH permeability through porcine skin. *J. Control. Rel.* **47**:81-89, (1997).

Bhatia, K.S. and Singh, J. Synergistic effect of iontophoresis and a series of fatty acids on LHRH permeability through porcine skin. *J. Pharm. Sci.* **87**:462-469, (1998).

Blank, I.H. Factors which influence the water content of the stratum corneum. *J. Invest. Dermatol.* **18**:433-440, (1952).

Boddé, H.E., de Haan, F.H.N., van der Brink, I. and Koerten, H.K. Visualisation of *in vitro* percutaneous penetration of mercuric chloride; transport through intercellular space versus cellular uptake through desmosomes. *J. Control. Rel.* **15**:227-236, (1991).

Boddé, H.E., Kruitof, M.A.M., Brussee, J. and Koertoen, H.K. Visualization of normal and enhanced $HgCl_2$ transport through human skin *in vitro*. *Int. J. Pharm* **53**:13-24, (1989).

Botarri, F., Carelli, V., Di Colo, F., Firinu, M.R. and Nannipieri, E. A method for studying drug complexation in semisolid vehicles. *Il Farmaco* **33**:3(1978).

Botarri, F., Carelli, V., Di Colo, G., Saettone, M.F. and Serafini, M.F. A new method for determining the diffusion coefficeint of drugs in semisolid vehicles from release data. *Int. J. Pharm* **2**:63(1979).

Bottari, F., Di Colo, G., Nannipieri, E., Saettone, M.F. and Serafini, M.F. Influence of drug concentration on *in vitro* release of salicylic acid from ointment bases. *J. Pharm. Sci* **63**:1779(1974).

Bouwstra, J.A., Gooris, G.S., Brussee, J., Salomons-de Vries, M.A. and Bras, W. The influence of alkyl-azones on the ordering of the lamellae in human stratum corneum. *Int. J. Pharm.* **79**:141-148, (1992a).

Bouwstra, J.A., Gooris, G.S., Salomons-de Vries, M.A., Van der Spek, J.A. and Bras, W. Structure of human stratum corneum as a function of temperature and hydration. *Int. J. Pharm* **84**:205-216, (1992b).

Bowser, P.A. and White, R.J. Isolation, barrier properties and lipid analysis of stratum compactum, a discrete region of the stratum corneum. *Br. J. Dermatol.* **112**:1-14, (1985).

Brain, K.R. and Walters, K.A. Molecular modelling of skin permeation enhancement by chemical agents. In: *Pharmaceutical Skin Penetration Enhancement*, edited by Walters, K.A. and Hadgraft, J. New York: Marcel Dekker Inc, 1993, p. 389-416.

Brand, R.M., Wahl, A. and Iversen, P.L. Effects of size and sequence on the iontophoretic delivery of oligonucleotides. *J. Pharm. Sci.* **87**:49-52, (1998).

Breathnach, A.S., Goodman, T., Stolinski, C. and Gross, M. Freeze-fracture replication of cells of stratum corneum of human epidermis. *J. Anat.* **114**:65-81, (1973).

Bronaugh, R.L., Congdon, E.R. and Scheuplein, R.J. The effect of cosmetic vehicles on the penetration of N-nitro-sodiethanolamine through excised human skin. *J. Invest. Dermatol* **76**:94-96(1981).

Bronaugh, R.L., Stewart, R.F. and Congdon, E.R. Methods for *in vitro* percutaneous absorption studies II. Animal models for human skin. *Toxicol. Appl. Pharmacol.* **62**:481-488 (1982).

Burnette, R.R. and Ongpipattanakul, B. Characterization of the permeselective properties of excised human skin during iontophoresis. *J. Pharm. Sci* **76**:765-773, (1987).

Burnette, R.R. and Ongipipattanakul, B. Characterization of the pore transport properties and tissue alteration of excised human skin during iontophoresis. *J. Pharm. Sci* **77**:132-137, (1988).

Cappel, M.J. and Kreuter, J. Effect of nonionic surfactants on transdermal drug delivery. I. Polysorbates. *Int. J .Pharm.* **69**:143-153(1991).

Chien, Y.-W., Lelawongs, P., Siddiqui, O., Sun, Y. and Shi, W.M. Facilitated transdermal delivery of therapeutic peptides and proteins by iontophoretic delivery devices. *J. Control. Rel.* **13**:263-278, (1990).

Chizmadzhev, Y.A., Indenbom, A.V., Kuzmin, P.I., Galichenko, S.V., Weaver, J.C. and Potts, R.O. Electrical Properties of skin at moderate voltages: Contribution of appendageal macropores. *Biophysical Journal* **74**:843-856, (1998).

Clemessy, M., Couarraze, G., Bevan, B. and Puisieux, F. Mechanisms involved in iontophoretic transport of angiotensin. *Pharm. Res.* **12**:998(1995).

Colthup, N.B., Daly, L.H. and Wiberley, S.E. *Introduction to infrared and raman spectroscopy*, New York:Academic Press, 1975. Ed.2 pp. 1-523.

Crank, J. *The Mathematics of diffusion*, New York:Oxford University, 1975. Ed.2

Cranne-van Hinsberg, W.I.H.M., Verhoef, J.C. and Bodde, H.E. Transdermal iontophoresis of peptides and proteins: Transport kinetics and electrical skin properties. In: *Drug Absorption Enhancement:Concepts,Possibilities,Limitations and Trends*, edited by de Boer, A.G. Chur: Harwood Academic, 1994, p. 199-220.

Cullander, C. Confocal Microscopy in the study of skin permeation: Utility and limitations. In: *Prediction of Percutaneous Penetration*, edited by Walters, K.A., Brain, K. and James, V.J. Cardiff: STS Publishing, 1996, p. 5-6.

Cullander, C. and Guy, R.H. Visualizing the pathways of iontophoretic current flow in real time with laser-scanning confocal microscopy and the vibrating probe electrode. In: *Prediction of Percutaneous Penetration*, edited by Scott, R.C., Guy, R.H. and Hadgraft, J. Southampton: IBC Technical Services, 1991,

De Bruijn, W.C. and Den Breejen, P. Glycogen, its chemistry and morphological appearance in the electron microscope. II. The complexes formed in the selective contrast staining of glycogen. *J.Histochem.* **7**:205-229, (1995).

Delgado-Charro, M.B. and Guy, R.H. Characterization of convective solvent flow during iontophoresis. *Pharm. Res.* **11**:929-935, (1994).

Delgado-Charro, M.B. and Guy, R.H. Iontophoretic delivery of nafarelin across the skin. *Int. J. Pharm.* **117**:165(1995).

Di Colo, G., Carelli, V., Giannaccini, B., Serafini, M.F. and Bottari, F. Vehicle effects in percutaneous absorption: *in vitro* study of influence of solvent power and microscopic viscosity of vehicle on benzocaine release from suspension hydrogels. *J. Pharm. Sci* **69**:387(1980).

Dyer, A., Hayes, G.G., Wilson, J.G. and Catterall, R. Diffusion through skin and model systems. *Int. J. Cosmet. Sci.* **1**:91(1979).

Edwardson, P.A.D., Walker, M., Gardner, R.S. and Jacques, E. The use of FT-IR for the determination of stratum corenum hydration *in vitro* and *in vivo*. *J. Pharm. Biomedical Analysis* **9**:1089-1094, (1991).

Edwardson, P.A.D., Walker, M. and Breheny, C. Quantitative FT-IR determination of skin hydration following occlusion with hydrocolloid containing adhesive dressings. *Int. J. Pharm.* **91**:51-57, (1993).

Fang, J.-Y., Huang, Y.-B., Wu, P.-C. and Tsai, Y.-H. Transdermal iontophoresis of sodium nonivamide acetate I. Consideration of electrical and chemical factors. *Int. J. Pharm.* **143** :46-58, (1996).

Fang, J.-Y., Fang, C.-L., Huang, Y.-B. and Tsai, Y.-H. Transdermal iontophoresis of sodium nonivamide acetate. III. Combined effect of pretreatment by penetration enhancers. *Int. J. Pharm* **149**:183-193, (1997).

Farenfort, J. Attenuated total reflection. A new principle for the production of useful infrared spectra of organic compunds. *Spectrochim Acta* **17**:697-8(1961).

Farinas, K.C., Doh, L., Venkatraman, S. and Potts, R.O. Characterization of solute diffusion in a polymer using ATR-FTIR spectroscopy and bulk transport techniques. *Macromolecules* **27**:5220-5222, (1994).

Fartasch, M. The nature of the epidermal barrier: structural aspects. *Advanced Drug Delivery Reviews* **18**:273-282, (1996).

Flynn, G.L. and Smith, R.W. Membrane diffusion. III: Influence of solvent compositions and permeant solubility on membrane transport. *J. Pharm. Sci* **60**:61-66, (1972).

Flynn, G.L. and Yalkowsky, S.H. Correlation and prediction of mass transport across membranes I: Influence of alkyl chain length of flux-determining properties of barrier and diffusant. *J. Pharm. Sci.* **61**:838(1972).

Francoeur, M.L., Golden, G.M. and Potts, R.O. Oleic acid: Its effects on stratum corneum in relation to (trans)dermal drug delivery. *Pharm. Res.* **7**:621-627, (1990).

French, E.J., Pouton, C.W. and Walters, K.A. Mechanisms and Prediction of Nonionic surfactant effects on Skin Permeability. In: *Pharmaceutical Skin Penetration Enhancement*, edited by Walters, K.A. and Hadgraft, J. New York: Mercel Dekker, 1993, p. 113-143.

Friedman, S., Koide, S.S. and Kincl, F.A. Sustained release hormonal preparations. *Steroids* **15**:679-684(1980).

Ganga, S., Ramarao, P. and Singh, J. Effect of Azone® on the iontophoretic transdermal delivery of metoprolol tartrate through human epidermis *in vitro*. *J. Control. Rel.* **42**:57-64, (1996).

Garrett, E.R. and Chemburkar, P.B. Evaluation, control, and prediction of drug diffusion through polymeric membranes I. *J. Pharm. Sci.* **57**:944(1968).

Gay, C.L., Green, P.G., R.H., G. and Francoeur, M.L. Iontophoretic delivery of piroxicam across the skin *in vitro*. *J. Control. Rel.* **22**:57-68, (1992).

Golden, G.M., Guzek, D.B., Harris, R.R., McKie, J.E. and Potts, R.O. Lipid thermotropic transitions in human stratum corneum. *J. Invest. Dermatol.* **86**:255-259, (1986).

Golden, G.M., McKie, J.E. and Potts, R.O. Role of Stratum corneum lipid fluidity in transdermal drug flux. *J. Pharm. Sci.* **76**:25-28, (1987).

Goodman, M. and Barry, B.W. Lipid-protein-partitioning(LPP) theory of skin enhancer activity: finite dose technique. *Int. J. Pharm.* **57**:29-40, (1989).

Grasso, P. Some aspects of the role of skin appendages in percutaneous absorption. *J. Soc. Cosm. Chem.* **22**:523 (1971).

Green, P.G., Flanagan, M., Shroot, B. and Guy, R.H. Iontophoretic Drug Delivery. In: *Pharmaceutical Skin Penetration Enhancement*, edited by Walters, K.A. and Hadgraft, J. New York: Marcel Dekker Inc, 1993, p. 311-333.

Green, P.G., Shroot, B., Bernerd, F., Pilgrim, W.R. and Guy, R.H. *In vitro* and *in vivo* iontophoresis of a tripeptide across nude rat skin. *J. Control. Rel.* **20**:209-218, (1992).

Gupta, S.K., Kumar, S., Bolton, S., Behl, C.R. and Malick, A.W. Effect of chemical enhancers and conducting gels on iontophoretic transdermal delivery of cromolyn sodium. *J. Control. Rel.* **31**:229-236, (1994).

Guy, R.H. Current status and future prospects of transdermal drug delivery. *Pharm. Res.* **13**:1765-1769, (1996).

Guy, R.H. and Hadgraft, J. Percutaneous penetration enhancement: Physicochemical considerations and implications for prodrug design. In: *Prodrugs: Topical and Ocular Drug Delivery,* edited by Sloan, B.K. New York: Marcel Dekker, 1992, p. 1-16.

Hadgraft, J. and Walters, K.A. Skin penetration enhancement. In: *Drug Absorption Enhancement*, edited by de Boer, A.G. Leiden: 1995, p. 177-198.

Hadgraft, J., Williams, D.G. and Allan, G. Azone®, Mechanisms of action and clinical effect. In: *Pharmaceutical Skin Penetration Enhancement*, edited by Walters, K.A. and Hadgraft, J. New York: Marcel Dekker, 1993,

Harrick, N.J. *Internal Reflectance spectroscopy*, U.S.A.:John Wiley & Sons, 1967.

Harrison, J.E., Groundwater, P.W., Brain, K.R. and Hadgraft, J. Azone® induced fluidity in human stratum corenum. A fourier transform infrared spectroscopy investigation using the predeuterated analogue. *J. Control. Rel.* **41**:283-290, (1996a).

Harrison, J.E., Watkinson, A.C., Green, D.M., Hadgraft, J. and Brain, K. The relative effect of Azone® and Transcutol® on permeant diffusivity and solubility in human stratum corneum. *Pharm. Res.* **13**:542-546, (1996b).

Haugland, R. P. Handbook of fluorescent Probes and Research Chemicals. 6. 1996. Molecular Probes® Catalog.

Herman, B. Single and multiphoton microscopy. In: *Fluorescence Microscopy*, edited by Herman, B. Oxford: Bios Scientific Publishers, 1998a, p. 89-97.

Herman, B. Fundamentals of fluorescence. In: *Fluorescence Microscopy*, edited by Herman, B. Oxford: Bios Scientific Publishers, 1998b, p. 1-16.

Higuchi, T. Physical chemical analysis of percutaneous absorption process from creams and ointments. *J. Soc. Cosmet. Chem.* **11**:85-97, (1960).

Hirvonen, J., Kontturi, K., Murtomaki, L., Paronen, P. and Urrti, A. Transdermal iontophoresis of Sotalol and Salicylate; the effect of skin charge and penetration enhancers. *J. Control. Rel.* **26**:109-117, (1993).

Hoogstraate, A.J., Verhoef, J., Brusee, J., Ijzerman, A.P., Spies, F. and Bodde, H.E. Kinetics, ultrastructural aspects and molecular modelling of transdermal peptide flux enhancement by N-alkylazacycloheptanones. *Int. J. Pharm.* **76**:(1991).

Horlick, G. Introduction to Fourier Transform Spectroscopy. *Applied Spectroscopy* **22**:617-626, (1968).

Houk, J. and Guy, R.H. Membrane models for skin penetration studies. *Chem. Rev.* **88**:455-471, (1988).

Idson, B. Vehicle effects in percutaneous absorption. *Drug Metabolism Reviews* **14**:207-222, (1983).

Johnson, C.G. and Mathias, L.J. Structural characterization of nylon 7 by solid state nuclear magnetic resonance, differential scanning calorimetry and attenuated total reflectance Fourier transform infra-red spectroscopy. *Polymer* **35**:66-74, (1994).

Juni, K., Nomoto, K., Nakano, M. and Arita, T. Drug release through a silicone capsular membrane from micellar solution, emulsion, and cosolvent systems and the correlation of release data *in vivo* with release profile *in vitro*. *J. Membr. Sci.* **5**:295(1979).

Kalia, Y. and Guy, R.H. Interaction between penetration enhancers and iontophoresis: effect on human skin impedance *in vivo*. *J. Control. Rel.* **44**:33-42, (1997).

Kemp, W. Infrared Spectroscopy. In: *Organic Spectroscopy*, edited by Kemp, W. Hong kong: Macmillan Education Ltd, 1991, p. 19-56.

Kendall, D.N. Infrared Radiation: Description and simple theory of absorption by molecules. In: *Applied Infrared Spectroscopy*, edited by Kendall, D.N. New York: Reinhold Publishing Corporation, 1966, p. 1-30.

Kim, A., Green, P.G., Rao, G. and Guy, R.H. Convective solvent flow across the skin during iontpophoresis. *Pharm. Res.* **10**:1315-1320, (1993).

Kincl, F.A., Benagiano, G. and Angee, I. Sustained release hormonal preparations. *Steroids* **11**:673(1968).

Kirkland, J.J. *Modern Practice of Liquid Chromatography*, New York:Wiley, 1971.

Knutson, K., Krill, S.L., Lambert, W.J. and Higuchi, W.I. Physiochemical aspects of transdermal permeation. *J. Control. Rel.* **6**:59-74, (1987).

Knutson, K., Krill, S.L. and Zheng, J. Solvent-mediated alterations of the stratum corneum. *J. Control. Rel.* **11**:93-103, (1989).

Komata, Y., Inaoka, M., Kaneko, A. and Fujie, T. *In vitro* percutaneous absorption of Thiamine disulfide from a mixture of propylene glycol and fatty acid. *J. Pharm. Sci.* **81**:744-746, (1992).

Kost, J. Phonophoresis. In: *Electronically Assisted Drug Delivery*, edited by Berner, B. and Dinh, S.M. New York: CRC Press, 1998, p. 215-228.

Kumar, S., Char, H., Patel, S., et al. *In vivo* transdermal iontophoretic delivery of growth hormone releasing factor (1-44) in hairless guinea pigs. *J. Control. Rel.* **18**:213(1992).

Kurihara, T.B., Knutson, K., DeNoble, L. and Goates, C. Percutaneous absorption enhancement of an ionic molecule by ethanol-water systems in human skin. *Pharm. Res.* 762-766, (1990).

Kushla, G. and Zatz, J.L. Correlation of water and Lidocaine flux enhancement by cationic surfactants *in vitro*. *J. Pharm. Sci.* **8**:1079-1083, (1991).

Landmann, L. Epidermal permeability barrier: transformation of lamellar granule-disks into intercellular sheets by a membrane-fusion process, a freeze fracture study. *J. Invest. Dermatol.* **87**:202-209, (1986).

Langkjaer, L., Brange, J., Grodsky, G.M. and Guy, R.H. Iontophoresis of monomeric insulin analogues *in vitro*: effects of insulin charge and skin pretreatment. *J. Control. Rel.* **51**:47-56, (1998).

Lau, D.T., Sharkey, J.W., Petryk, L., Mancuso, F.A., Yu, Z. and Tse, F.L. Effect of current magnitude and drug concentration on iontophoretic delivery of octreotide acetate (Sandostatin) in the rabbit. *Pharm. Res.* **11**:1742 (1994).

LeDuc, S. Introduction of medicinal substances into the depth of tissues by electric current. *Ann.d'Electrobiol* **3**:560 (1900).

Lee, S.J., Kurihara-Bergstrom, T. and Kim, S.W. Ion-paired drug diffusion through polymer membranes. *Int. J. Pharm.* **47**:59-73, (1987).

Lelawongs, P., Liu, J.-C., Siddiqui, O. and Chien, Y.W. Transdermal iontophoretic delivery of arginine-vasopressin (I): Physiochemical considerations. *Int. J. Pharm.* **56**:13 (1989).

Leo, A., Hansch, C. and Elkins, D. Partition coefficients and their uses. *Chemical Reviews* **71**:525-555, (1971).

Lewis, D. and Hadgraft, J. Mixed monolayers of dipalmitylphosphatidylcholine with Azone® or oleic acid at the air/water interface. *Int. J. Pharm.* **65**:211-218, (1990).

Li, S.K., Ghanem, A.-H., Peck, K.D. and Higuchi, W.I. Iontophoretic transport across a synthetic membrane and human epidermal membrane: A study of the effects of permeant charge. *J. Pharm. Sci.* **86**:680-689, (1997).

Lin., S.-Y. and Liang, R.-C. The effect of ultraviolet B irradiation on the isolated porcine stratum corneum: colorimetric and ATR/FTIR spectroscopic investigations. *Biomedical Research* **15**:9-15, (1994).

Liu, P., Kurihara-Bergstrom, T. and Good, W.R. Cotransport of estradiol and ethanol through human skin *in vitro*: Understanding the permeant/enhancer flux relationship. *Pharm. Res.* **8**:938-944, (1991).

Illel, B. Formulation for transfollicular drug administration: Some recent advances. *CriticalReviews in Therapeutic drug carrier Systems* **14**:207-219, (1997).

Illel, B., Saunal, H., Muller, D. and Schaefer, H. Skin surface biopsy methodology applied to penetration enhancing techniques:Evaluation of skin penetration pathways . In: *Prediction of Percutaneous Penetration*, edited by Walters, K.A., James, V.J. and Brain, K. Cardiff: STS Publishing, 1993, p. 149-160.

Madison, K.C., Swartzendruber, D.C., Wertz, P.W. and Downing, D.T. Presence of intact intercellular lipid lamellae in the upper layers of the stratum corneum. *J. Invest. Dermatol.* **88**:714-718, (1987).

Maher, L.J. Prospects for the therapeutic use of antigene oligonucleotides. *Cancer Investigation* **14**:66-82, (1996).

Maitani, Y., Sato, H. and Nagai, T. Effect of ethanol on the true diffusion coefficient of diclofenac and its sodium salt in silicone membrane. *Int. J. Pharm.* **113**:165-174, (1995).

Mak, V.H.W., Potts, R.O. and Guy, R.H. Oleic acid concentration and effect in human stratum corneum: Non-invasive determination by attenuated total reflectance infrared spectroscopy in vivo. *J. Control. Rel.* **12**:67-75, (1990a).

Mak, V.H.W., Potts, R.O. and Guy, R.H. Percutaneous penetration enhancement *in vivo* measured by attenuated total reflectance infrared spectroscopy. *Pharm. Res.* **7**:835-841, (1990b).

Margarida, A., Tralhao, L., Watkinson, A.C., Brain, K.R., Hadgraft, J. and Armstrong, N.A. Use of ATR-FTIR spectroscopy to study the diffusion of ethanol through glycerogelatin films. *Pharm. Res.* **12**:572-575, (1995).

Markovich, R.J. and Pidgeon, C. Introduction to Fourier Transform infrared spectroscopy and applications in the pharmaceutical sciences. *Pharm. Res.* **8**:663-675, (1991).

Martin, M., Curley, P., Devane, J. and Kelly, J. *In-vitro* transdermal delivery of desmopressin. In: *Prediction of Percutaneous Penetration*, edited by Scott, R.C., Guy, R.H., Hadgraft, J. and Bodde, H.E. London: IBC Technical Services Ltd, 1991, p. 97

Megrab, N.A., Williams, A.C. and Barry, B.W. Oestradiol permeation across human skin, silastic and skin membranes: The effects of ethanol/water co-solvent systems. *Int. J. Pharm.* **116**:101-112, (1995a).

Megrab, N.A., Williams, A.C. and Barry, B.W. Oestradiol permeation through human skin and silastic membrane: effects of propylene glycol and supersaturation. *J. Control. Rel.* **36**:277-294, (1995b).

Michniak, B.B., Player, M.R., Godwin, D.A., Phillips, C.A. and Sowell Sr, J.W. *In vitro* evaluation of a series of Azone® analogs as dermal penetration enhancers; IV. Amines. *Int. J. Pharm.* **116**:201-209, (1995).

Michniak, B.B., Player, M.R., Godwin, D.A., Lockhart, C.C. and Sowell, J.W. *In vitro* evaluation of Azone® analogs as dermal penetration enhancers. *Int. J. Pharm.* **161**:169-178, (1998).

Miller, L.L., Kolaskie, C.J., Smith, G.A. and Rivier, J. Transdermal iontophoresis of gonadotropin-releasing hormone(LHRH) and two analogues. *J. Pharm. Sci.* **79**:490(1989).

Mollgaard, B. Synergistic effects in percutaneous enhancement. In: *Pharmaceutical Skin Penetration Enhancement*, edited by Walters, K.A. and Hadgraft, J. 1993, p. 229-242.

Mollgaard, B. and Hoelgaard, A. Vehicle effect on topical drug delivery. I. Influence of glycols and drug concentration on skin transport. *Acta. Pharm. Suec.* **20**:433-442, (1983).

Montagna, W., Kligman, A.M. and Carlisle, K.S. *Atlas of Normal Skin*, New York:Springer-Verlag Inc, 1992.

Naik, A., Pechtold, L. A. R. M., Potts, R. O., and Guy, R. H. Mechanism of skin penetration enhancement, *in vivo*, in man. *In Prediction of Percutaneous Penetration.*, edited by Brain, K. 3B, 161-165. 1993. Cardiff, STS Publishing.

Nakano, M. and Pater, N.K. Release, uptake and permeation behaviour of salicylic acid in ointment bases. *J. Pharm. Sci.* **59**:985(1970).

Nemanic, M.K. and Elias, P.M. *In situ* precipitation: A novel cytochemical technique for visualistaion of permeability pathways in mammalian startum corneum. *J. Hist. Cytochem.* **28**:573-578, (1980).

Odland, G.F. Structure of the skin. In: *Physiology, Biochemistry, and Molecular Biology of the Skin*, edited by Goldsmith, L.A. New York: Oxford University Press, 1991, p. 3-62.

Ogiso, T. and Shintani, M. Mechanism for the enhancement effect of fatty acids on the percutaneous absorption of propranolol. *J. Pharm. Sci.* **79**:1065-1071, (1990).

Ogiso, T., Paku, T., Iwaki, M., Tanino, T. and Nisioka, S. Percutaneous absorption of physiologically active peptides, Ebiratide and Elcatonin, in rats. *Biol. Pharm. Bull.* **17**:1094-110, (1994a).

Ogiso, T., Paku, T., Iwaki, M. and Tanino, T. Mechanism of the enhancement effect of n-Octyl-B-D-thioglucoside on the transdermal penetration of fluorescein isothiocyanate-labelled dextrans and the molecular weight dependance of water-soluble penetrants through stripped skin. *J. Pharm. Sci.* **83**:1676-1681, (1994b).

Ogiso, T., Paku, T., Iwaki, M. and Tanino, T. Percutaneous penetration of fluorescein Isothiocyanate-Dextrans and the mechanism for enhancement effect of enhancers on the intercellular penetration. *Biol. Pharm. Bull.* **18**:1566-1571, (1995).

Oh, S.Y., Jeong, S.Y., Park, T.G. and Lee, J.H. Enhanced transdermal delivery of AZT (Zidovudine) using iontophoresis and penetration enhancer. *J. Control. Rel.* **51**:161-168, (1998).

Ongpipattanakul, B., Burnette, R.R., Potts, R.O. and Francoeur, M.L. Evidence that oleic acid exists in a separate phase within stratum corneum lipids. *Pharm. Res.* **8**:350-354, (1991).

Park, A.C. and Baddeil, C.B. Rheology of stratum corneum II: A physico-chemical investigation of factors influencing the water content of the corneum. *J. Soc. Cosmet. Chem.* **23**:13-21, (1972).

Patil, S., Singh, P., Szolar-Platzer, C. and Maibach, H. Epidermal enzymes as pentration enhancers in transdermal drug delivery. *J. Pharm. Sci.* **85**:249-252, (1996).

Pellet, M. A., Watkinson, A. C., Brain, K. R., and Hadgraft, J. An investigation into the validity of deuterated labelling of compounds in relation to their diffusion within synthetic membranes. In 4th UKaps AnnualConference proc., edited by Kellaway, I. W. and Hadgraft, J. 68. 1995. Cardiff, STS Publishing.

Pellet, M.A., Watkinson, A.C., Hadgraft, J. and Brain, K.R. Comparison of permeability data from traditional diffusion cells and ATR-FTIR spectroscopy. Part II. Determination of diffusional pathlengths in synthetic membranes and human stratum corneum. *Int. J. Pharm.* **154**:217-227, (1997a).

Pellet, M.A., Watkinson, A.C., Hadgraft, J. and Brain, K.R. Comparison of permeability data from traditional diffusion cells and ATR-FTIR spectroscopy Part I. Synthetic membranes. *Int. J. Pharm.* **154**:205-215, (1997b).

Pikal, M.J. The role of electroosmotic flow in transdermal iontophoresis. *Adavnced Drug Delivery Reviews* **9**:201-237, (1992).

Pikal, M.J. and Shah, S. Transport Mechanisms in Iontophoresis.III. An experimental study of the contributions of electroosmotic flow and permeability change in transport of low and high molecular weight solutes. *Pharm. Res.* **7**:222-229, (1989).

Pirot, F. Characterization of the permeability barrier of human skin *in vivo*. Proc. Natl. Acad. Sci. 94, 1562-1567. 1996.

Potts, R.O. and Francoeur, M.L. The influence of stratum corneum morphology on water permeability. *J. Invest. Dermatol.* **96**:495-499, (1991).

Praustnitz, M.R. Reversible skin permeabilization for transdermal delivery of macromolecules. *Critical Reviews in Therapeutic Drug Carrier Systems* **14**:455-483, (1997).

Prausnitz, M.R. Electroporation. In: *Electronically assisted drug delivery*, edited by Berner, B. and Dinh, S.M. New York: CRC Press, 1998, p. 185-214.

Pugh, W.J., Roberts, M.S. and Hadgraft, J. Epidermal permeability - penetrant structure relationships; 3. The effect of hydrogen bonding interactions and molecular size on diffusion across the stratum corneum. *Int. J. Pharm.* **138**:149-165, (1996).

Puttnam, N.A., Baxter, B.H., Lee, S. and Stott, P.L. Application of attenuated total reflectance IR spectroscopy to toilet articles and household products, 2.-Quantitative analysis. *J. Soc. Cosm. Chem.* **17**:9-16, (1966).

Rhein, L.D., Robbins, C.R., Fernee, K. and Cantore, R. Surfactant structure effects on swelling of isolated human stratum corneum. *J. Soc. Cosm. Chem.* **37**:125(1986).

Riviere, J.E. and Heit, M.C. Electrically-assisted transdermal drug delivery. *Pharm. Res.* **14**:687-697, (1997).

Roberts, M.S., Favretto, W.A., Meyer, A., Reckmann, M. and Wongesclashote, T. Topical bioavailability of methyl salicylate. *Aust.N.Z.J.Med.* **12**:303-305, (1982).

Roberts, M.S., Pugh, W.J. and Hadgraft, J. Epidermal permeability - penetrant structure relationships: 2. The effect of H-bonding groups in penetrants on their diffusion through the stratum corneum. *Int. J. Pharm.* **132**:23-32, (1996).

Roberts, M.S. and Walker, M. Water: The most natural penetration enhancer. In: *Pharmaceutical Skin Penetration Enhancement*, edited by Walters, K.A. and Hadgraft, J. New York: Marcel Dekker, 1993, p. 1-30.

Santus, G.C. and Baker, R.W. Transdermal enhancer patent literature. *J. Control. Rel.* **25**:1-20, (1993).

Scheuplein, R.J. Mechanism of percutaneous absorption. I. Routes of penetration and the influence of solubility. *J. Invest. Dermatol.* **45**:334-346, (1967).

Scheuplein, R.J. Permeability of the skin: A review of major concepts. *Curr. Probl. Dermatol.* **7**:172-186, (1978a).

Scheuplein, R.J. The skin as a barrier. In: *The Physiology and Pathophysiology of Skin*, edited by Jarret, A. London: Academic Press, 1978b, p. 1669-1692.

Scheuplein, R.J. and Bronaugh, R.L. *Biochemistry and Physiology of the Skin*, New York:Oxford University, 1983. pp. 1255

Scheuplein, R.J. and Dugard, P.H. Effects of ionic surfactants on the permeability of human epidermis: an electrometric study. *J. Invest. Dermatol.* **60**:(1973).

Scott, E.R., Laplaza, A.I., White, H.S. and Phipps, J.B. Transport of ionic species in skin: Contribution of pores to the overall skin conductance. *Pharm. Res.* **10**:1699-1709, (1993).

Sharata, H. and Burnette, R. Effect of dipolar aprotic permeability enhancers on the basal stratum corneum. *J. Pharm. Sci.* **77**:27-32, (1988).

Siddiqui, O., Roberts, M.S. and Polack, A.E. The effect of iontophoresis and vehicle pH on the *in vitro* permeation of lignocaine through human stratum corneum. *J. Pharm. Pharmacol.* **37**:732-735, (1985).

Simonetti, O., Hoogstraate, A.J., Bialik, W., Ponec, M. and Boddé, H.E. Visualization of diffusion pathways across the stratum corneum of native and *in-vitro*-reconstructed epidermis by confocal laser scanning microscopy. *Arch. Dermatol. Res.* **287**:465-473, (1995).

Singh, P. and Maibach, H.I. Iontophoresis in drug delivery: Basic principles and applications. *Critical Reviews in Therapeutic Drug Carrier Systems* **11**:161-213, (1994).

Singh, P. and Maibach, H.I. Iontophoresis: an alternative to the use of carriers in cutaneous drug delivery. *Advanced Drug Delivery Reviews* **18**:379-394, (1996).

Singh, S. and Singh, J. Transdermal drug Delivery by passive diffusion and iontophoresis: A review. *Medicinal research reviews* **13**:569-621, (1993).

Smith, A.L. *Applied Infrared Spectroscopy*, New York:John Wiley & Sons, 1980. pp. 322

Smith, E.W. and Maibach, H.I. *Percutaneous Penetration Enhancers*, Boca Raton:CRC Press, 1995.

Spruit, D. and Malten, K.E. Epidermal water-barrier formation after stripping of normal skin. *J. Invest. Dermatol.* **45**:6-14, (1965).

Srinivasasn, V., Su, M.-H., Higuchi, W.I. and Behl, C.R. Iontophoresis of polypeptides: Effect of ethanol pretreatment of human skin. *J. Pharm. Sci.* **79**:588-591, (1990).

Steinstrasser, I. and Merkle, H.P. Dermal metabolism of topically applied drugs: pathways and models reconsidered. *Pharm. Acta. Helv.* **70**:3-24, (1995).

Sternhell, S. and Kalman, J.R. *Organic structures from spectra*, Chicester:John Wiley & Sons Ltd, 1986. pp. 1-202.

Subramanian, D.V. A spectroscopic method for the evaluation of the substantivity of N-lauroyl sarcosinate to human skin. *J. Soc. Cosmet. Chem.* **46**:153-162, (1995).

Swartzendruber, D.C., Manganaro, A., Madison, K.C., Kremer, M., Wertz, P.W. and Squier, C.A. *Cell Tissue Res.* **279**:271-276, (1995).

Sweeny, T.M. and Downing, D.T. The role of the epidermal barrier to water diffusion. *J. Invest. Dermatol.* **55**:135-140, (1970).

Takeuchi, Y., Yasukawa, H., Yamaoka, Y. Effects of Oleic acid/Propylene Glycol on rat abdominal stratum corneum: Lipid extraction and appearance of propylene glycol in the dermis measured by fourier transform infrared/attenuated total reflectance (FT-IR/ATR) spectroscopy. *Chem. Pharm. Bull.* .**41**:1434-1437, (1993).

Takeuchi, Y., Yasukawa, H., Yamaoka, Y. Behavior of propylene glycol (PG) in dermis after treatment of rat intact skin surface with fatty acids, fatty amines or Azone® dissolved in PG. *Biol. Pharm. Bull.* **18**:304-309, (1995).

Theiβ, U. and Lucker, P.W. Iontophoresis - Is there a future for clinical application? *Meth. Find. Exp. Clin. Pharmacol.* **13**:353-359, (1991).

Thysman, S., Hanchard, C. and Preat, V. Human calcitonin delivery in rats by iontophoresis. *J. Pharm. Pharmacol.* **46**:725(1994).

Turner, N.G., Ferry, L., Price, M., Cullander, C. and Guy, R.H. Iontophoresis of Poly-L-lysines: The role of molecular weight? *Pharm. Res.* **14**:1322-1331, (1997).

Turner, N.G. and Guy, R.H. Iontophoretic transport pathways: Dependance on penetrant physicochemical properties. *J. Pharm. Sci.* **86**:1385-1389, (1997).

Turner, N.G. and Nonato, L.B. Visualization of stratum corneum and transdermal permeation pathways. In: *Mechanisms of Transdermal Drug Delivery*, edited by Potts, R.O. and Guy, R.H. New York: Marcel Dekker Inc, 1997, p. 1-40.

Twist, J.N. and Zatz, J.L. Membrane-solvent-solute interaction in a model permeation system. *J. Pharm. Sci.* **77**:536-540, (1988).

Van der Geest, R. PK/PD based drug delivery system design: Iontophoretic apomorphine delivery in patients with Parkinson's disease. 238. 1998. PhD Thesis, University of Leiden.

Van der Geest, R., Danhof, M. and Bodde, H.E. Iontophoretic delivery of Apomorphine I: *In vitro* optimization and validation. *Pharm. Res.* **14**:1798-1803, (1997).

Van Dijk-Wolthuis, W. Biodegradable dextran hydrogels for pharmaceutical applications. 1-158. 1997. PhD Thesis,University of Utrecht.

Volpato, N.M., Santi, P. and Colombo, P. Iontophoresis enhances the transport of acyclovir through nude mouse skin by electrorepulsion and electroosmosis. *Pharm. Res.* **12**:1623-1626, (1995).

Vroom, J. Two-photon excitation fluorescence lifetime imaging: development and biological applications. 1-93. 1998. PhD Thesis, Academic Department: Universiteit Utrecht, Faculteit Natuur-en Sterrenkunde.

Walker, M. and Hadgraft, J. Oleic acid - a membrane 'fluidiser' or fuid within the membrane? *Int. J. Pharm.* **71**:R1-R4(1991).

Walker, R.B. and Smith, E.W. The role of percutaneous penetration enhancers. *Advanced Drug Delivery Reviews* **18**:295-301, (1996).

Walkow, J.C. and McGinity, J.W. The effect of physiochemical properties on the *in vitro* diffusion of drug through synthetic membranes and pigskin. I Methyl salicylate. *Int. J. Pharm.* **35**:91-102, (1987a).

Walkow, J.C. and McGinty, J.W. The effect of physiochemical properties on the *in vitro* diffusion of drug through synthetic membranes and pigskin. II. Salicylic acid. *Int. J. Pharm.* **35**:103-109, (1987b).

Walters, K.A. Surfactants and percutaneous absorption. In: *Prediction of Percutaneous Penetration Methods, Measurements, Modelling*, edited by Scott, R.C., Guy, R.H. and Hadgraft, J. 1989, p. 148-162.

Walters, K.A. and Hadgraft, J. *Pharmaceutical Skin Penetration Enhancement*, New York: Marcel Dekker Inc, 1993.

Watkinson, A.C., Hadgraft, J., Walters, K.A. and Brain, K.R. Measurement of diffusional parameters in membranes using ATR-FTIR spectroscopy. *Int. J. Cosm. Sci.* **16**:199-210, (1994a).

Watkinson, A. C., Hadgraft, J., and Brain, K. R. The Deconvolution of diffusion and partition coefficeints in permeability studies. 21st Controlled Release Society Conference, 160-161. 1994b. Nice.

Watkinson, A.C., Joubin, H., Green, D.M., Brain, K.R. and Hadgraft, J. The influence of vehicle on permeation from saturated solutions. *Int. J. Pharm.* **121**:27-36, (1995).

Wearley, L. and Chien, Y.W. Enhancement of the *in vitro* skin permeability of Azidothymidine (AZT) via iontophoresis and chemical enhancer. *Pharm. Res.* **7**:34-40, (1990).

Wertz, P.W. and Van den Bergh, B. The physical, chemical and functional properties of lipids in the skin and other biological barriers. *Chemistry and Physics of Lipids* **91**:85-96, (1998).

Wester, R.C., Christoffel, J., Hartway, T., Poblete, N., Maibach, H. and Forsell, J. Human cadaver skin viability for *In vitro* percutaneous absorption: Storage and detrimental effects of heat-separation and freezing. *Pharm. Res.* **15**:82-84, (1998).

Wiechers, J. W. Absorption, distribution, metabolism and excretion of the cutaneous penetration enhancer Azone®. PhD Thesis, University of Leiden. 152. 1989.

Wotton, P.K., Mollgaard, B., Hadgraft, J. and Hoelgaard, A. Vehicle effect on topical drug delivery. III. Effect of Azone® on the cutaneous permeation of metronidazole and propylene glycol. *Int. J. Pharm.* **25**:19-26, (1985).

Wurster, D.E., Buraphacheep, V. and Patel, J.M. The determination of diffusion coefficients in semisolids by fourier transform infrared (FT-IR) spectroscopy. *Pharm. Res.* **10**:616-620, (1993).

Yamaguchi, Y. Evaluation of skin permeability of drugs by newly prepared polymer membranes. *Chem. Pharm. Bull.* **45**:537-541, (1997).

Yamamoto, T. and Yamamoto, Y. Electrical properties of the epidermal stratum corneum. *Medical and Biological Engineering* 151-158, (1976).

Yamane, M.A., Williams, A.C. and Barry, B.W. Effects of terpenes and oleic acid as skin penetration enhancers towards 5-fluorouracil as assessed with time; permeation, partitioning and differential scanning calorimetry. *Int. J. Pharm.* **116**:237-251, (1995).

Yoshida, N. and Roberts, M. Solute molecular size and transdermal iontophoresis across excised human skin. *J. Control. Rel.* **25**:177-195, (1993).

Yuk, S.H., Cho, S.H. and Lee, H.B. Composite membrane for transdermal delivery of Beta-estradiol. 22nd Controlled Release Society Conference, **22**:636-637, (1995).